The Search for *Hypercloso* Metallacarboranes Through Ligand Manipulation

John J. Jones

Submitted for the degree of Doctor of Philosophy at Heriot-Watt University, on completion of research in the school of Engineering and Physical Sciences.

June 2018

Abstract

Chapter one is an introduction to carborane and metallacarborane chemistry, with a particular focus on "non-Wadian", including *hypercloso*, heteroboranes. The chapter then discusses the various methods that could be used to synthesise *hypercloso* boranes and heteroboranes before identifying generating *hypercloso* metallacarboranes through ligand set manipulation as the objective of this project.

Chapter two contains a discussion of attempts to synthesise *hypercloso* molybdacarboranes through ligand abstraction. A reaction between the species $[NEt_4][1,7\text{-}Me_2\text{-}2,2,2\text{-}(CO)_3\text{-}2\text{-}I\text{-}closo\text{-}2,1,7\text{-}MoC_2B_9H_9]$ and $Ag[BF_4]$ was found unexpectedly to regenerate $1,7\text{-}Me_2\text{-}2,2,2,2\text{-}(CO)_4\text{-}closo\text{-}2,1,7\text{-}MoC_2B_9H_9$ through a process referred to as carbonyl stealing. Further related experiments also produced results consistent with carbonyl stealing.

In chapter three efforts are instead directed at synthesising *hypercloso* ruthenacarboranes. In the process two new routes to *closo* ruthenacarboranes were developed. The first leads to anions of the general formula $[1,2\text{-}R_2\text{-}3\text{-}Cl\text{-}3,3\text{-}(PPh_3)_2\text{-}closo\text{-}3,1,2\text{-}RuC_2B_9H_9]^-$ whilst the second (which follows from this) was used to synthesise a diverse family of mixed ligand ruthenacarboranes. Attempts to synthesise *hypercloso* ruthenacarboranes instead produced highly complex product mixtures from which several unusual "wedged" species were isolated.

Chapter four describes efforts directed towards synthesising *hypercloso* ruthenacarboranes using the same methodology as in chapter three but by also exploiting steric factors. This once again resulted in complex product mixtures from which some highly unusual species were isolated, including an additional "wedged" species as well as two "symbiotic" species, one of which is without precedent in the literature.

Chapter five contains a summary of the research contained within this thesis whilst chapter six contains experimental details for all of the novel compounds prepared as well as alternative or improved syntheses for some literature compounds.

Acknowledgements

Firstly, I would like to thank my PhD supervisor, Prof. Alan Welch, who has been indescribably helpful and encouraging for the duration of my PhD. Alan sets high standards for his PhD students but I believe he does so because he wants his students to develop into the best chemists they can possibly be. It has been a privilege to work for a supervisor who has such enthusiasm for chemistry and such a wealth of knowledge and experience.

I would also like to thank my parents and wider family for all of their love and support without which I would not be where I am today. My parents support during the time I was writing my thesis was particularly important and so I am particularly grateful for that. At this point in time they are presumably just very relieved that I finally have an actual job.

Other people who have aided me throughout my PhD include Dr Dave Ellis and Dr Georgina Rosair. I am very grateful for their time and expertise. Additionally, I would like to thank the Leverhulme trust for funding my project.

Thank you to the current and former members of the heteroborane group for both abetting me and for making W.P. 2.12 such an enjoyable environment to work in. I would like to thank Tony, Bex, Mandy, Laura, Sam, Dipendu, Steve, the other Laura (Woodward) but especially Dr Ally Robertson, who invested so much into my development as a chemist. I wish him and his young family all the good will in the world. I would also like to thank Dr Mansell and Dr Vilela for their support.

I would also like to thank all of the current and former chemistry PhD students and post-docs with whom I have become friends with but also Robert Newland. I wish Rob good fortune in his attempts to become a professional skateboarder. I would also like to thank my best friend and debating partner Michael, whose friendship has been invaluable. I should also take this opportunity to apologise to my co-workers and fellow PhD students for my “occasional” grumpiness. Recognise that this statement does not amount to an admission of guilt and has no cash value.

HERIOT WATT UNIVERSITY

ACADEMIC REGISTRY
Research Thesis Submission

Name:	John J. Jones		
School:	Engineering and Physical Sciences		
Version: *(i.e. First, Resubmission, Final)*	First	Degree Sought:	Doctor of Philosophy

Declaration

In accordance with the appropriate regulations I hereby submit my thesis and I declare that:

1) the thesis embodies the results of my own work and has been composed by myself
2) where appropriate, I have made acknowledgement of the work of others and have made reference to work carried out in collaboration with other persons
3) the thesis is the correct version of the thesis for submission and is the same version as any electronic versions submitted*.
4) my thesis for the award referred to, deposited in the Heriot-Watt University Library, should be made available for loan or photocopying and be available via the Institutional Repository, subject to such conditions as the Librarian may require
5) I understand that as a student of the University I am required to abide by the Regulations of the University and to conform to its discipline.
6) I confirm that the thesis has been verified against plagiarism via an approved plagiarism detection application e.g. Turnitin.

* *Please note that it is the responsibility of the candidate to ensure that the correct version of the thesis is submitted.*

Signature of Candidate:	John	Date:	28/6/18

Submission

Submitted By *(name in capitals)*:	JOHN J. JONES
Signature of Individual Submitting:	John
Date Submitted:	28/6/18

For Completion in the Student Service Centre (SSC)

Received in the SSC by *(name in capitals)*:			
Method of Submission *(Handed in to SSC; posted through internal/external mail)*:			
E-thesis Submitted ***(mandatory for final theses)***			
Signature:		Date:	

Please note this form should be bound into the submitted thesis.

Table of Contents

List of Abbreviations

[9]aneS_3	1,4,7-Trithiacyclononane
<δ(^{11}B)>	Weighted average ^{11}B NMR chemical shift
acac	Acetylacetonate
BHD	Boron-hydrogen-distance
Bz	Benzyl group
BNCT	Boron neutron capture therapy
BTMA	Benzyltrimethylammonium
Cb*	Tetramethylcyclobutadiene
CHN	Elemental analysis (Carbon-Hydrogen-Nitrogen)
COD	Cyclooctadiene
CoSAN	[(*closo*-1,2-$C_2B_9H_{11})_2Co]^-$ ("Cobalt Sandwich")
Cp	Cyclopentadienyl
Cp*	Pentamethylcyclopentadienyl
CSD	Cambridge Structural Database
Cy	Cyclohexyl
d	Doublet
DEI	Direct electrophilic insertion
DSD	Diamond-square-diamond
EIMS	Electron ionisation mass spectrometry
E_k	Kinetic energy
Et	Ethyl
FeSAN	[(*closo*-1,2-$C_2B_9H_{11})_2Fe]^{n-}$ ("Fe Sandwich")
FTIR	Fourier-transform infrared
^{i}Pr	Isopropyl
IR	Infrared
IUPAC	International Union of Pure and Applied Chemistry
L	L type ligand
m	Multiplet
Me	Methyl
MeV	Mega electron volts
MO	Molecular orbital
^{n}Bu	*n*-Butyl
NMR	Nuclear magnetic resonance
o-tolyl	Orthomethylated phenyl

p-cymene	1-^{i}Pr-4-Me-C_6H_4
Petrol	40:60 petroleum ether
Ph	Phenyl
phen	Phenanthroline
PNP	Bis(triphenylphosphine)iminium $[Ph_3P=N=PPh_3]^+$
ppm	Parts per million
R_f	Retention factor
RuSAN	$[(closo\text{-}1,2\text{-}C_2B_9H_{11})_2Ru]^{n-}$ (“Ruthenium Sandwich”)
s	Singlet
SEP	Skeletal electron pair
STE	Structural trans effect
t	Triplet
^{t}Bu	*t*-Butyl
TFR	Triangular face rotation
THF	Tetrahydrofuran
TLC	Thin layer chromatography
VCD	Vertex-to-centroid-distance
X	X type ligand

List of Abbreviations for Specific Compounds

List of Abbreviations for New Compounds

1 4,4,4,4-$(CO)_4$-*closo*-4,1,6-$MoC_2B_{10}H_{12}$

2 1,7-Me_2-2,2,2,2-$(CO)_4$-*closo*-2,1,7-$MoC_2B_9H_9$

3 [1,7-Me_2-2,2,2-$(CO)_3$-2-I-*closo*-2,1,7-$MoC_2B_9H_9$]$^-$

4 1,8-Me_2-2,2,2,2-$(CO)_4$-*closo*-2,1,8-$MoC_2B_9H_9$

5 3,3-$(PPh_3)_2$-3-^{t}BuNC-*closo*-3,1,2-$RuC_2B_9H_{11}$

6 3-PPh_3-3,3-$(PMe_3)_2$-*closo*-3,1,2-$RuC_2B_9H_{11}$

10 [7,8′-*exo*-(Ru{PPh_3}$_2$)-7,8′-μ-$(H)_2$-*commo*-3,3′-Ru(1,2-Me_2-1,2-$C_2B_9H_8$) (1′,2′-Me_2-1′,2′-$C_2B_9H_8$)]

11 1-^{t}Bu-2-Me-*closo*-1,2-$C_2B_{10}H_{10}$

12 K[7-^{t}Bu-8-Me-*nido*-7,8-$C_2B_9H_{10}$]

13 5,6,10-[Cl(Ph_3P)$_2$Ru]-5,6,10-μ-$(H)_3$-7-^{t}Bu-8-Me-10-H-7,8-$C_2B_9H_6$

14 1-^{t}Bu-2-Me-3-PPh_3-3,3-(^{t}BuNC)$_2$-*closo*-3,1,2-$RuC_2B_9H_9$

17 5,6,10-[Cl(Ph_3P)$_2$Ru]-5,6,10-μ-$(H)_3$-7,8-Ph_2-10-H-7,8-$C_2B_9H_6$

18 1,2-Ph_2-3-(^{t}BuNC)$_2$-3-PPh_3-1,2-Ph_2-*pseudocloso*-3,1,2-$RuC_2B_9H_9$

19 1,2-Ph_2-3-PPh_3-3,3-$(CO)_2$-*pseudocloso*-3,1,2-$RuC_2B_9H_9$

20 [{1,2-Ph_2-*pseudocloso*-3,1,2-$RuC_2B_9H_9$}{1′,8′-Ph_2-*closo*-2′,1′,8′-$RuC_2B_9H_9$}]

21 [{1,2-Ph_2-*pseudocloso*-3,1,2-$RuC_2B_9H_9$}{1′,8′-Ph_2-*closo*-2′,1′,8′-$RuC_2B_9H_9$} {1″,8″-Ph_2-*closo*-2″,1″,8″-$RuC_2B_9H_9$}]

List of Abbreviations for Literature Compounds

I $Mo(CO)_2(MeCN)_2(C_3H_5)Br$

II 1,2-Me_2-3,3,3,3-$(CO)_4$-*closo*-3,1,2-$MoC_2B_9H_9$

III [1,6-Me_2-4,4-$(CO)_2$-4-(C_3H_5)-*closo*-4,1,6-$MoC_2B_{10}H_{10}$]$^-$

IV [1,8-Me_2-2-I-2,2,2-$(CO)_3$-*closo*-2,1,8-$MoC_2B_9H_9$]$^-$

V 5,6,10-[Cl(Ph_3P)$_2$Ru]-5,6,10-μ-$(H)_3$-10-H-7,8-$C_2B_9H_8$

VI [3-Cl-3,3-$(PPh_3)_2$-*closo*-3,1,2-$RuC_2B_9H_{11}$]$^-$

VII 3,3-$(PPh_3)_2$-3-CO-*closo*-3,1,2-$RuC_2B_9H_{11}$

VIII 5,6,10-[Cl(Ph_3P)$_2$Ru]-5,6,10-μ-$(H)_3$-7,8-Me_2-10-H-7,8-$C_2B_9H_6$

IX 1-^{t}Bu-*closo*-1,2-$C_2B_{10}H_{11}$

1.0 Introduction

1.1 Boron

Boron is the fifth element in the periodic table and was discovered in 1808 by Davy, Thenard and Gay-Lussac.[1] Boron does not exist freely in nature and therefore must be extracted from ores, such as borax, $Na_2[B_4O_5(OH)_4]\cdot 8H_2O$, which can be reduced to give elemental boron. Elemental boron is like its neighbour carbon in its capacity to form stable covalently bonded molecular networks.

Boron is a group thirteen element and possesses only three valence electrons. Boron therefore is electron deficient, as it cannot make enough covalent bonds to fill its outer shell in the same way that other p-block elements like carbon and nitrogen can. However, boron is unlike other group thirteen elements, which are more metallic in character and have lower ionisation potentials, meaning that they can be ionised relatively easily to give cations, something not true of boron.

There are only two naturally occurring isotopes of boron, ^{10}B and ^{11}B, which make up 20% and 80% of naturally occurring boron, respectively. Both nuclei are NMR-active but ^{11}B NMR spectroscopy is used much more pervasively than ^{10}B NMR spectroscopy, as the former isotope is more abundant.

1.2 Boranes

Boron forms complexes with hydrogen known as boron hydrides, the simplest of which is BH_3, which is a Lewis acid as it has an unoccupied p orbital. Because of this, BH_3 is very reactive and cannot be concentrated without dimerising to form B_2H_6, shown in figure 1.2.1. The structure of B_2H_6, confirmed by Bauer,[2] contains four terminal hydrogen atoms and two bridging hydrogen atoms. It is not possible to describe all four of these bonds as conventional two-centre, two-electron bonds because each boron atom only has three valence electrons available for covalent bonding. Instead, each bridging hydrogen atom can be thought of as being the centre of a three-centre, two-electron bond, as proposed by Longuet-Higgins.[3] This allows each boron atom to complete its octet. The bonding character is also reflected in some of the properties of the molecule. For example, the terminal B-H bonds are shorter than the bridging B-H bonds, as the bridging bonds are weaker and therefore longer than conventional two-centre, two-electron bonds.

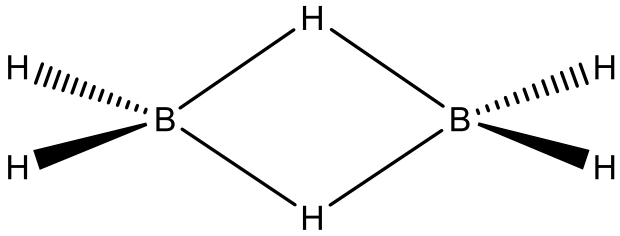

Figure 1.2.1: Structure of B_2H_6.

An alternative method of conceptualising the bonding in B_2H_6 would instead be to utilise Molecular Orbital (MO) theory. Using the ligand orbital approach, it is possible to consider the interactions between a pair of bridging H atoms and the remaining B_2H_4 fragment, the MO diagram for which is shown in figure 1.2.2. An important conclusion of the MO model is that, instead of having two distinct three centre, two electron bonds, the electron density is instead delocalised over all four atoms of the bridging $\{B_2H_2\}$ unit.

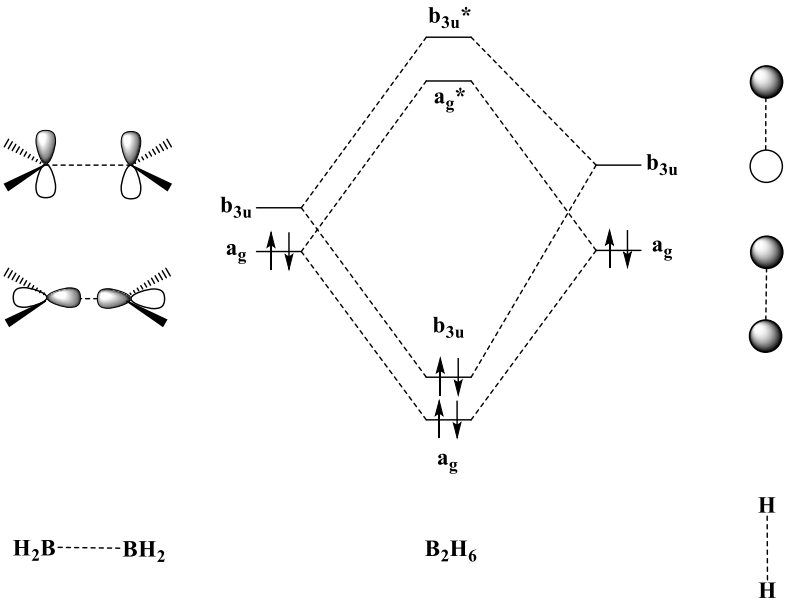

Figure 1.2.2: MO diagram for B_2H_6.

This multiple centre bonding also occurs within larger boranes, which form polyhedral clusters. These contain highly connected boron atoms that are connected to more than four other vertices. The linkages between boron vertices are referred to as connectivities, not bonds, as the latter implies two-centre, two-electron bonding as opposed to multiple centre bonding. In the case of large enough borane clusters, such as $[B_{12}H_{12}]^{2-}$, shown in figure 1.2.3, the bonding can be considered as being delocalised over the entire cluster, in a way that can be thought of as a three-dimensional analogue of an aromatic molecule.

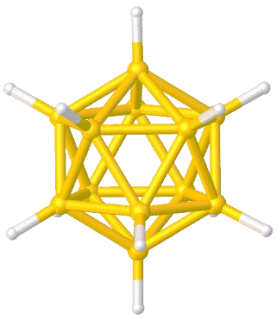

Figure 1.2.3: Structure of $[B_{12}H_{12}]^{2-}$.

1.3 Wade's Rules

Originally articulated by Kenneth Wade,[4] Wade's rules relate the observed geometries of cluster compounds to their number of vertices and number of skeletal electron pairs (SEPs), which are the electrons involved in cluster bonding.

If a species has n vertices and n+1, n+2 or n+3 SEPs then it is classified as *closo*, *nido* or *arachno*, respectively. These are the three most common classifications encountered, though species with even more than n+3 SEPs do exist, e.g. species with n vertices and n+4 SEPs are classified as *hypho*.

To classify a cluster compound the number of SEPs must be known. This is determined by the number of electrons the vertices cumulatively contribute to cluster bonding plus or minus any contribution from the overall charge of the molecule. The number of electrons a vertex donates to cluster bonding (s) is equal to its valence electron count (v), plus the number of electrons provided by any *exo*-polyhedral substituent (x) minus any electrons that are involved in bonding *exo* to the cluster (y).

$$s = v + x - y$$

s = no. of electrons available for cluster bonding.
v = no. of valence electrons possessed by vertex atom.
x = no. of electrons provided by any *exo*-polyhedral substituents bound to vertex.
y = no. of electrons involved in *exo*-polyhedral bonding, commonly equal to two in the case of a vertex with either a lone pair or a single bond *exo* to the cluster.

For example, a {BH} vertex consists of a boron atom with three valence electrons (v=3). The hydrogen atom contributes one electron (x=1), but two electrons are involved in the B-H bond (y=2), which is *exo* to the cluster. The number of electrons a {BH} vertex donates to cluster bonding (s) is therefore equal to two.

To calculate the overall number of SEPs a species possesses one must take into account both the number of electrons contributed by each vertex and the overall charge of the molecule. For example, each of the twelve boron vertices in $[B_{12}H_{12}]^{2-}$ contributes two electrons to cluster bonding, contributing 24 electrons in total. Additionally, two electrons are available from the negative charge, bringing the total to 26 electrons, or 13 pairs of electrons. As the species has twelve vertices this means that it has n+1 SEPs, classifying the structure as *closo*.

Wade's rules are not limited in their application to boranes, as they are applicable to clusters generally. A wide range of other elements can be incorporated into the cage of boron-based clusters, including transition metals and main group elements such as carbon, nitrogen and phosphorus.[5] Additionally, clusters containing no boron at all have also been observed to obey Wade's rules. For example, $[Pb_{10}]^{2-}$ is a *closo* species with ten vertices and eleven SEPs.[6] This is because each vertex atom has four valence electrons (v=4), no *exo*-polyhedral bonds (x=0) and a single lone pair *exo* to the cluster (y=2), giving a total of two electrons available for cluster bonding (s) per vertex. $[Pb_{10}]^{2-}$ is therefore analogous to $[B_{10}H_{10}]^{2-}$, both of which are *closo* ten vertex species which assume a bicapped square antiprismatic structure, as shown in figure 1.3.1.

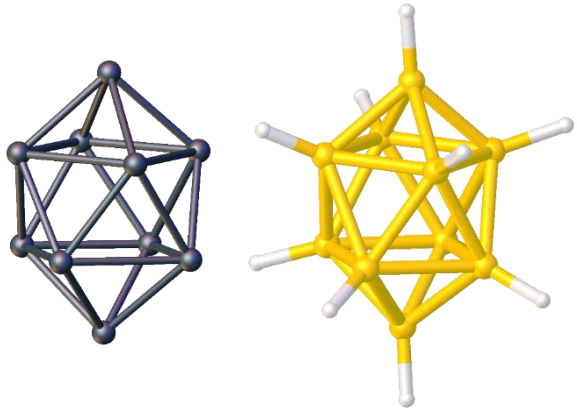

Figure 1.3.1: A comparison of the structures of the ten vertex *closo* species $[Pb_{10}]^{2-}$ and $[B_{10}H_{10}]^{2-}$.

Observations of the molecular structures of boranes and other species which obey Wade's rules allowed Williams to realise that there is a relationship between many of the geometries of *closo*, *nido* and *arachno* species with n, n-1 and n-2 vertices.[7] Successive removal of the most connected vertex from a series of compounds starting with a *closo* species, reveals this relationship. Removal of the most connected vertex from a *closo* species with n vertices affords a *nido* species with n-1 vertices. Subsequent removal of

the most connected vertex in the open face of the resultant *nido* species generates an *arachno* species with n-2 vertices. This relationship is known as the Wade-Williams structural matrix and is displayed in figure 1.3.2.

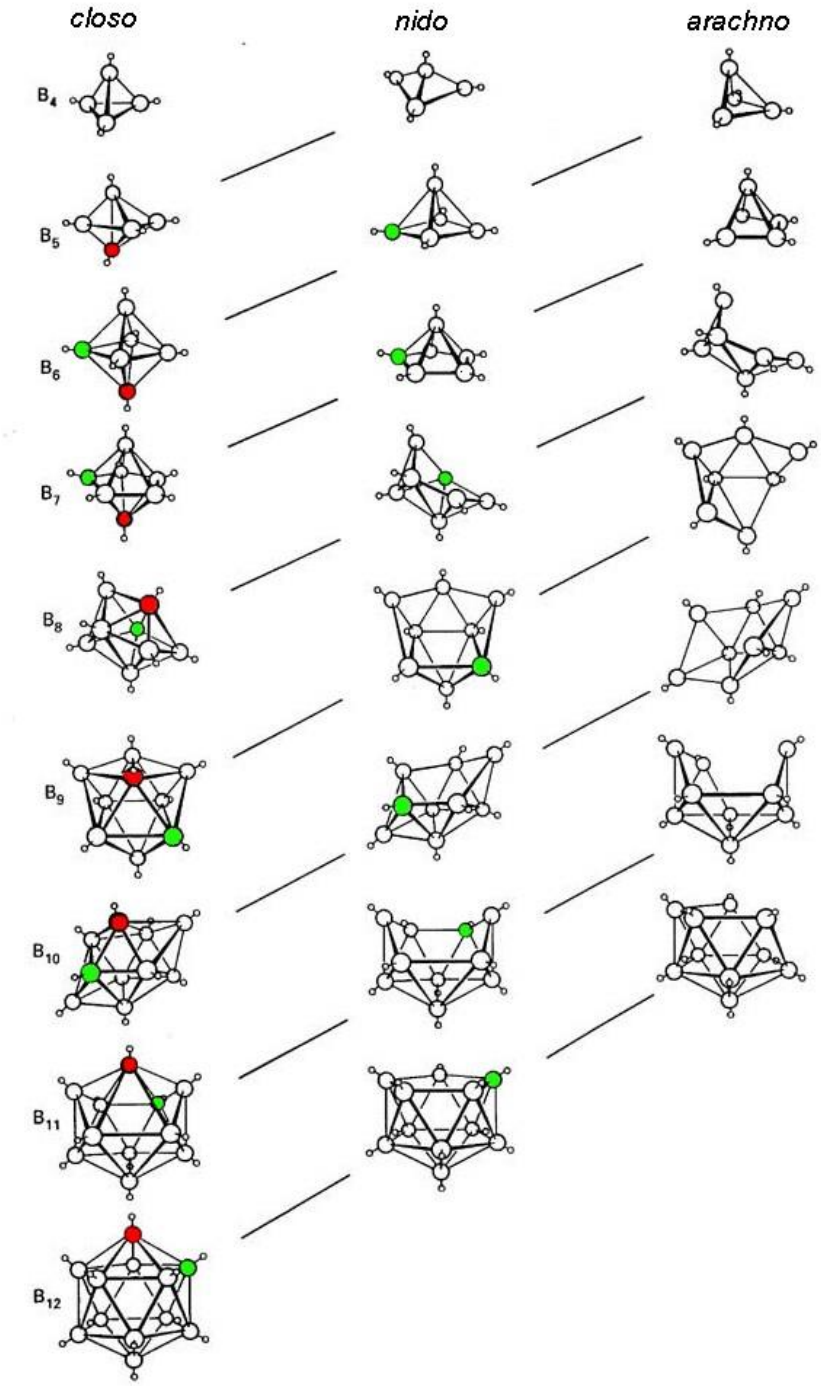

Figure 1.3.2: Wade-Williams matrix, revealing the relationship between *closo*, *nido* and *arachno* species. In each case the first atom to be removed is the most highly connected vertex, coloured red, which affords a *nido* species. The second vertex to be removed is the most highly connected vertex of the open face of the *nido* species, coloured green. This affords an *arachno* species.[7]

However, steric interactions can sometimes mean that boranes and heteroboranes do not assume the geometry predicted by Wade's rules. One such example is the family of species referred to as *pseudocloso*. These are species that have *closo* electron counts but have distorted structures, usually due to steric interactions between bulky functional groups. One example, [9]aneS$_3$-Ru-Ph$_2$C$_2$B$_9$H$_9$, reported by Welch and Weller, is shown in figure 1.3.3, alongside the closely related *closo* species [9]aneS$_3$-Ru-PhC$_2$B$_9$H$_{10}$, shown for comparison.[8] However, it should be noted that electronic effects can also give rise to *pseudocloso* species.[9–11]

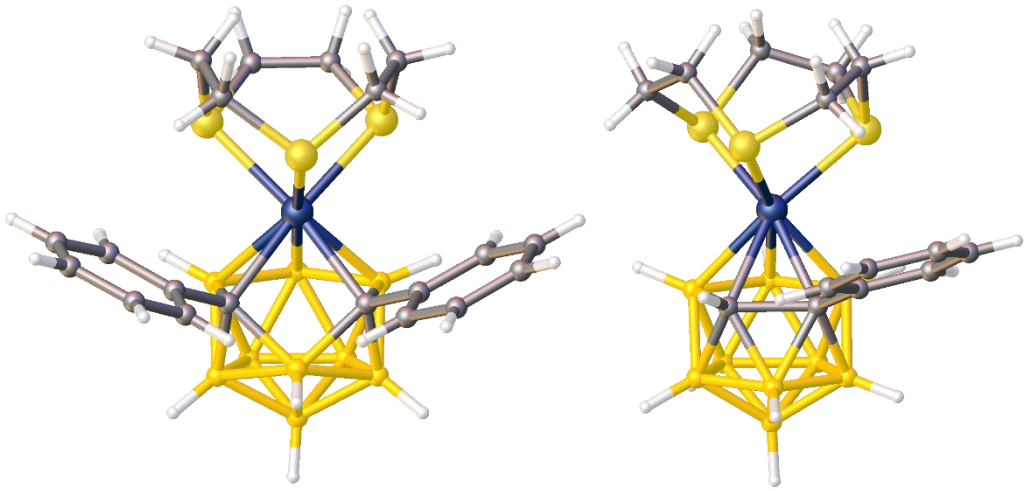

Figure 1.3.3: A comparison of the structures of *pseudocloso* [9]aneS$_3$-RuPh$_2$C$_2$B$_9$H$_9$ and *closo* [9]aneS$_3$-RuPhC$_2$B$_9$H$_{10}$.

The two cage carbon atoms of [9]aneS$_3$-Ru-Ph$_2$C$_2$B$_9$H$_9$ both have bulky phenyl units attached and have therefore separated, distorting the usual icosahedral geometry expected for a 12-vertex species with a *closo* electron account. In contrast, no such distortion occurs in [9]aneS$_3$-Ru-PhC$_2$B$_9$H$_{10}$. This is reflected in the distances between the two cage carbon atoms in the two molecules, 2.504(7) Å and 1.676(7) Å, respectively, a significant lengthening in the case of the former species.[8]

It should be noted that the phenyl units of [9]aneS$_3$-Ru-Ph$_2$C$_2$B$_9$H$_9$ only interact with each other in such a way to force the carbon atoms apart because of the presence of the metal fragment. This is because in the absence of the metal fragment the phenyl groups would align in space to avoid interacting with each other. For example, in the case of Ph$_2$C$_2$B$_{10}$H$_{10}$, shown in figure 1.3.4, the phenyl groups lie parallel to one another to

minimise steric interaction.[12] However, once a bulky metal fragment is inserted into the cage in a position adjacent to both carbon atoms this is no longer possible, as the steric bulk from the ligands force the phenyl units into a position where they clash sterically with each other.

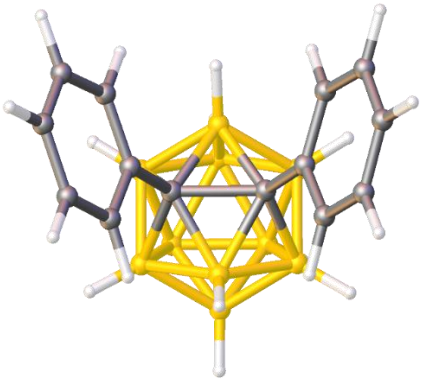

Figure 1.3.4: $Ph_2C_2B_{10}H_{10}$.

1.4 Carboranes

Carboranes are species in which one or more carbon atoms are present within a boron cluster. The bonding in these species can be conceptualised in the same way as that of borane clusters, involving multiple centre bonding and vertices, including carbon atoms, that have more than four connectivities.

Carboranes commonly contain either one or two carbon atoms within the cage, although it is possible to have as many as six carbon atoms present.[13] However, all of the research contained within this thesis concerns carboranes containing two cage carbon atoms, e.g. $C_2B_{10}H_{12}$.

Exchanging a cage boron atom for a carbon atom has effects on the electron counting. For example, both $C_2B_{10}H_{12}$ and $[B_{12}H_{12}]^{2-}$ are regular twelve vertex icosahedra, as both are closo species with n+1 SEPs. In this case the difference is that carbon has one more valence electron than boron, which it donates to cluster bonding, allowing the molecule to achieve a *closo* electron count without being an anion.

Incorporating carbon atoms into the cage also has effects on the reactivity of the boron atoms of the cage. Carbon is more electronegative than boron and so boron vertices in close proximity to carbon atoms become relatively electron poor. The consequences of this include increased susceptibility of boron vertices to nucleophilic attack.[14]

1.4.1 Isomerisation of Carboranes

The carbon atoms in $C_2B_{10}H_{12}$ can assume three different relative positions to give three different isomers. Th

ese are ortho-carborane, where the two carbon atoms are adjacent to each other, meta-carborane, where the two carbon atoms are separated by one boron vertex, and para-carborane, where the carbon atoms are separated by two boron vertices and are therefore directly opposite to each other. Ortho-carborane can be converted to meta-carborane by heating to 450°C,[15] whilst meta-carborane can then be converted to para-carborane by

heating to 600°C using vacuum pyrolysis, as shown in figure 1.4.1.1.[16] The driving force for this isomerisation is the mutual repulsion between the two relatively electronegative (and therefore δ−) carbon vertices.[17]

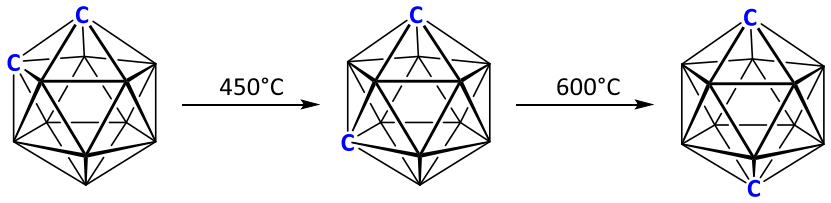

Figure 1.4.1.1: Thermal conversion of different isomers of $C_2B_{10}H_{12}$.

However, the high temperatures required for this process inhibit study of the mechanism of isomerisation. In the absence of direct evidence, two prominent theories have been presented. Lipscomb postulated the diamond-square-diamond (DSD) mechanism which occurs in a diamond consisting of four vertices of a deltahedron.[18] In the DSD process, shown in figure 1.4.1.2, the central connectivity of the diamond elongates and then breaks, to give a square, before a new connectivity is formed perpendicular to the original connectivity, reforming a diamond.

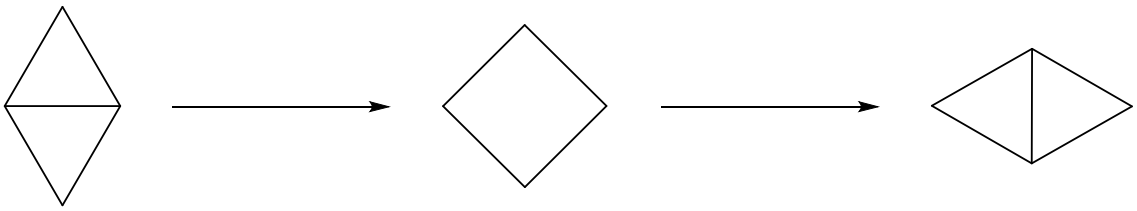

Figure 1.4.1.2: DSD process on one face of a polyhedron.

Lipscomb has utilised the DSD theory to rationalise the isomerisation of ortho to meta-carborane, in which ortho-carborane undergoes a concerted sextuple DSD process, illustrated in figure 1.4.1.3. Firstly, six connectivities break throughout the species, including the carbon-carbon bond, generating a cubeoctahedral species containing six square faces. Next, all six square faces have connectivities reform across them to regenerate an icosahedral species, meta-carborane in this case.[18]

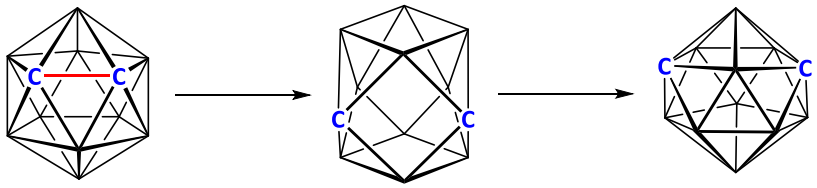

Figure 1.4.1.3: Suggested DSD process for thermal rearrangement of ortho-carborane to meta-carborane.

Isomerisation from meta-carborane to para-carborane cannot be rationalised by a DSD arrangement *via* a cubeoctahedral intermediate. However, work by Wales has been able to rationalise the formation of both meta-carborane and para-carborane *via* a process that consists primarily of sequential DSD transitions through low-symmetry intermediates.[19]

The other dominant theory is triangular face rotation (TFR), also proposed by Lipscomb, in which a single triangular face rotates through 120°.[20] This theory can also be used to conceptualise the conversion of ortho to meta-carborane, as shown in figure 1.4.1.4, as well as the conversion of meta to para-carborane. Additionally, work by McKee has demonstrated that one TFR step can be explained by three consecutive DSD steps.[21]

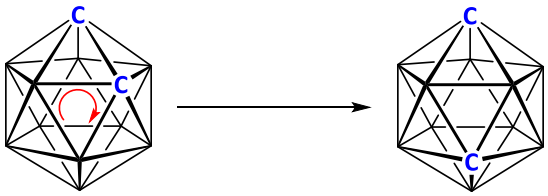

Figure 1.4.1.4: Hypothesised TFR process for thermal rearrangement of ortho-carborane to meta-carborane.

1.4.2 Numbering In Heteroboranes

Carboranes can be numbered, as can metallacarboranes and heteroboranes more generally. IUPAC rules for numbering such species stipulate that numbering is to be based on the highest order symmetry axis of the parent polyhedron. Numbering proceeds in one direction around the symmetry axis with vertices being labelled sequentially. For example, this means that for a species with a bicapped square antiprismatic geometry one

of the two vertices in capping positions must be assigned as vertex one. Once a belt has been completely labelled the positions on the next belt down are then labelled, proceeding in the same direction. However, before numbering can resume a connectivity on the lower belt is crossed without being numbered. An example of this is given in figure 1.4.2.1.

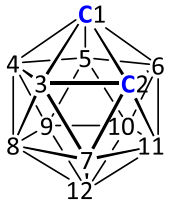

Figure 1.4.2.1: Numbering of vertices in *closo*-1,2-$C_2B_{10}H_{12}$. Note that a connectivity is crossed on the lower belt before vertex seven is labelled.

Elements with higher atomic numbers are given higher priority when it comes to assigning numbers, hence why carbon is assigned as vertex 1 in figure 1.4.2.1. For example, in the case of a heteroborane that incorporated both phosphorus and sulfur into the cage sulfur would be assigned as the highest priority vertex and the cage would be numbered in such a way as to assign to sulfur a lower number than phosphorus. An exception to this rule occurs when assigning numbers to heteroboranes that contain carbon, e.g. metallacarboranes or phosphacarboranes, in which case carbon is given highest priority. This system also means that ortho, meta and para-carborane can be referred to as *closo*-1,2-$C_2B_{10}H_{12}$, *closo*-1,7-$C_2B_{10}H_{12}$ and *closo*-1,12-$C_2B_{10}H_{12}$, respectively.

1.4.3 Synthesis of Carboranes and Functionalisation at Carbon

Ortho-carborane can be synthesised by inserting acetylene into decaborane (the *nido* species $B_{10}H_{14}$) with the assistance of a Lewis base.[22] This reaction can be carried out with a range of functionalised acetylenes to give C-substituted carboranes, as shown in figure 1.4.3.1. However, this process has limitations as it cannot be used to insert either very sterically encumbered acetylenes (e.g. ^{t}BuC≡C^{t}Bu) or acetylenes containing acidic groups (e.g. COOH), as these are incompatible with the decaborane-Lewis base adduct.[23]

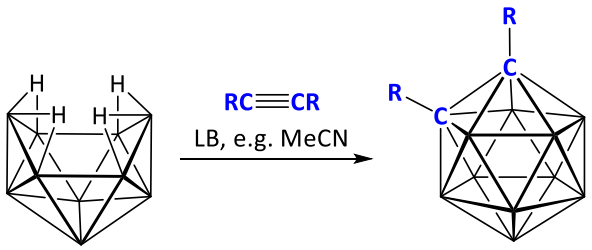

Figure 1.4.3.1: Synthesis of ortho-carborane and C-substituted ortho-carborane derivatives. R = H, alkyl, haloalkyl, aryl, alkenyl and alkynyl.

Alternatively, C-substituted carboranes can be made from unfunctionalised carboranes. The C-H protons of the cage are acidic and can therefore be removed with *n*-BuLi to give $Li_2[C_2B_{10}H_{10}]$. This can then undergo reaction with electrophiles such as alkyl halides to give C-substituted carboranes, as shown in figure 1.4.2.2. However, it should be noted that this reaction only works for primary alkyl halides. Additionally, $Li_2[C_2B_{10}H_{10}]$ can be used to generate carboranes with heteroatoms attached to the cage carbon atoms, including phosphorus, silicon and boron, as shown in figure 1.4.3.2.[24]

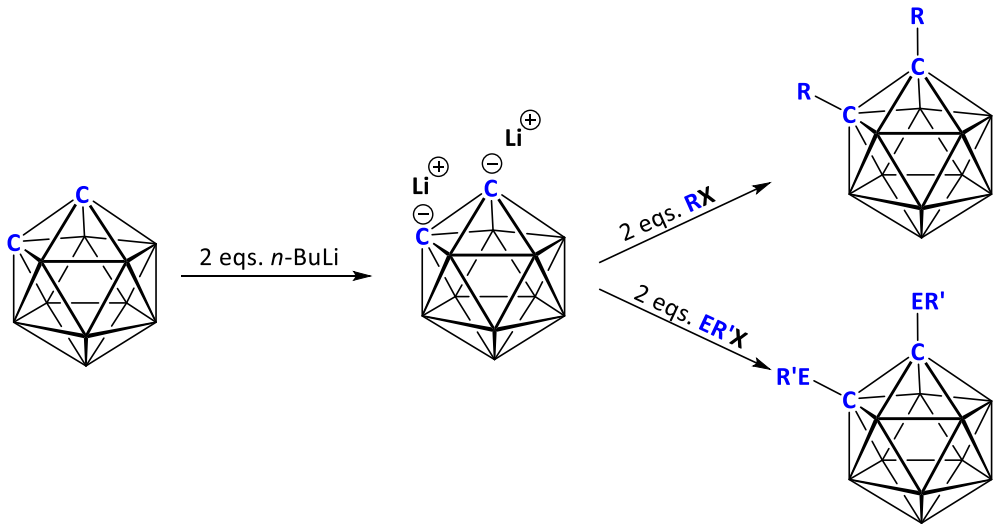

Figure 1.4.3.2: Functionalisation of ortho-carborane at carbon atoms. R = primary alkyl group, ER′ = a heteroatom with appropriate functional groups, e.g. a PPh_2 unit, and X = a halogen or other appropriate leaving group.

1.5 Decapitation and Reduction

Decapitation is the process where a boron vertex is removed from a *closo* caborane. For example, decapitation can be carried out on *closo*-1,2-$C_2B_{10}H_{12}$.[14] In this case, the two boron vertices adjacent to the two carbon vertices are both susceptible to nucleophilic attack due to the electronegative pull of the two carbon atoms. It should be noted that both boron vertices adjacent to the carbon atoms are equivalent as the molecule has C_{2v} symmetry. Therefore, upon exposure to a nucleophile, such as $[EtO]^-$, one of these two boron vertices will undergo nucleophilic attack and be removed from the cage as a boric ester, e.g. $B(OEt)_3$. This gives rise to [*nido*-7,8-$C_2B_9H_{12}]^-$, a species with an *endo* proton which can be removed with strong bases such as *n*-BuLi to give [*nido*-7,8-$C_2B_9H_{11}]^{2-}$. This process is shown in figure 1.5.1.

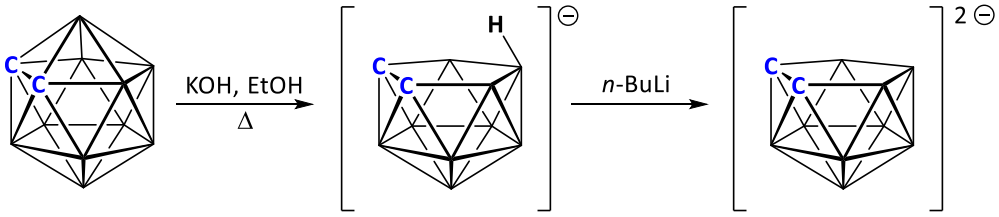

Figure 1.5.1: Decapitation of *closo*-1,2-$C_2B_{10}H_{12}$ followed by subsequent removal of the *endo* proton to form [*nido*-7,8-$C_2B_9H_{11}]^{2-}$.

Carboranes other than *closo*-1,2-$C_2B_{10}H_{12}$ can also be decapitated, with decapitation being made more difficult by both steric crowding of the most electron poor boron vertex and by electron donating groups reducing the electrophilicity of the cage boron atoms. Conversely, carboranes containing electron withdrawing groups undergo decapitation more easily.

The structure of the *nido* species formed depends on the location of the carbon atoms within the *closo* species that is to be decapitated. If *closo*-1,2-$C_2B_{10}H_{12}$ is decapitated and then deprotonated it will produce [*nido*-7,8-$C_2B_9H_{11}]^{2-}$. If instead *closo*-1,7-$C_2B_{10}H_{12}$ or *closo*-1,12-$C_2B_{10}H_{12}$ are chosen they will produce [*nido*-7,9-$C_2B_9H_{11}]^{2-}$ and [*nido*-2,9-$C_2B_9H_{11}]^{2-}$ respectively, as shown in figure 1.5.2.

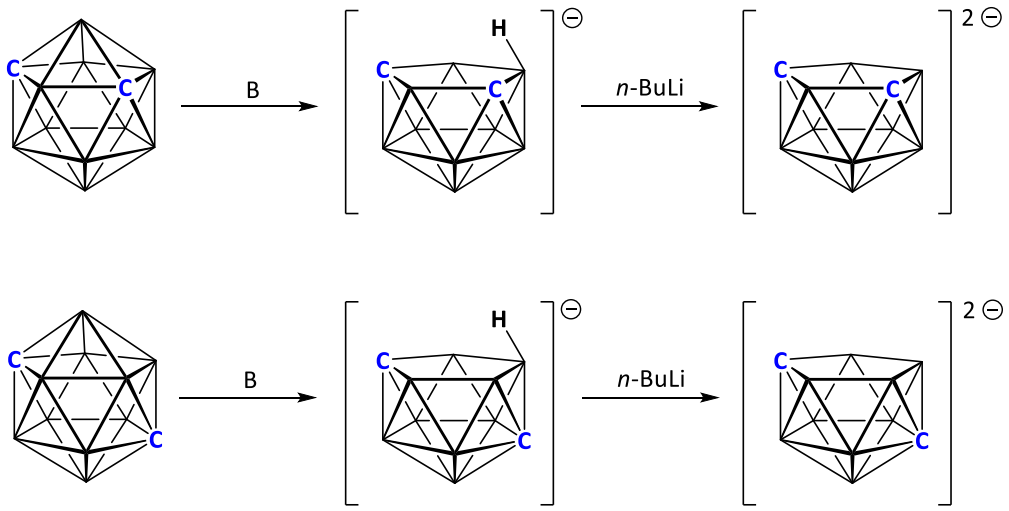

Figure 1.5.2: Decapitation and subsequent deprotonation of *closo*-1,7-$C_2B_{10}H_{12}$ and *closo*-1,12-$C_2B_{10}H_{12}$, shown with generic base, B.

Alternatively, a *nido* dianion can be made simply by a two electron reduction of the analogous *closo* species.[25] This is commonly done using sodium naphthalenide. For example, the reaction of *closo*-1,2-$C_2B_{10}H_{12}$ and two equivalents of sodium naphthalenide in THF produces Na_2[*nido*-7,9-$C_2B_{10}H_{12}$], as shown in figure 1.5.3.

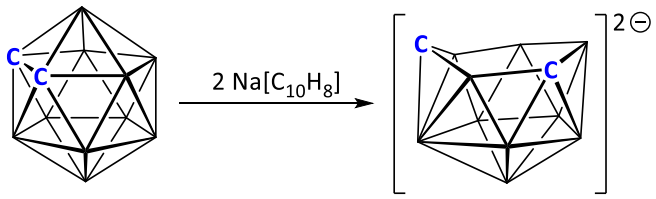

Figure 1.5.3: Two electron reduction of *closo*-1,2-$C_2B_{10}H_{12}$ to form Na_2[*nido*-7,9-$C_2B_{10}H_{12}$].

Regardless of synthetic route, *nido* dianions have an 'open face' which can be capped by an appropriate reagent, incorporating a new atom into the cage as a vertex. For this purpose main group elements such as phosphorus or boron can be incorporated.[5] Alternatively this procedure can be used to incorporate transition metals into the cage of a carborane. The general procedure for this is shown in figure 1.5.4 using [7,8-R_2-*nido*-7,8-$C_2B_9H_9$]$^{2-}$ as an example.

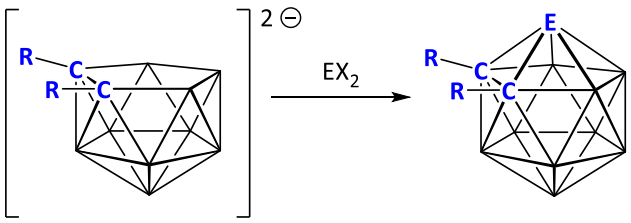

Figure 1.5.4: Capitation of open face of [7,8-R_2-*nido*-7,8-$C_2B_9H_9$]$^{2-}$ with generic element E.

1.6 Metallacarboranes

Metallacaboranes can be considered as either species in which one or more transition metal atoms have been incorporated as vertices in the cage of a carborane or as transition metal complexes containing a carborane ligand. In this respect, a carboranyl $[C_2B_9H_{11}]^{2-}$ anion is conceptually similar to the cyclopentadienide $[C_5H_5]^-$ anion, an observation first made by Hawthorne. A comparison of the non-symmetry adapted frontier orbitals of [*nido*-7,8-$C_2B_9H_{11}]^{2-}$ and $[C_5H_5]^-$ is shown in figure 1.6.1.[26] It should be noted however that in the case of $[C_5H_5]^-$ the orbitals are perpendicular to the ring where as in [*nido*-$C_2B_9H_{11}]^{2-}$ the orbitals are orientated towards the point in space which would be occupied by a vertex in an analogous twelve vertex *closo* species such as $C_2B_{10}H_{12}$.

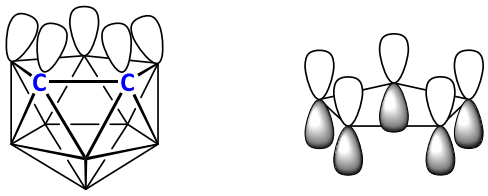

Figure 1.6.1: A comparison between the non-symmetry adapted frontier orbitals of [*nido*-$C_2B_9H_{11}]^{2-}$ and $[C_5H_5]^-$.

The first metallacarborane, $[(C_2B_9H_{11})_2Fe]^{2-}$, reported by Hawthorne, is a species that is frequently compared to ferrocene (Cp_2Fe) as the two have obvious structural similarities.[26] The synthesis of $[(C_2B_9H_{11})_2Fe]^{2-}$ is shown in figure 1.6.2. In addition to this, other carborane-metal-carborane 'sandwich' compounds can be formed, including $[(C_2B_9H_{11})_2Co]^-$, commonly known as 'CoSAN' ('Cobalt Sandwich'), one of the most studied metallacarboranes in the literature.[27] The notation used for metallacarboranes containing more than one cage differentiates between said cages by assigning all of the atoms of one cage a prime symbol (′). For example, the full systematic formula for FeSAN is $(C_2B_9H_{11})Fe(C'_2B'_9H'_{11})$.

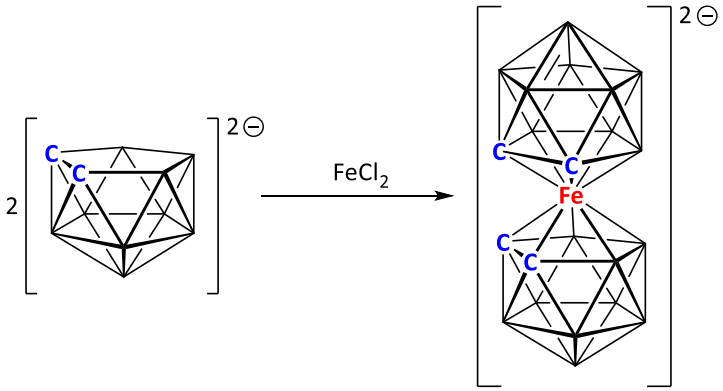

Figure 1.6.2: Synthesis of $[(C_2B_9H_{11})_2Fe]^-$.

Alternatively, metallacarboranes can be synthesised that consist of one cage containing a metal which has ligands bound to it *exo* to the cluster. This is commonly done by reacting a *nido* carborane of general formula $[R_2C_2B_nH_n]^{2-}$ with a source of a metal fragment, often supplying the metal fragment as a cation or a dication to give a monoanionic or neutral metallacarborane, respectively. In such situations the metal fragment is said to cap the open face of the *nido* carborane. For example, $[nido\text{-}7,8\text{-}C_2B_9H_{11}]^{2-}$ can react with an appropriate source of a metal fragment of the general formula $\{ML_n\}$ to give a twelve vertex metallacarborane of formula $L_nMC_2B_9H_{11}$.

The number of electrons a metal fragment donates to cluster bonding varies and depends on both the metal valence electron count and the number of electrons donated by any ligands bound to the metal. Most commonly, the number of electrons donated by the metal fragment to cluster bonding (s) is equal to the number of valence electrons possessed by the metal atom (v) plus the number of electrons provided by any *exo*-polyhedral ligands (x) minus twelve. Of these twelve electrons unavailable for cluster bonding six are involved in *exo*-polyhedral bonding to ligands and an additional six are located in non-bonding orbitals.

$$s = v + x - 12$$

s = no. of electrons available for cluster bonding.

v = no. of valence electrons possessed by vertex atom.

x = no. of electrons provided by any *exo*-polyhedral substituents bound to vertex.

12 = no. of electrons involved in both *exo*-polyhedral bonds (six in total) and non-bonding orbitals (six in total).

Metal fragments can be classified as either three-electron, two-electron, one-electron or zero-electron fragments. For example, in the case of $\{Fe(CO)_3\}$ being incorporated into a carborane, the number of electrons donated to cluster bonding (s) is equal to two, as iron has eight valence electrons (v=8) and the three carbonyl ligands each provide two electrons (x=6). Therefore, $\{Fe(CO)_3\}$ is a one-vertex, two-electron fragment. This is supported by experimental evidence, as a wide range of metallacarboranes and metallaboranes containing the $\{Fe(CO)_3\}$ fragment have identical charges and geometries to analogous carboranes and boranes with the same number of vertices.

Metallacaboranes undergo thermal rearrangement at lower temperatures than comparable carboranes do, which often need to be heated to several hundred degrees centigrade in order to isomerise. In contrast, many metallacarboranes, especially those which are sterically crowded, have proved able to isomerise at room temperature.

1.7 Applications of Carboranes and Metallacarboranes

Carboranes and metallacarboranes have been the subject of research for applications in fields as diverse as medicine, organic chemistry, materials, electronic devices and the separation and storage of gas molecules within metal-organic-frameworks. For a more expansive discussion of the applications of carboranes than is contained within this chapter, see work by Grimes.[28,29]

The medicinal uses of carboranes include their incorporation into drug molecules. Carboranes have properties that are desirable within this field, such as their low toxicity and lipophilic character. Their lipophilicity arises from the hydridic nature of their B-H bonds and can be useful in certain contexts within drug delivery, such as allowing them to occupy hydrophobic pockets within proteins.[30]

Another prominent medicinal use of carboranes in boron neutron capture therapy (BNCT), which has been one of the dominant areas of research into medicinal applications of carboranes for some time now. This technique utilises the capacity of the nonradioactive ^{10}B isotope, which accounts for 20% of naturally occurring boron, to absorb low energy thermal neutrons. Upon absorption of a neutron the ^{10}B nucleus becomes a metastable $^{11}B^{*}$ nucleus that then undergoes nuclear fission to produce a ^{7}Li nucleus and a high energy alpha particle, as shown in figure 1.7.1.[31] The alpha particles generated have a kinetic energy (E_k) of between 2.31 and 2.79 MeV, which results in the alpha particles having a path length of between 5 and 9 μm, which is approximately the diameter of one cell.[29] This therefore contains the destructive alpha particles within the target cell. The implications of this are that if cancerous cells can be enriched with a boron containing molecule then they can be selectively targeted and destroyed by this technique. Carboranes are ideal for this application as they are both very boron-dense and non-toxic.

Figure 1.7.1: The capture of a low energy neutron by ^{10}B leads to the formation of meta-stable $^{11}B^{*}$, which rapidly decays to release an alpha particle with significant E_k.

Carboranes have also found applications within organic chemistry. Derivatives of [*closo*-$CB_{11}H_{12}]^-$ have been used to isolate highly reactive cations such as R_3Si^+. This is made possible by the fact that such carboranes have very low nucleophilicity and are extremely weakly coordinating due to the negative charge being delocalised over the 3D aromatic system of the carborane. This also means that compounds based around derivatives of $[CB_{11}H_{12}]^-$ have been found to behave as extremely strong acids, such as $H[CHB_{11}F_{11}]$, which was the strongest Brønsted acid known at the time of its discovery in 2014 by Reed and co-workers. This acid displays the remarkable ability to protonate hydrocarbons such as benzene and tertiarybutane at room temperature.[32]

Carboranes and metallacarboranes have been the subject of intense investigation into their application as catalysts in the production of organic molecules. One such example is the catalytic system developed by Lyubimov and co-workers for hydrogenation of prochiral olefins. This system utilises $[Rh(COD)_2]BF_4$ and an aryl phosphite connected to a carborane, an example of which is given in figure 1.7.2. This system is able to achieve up to 99.5% enantiomeric excess.[33]

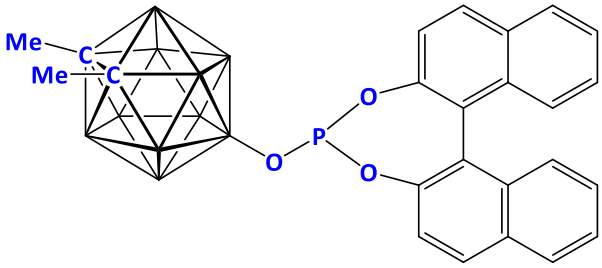

Figure 1.7.2: 9-$OPO_2C_{20}H_{12}$-1,2-Me_2-*closo*-1,2-$C_2B_{10}H_9$.

1.8 Methods of Distinguishing Between Boron and Carbon Atoms in Crystal Structures

Boron and carbon are periodically adjacent. This gives them very similar X-ray scattering powers, meaning that distinguishing between cage boron and cage carbon atoms within the crystal structures of carboranes and metallacarboranes can be difficult. This problem does not arise if either category of vertex has an *exo*-polyhedral substituent other than hydrogen, which functions as an effective label. However, this is not always possible.

Welch and co-workers developed the vertex-to-centroid-distance (VCD) method to distinguish between cage boron and cage carbon atoms.[34,35] This method is predicated on the fact that carbon has a smaller atomic radius than boron, due to the additional nuclear charge. During refinement all vertices are labelled as boron atoms and the distance between the centroid of the cluster and each vertex is measured. As carbon has a smaller radius than boron this means that the carbon vertices will appear closer to the centroid than the boron vertices, allowing differentiation between the two. The VCD method is applicable to *closo* carboranes, *nido* carboranes and heterocarboranes.

Another method of differentiating between cage boron and cage carbon atoms is the boron-hydrogen-distance (BHD) method, also developed by Welch and co-workers.[35,36] This process is similar to the VCD method as it relies on assigning all vertices as boron atoms during refinement. This will leave the carbon atoms as having been modelled with less electron density than they actually possess, which results in the hydrogen atom moving closer to the vertex to compensate for this. This means that carbon vertices can be identified by unusually short vertex-hydrogen distances.

1.9 "Non-Wadian" Boranes and Heteroboranes

As previously noted, Wade's rules define a *closo* species as having n vertices and n+1 SEPs. However, what happens if a borane or heteroborane has fewer than the n+1 SEPs required to form a *closo* species? Such species are referred to as "non-Wadian" as they fall outside of the range of species conventionally covered in discussions of Wade's rules. Whilst species with fewer than n+1 SEPs are referred to as non-Wadian, species that have n vertices and n SEPs are specifically referred to as *hypercloso* species. Despite non-Wadian species being reported as early as 1975, there exists a relatively small number of non-Wadian species in the literature, many of which were synthesised serendipitously. The aim of this project is to develop deliberate and systematic routes to non-Wadian metallacarboranes.

1.9.1 Geometries and Structural Properties of *Hypercloso* Species

Hypercloso species usually do not have the same geometry as analogous *closo* species but instead adopt structures related to the structure of the *closo* species by a single DSD transition. An example is given in figure 1.9.1.1, of 2,6-Cp_2-*closo*-2,6,1,10-$Co_2C_2B_6H_8$ and *hypercloso* $(CpFe)_2C_2B_6H_8$, which are related by a DSD rearrangement of the 2-6-10-9 diamond of the former polyhedron.[37,38] Such *hypercloso* species often have one or more unusually highly connected vertex, often a metal atom. In the case of $(CpFe)_2C_2B_6H_8$ one Fe atom is a highly connected degree six vertex (meaning that it has six connectivities to other vertices in the cage).

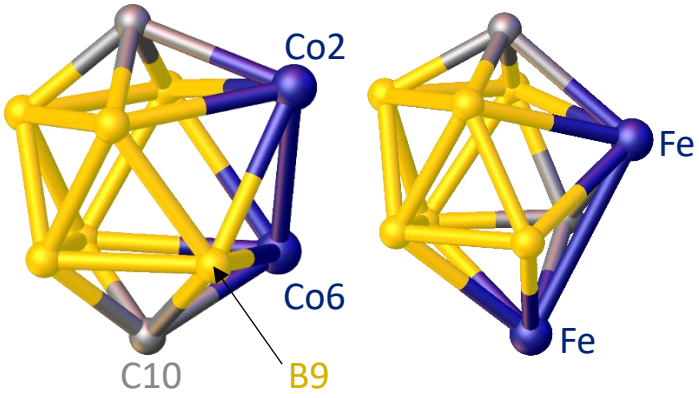

Figure 1.9.1.1: *Closo* $(CpCo)_2C_2B_6H_8$ (left) and *hypercloso* $(CpFe)_2C_2B_6H_8$ (right) (Cp groups omitted for clarity).

Additionally, non-Wadian species often have fewer degrees of symmetry than Wadian species. This can result in difficulties numbering the vertices of non-Wadian species, as the rules used for Wadian species cannot be applied and no alternative set of rules is yet established, a consequence of the fact that this area of research is still underdeveloped.

A number of twelve vertex *hypercloso* species are also known within the literature, many of which display traits characteristic of *hypercloso* species. For example, $[(PEt_3)_2Pt(CO)_2W(Me_2C_2B_9H_8CH_2C_6H_4Me)]$, shown in figure 1.9.1.2, adopts a geometry related to that of a twelve vertex *closo* species by a single DSD transition. Additionally, this species also has an unusually highly connected vertex, occupied by a degree six tungsten atom.[39,40]

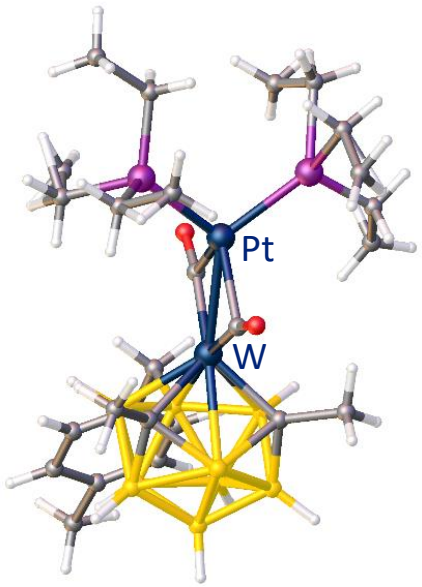

Figure 1.9.1.2: *Hypercloso* $[(PEt_3)_2Pt(CO)_2W(Me_2C_2B_9H_8CH_2C_6H_4Me)]$.

Unlike Wadian species, it is not possible to easily predict what geometry a *hypercloso* species will assume and so this information must be derived from X-ray crystallography. Figure 1.9.1.3 contains a comparison of the geometries of three twelve vertex species, one *closo*, $[B_{12}H_{12}]^{2-}$,[41] and two *hypercloso* species, $B_{12}O_{12}(CH_2Ph)_{12}$[42] and $(Cp^*Rh)_2B_{10}H_8(OH)_2$.[43] The two *hypercloso* species have different geometries, despite both being twelve vertex *hypercloso* species. The former has a distorted icosahedral structure closely related to the icosahedron assumed by the *closo* species but with distortions in the lengths of and angles between the B-B connectivities. The latter species has undergone a DSD transition and so has a totally different, novel and yet unnamed geometry.

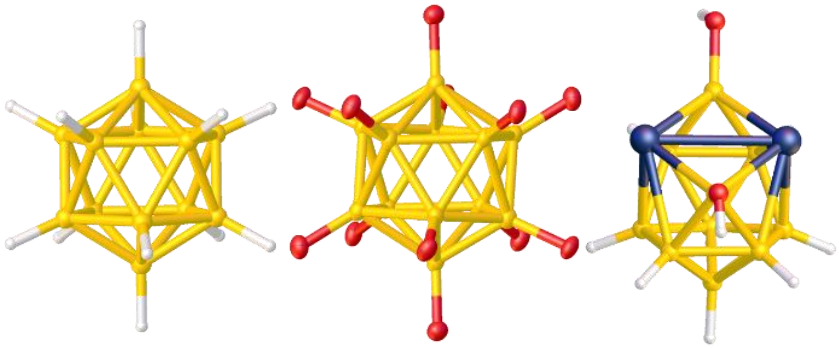

Figure 1.9.1.3: *Closo* $[B_{12}H_{12}]^{2-}$, *hypercloso* $B_{12}O_{12}(CH_2Ph)_{12}$ and *hypercloso* $(Cp^*Rh)_2B_{10}H_8(OH)_2$, (Bz and Cp* groups omitted for clarity).

The distorted icosahedral geometry of $B_{12}O_{12}(CH_2Ph)_{12}$ results in an unusually wide range of B-B distances as compared to an analogous *closo* species, as demonstrated in table 1.9.1.4, a comparison of $B_{12}O_{12}(CH_2Ph)_{12}$ and $[B_{12}H_{12}]^{2-}$, the latter of which has B-B connectivity lengths typical of those in a twelve vertex *closo* borane. Several *hypercloso* boranes, of general formula $B_{12}R_{12}/B_{12}X_{12}$ (where R=O-alkyl, O-benzyl and derivatives thereof and X=a halogen), are reported in the literature all of which display the same distorted icosahedral geometry as $B_{12}O_{12}(CH_2Ph)_{12}$.[42,44]

Species	Range of B-B connectivity lengths (Å)
[*closo*-$B_{12}H_{12}]^{2-}$	1.7804(6)-1.7910(6)
hypercloso-$B_{12}O_{12}(CH_2Ph)_{12}$	1.755(2)-1.918(2)

Table 1.9.1.4: A comparison of the B-B connectivity lengths in $[B_{12}H_{12}]^{2-}$ and $B_{12}O_{12}(CH_2Ph)_{12}$.[41,42]

As a result of the general observation that it is not possible to predict the geometries of non-Wadian species, postulated non-Wadian species are best represented graphically in a format that does not specify geometry. An illustration of this for generic non-Wadian species $LMR_2C_2B_nH_n$ is given in figure 1.9.1.5.

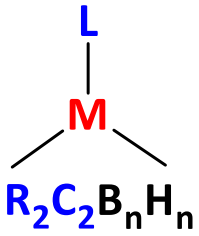

Figure 1.9.1.5: Generic non-Wadian species $LMR_2C_2B_nH_n$.

A notable exception to the general observation that *hypercloso* species assume different geometries to their *closo* analogues exists for thirteen vertex species. In this case both *hypercloso* and *closo* species assume a docosahedral geometry. This is because the thirteen vertex parent polyhedron (the docosahedron) has non-degenerate frontier orbitals and hence does not change shape if only n SEPs are present.[45] An example of this phenomenon is given in figure 1.9.1.6, a comparison between *closo* 4,5-(*p*-cymene)$_2$-4,5,2,3-$Ru_2C_2B_9H_{11}$ and *hypercloso* 4,5-Cp*$_2$-4,5,2,3-$Ru_2C_2B_9H_{11}$.[46,47]

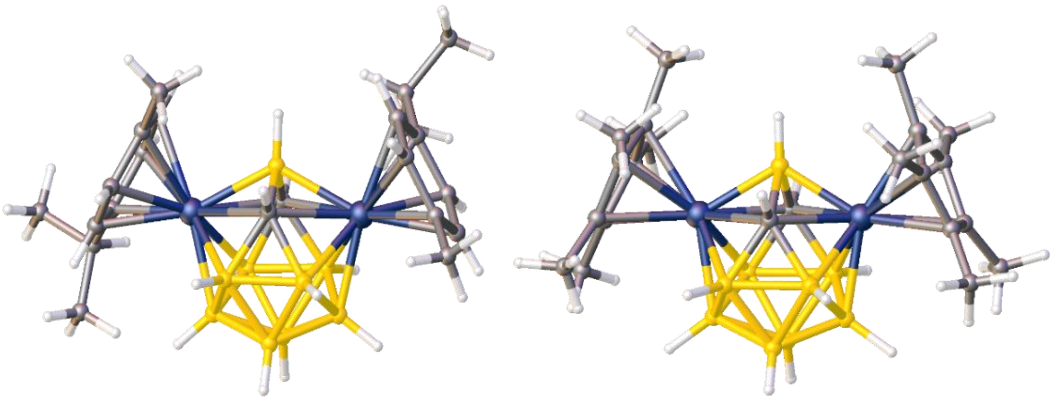

Figure 1.9.1.6: *Closo* 4,5-(*p*-cymene)$_2$-4,5,2,3-$Ru_2C_2B_9H_{11}$ (left) and *Hypercloso* 4,5-Cp*$_2$-4,5,2,3-$Ru_2C_2B_9H_{11}$ (right).

1.9.2 Conversion of *Hypercloso* to *Closo* Species

Evidence exists within the literature that *hypercloso* species can undergo two electron reductions and in the process assume both a *closo* electron count and geometry, just as heteroboranes with Wadian electron counts can interconvert between categories such as *closo* and *nido* upon addition of two electrons. The first reported example of this process is the reversible two electron reduction of *hypercloso* 1-C_6Me_6-1-RuB_9H_9 to *closo* [1-C_6Me_6-1-RuB_9H_9]$^{2-}$, shown in figure 1.9.2.1, reported by Spencer and co-workers. Interestingly, the resultant *closo* species is highly air-sensitive and is readily oxidised by air to reform the *hypercloso* species.[48]

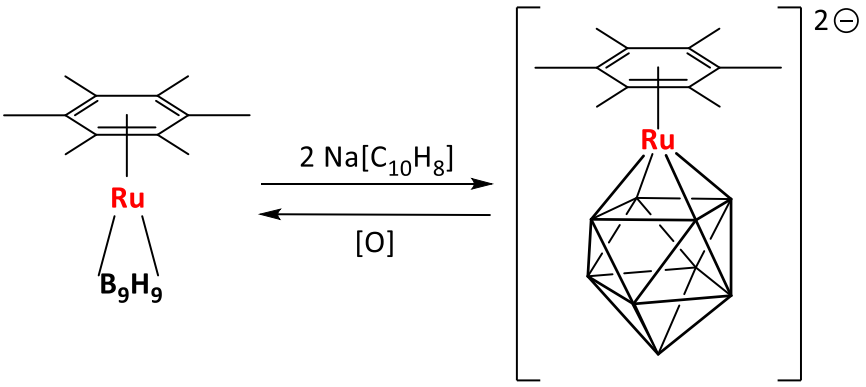

Figure 1.9.2.1: Reversible two electron reduction of *hypercloso* 1-C_6Me_6-1-RuB_9H_9 to *closo* [1-C_6Me_6-1-RuB_9H_9]$^{2-}$.

Additionally, evidence exists within the literature that *hypercloso* metallacarboranes can also be converted to *closo* species *via* addition of an L type ligand, which provides two additional electrons to the metal, thereby increasing the number of electrons available for cluster bonding by two. Work by Stone and co-workers has demonstrated that the *hypercloso* species [$(PEt_3)_2Pt(\mu\text{-}CO)_2W(Me_2C_2B_9H_8CH_2C_6H_4Me)$] can be converted to the *closo* species [$(PEt_3)_2Pt(CO)_2(PMe_3)W(Me_2C_2B_9H_8CH_2C_6H_4Me)$] *via* ligand addition, as shown in figure 1.9.2.2.[39]

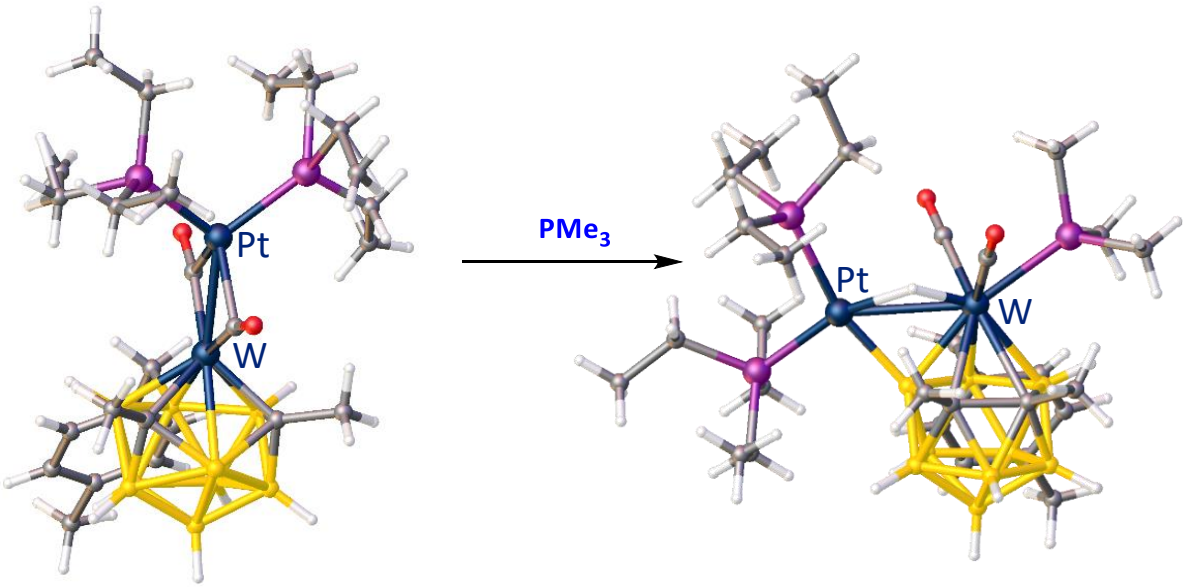

Figure 1.9.2.2: Conversion of *hypercloso* $[(PEt_3)_2Pt(\mu\text{-}CO)_2W(Me_2C_2B_9H_8CH_2C_6H_4Me)]$ to *closo* $[(PEt_3)_2Pt(CO)_2(PMe_3)W(Me_2C_2B_9H_8CH_2C_6H_4Me)]$ *via* addition of a two electron donating L type ligand, PMe_3.

1.9.3 NMR Spectroscopic Properties of Non-Wadian Species

Non-Wadian species frequently produce ^{11}B NMR spectra with unusual properties not typically found in Wadian heteroboranes, including unusually high frequency shifts and unusually wide ranges of shifts. One such species is $[2,7\text{-}Cp^*_2\text{-}2,7,1,12\text{-}Ru_2C_2B_{10}H_{12}]$, reported by Welch and co-workers, the $^{11}B\{^1H\}$ NMR spectrum of which is shown in figure 1.9.3.1. The spectrum displays both two unusually high frequency shifts, at 58.4 ppm and 54.1 ppm, as well as an unusually wide range of shifts, from 58.4 to -22.9 ppm.[49]

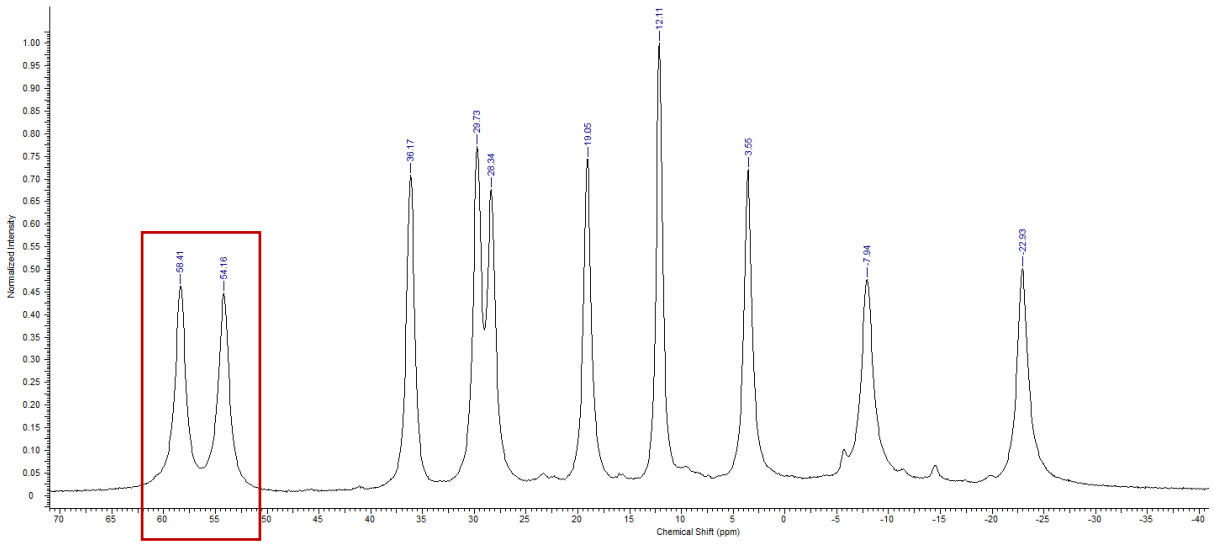

Figure 1.9.3.1: $^{11}B\{^1H\}$ NMR spectrum of $[2,7\text{-}Cp^*_2\text{-}2,7,1,12\text{-}Ru_2C_2B_{10}H_{12}]$.

1.9.4 Existing Crystallographically Determined Twelve Vertex *Hypercloso* Boranes and Heteroboranes

As previously noted, there exists a relatively small number of "non-Wadian" species within the scientific literature. The underdevelopment of this area of chemistry is reflected in the fact that, despite *hypercloso* boron based clusters being reported as early as 1975,[37] there exists a very limited number of crystallographically determined *hypercloso* twelve vertex species within the literature. This is in contrast with the enormous number of Wadian twelve vertex boranes and heteroboranes reported. A summary of all of the crystallographically determined *hypercloso* boranes and heteroboranes known is provided in figures 1.9.4.1 to 1.9.4.6. Note that where a family of species with highly similar structures exists, e.g. $(Cp^*Rh)_2B_{10}H_{10-n}(OH)_n$ (where n=0, 1 or 2), a single representative example is given within the figure (figure 1.9.4.1 in this case).

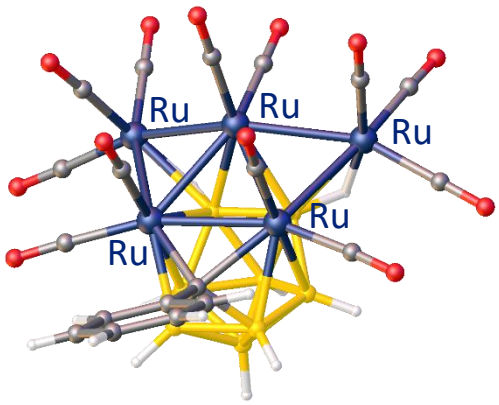

Figure 1.9.4.1: Stone reports four related twelve-vertex *hypercloso* 'raft' species, of which a representative example is shown here, [2,3,7-{$Ru(CO)_3$}-3,4,8-{$Ru(CO)_3$}-7,8-(μ-H)$_2$-1-Ph-2,2,3,3,4,4-$(CO)_6$-*hypercloso*-2,3,4,1-$Ru_3CB_8H_6$]$^-$ (numbered as in publication). The author uses the term 'raft' to refer to the collection of metal atoms, two of which lie *exo* to the cage in this case.[50]

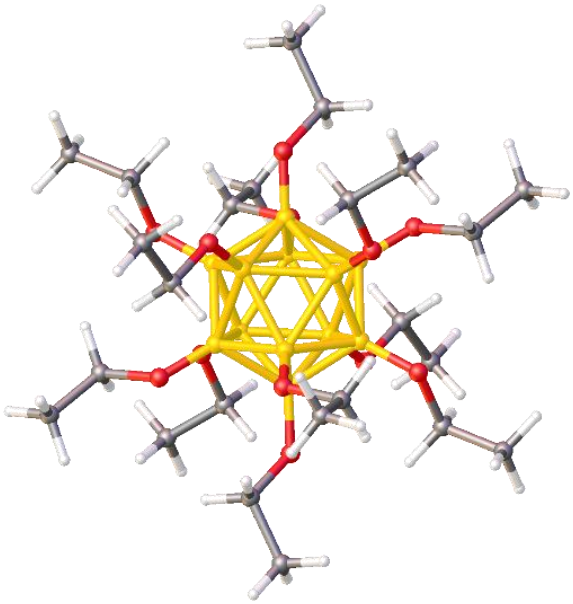

Figure 1.9.4.2, $B_{12}(OEt)_{12}$: Several *hypercloso* twelve vertex boranes are reported in the literature, of general formula $B_{12}R_{12}$, where R can be O-alkyl, O-benzyl and derivatives there of (e.g. $OCH_2C_6H_4F$). Additionally a number of $B_{12}X_{12}$ species are reported where X=a halogen. All of these species have the same distorted icosahedral geometry,[42,44] as discussed in section 1.9.1.

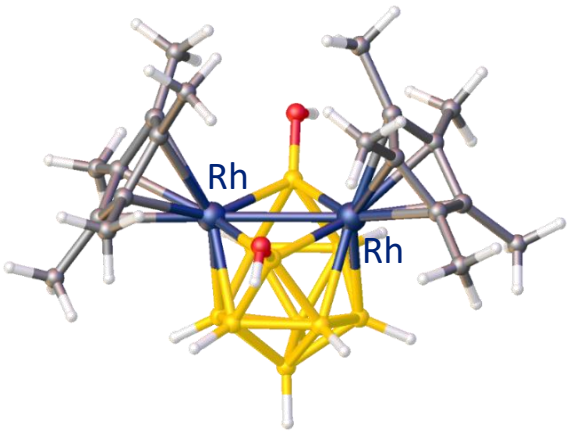

Figure 1.9.4.3: $(Cp^*Rh)_2B_{10}H_8(OH)_2$. Ghosh and co-workers report three *hypercloso* species of general formula $(Cp^*Rh)_2B_{10}H_{10-n}(OH)_n$, where n=0, 1 or 2.[43]

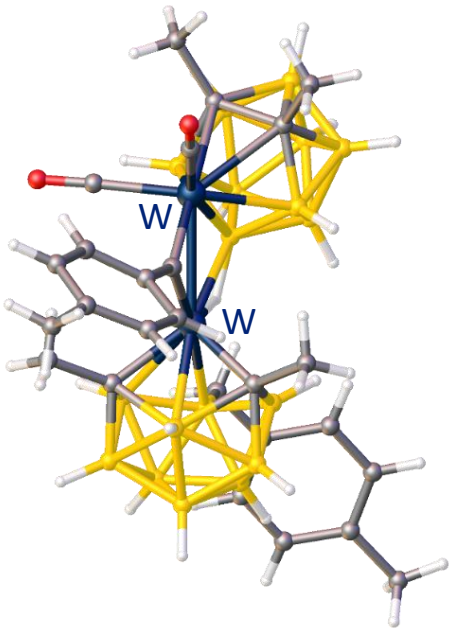

Figure 1.9.4.4: $[W_2(\mu\text{-}CC_6H_4Me\text{-}4)(CO)_2(7,8\text{-}Me_2\text{-}7,8\text{-}C_2B_9H_9)(7,8\text{-}Me_2\text{-}7,8\text{-}C_2B_9H_9\text{-}10\text{-}(CH_2C_6H_4Me\text{-}4)]^-$ (numbered as in publication), reported by Stone. Only one of the cages (positioned below) is *hypercloso*.[51]

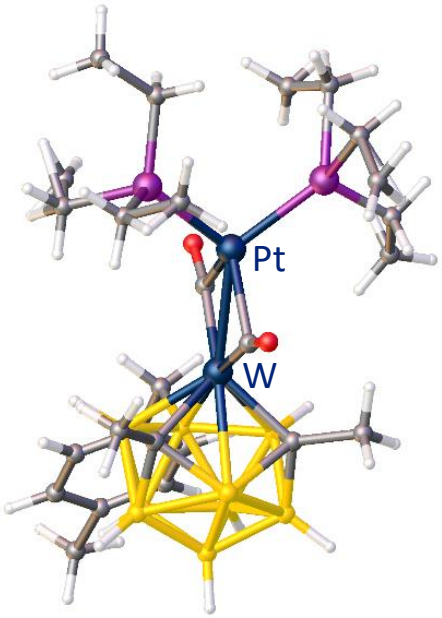

Figure 1.9.4.5: $(PEt_3)_2Pt(CO)_2W(Me_2C_2B_9H_8CH_2C_6H_4Me)$, reported by Stone.[39,40]

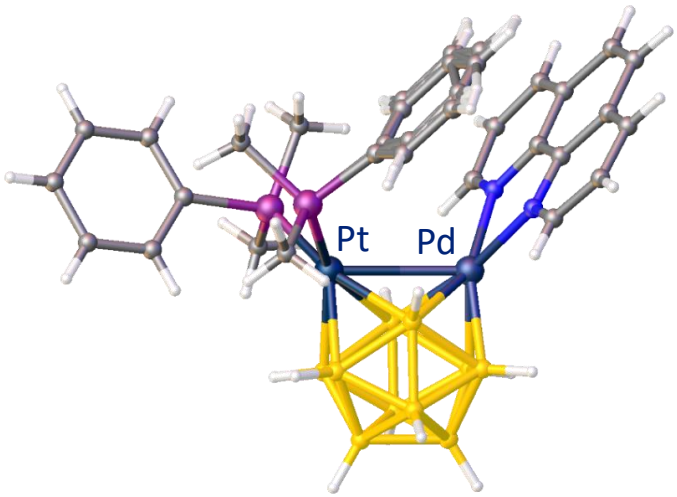

Figure 1.9.4.6: $(PMe_2Ph)_2PtPd(phen)B_{10}H_{10}$, reported by Kennedy.[52]

1.10 Synthetic Routes to *Hypercloso* Boranes and Heteroboranes

There are several routes to non-Wadian species found within the literature. However, as noted previously many of these species have been generated serendipitously and their synthesis often reflects this. One such example is the family of six related *hypercloso* rhodaboranes reported by Ghosh and co-workers, synthesised by the thermolysis of $[Cp^*RhCl_2]_2$, $[LiBH_4{\cdot}THF]$ and $[BH_3{\cdot}THF]$ in toluene at 105 °C for five days. This created a complex product mixture from which a number of species were isolated. Three examples of this family, ten vertex $[(Cp^*Rh)_4B_6H_6]$, fifteen vertex $[(Cp^*Rh)_2B_{13}H_{13}]$ and sixteen vertex $[(Cp^*Rh)_3B_{12}H_{12}Rh\{Cp^*RhB_4H_9\}]$, are provided in figure 1.10.1. The latter species was the first sixteen vertex boron based cluster reported.[43]

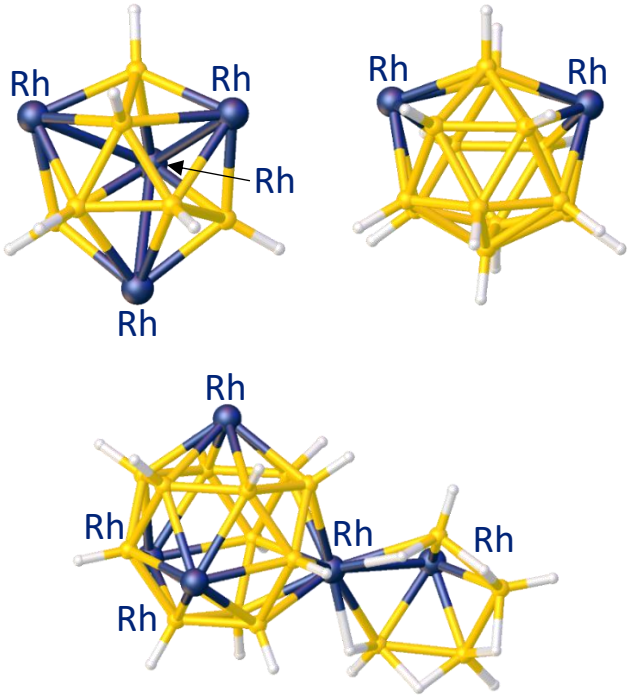

Figure 1.10.1: *Hypercloso* $[(Cp^*Rh)_4B_6H_6]$, $[(Cp^*Rh)_2B_{13}H_{13}]$ and $[(Cp^*Rh)_3B_{12}H_{12}Rh\{Cp^*RhB_4H_9\}]$, clockwise from top left (Cp* groups omitted for clarity).

However, as remarkable as the compounds reported by Ghosh and co-workers are their synthetic methodology does not have much wider applicability as it allows very little control or predictability. Furthermore, the extreme reaction conditions render the reaction mechanism difficult to investigate which therefore inhibits any logical alterations or improvements designed to obtain a particular target compound. As the aim of this project is to develop deliberate synthetic routes to non-Wadian species and to determine their geometries this approach was deemed inappropriate.

It is possible to envisage three potential routes to *hypercloso* species which meet the criteria of being deliberate and having wide applicability. These are: 1) two electron oxidation of *closo* species; 2) inserting electron deficient metal fragments into boranes or heteroboranes; and 3) manipulating the ligand set of a *closo* metallaborane or metallacarborane in such a way as to reduce the number of electrons involved in cluster bonding by two, e.g. by removing an L type or X^- type ligand. There exists some precedent for all three of these methodologies within the literature.

1.10.1 Two Electron Oxidation of *Closo* Species

If a *closo* species were to undergo a two electron oxidation it would then possess a *hypercloso* electron count. There exists within the literature a large number of *closo* dianions, particularly in borane chemistry, which could be oxidised in such a fashion. In one such example, Hawthorne and co-workers successfully synthesised *hypercloso* $B_{12}(O_{12}CH_2Ph)_{12}$ *via* a two electron oxidation of *closo* $[B_{12}(O_{12}CH_2Ph)_{12}]^{2-}$, as shown in figure 1.10.1.1.[42]

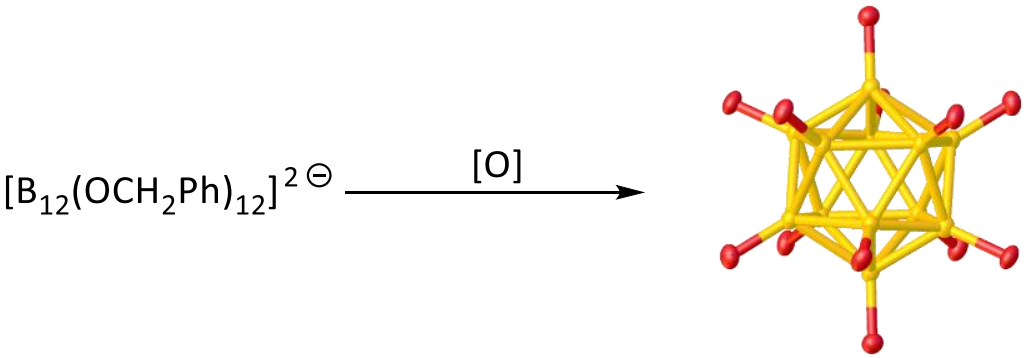

Figure 1.10.1.1: Two electron oxidation of $[B_{12}(O_{12}CH_2Ph)_{12}]^{2-}$ to produce *hypercloso* $B_{12}(O_{12}CH_2Ph)_{12}$ (benzyl groups omitted for clarity).

However, applications of this approach within carborane chemistry are limited, as *closo* carboranes exist as neutral species (or monoanions in the case of carboranes which only have one carbon atom incorporated into the cage), and are therefore significantly harder to oxidise.

1.10.2 Insertion of Electron Deficient Metal Fragments

A *hypercloso* metallacarborane can also be synthesised by inserting one or more electron poor metal fragments into the cage of a carborane. This process can be achieved using two slightly different approaches: either by incorporating into the cage a single one-vertex, zero-electron metal fragment (e.g. Cp*Re) or two one-vertex, one-electron fragments (e.g. Cp*Ru). The methodology for inserting a single one-vertex, zero-electron metal fragment into a carborane is conceptually simple and consists of inserting the desired metal fragment as a dication into the open face of a *nido* carborane of general formula $[R_2C_2B_nH_n]^{2-}$. An example of this process using $[R_2C_2B_9H_9]^{2-}$ is shown in figure 1.10.2.1.

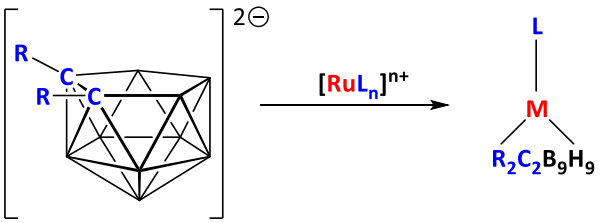

Figure 1.10.2.1: Synthesis of generic *hypercloso* species $LMR_2C_2B_9H_9$ *via* insertion of a generic one-vertex, zero-electron metal fragment.

The methodology for inserting two one-vertex, one-electron metal fragments into the cage is slightly more complex and consists of two steps, as shown in figure 1.10.2.2. Firstly, a one-vertex, one-electron metal fragment is supplied as a monocation and inserts into a *nido* carborane of general formula $[R_2C_2B_nH_n]^{2-}$ to give a *closo* species of general formula $[L_nMR_2C_2B_nH_n]^{-}$. This species then undergoes a reaction with an additional source of a monocationic one-vertex, one-electron metal fragment which is incorporated into the cage through a process called Direct Electrophilic Insertion (DEI). This process can be carried out in one step using a one pot synthesis and two equivalents of an appropriate source of the desired metal fragment. Alternatively, this process can be carried out

sequentially, allowing for the possibility of inserting two different metal fragments in order to give a mixed-metal *hypercloso* species, as is the case for the synthesis of 4-Cp*-5-Cb*-4,5,2,3-$RuCoC_2B_9H_{11}$, reported by Kudinov and co-workers, shown in figure 1.10.2.3.[53]

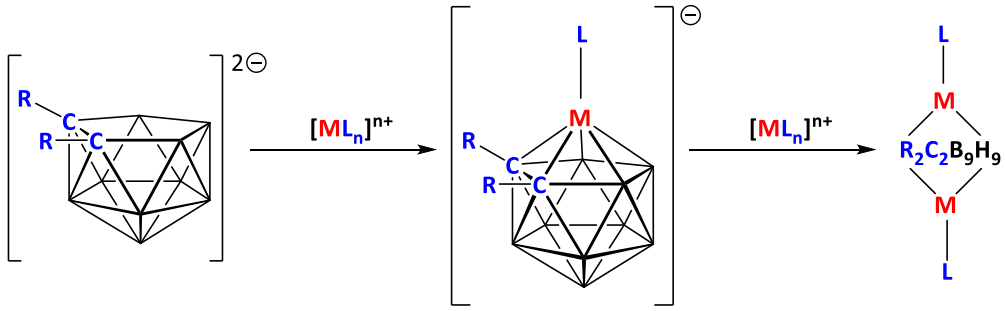

Figure 1.10.2.2: Synthesis of generic *hypercloso* species $LMR_2C_2B_9H_9$ *via* sequential insertion of two generic one-vertex, one-electron metal fragments.

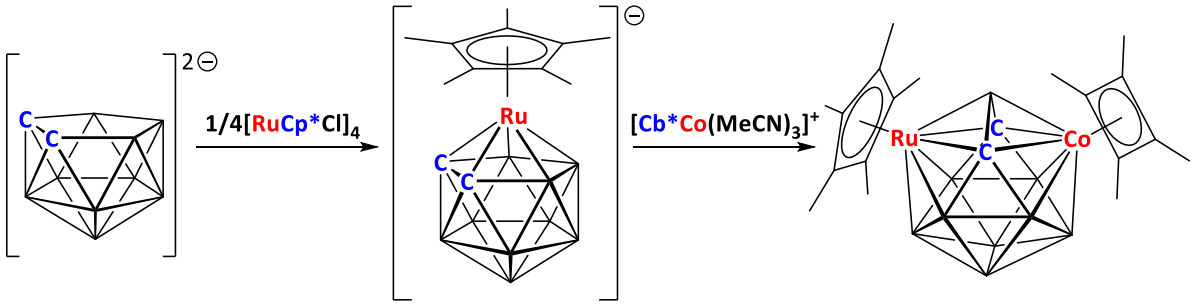

Figure 1.10.2.3: Synthesis of mixed-metal *hypercloso* species 4-Cp*-5-Cb*-4,5,2,3-$RuCoC_2B_9H_{11}$.

It was by this process of sequential addition of two one-vertex, one-electron metal fragments that three isomers of $(Cp^*Ru)_2C_2B_{10}H_{12}$, the first and to date only examples of fourteen vertex *hypercloso* heteroboranes, were synthesised by Welch and co-workers.[49] All three of these isomers were found to have the same geometry, with variations in which vertices were occupied by carbon atoms instead of boron atoms. The authors have therefore devised their own numbering system for this geometry. One of the isomers is shown in figure 1.10.2.4. The observed geometry is unique, containing a four atom trapezoidal face, and distinct from the bicapped hexagonal antiprismatic geometry assumed by *closo* fourteen vertex species. All three isomers also displayed other properties characteristic of *hypercloso* species, including an unusually wide range of ^{11}B

NMR shifts and unusually high frequency shifts. Additionally, all three isomers contain two unusually highly connected vertices, both of which are occupied by degree six ruthenium atoms.[49]

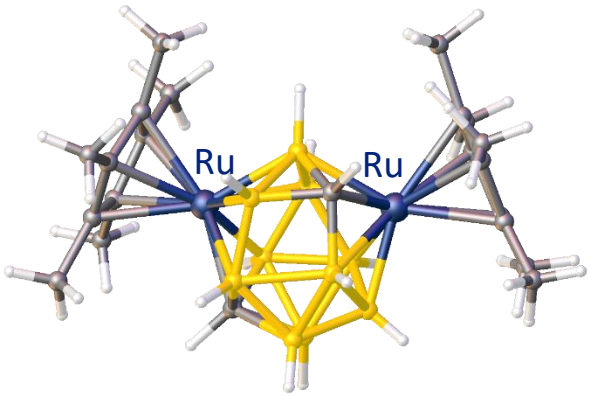

Figure 1.10.2.4: The fourteen vertex *hypercloso* species 2,7-Cp*$_2$-2,7,1,12-$Ru_2C_2B_{10}H_{12}$.

1.10.3 Ligand Set Manipulation

The final approach discussed that could be used to generate *hypercloso* species is that of ligand set manipulation. This process can be conceptualised as removing an L or X^- type ligand from a metal atom incorporated into a *closo* metallacarborane, thereby reducing the number of electrons available for cluster bonding by two, therefore converting the species from *closo* to *hypercloso*.

This can be done using one of two slightly different methods. One method would be to remove an X type ligand as X^- (e.g. by abstracting Cl^-) from a one vertex, one electron metal fragment incorporated into a *closo* metallacarborane of general formula $[XL_nMR_2C_2B_nH_n]^-$ to give a *hypercloso* species of general formula $L_nMR_2C_2B_nH_n$. Alternatively, an L type ligand could be abstracted from a one vertex, two electron metal fragment incorporated into a *closo* metallacarborane of general formula $L_{n+1}MR_2C_2B_nH_n$ to give a *hypercloso* species of general formula $L_nMR_2C_2B_nH_n$. It should be noted that loss of two X type ligands could be substituted for loss of an L type ligand in this case, e.g. by loss of hydrogen gas. Graphical representations of both of these processes are given in figure 1.10.3.1.

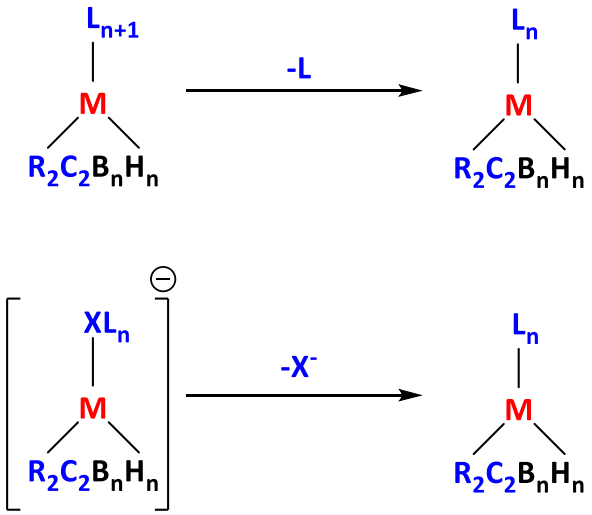

Figure 1.10.3.1: Generation of generic *hypercloso* species $L_nMR_2C_2B_nH_n$ from removal of either an L or X^- type ligand from generic *closo* metallacarboranes $L_{n+1}MR_2C_2B_nH_n$ or $[XL_nMR_2C_2B_nH_n]^-$.

Examples of *hypercloso* species synthesised by ligand manipulation are comparatively rare. However, some evidence exists within the literature that *hypercloso* metallacarboranes can be generated by this methodology. Hawthorne and co-workers report the synthesis of *hypercloso* $(PPh_3)_2RuC_2B_9H_{11}$, achieved by heating *closo* $(PPh_3)_2(H)_2RuC_2B_9H_{11}$ to 160 °C *in vacuo*, which leads to the evolution of hydrogen gas, as shown in figure 1.10.3.2. However, no crystal structure was reported for the *hypercloso* species formed.[54,55]

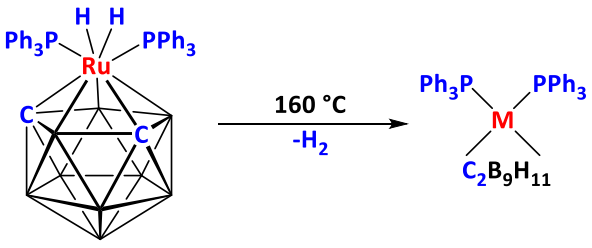

Figure 1.10.3.2: Dehydrogenation of 2,2-$(PPh_3)_2$-2,2-H_2-2,1,7-$RuC_2B_9H_{11}$.

Ligand manipulation is potentially an extremely useful synthetic route to *hypercloso* metallacarboranes. This is because there exists an extremely large number and wide range of *closo* metallacarboranes that are either monoanions with X type ligands or neutral species with L type ligands that could theoretically undergo ligand abstraction in order to

generate a *hypercloso* species. Despite this, and despite some literature precedent for this methodology, this particular approach has been under-explored within the literature and has not been explored previously within the group. Therefore, the synthesis of *hypercloso* metallacarboranes through ligand manipulation was designated as the objective of this project.

1.11 References

1 J. Daintith, *Dictionary of Chemistry*, Oxford University Press, Oxford, UK, 3rd edn., 1996.

2 S. H. Bauer, *J. Am. Chem. Soc.*, 1937, **59**, 1096.

3 H. C. Longuet-Higgins, *Proc. Roy. Soc.*, 1945, **183**, 357.

4 K. Wade, *J. Chem. Soc. D*, 1971, 792.

5 M. Driess and H. Nöth, *Molecular Clusters of the Main Group Elements*, Wiley, Weinheim, Germany, 2005.

6 A. Spiekermann, S. D. Hoffmann and T. F. Fässler, *Angew. Chemie - Int. Ed.*, 2006, **45**, 3459.

7 R. E. Williams, *Inorg. Chem.*, 1971, **10**, 210.

8 A. J. Welch and A. S. Weller, *Inorg. Chem.*, 1996, **35**, 4548.

9 J. Bould and J. D. Kennedy, *J. Organomet. Chem.*, 2014, **749**, 163.

10 L. S. Alekseev, A. V. Safronov, F. M. Dolgushin, A. A. Korlyukov, I. A. Godovikov and I. T. Chizhevsky, *J. Organomet. Chem.*, 2009, **694**, 1727.

11 L. S. Alekseev, F. M. Dolgushin and I. T. Chizhevsky, *J. Organomet. Chem.*, 2008, **693**, 3331.

12 Z. G. Lewis and A. J. Welch, *Acta Crystallogr. Sect. C Cryst. Struct. Commun.*, 1993, **49**, 705.

13 B. Wrackmeyer, H. J. Schanz, M. Hofmann and P. V. R. Schleyer, *Angew. Chemie - Int. Ed.*, 1998, **37**, 1245.

14 R. A. Wiesboeck and M. F. Hawthorne, *J. Am. Chem. Soc.*, 1964, **86**, 1642.

15 D. Grafstein and J. Dvorak, *Inorg. Chem.*, 1963, **2**, 1128.

16 S. Papetti and T. L. Heying, *J. Am. Chem. Soc.*, 1964, **86**, 2295.

17 G. Thiripuranathar, W. Y. Man, C. Palmero, A. P. Y. Chan, B. T. Leube, D. Ellis, D. McKay, S. A. Macgregor, L. Jourdan, G. M. Rosair and A. J. Welch, *Dalton Trans.*, 2015, **44**, 5628.

18 W. N. Lipscomb, *Science*, 1966, **153**, 373.

19 D. J. Wales, *J. Am. Chem. Soc.*, 1993, **115**, 1557.

20 H. D. Kaesz, R. Bau, H. A. Beall and W. N. Lipscomb, *J. Am. Chem. Soc.*, 1967, **89**, 4218.

21 C. A. Brown and M. L. McKee, *J. Mol. Model.*, 2006, **12**, 653.

22 T. L. Heying, J. W. Ager, S. L. Clark, D. J. Mangold, H. L. Goldstein, M. Hillman, R. J. Polak and J. W. Szymanski, *Inorg. Chem.*, 1963, **2**, 1089.

23 R. Rosen, R. L. Ernest, W. Quintana, L. G. Sneddon and P. J. Carroll, *Organometallics*, 1987, **6**, 80.

24 R. P. Alexander and H. Schroeder, *Inorg. Chem.*, 1963, **2**, 1107.

25 B. M. Ramachandran, S. M. Trupia, W. E. Geiger, P. J. Carroll and L. G. Sneddon, *Organometallics*, 2002, **21**, 5078.

26 M. F. Hawthorne, D. C. Young and P. A. Wegner, *J. Am. Chem. Soc.*, 1965, **87**, 1818.

27 M. F. Hawthorne and J. N. Francis, *Inorg. Chem.*, 1971, **10**, 863.

28 R. N. Grimes, *Dalton Trans.*, 2015, **44**, 5939.

29 R. N. Grimes, *Carboranes*, Elsevier, London, UK, 2nd edn., 2011.

30 M. F. Hawthorne and A. Pushechnikov, *Pure Appl. Chem.*, 2012, **84**, 2279.

31 R. F. Barth, J. A. Coderre, M. G. H. Vincente and T. E. Blue, *Clin. Cancer Res.*, 2005, **11**, 3987.

32 M. Nava, I. V. Stoyanova, S. Cummings, E. S. Stoyanov and C. A. Reed, *Angew. Chemie - Int. Ed.*, 2014, **53**, 1131.

33 S. E. Lyubimov, I. V. Kuchurov, A. A. Tyutyunov, P. V. Petrovskii, V. N. Kalinin, S. G. Zlotin, V. A. Davankov and E. Hey-Hawkins, *Catal. Commun.*, 2010, **11**, 419.

34 A. McAnaw, G. Scott, L. Elrick, G. M. Rosair and A. J. Welch, *Dalton Trans.*, 2013, **42**, 645.

35 A. J. Welch, *Crystals*, 2017, **7**, 234.

36 A. McAnaw, M. E. Lopez, D. Ellis, G. M. Rosair and A. J. Welch, *Dalton Trans.*, 2014, **43**, 5095.

37 K. P. Callahan, W. J. Evans, F. Y. Lo, C. E. Strouse and M. F. Hawthorne, *J. Am. Chem. Soc.*, 1975, **97**, 296.

38 E. L. Hoel, C. E. Strouse and M. F. Hawthorne, *Inorg. Chem.*, 1974, **13**, 1388.

39 M. J. Attfield, J. A. K. Howard, A. N. D. M. Jelfs, C. M. Nunn and F. G. A. Stone, *J. Chem. Soc. Dalton Trans.*, 1987, 2219.

40 M. J. Attfield, J. A. K. Howard, A. N. D. M. Jelfs, C. M. Nunn and F. G. A. Stone, *J. Chem. Soc. Chem. Commun.*, 1986, 918.

41 I. Tiritiris and T. Schleid, *Z. Anorg. Allg. Chem.*, 2004, **630**, 541.

42 O. K. Farha, R. L. Julius, M. W. Lee, R. E. Huertas, C. B. Knobler and M. F. Hawthorne, *J. Am. Chem. Soc.*, 2005, **127**, 18243.

43 S. Ghosh, D. K. Roy, B. Mondal, P. Shankhari, R. S. Anju, K. Geetharani and S. M. Mobin, *Inorg. Chem*, 2013, **52**, 6705.

44 R. T. Boerø, J. Derendorf, C. Jenne, S. Kacprzak, M. Keßler, R. Riebau, S. Riedel, T. L. Roemmele, M. Rühle, H. Scherer, T. Vent-Schmidt, J. Warneke and S. Weber, *Chem. - a Eur. J.*, 2014, **20**, 4447.

45 M. E. O'Neill and K. Wade, *Polyhedron*, 1984, **3**, 199.

46 M. E. Lopez, M. J. Edie, D. Ellis, A. Horneber, S. A. Macgregor, G. M. Rosair and A. J. Welch, *Chem. Commun.*, 2007, **2**, 2243.

47 A. R. Kudinov, D. S. Perekalin, S. S. Rynin, K. A. Lyssenko, G. V. Grintselev-Knyazev and P. V. Petrovskii, *Angew. Chemie - Int. Ed.*, 2002, **41**, 4112.

48 R. Littger, U. Englich, K. Ruhlandt-Senge and J. T. Spencer, *Angew. Chemie - Int. Ed.*, 2000, **39**, 1472.

49 A. P. M. Robertson, N. A. Beattie, G. Scott, W. Y. Man, J. J. Jones, S. A. Macgregor, G. M. Rosair and A. J. Welch, *Angew. Chemie - Int. Ed.*, 2016, **55**, 8706.

50 S. Du, B. E. Hodson, P. Lei, T. D. McGrath and F. G. A. Stone, *Inorg. Chem.*, 2007, **46**, 6613.

51 N. Carr, D. F. Mullica, E. L. Sappenfield and F. G. A. Stone, *Organometallics*, 1992, **11**, 3697.

52 J. Bould and J. D. Kennedy, *Chem. Commun.*, 2008, 2447.

53 D. S. Perekalin, K. A. Lyssenko, A. R. Kudinov, M. Corsini and F. Fabrizi De Biani, *Dalton Trans.*, 2017, **46**, 15710.

54 E. H. S. Wong and M. F. Hawthorne, *Inorg. Chem.*, 1978, **17**, 2863.

55 E. H. S. Wong and M. F. Hawthorne, *J. Chem. Soc. Chem. Commun.*, 1976, 257.

2.0 Attempts To Synthesise *Hypercloso* Molybdacarboranes

2.1 Introduction to Molybdacarboranes

The first molybdacarborane reported in the scientific literature was $[HNMe_3]_2[3,3,3\text{-}(CO)_3\text{-}closo\text{-}3,1,2\text{-}MoC_2B_9H_{11}]$, shown in figure 2.1.1, synthesised by Hawthorne and co-workers in 1968. The structure of this anion was later crystallographically determined by Do and co-workers as the tetramethylammonium salt.[1,2]

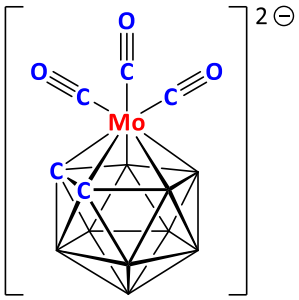

Figure 2.1.1: Structure of $[3,3,3\text{-}(CO)_3\text{-}closo\text{-}3,1,2\text{-}MoC_2B_9H_{11}]^{2-}$.

There exists a significant number of molybdacarboranes within the scientific literature, with at least 59 such examples known, which have between six and thirteen vertices.[3] An example of a thirteen vertex molybdacarborane, $[4,4,4\text{-}(CO)_3\text{-}closo\text{-}4,1,6\text{-}MoC_2B_{10}H_{12}]^{2-}$, and an example of a six vertex molybdacarborane, $[1,1\text{-}(CO)_2\text{-}2,3\text{-}Et_2\text{-}nido\text{-}1,2,3\text{-}MoC_2B_3H_5]_2(\mu\text{-}Br)_2$, are given in figure 2.1.2.[4,5]

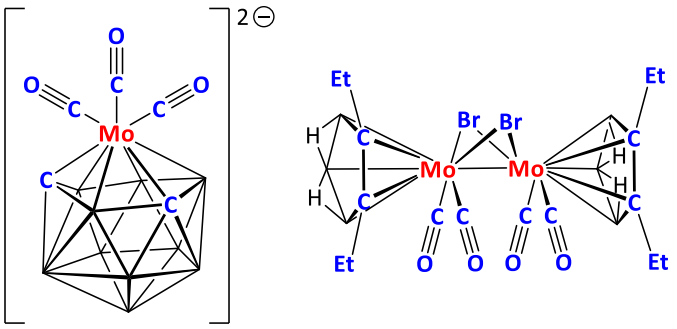

Figure 2.1.2: Thirteen vertex [4,4,4-$(CO)_3$-*closo*-4,1,6-$MoC_2B_{10}H_{12}]^{2-}$, reported by Stone and co-workers, and [1,1-$(CO)_2$-2,3-Et_2-*nido*-1,2,3-$MoC_2B_3H_5]_2(\mu$-$Br)_2$, a dimer of two six vertex molybdacarboranes, reported by Grimes and co-workers.[4,5]

Molybdacarboranes containing a wide range of ligands have been reported. These include L type ligands, such as phosphines, alkenes and alkynes, and X type ligands, such as halides. However, CO is by far the most common ligand encountered. Some examples are shown in figure 2.1.3.

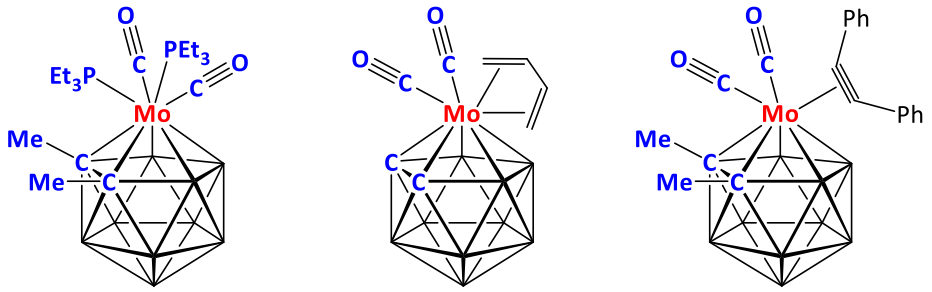

Figure 2.1.3: 1,2-Me_2-3,3-$(PEt_3)_2$-3,3-$(CO)_2$-*closo*-3,1,2-$MoC_2B_9H_9$, 3,3-$(CO)_2$-3-(C_4H_6)-*closo*-3,1,2-$MoC_2B_9H_{11}$, 1,2-Me_2-3,3-$(CO)_2$-3-(PhCCPh)-*closo*-3,1,2-$MoC_2B_9H_9$, respectively.[6,7]

2.2 Routes to *Hypercloso* Molybdacarboranes

As noted in 1.10, a metallacarborane of general formula $L_xMR_2C_2B_nH_n$ will have a *hypercloso* electron count if the metal vertex can be considered a one vertex, zero electron metal fragment. A metal fragment can be considered to be a one vertex, zero electron fragment if the valence electron count of the metal plus any electrons donated by ligands is equal to twelve. As group six metals, a molybdenum, tungsten or chromium atom incorporated as a vertex with three L type ligands can be considered a one vertex, zero electron fragment. Chromacarboranes are known within the literature but are less common than molybdacarboranes and tungstacarboranes and more frequently form dimeric "sandwich" compounds (similar to FeSAN and CoSAN, noted in 1.6) than single cage metallacarboranes with *exo*-polyhedral ligands which can be abstracted. $\{L_3Cr\}$ can therefore be eliminated as a target metal fragment.

The vast majority of molybdacarboranes and tungstacarboranes have at least one carbonyl ligand bound to the metal vertex. This is because the starting materials used in this area of chemistry, $Mo(CO)_6$ and $W(CO)_6$, both have multiple carbonyl ligands and it is difficult to remove all of these from the metal. However, carbonyl ligands are a desirable target for ligand abstraction as there are well-known methods to remove carbonyl ligands within the literature. One such method is photolysis, which commonly removes CO ligands as free CO gas from metal centres. Another method is to use Me_3NO, which abstracts CO ligands by reacting to form free CO_2 gas and NMe_3, as shown in figure 2.2.1.

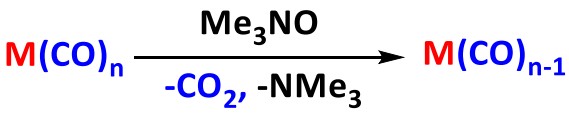

Figure 2.2.1: Generic scheme for abstraction of a carbonyl from a metal centre by Me_3NO.

Within metallacarborane chemistry there exist examples of using Me_3NO to abstract a carbonyl ligand, as demonstrated in work by Stone and co-workers, shown in figure 2.2.2.[8] In this case Me_3NO abstracts a carbonyl ligand bound to the iron centre before the resulting vacant coordination site is rapidly occupied by the intramolecular alkyne.

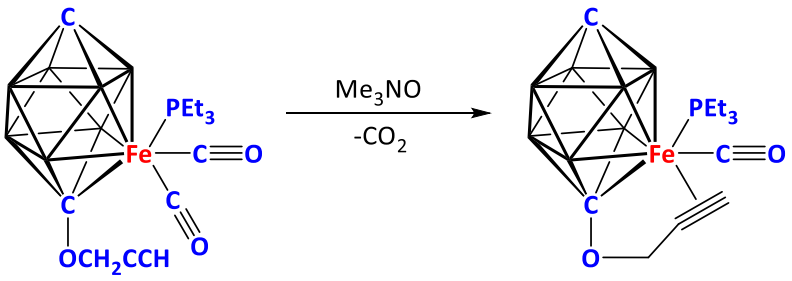

Figure 2.2.2: Abstraction of CO by Me_3NO and subsequent binding of alkyne to Fe.

Alternatively, an $\{L_3M\}$ fragment could be formed by abstracting an X^- type ligand from a molybdacarborane of general formula $[XL_3MoR_2C_2B_nH_n]^-$. A number of molybdacarboranes are reported in the literature of general formula $[X(CO)_3MoR_2C_2B_nH_n]^-$, where R=Me or H, which would be appropriate candidates. Halide ligands can be frequently abstracted from metal atoms by silver salts, e.g. $Ag[BF_4]$.[9–12] Examples of a halide being abstracted from a metal centre using a silver salt are given in figure 2.2.3.[11] In this case the metal then reacts with another metal complex to form a family of heterobimetallic compounds.

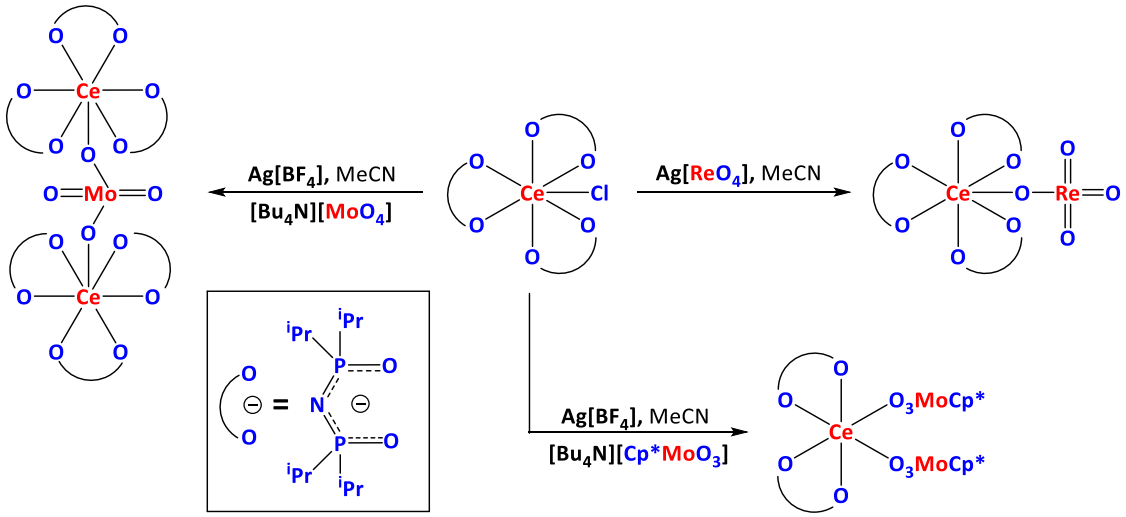

Figure 2.2.3: Abstraction of chloride from $Ce(N\{^iPr_2PO\}_2)_3Cl$ by silver reagents and subsequent bonding of a range of metal oxides to the resultant vacant coordination site.

When deciding on potential *hypercloso* molybdacarboranes to study a choice exists between twelve and thirteen vertex systems, both of which can be accessed easily using $[R_2C_2B_9H_9]^{2-}$ and $[R_2C_2B_{10}H_{10}]^{2-}$, respectively. As noted in 1.9, an important difference exists between twelve and thirteen vertex *hypercloso* heteroboranes in that thirteen vertex

species are unusual in that both *closo* and *hypercloso* species share the same docosahedral structure. As a result, thirteen vertex species have a potential advantage when it comes to the formation of *hypercloso* metallacarboranes through abstracting an L type ligand from a *closo* metallacarborane. As no change in shape would be anticipated for such a process, this implies that generating a thirteen vertex species *via* this route could be easier than for other systems which do have to undergo a change in shape. However, this also has a significant disadvantage as it means that the resulting *hypercloso* species will not have a novel geometry and could therefore be of limited interest versus a *hypercloso* twelve vertex species.

2.3 Attempts to Synthesise *Hypercloso* Molybdacarboranes Through Carbonyl Abstraction

[BTMA][4,4-$(CO)_2$-4-(C_3H_5)-*closo*-4,1,6-$MoC_2B_{10}H_{12}$] was prepared by literature methods, including an improved synthesis of the starting material $Mo(CO)_2(MeCN)_2(C_3H_5)Br$ (**I**).[13,14] From this 4,4,4,4-$(CO)_4$-*closo*-4,1,6-$MoC_2B_{10}H_{12}$ (**1**) was prepared by the route shown in figure 2.3.1, adapting a synthesis reported by Stone and co-workers to make twelve vertex molybdacarboranes.[7]

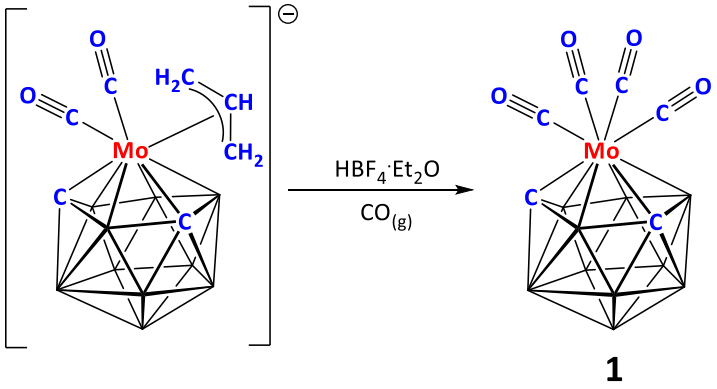

Figure 2.3.1: Synthesis of 4,4,4,4-$(CO)_4$-*closo*-4,1,6-$MoC_2B_{10}H_{12}$ (**1**).

^1H NMR data obtained for **1** displays only one cage CH resonance (δ=4.38 ppm) despite having two inequivalent carbon vertices at positions 1 and 6. This is because 4,1,6-$MR_2C_2B_{10}H_{10}$ species are commonly fluxional in solution at room temperature, a phenomenon first discovered by Hawthorne and co-workers for 4-Cp-4,1,6-$CoC_2B_{10}H_{12}$.[15,16] As can be seen from the mechanism of fluxionality, reported by Hawthorne and co-workers and shown in figure 2.3.2, this process means the carbon atoms are equivalent in solution at room temperature on the NMR timescale and that the molecule has overall C_s symmetry.[16,17] $^{11}B\{^1H\}$ NMR data obtained for **1** shows six signals in the ratio 1:1:2:2:1:3 (from high frequency to low frequency), which can also be rationalised by fluxionality, as if **1** was non-fluxional then it would instead generate a $^{11}B\{^1H\}$ NMR spectrum containing up to ten distinct boron signals.

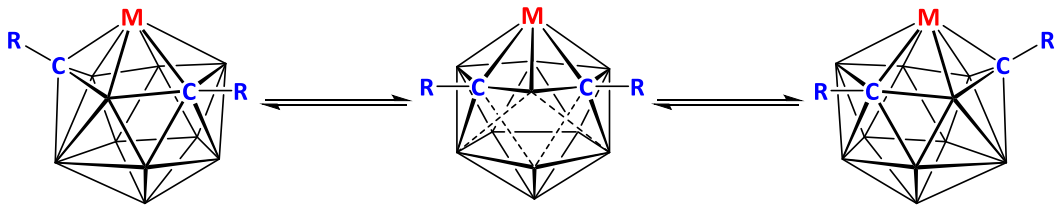

Figure 2.3.2: Mechanism of fluxionality in 4,1,6-$MR_2C_2B_{10}H_{10}$ metallacarboranes.

A reaction between **1** and Me_3NO was then carried out, as shown in figure 2.3.3. The desired *hypercloso* species was not isolated. Instead, $^{11}B\{^1H\}$ NMR spectroscopy revealed that the reaction mixture contained **1** as the major component. Additionally, a large amount of an unknown, dark, insoluble material was present in the reaction mixture. A plausible explanation for these observations is given in 2.4.

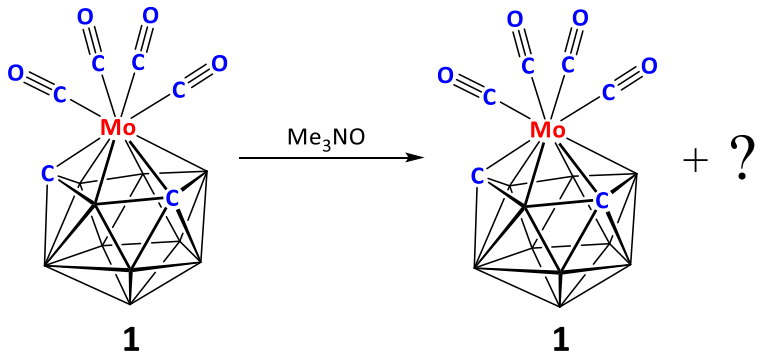

Figure 2.3.3: Reaction of **1** and Me_3NO.

An alternative method for removing carbonyl ligands from metal centres is photolysis. To this end the twelve-vertex literature species 1,2-Me_2-3,3,3,3-$(CO)_4$-*closo*-3,1,2-$MoC_2B_9H_9$ (**II**)[7] in C_6D_6 was photolysed in a J. Young NMR tube, with the progress of the reaction monitored by $^{11}B\{^1H\}$ NMR spectroscopy at intervals of 15 minutes, 45 minutes, 3 hours and 6 hours. The spectra produced are overlaid in figure 2.3.4. The large number of signals produced over time does not indicate conversion to a single species as desired, but instead suggests partial decomposition. This hypothesis is supported by the observation that the reaction mixture turned from a yellow solution to a thick black tar during the course of the experiment. Additionally, the signals produced are not in the region of the spectrum characteristic of *hypercloso* species, which tend to produce high

frequency signals. As with the reaction between **1** and Me_3NO, a hypothesised explanation for these observations is given in 2.4.

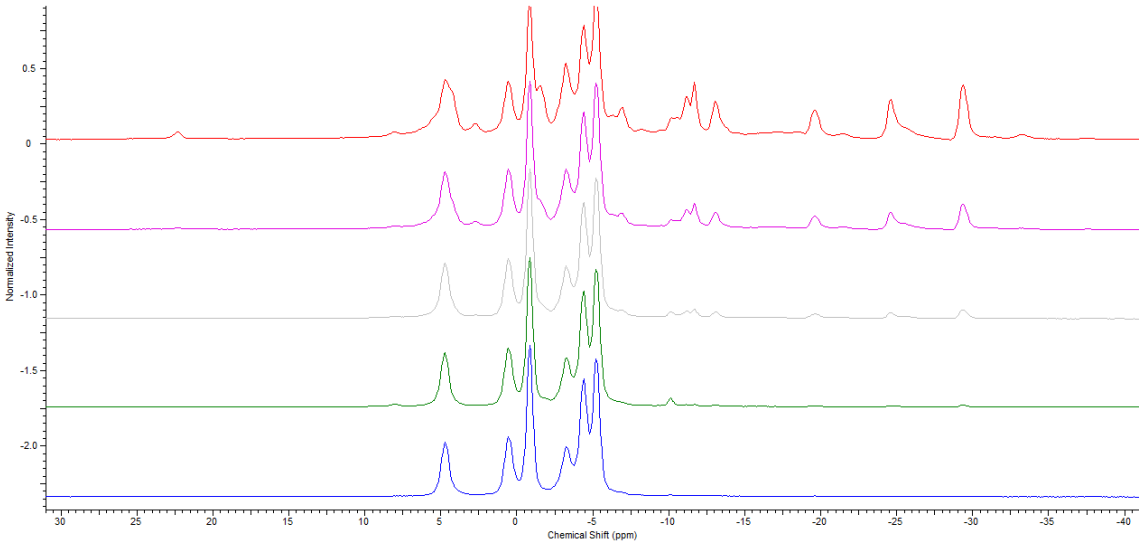

Figure 2.3.4: Overlaid $^{11}B\{^1H\}$ NMR spectra of photolysis of **II** in C_6D_6. From the bottom to the top the spectra relate to the sample at 0 minutes (blue), 15 minutes (green), 45 minutes (grey), 3 hours (pink) and 6 hours (red).

2.4 Attempts to Synthesise *Hypercloso* Molybdacarboranes Through Iodide Abstraction

Given the failure of both methods of carbonyl abstraction to generate a *hypercloso* species, an alternative approach was required. One such method of ligand abstraction would be to instead create a monoanionic *closo* metallacarborane containing a halide ligand which could be abstracted as X^- by $Ag[BF_4]$, as shown for generic molybdacarborane $[L_3XMoR_2C_2B_nH_n]^-$ in figure 2.4.1.

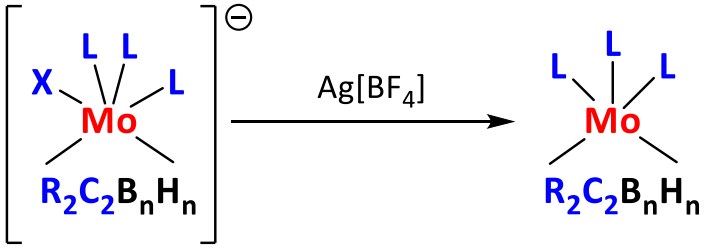

Figure 2.4.1: Abstraction of X^- from generic molybdacarborane $[L_3XMoR_2C_2B_nH_n]^-$.

To this end attempts were made to synthesise and then abstract an iodide from [1,6-Me_2-4-I-4,4,4-$(CO)_3$-*closo*-4,1,6-$MoC_2B_{10}H_{10}$]$^-$. In this case a species with methyl groups attached to the cage carbon atoms was chosen as the methyl groups would aid crystallographic determination of the location of the carbon atoms in any subsequent *hypercloso* species formed. The objective was to synthesise this molecule in a two step process, as shown in figure 2.4.2.

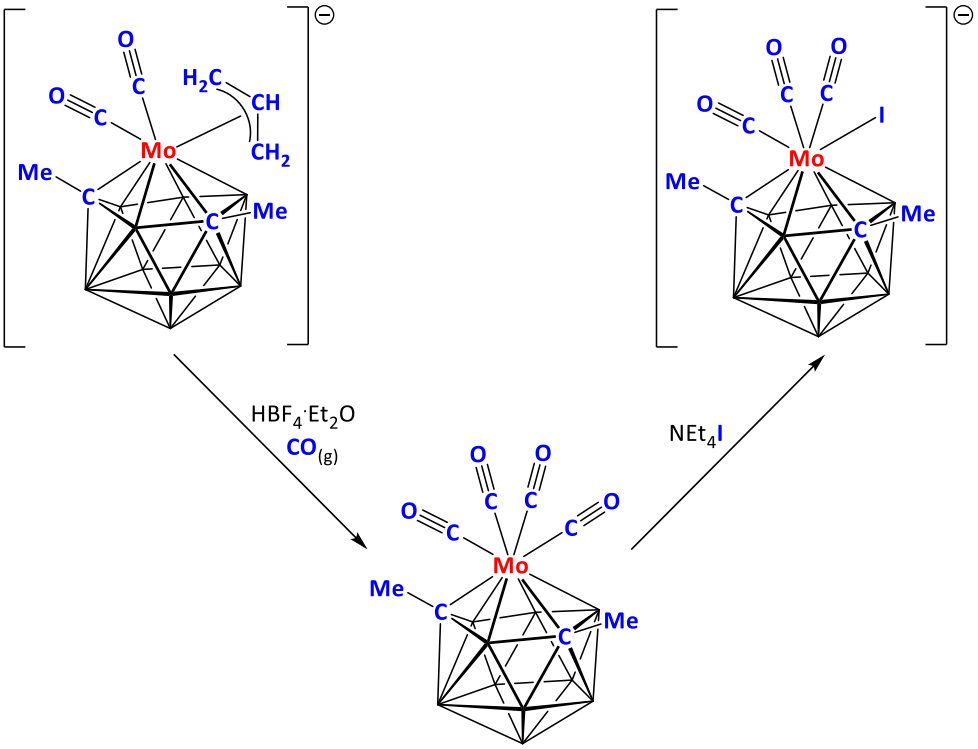

Figure 2.4.2: Planned synthesis of [1,6-Me_2-4-I-4,4,4-$(CO)_3$-*closo*-4,1,6-$MoC_2B_{10}H_{10}$]$^-$.

[PNP][1,6-Me_2-4,4-$(CO)_2$-4-(C_3H_5)-*closo*-4,1,6-$MoC_2B_{10}H_{10}$] ([PNP]**III**) was synthesised by literature methods and the molecular structure determined. The structure of the anion is shown in figure 2.4.3.[18]

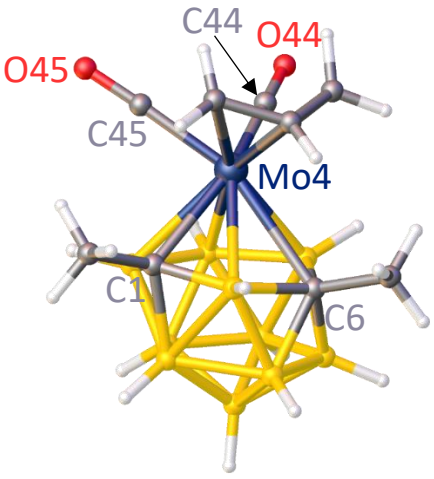

Figure 2.4.3: Structure of [1,6-Me_2-4,4-$(CO)_2$-4-(C_3H_5)-*closo*-4,1,6-$MoC_2B_{10}H_{10}$]$^-$ (**III**).

The orientation of the ligands in **III** relative to the carbon atoms of the cage can be rationalised by considering the Structural *Trans* Effect (STE) that each ligand and cage atom exerts. The boron atoms of the cage contribute more to the frontier molecular orbitals of the cage than the cage carbon atoms do, which results in the M-B_{cage} bonds being stronger than the M-C_{cage} bonds. The result of this is that the cage boron atoms exert a greater STE than the cage carbon atoms, which has an effect on any ligands bound *exo* to the cluster.[19] For a homogeneous ligand set this means any ligands *trans* to cage boron atoms will be bound more weakly than ligands bound *trans* to cage carbon atoms, resulting in bond lengthening in the former case relative to the latter. It should be noted that thirteen vertex metallacarboranes commonly contain carbon atoms with only four connectivities. These exert a greater STE than carbon atoms with five connectivities but still exert less of an effect than a boron atom.[20] If the ligand set is not homogeneous then the orientation of the ligands will be influenced by the STEs of the cage atoms. Ligands with a smaller STE will be *trans* to cage boron atoms whilst ligands with a larger STE will be *trans* to cage carbon atoms.

The relative STE of cage B and C vertices is evident in the structure of **III**. One CO ligand (CO45) is *trans* to C6, a connectivity five carbon vertex, whilst the other (CO44) is *trans* to a boron vertex and C1, a connectivity four carbon vertex. The M-C_{CO} distance of CO45 is, as expected, shorter than the other (CO44), at 1.948(2) Å vs 1.9621(19) Å, a statistically significant difference of over 5σ. Additionally, the orientation of the *exo*-polyhedral ligands suggests that the allyl group exerts a weaker STE than the carbonyl ligands, as the allyl group lies *trans* to boron vertices.

However, the reaction of [PNP]**III** with $HBF_4{\cdot}Et_2O$ and CO did not produce the anticipated thirteen vertex species 1,6-Me_2-4,4,4,4-$(CO)_4$-*closo*-4,1,6-$MoC_2B_{10}H_{10}$, but instead unexpectedly produced a twelve vertex species as the only isolatable product. This can be observed from the $^{11}B\{^1H\}$ NMR spectrum, shown in figure 2.4.4, which contains evidence for only nine boron atoms. The exact mechanism of this reaction is unclear, but presumably includes the ejection of a {BH} fragment.

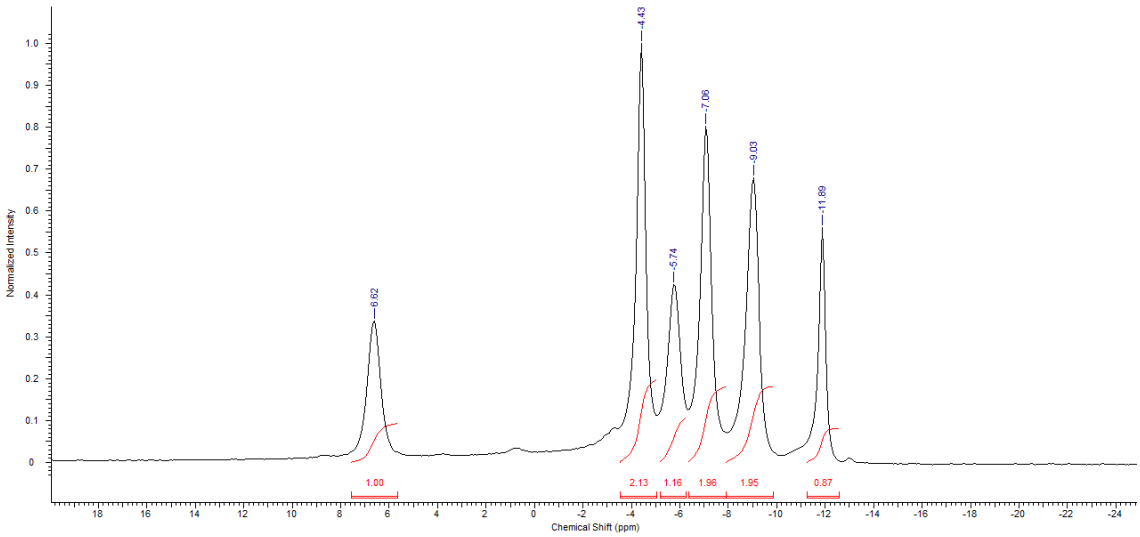

Figure 2.4.4: $^{11}B\{^{1}H\}$ NMR spectrum of "$(CO)_4MoMe_2C_2B_9H_9$" (**2**) in $CDCl_3$.

The NMR data obtained is consistent with 1,7-Me_2-*closo*-2,2,2,2-$(CO)_4$-2,1,7-$MoC_2B_9H_9$ (**2**), as shown in figure 2.4.5. The ^{1}H NMR spectrum contains a single signal for the methyl groups, meaning the cage carbon atoms must be equivalent, eliminating a large number of potential isomers. Additionally, the 3,1,2-MoC_2B_9 isomer can be eliminated from consideration as 1,2-Me_2-3,3,3,3-$(CO)_4$-*closo*-3,1,2-$MoC_2B_9H_9$ is a literature species and the $^{11}B\{^{1}H\}$ and ^{1}H NMR data obtained are not consistent with the data reported for this species.[7] This leaves the 2,1,7-MoC_2B_9 isomer as the most likely species. Additionally, both the $^{11}B\{^{1}H\}$ and $^{1}H\{^{11}B\}$ NMR data indicate the presence of six different boron environments of ratio 2:2:2:1:1:1, which is also consistent with 1,7-Me_2-2,2,2,2-$(CO)_4$-*closo*-2,1,7-$MoC_2B_9H_9$ (**2**). Moreover, the structure of a related species (**3**) synthesised from **2** was crystallographically determined and found to be the 2,1,7-MoC_2B_9 isomer.

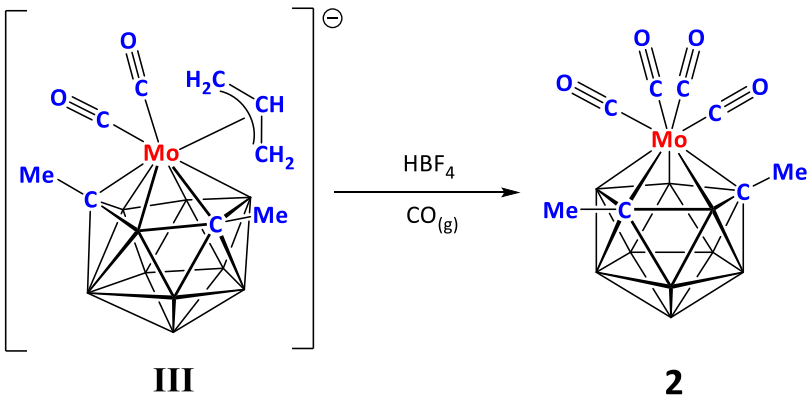

Figure 2.4.5: Synthesis of 1,7-Me_2-2,2,2,2-$(CO)_4$-*closo*-2,1,7-$MoC_2B_9H_9$ (**2**).

Although the synthesis of **2** was not the objective, it is nonetheless a tetracarbonyl molybdacarborane that could be converted into a monoanionic molybdacarborane containing a halide which could then be abstracted. [NEt_4][1,7-Me_2-2-I-2,2,2-$(CO)_3$-*closo*-2,1,7-$MoC_2B_9H_9$] ([NEt_4]**3**) was therefore synthesised, as shown in figure 2.4.6.

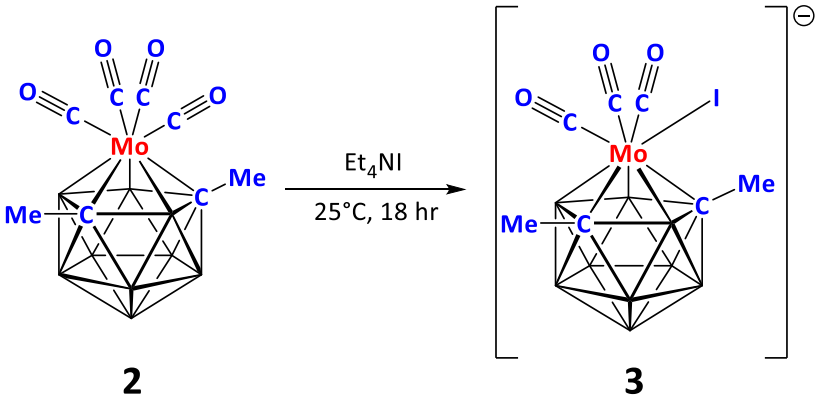

Figure 2.4.6: Synthesis of [1,7-Me_2-2-I-2,2,2-$(CO)_3$-*closo*-2,1,7-$MoC_2B_9H_9$]$^-$ (**3**).

The ^{1}H NMR spectrum of [NEt_4]**3** contains three sharp signals, two of which arise from the [NEt_4]$^+$ cation and one signal for the cage methyl groups, indicating that the cage carbon atoms are equivalent, which is consistent with the 2,1,7-MoC_2B_9 isomer. The ^{11}B{^{1}H} NMR spectrum contains four signals of ratio 3:3:2:1 whereas the expected ^{11}B{^{1}H} NMR spectrum for the 2,1,7-MoC_2B_9 isomer could contain up to six signals of ratio 2:2:2:1:1:1. However, this can be explained by two of the signals of integral one each coinciding with a signal of integral two.

[NEt_4]**3** was also studied crystallographically and the anion shown to be the 2,1,7-MoC_2B_9 isomer, as shown in figure 2.4.7, strongly supporting the hypothesis that **2** is indeed 1,7-Me_2-2,2,2,2-$(CO)_4$-*closo*-2,1,7-$MoC_2B_9H_9$.

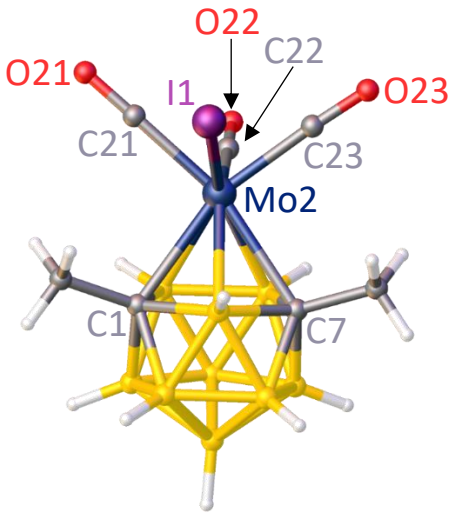

Figure 2.4.7: Structure of the anion [1,7-Me_2-2-I-2,2,2-$(CO)_3$-*closo*-2,1,7-$MoC_2B_9H_9$]$^-$ (**3**).

As can be seen from the structure of **3**, the iodide ligand assumes a position *trans* to two boron atoms, which is to be expected as the iodide is the ligand with the weakest STE. However, the M-C_{CO} bond lengths of CO21 and CO23, the two carbonyls *trans* to cage carbon atoms (C1 and C7) are unexpectedly longer than the M-C_{CO} bond length of CO22, the carbonyl *trans* to boron. The difference in bond lengths is statistically significant, with bond lengths of 2.003(3) Å, 1.994(4) Å and 1.971(3) Å respectively.

The reaction between [NEt_4]**3** and Ag[BF_4] was carried out with the intention of producing the *hypercloso* species $(CO)_3MoMe_2C_2B_9H_9$. However, this reaction was found by $^{11}B\{^1H\}$ NMR spectroscopy to unexpectedly regenerate 1,7-Me_2-2,2,2,2-$(CO)_4$-*closo*-2,1,7-$MoC_2B_9H_9$ (**2**), as shown in figure 2.4.8.

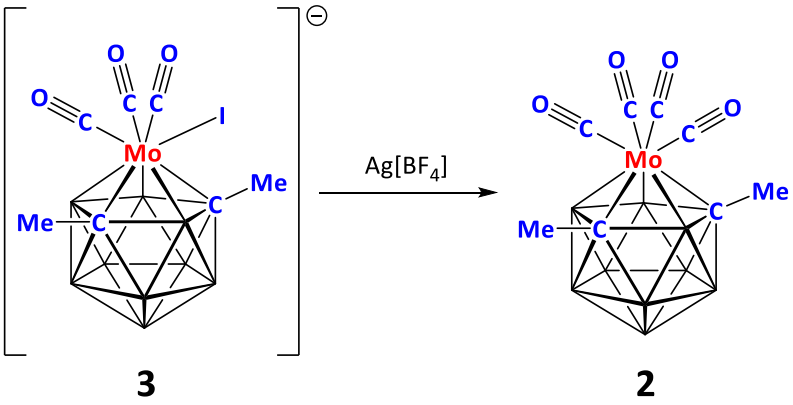

Figure 2.4.8: Unexpected regeneration of **2** from the reaction between $[NEt_4]$**3** and $Ag[BF_4]$.

Exactly how **2** is regenerated is unclear, but a postulated mechanism is shown in figure 2.4.9. In this process the iodide is first abstracted from **3** by $Ag[BF_4]$ to produce the transient species "$(CO)_3MoMe_2C_2B_9H_9$" which then reacts with one equivalent of itself to produce one molecule of **2** through a process referred to as carbonyl stealing. This also produces one molecule of "$(CO)_2MoMe_2C_2B_9H_9$", an extremely electron deficient species that would presumably undergo rapid decomposition. Alternatively, it is possible that "$(CO)_3MoMe_2C_2B_9H_9$" reacts with a molecule of **3** to form "$I(CO)_2Me_2C_2B_9H_9$", which presumably then undergoes decomposition. The hypothesised explanation for this is that it is more energetically favourable to regenerate a *closo* species *via* carbonyl stealing than to instead have to undertake the change in geometry that a twelve vertex *hypercloso* species would likely undergo.

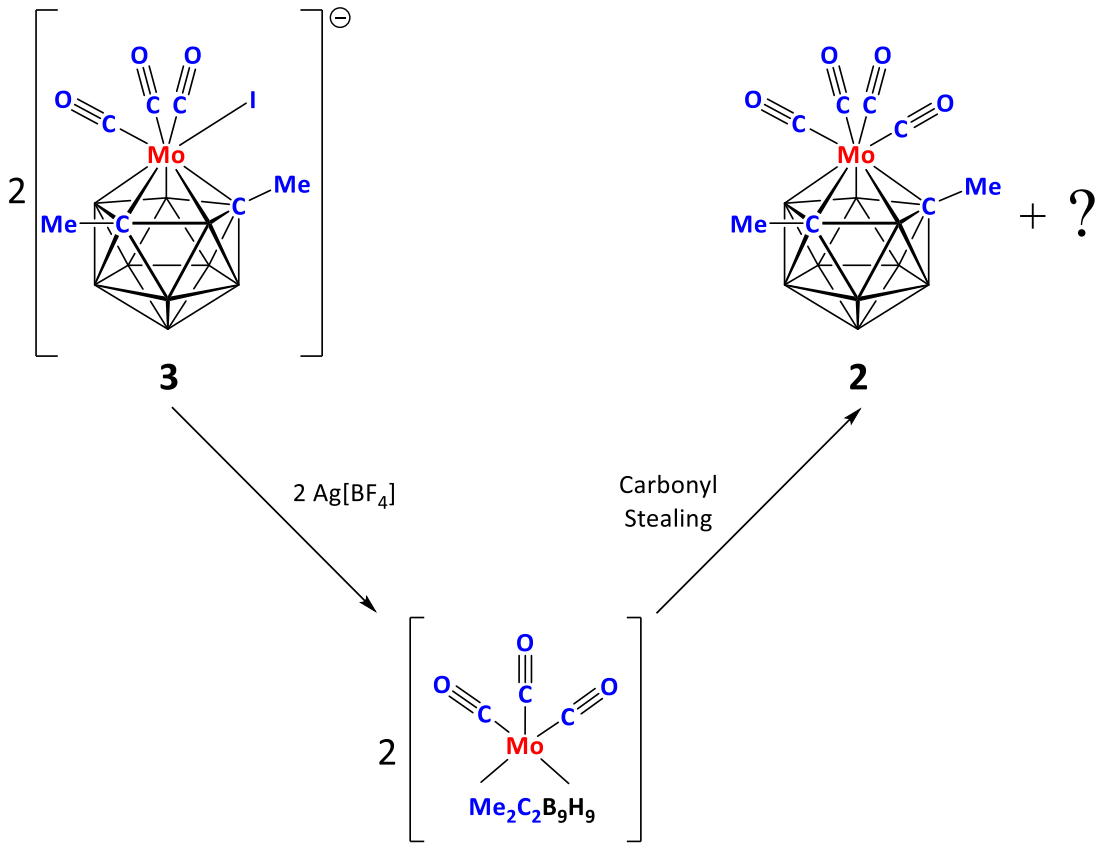

Figure 2.4.9: Iodide abstraction from [NEt$_4$]**3** and subsequent postulated mechanism of regeneration of **2**.

This suggestion is supported by evidence of decomposition provided by $^{11}B\{^1H\}$ NMR spectra of the petrol washings of the crude material, shown in figure 2.4.10. As can be seen, there is a sharp singlet at 0.8 ppm, which does not couple in the ^{11}B NMR spectrum (and therefore remains a singlet), shown in figure 2.4.11. This is typical of a species that contains a single boron atom with no protons attached directly to it, a category of species frequently formed in the decomposition of carboranes and metallacarboranes.

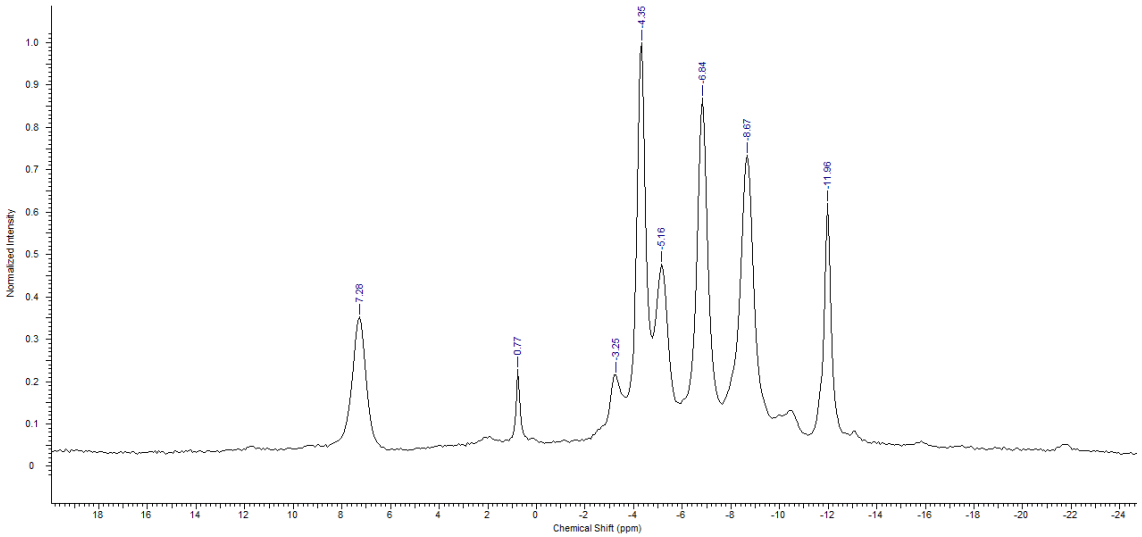

Figure 2.4.10: $^{11}B\{^{1}H\}$ NMR spectrum of petrol washings of the reaction of $[NEt_4]$**3** and $Ag[BF_4]$ in C_6D_6.

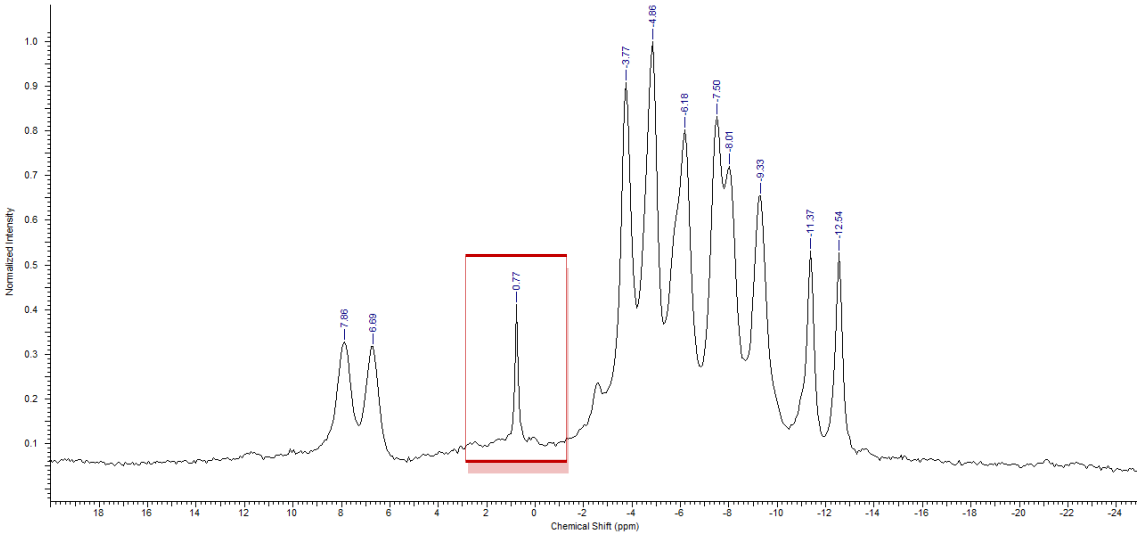

Figure 2.4.11: ^{11}B NMR spectrum of petrol washings of the reaction of $[NEt_4]$**3** and $Ag[BF_4]$ in C_6D_6.

This result also provides a potential explanation for the observed products from both the reaction of **1** and Me_3NO and the photolysis of **II**. In the former case the reaction mixture was found to contain **1** and insoluble dark material, consistent with decomposition. In the latter case the $^{11}B\{^{1}H\}$ NMR spectrum indicates the presence of **II** and a range of non-*hypercloso* boron containing compounds, also consistent with decomposition. These

observations are consistent with the suggestion that something similar to the carbonyl stealing postulated in figure 2.4.9 was occurring in both of these reactions.

Attempts were made to avoid ligand stealing by replacing a carbonyl ligand with a phosphine. It was hypothesised that if a species of generic formula [NEt_4][1,7-Me_2-2-I-2-PR_3-2,2-$(CO)_2$-*closo*-2,1,7-$MoC_2B_9H_9$] (where PR_3=a bulky phosphine) could be synthesised then, upon formation of "$PR_3(CO)_2MoMe_2C_2B_9H_9$" *via* iodide abstraction, the steric bulk of the phosphine may protect the molybdenum centre from carbonyl stealing by blocking another molybdenum centre from approaching. Attempts were made to synthesise 1,7-Me_2-2-PR_3-2,2,2-$(CO)_3$-*closo*-2,1,7-$MoC_2B_9H_9$ (where PR_3=PCy_3 or P{*o*-tolyl}$_3$), which would then undergo reaction with [NEt_4]I, by simple carbonyl displacement. However, these reactions were unsuccessful, as shown in figure 2.4.12.

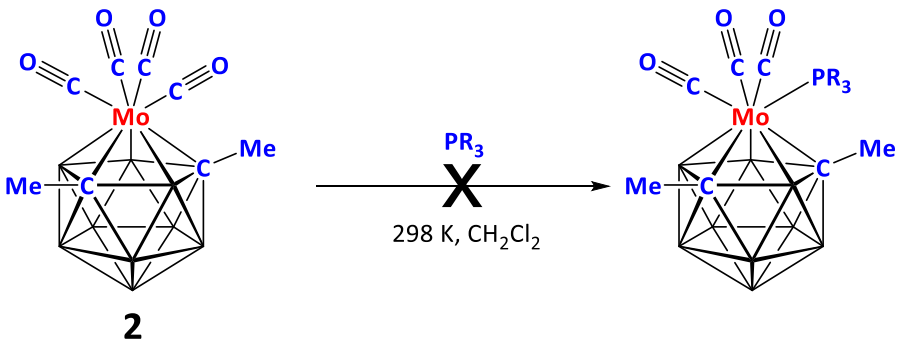

Figure 2.4.12: Attempted synthesis of 1,7-Me_2-2-PR_3-2,2,2-$(CO)_3$-*closo*-2,1,7-$MoC_2B_9H_9$, where PR_3=PCy_3 and P(*o*-tolyl)$_3$.

2.5 Attempts to Synthesise *Hypercloso* Molybdacarboranes Through Iodide Abstraction From [1,8-Me_2-2-I-2,2,2-$(CO)_3$-*closo*-2,1,8-$MoC_2B_9H_9$]$^-$

Having failed to produce a *hypercloso* species by abstraction of an iodide from [NEt_4]**3**, efforts were directed towards attempting to generate a *hypercloso* species by abstracting an iodide from an a different molybdacarborane containing a {$I(CO)_3Mo$} fragment. However, experience of working with thirteen vertex systems had provided evidence that such species can undergo decomposition to form twelve vertex species. As such, research was instead directed towards twelve vertex systems and specifically intentional routes to twelve vertex species, as synthesising the twelve vertex species **2** *via* decomposition of a thirteen vertex precursor was inefficient, low-yielding and ultimately unpredictable.

One such species is [PNP][1,8-Me_2-2-I-2,2,2-$(CO)_3$-*closo*-2,1,8-$MoC_2B_9H_9$] ([PNP]**IV**), a literature compound reported by Stone and Li.[21] This species has methyl groups attached to the cage carbon atoms which would aid crystallographic location of the carbon atoms in any *hypercloso* species generated. This species was prepared as the $[NEt_4]^+$ salt by a different route to that published by Stone and was also crystallographically characterised, as shown in figures 2.5.1 and 2.5.2. ^{1}H (cage) and ^{11}B{^{1}H} NMR spectra obtained for [NEt_4]**IV** were consistent with the reported spectra.

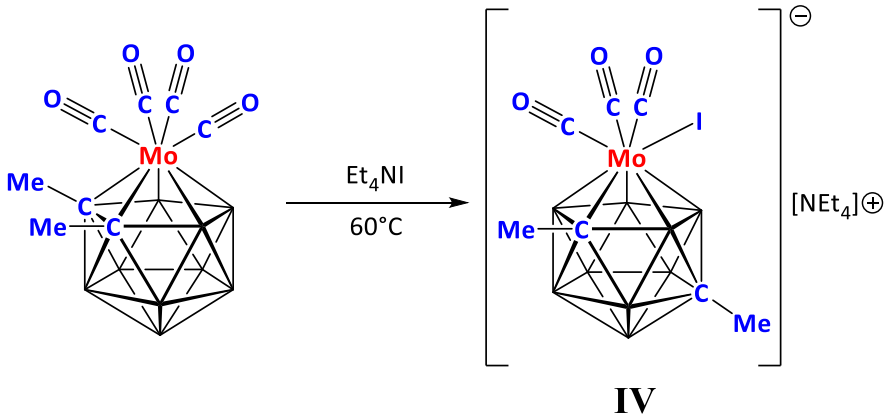

IV

Figure 2.5.1: Synthesis of [NEt_4][1,8-Me_2-2-I-2,2,2-$(CO)_3$-*closo*-2,1,8-$MoC_2B_9H_9$] ([NEt_4]**IV**).

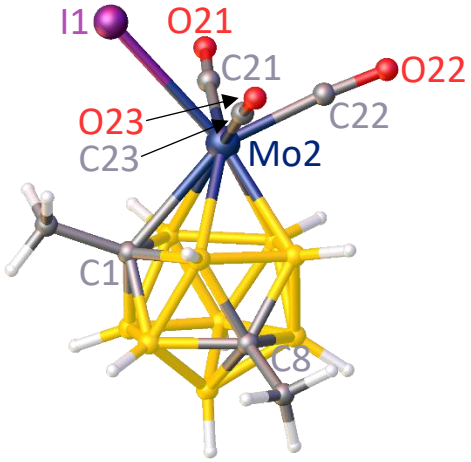

Figure 2.5.2: Structure of **IV**$^{-}$.

From the molecular structure of **IV**$^{-}$ it can be seen that the iodide ligand is positioned *trans* to the cage boron atoms. This is to be expected given that iodide is the *exo*-polyhedral ligand with smallest STE. Conversely, CO22 lies almost perfectly *trans* to C1, the cage carbon atoms present in the upper belt. As would be predicted, this M-C_{CO} bond is significantly shorter than those of CO21 and CO23, the two carbonyl ligands *trans* to boron, at 1.9346(16) Å, 2.0475(17) Å and 2.0430(17) Å, respectively. Additionally, the lengths of the C-O bonds of the carbonyl ligands are statistically different, with the bond lengths of CO21 and CO23 being shorter, at 1.141(2) and 1.139(2) Å, than the C-O bond length of CO22, at 1.1660(19) Å. This is unsurprising as the stronger M-C_{CO} bond between Mo2 and CO22 means there is more back donation from the molybdenum to the π^* antibonding orbital of the carbonyl ligand, weakening and therefore lengthening the C-O bond.

A reaction between [NEt_4]**IV** and Ag[BF_4] was carried out. However, no *hypercloso* species were isolated. Instead, evidence from the $^{11}B\{^1H\}$ NMR spectrum, shown in figure 2.5.3, suggests the formation of a twelve vertex *closo* species, as the signals produced lie in the region of the spectrum typical for *closo* species and integrate to nine boron atoms. Additionally, no high-frequency resonances characteristic of *hypercloso* species are observed in the $^{11}B\{^1H\}$ spectrum. The product isolated is instead consistent with 2,2,2,2-$(CO)_4$-1,8-Me_2-*closo*-2,1,8-$MoC_2B_9H_9$ (**4**), as shown in figure 2.5.4, a species unreported in the literature.

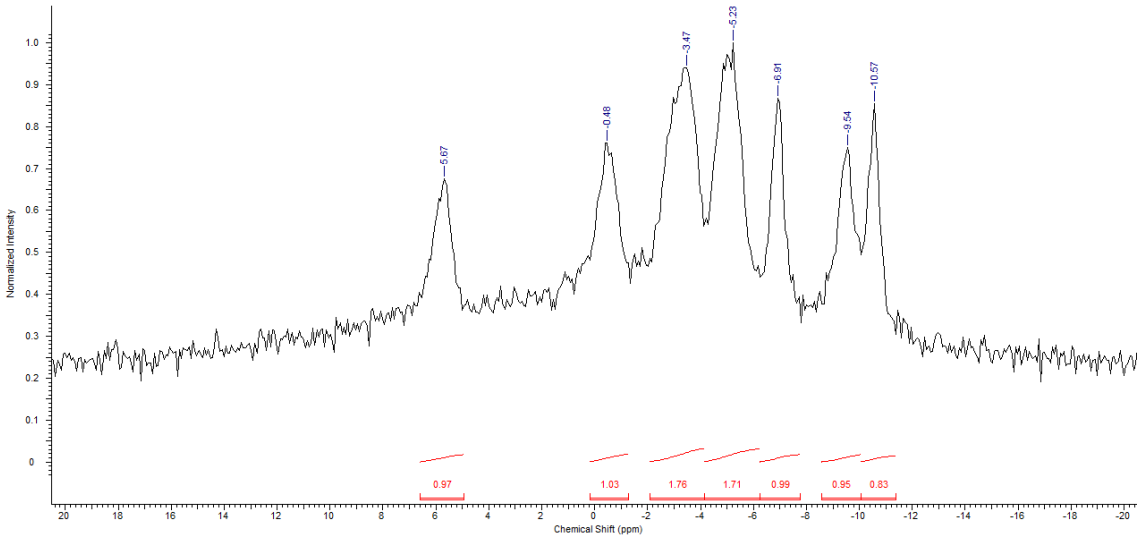

Figure 2.5.3: $^{11}B\{^{1}H\}$ spectrum of hypothesised 1,8-Me_2-2,2,2,2-$(CO)_4$-*closo*-2,1,8-$MoC_2B_9H_9$ (**4**).

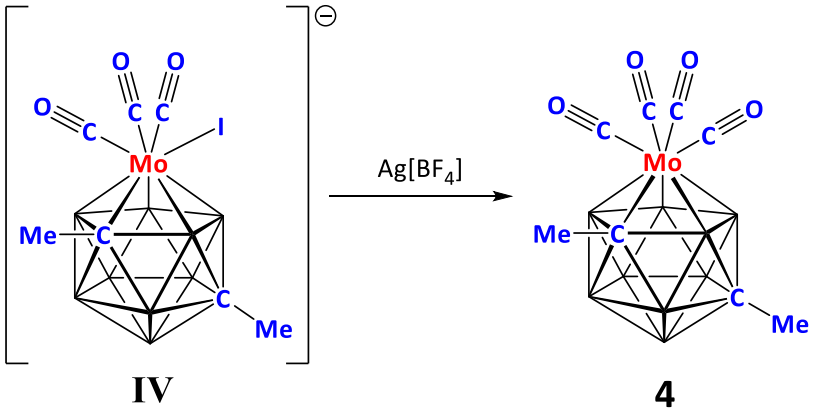

Figure 2.5.4: Postulated synthesis of **4** *via* carbonyl stealing.

Attempts to crystallise **4** from CH_2Cl_2/petrol and C_6F_6/petrol were unsuccessful. However, EIMS data supports the suggestion that **4** is 1,8-Me_2-2,2,2,2-$(CO)_4$-*closo*-2,1,8-$MoC_2B_9H_9$. The data, shown in figure 2.5.5, contains an envelope centred at *m/z* 368, the correct mass for **4**, which is followed by a series of envelopes at 340, 312, 284 and 256, all of which indicate the sequential loss of four carbonyl ligands. The envelopes produced are typical of boranes and heteroboranes and result from the fact that boron exists as two isotopes, ^{11}B and ^{10}B. Elemental analysis obtained for **4** is also consistent with the proposed structure.

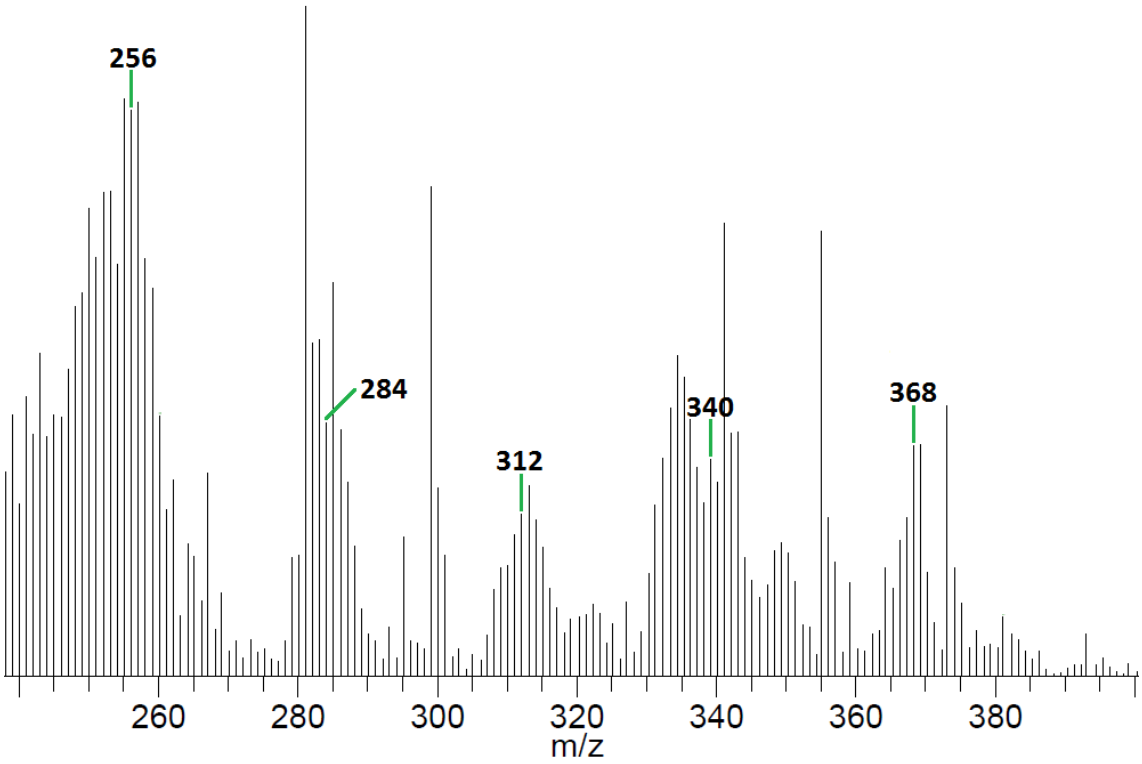

Figure 2.5.5: EIMS data for **4**.

It can be seen from the ^{1}H NMR data that this species has two inequivalent methyl groups, as expected for a 2,1,8-MoC_2B_9 molybdacarborane. Additionally, the ^{1}H NMR spectrum contains no signals other than the methyl groups, meaning that whatever ligands are bound to the metal must all be ^{1}H NMR-silent. This is consistent with carbonyl stealing generating a tetracarbonyl molybdacarborane *via* a mechanism similar to that postulated for the reaction between [NEt_4]**3** and Ag[BF_4], shown in figure 2.4.9. Finally, the species produced has the same yellow colour characteristic of other tetracarbonyl molybdacarboranes such as **1** and **2**.

2.6 Attempts to Synthesise *Hypercloso* Molybdacarboranes Containing 1,4,7-Trithiacyclononane

One approach which could avoid the problems associated with ligand abstraction would be to instead make a molybdacarborane that contains a polydentate ligand bound to molybdenum. If such a ligand had three heteroatoms capable of donating a lone pair to the metal atom then it would be equivalent to three L type ligands, producing a $\{L_3Mo\}$ fragment. Ligand stealing of the type seen for carbonyls would then be significantly less likely, as the chelate effect should prevent the polydentate ligand dissociating from the molybdenum centre. Therefore, if a *closo* molybdacarborane of general formula $L'L_3MoR_2C_2B_nH_n$, containing a tridentate ligand (L_3) and a single additional L type ligand (L') could be constructed then L' could be abstracted to generate a *hypercloso* species of formula $L_3MoR_2C_2B_nH_n$, as shown in figure 2.6.1 for n=9. Alternatively, X^- could be abstracted from a monoanionic *closo* species, containing an X type ligand and a tridentate ligand, to give a *hypercloso* species, as also shown in figure 2.6.1 for n=9.

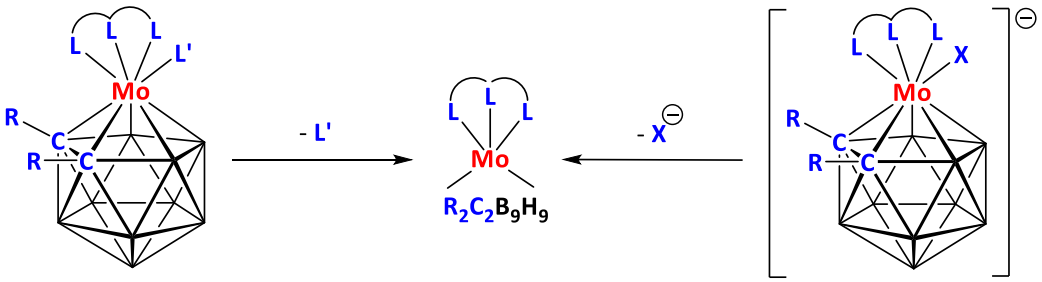

Figure 2.6.1: Generation of generic *hypercloso* species $L_3MoR_2C_2B_9H_9$ from abstracting an L type ligand from *closo* $L'L_3MoR_2C_2B_9H_9$ or an X^- type ligand from *closo* $[XL_3MoR_2C_2B_9H_9]^-$. L_3=a tridentate L type ligand, L'=a monodentate L type ligand.

To this end, 1,4,7-trithiacyclononane ([9]aneS_3) was designated as a target ligand, a tridentate ligand with three sulphur atoms which can act as L type ligands. The intention was to insert a {[9]aneS_3(CO)Mo} fragment into a cage to produce 1,2-Me_2-3,3,3-[9]aneS_3-3-CO-*closo*-3,1,2-$MoC_2B_9H_9$ before abstracting a carbonyl ligand using Me_3NO to generate *hypercloso* [9]ane$S_3MoMe_2C_2B_9H_9$, as shown in figure 2.6.2. Previous work involving Me_3NO and **1** did not generate the desired *hypercloso* species but instead generated starting material and insoluble, dark material. However, it is

suspected that this occurred because of ligand stealing, something that should be significantly more difficult in this case.

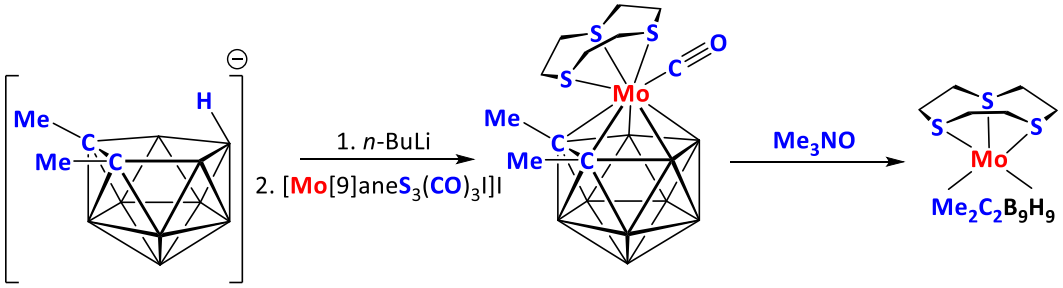

Figure 2.6.2: Proposed synthesis of 1,2-Me_2-3,3,3-[9]aneS_3-3-CO-*closo*-3,1,2-$MoC_2B_9H_9$ and subsequent carbonyl abstraction to form *hypercloso* [9]aneS_3Mo$Me_2C_2B_9H_9$.

However, the reaction between [Mo[9]aneS_3(CO)$_3$I]I, prepared *via* literature methods,[22] and Li_2[7,8-Me_2-*nido*-7,8-$C_2B_9H_9$] did not give the intended product. Instead Li[7,8-Me_2-*nido*-7,8-$C_2B_9H_{10}$] was recovered, as demonstrated by $^{11}B\{^1H\}$ and ^1H NMR spectra. This suggests that the metal fragment failed to cap the open face of the cage, as shown in figure 2.6.3.

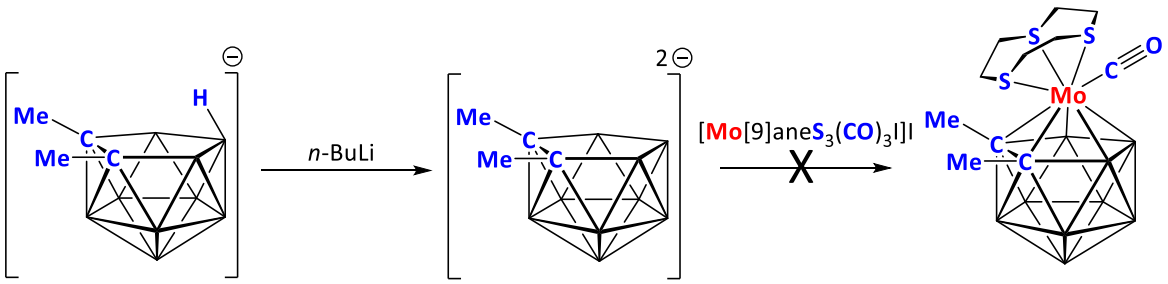

Figure 2.6.3: Attempted synthesis of 1,2-Me_2-3,3,3-[9]aneS_3-3-CO-*closo*-3,1,2-$MoC_2B_9H_9$.

2.7 Chapter Summary

Attempts to synthesise *hypercloso* molybdacarboranes were ultimately unsuccessful. Both the reaction of **1** and Me_3NO and the photolysis of **II**, shown in figures 2.7.1 and 2.7.2, produced product mixtures from which *hypercloso* species could not be isolated. Instead both mixtures contained a combination of starting material and unidentified boron containing compounds, consistent with decomposition. These observations are consistent with carbonyl stealing.

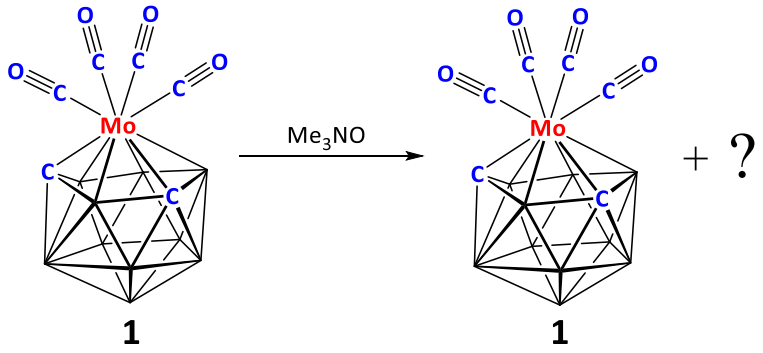

Figure 2.7.1: Reaction of **1** and Me_3NO.

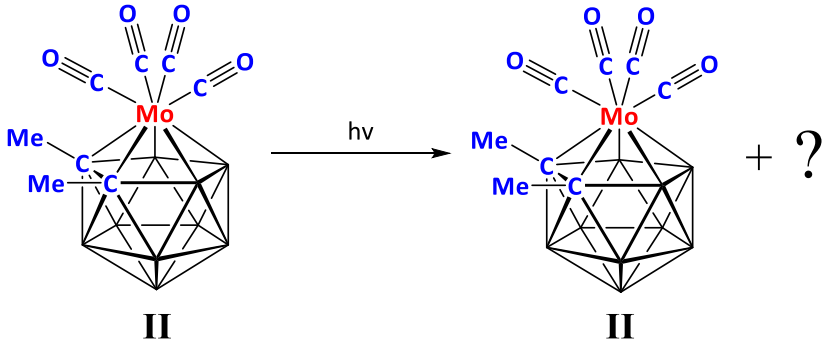

Figure 2.7.2: Photolysis of **II**.

Attempts to synthesise *hypercloso* "$(CO)_3MoMe_2C_2B_9H_9$" by abstracting I^- from $[NEt_4]$**3** using $Ag[BF_4]$ instead regenerated **2**, as shown in figure 2.7.3. This is postulated to have occurred *via* carbonyl stealing, as described in 2.4.

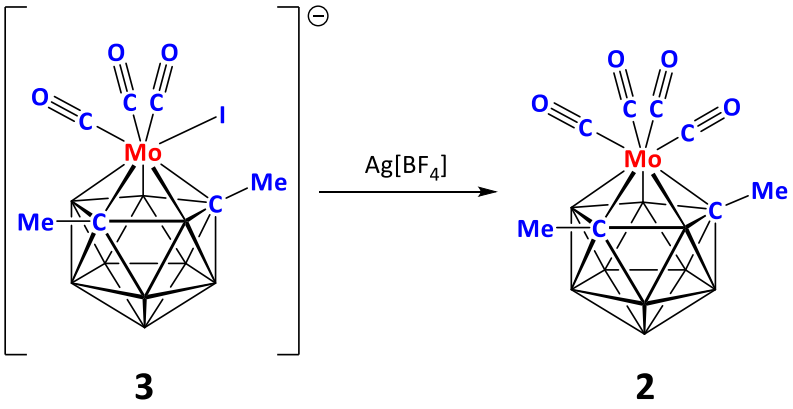

Figure 2.7.3: Unexpected regeneration of **2** *via* carbonyl stealing.

Further evidence for carbonyl stealing was also obtained for the reaction between [NEt_4]**IV** and Ag[BF_4], which produced a species consistent with **4**, as shown in figure 2.7.4, a species currently unknown. In this case EIMS, $^{11}B\{^1H\}$ and ^1H NMR evidence are consistent with the proposed structure.

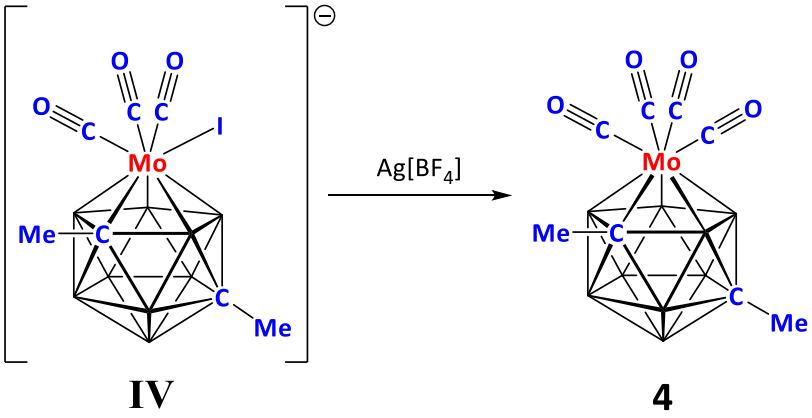

Figure 2.7.4: Postulated synthesis of **4** *via* carbonyl stealing.

Different approaches were envisaged to avoid ligand stealing. The first was to use a bulky phosphine ligand to shield the molybdenum centre. To this end attempts were made to synthesise 1,7-Me_2-2-PR_3-2,2,2-$(CO)_3$-*closo*-2,1,7-$MoC_2B_9H_9$ (where PR_3=PCy_3 and P(*o*-tolyl)$_3$), as shown in figure 2.7.5, *via* addition of PR_3 to **2**, which would then undergo reaction with NEt_4I to form [NEt_4][1,7-Me_2-2-I-2-PPh_3-2,2-$(CO)_2$-*closo*-2,1,7-$MoC_2B_9H_9$]. However, this approach produced no reaction for both PCy_3 and P(*o*-tolyl)$_3$.

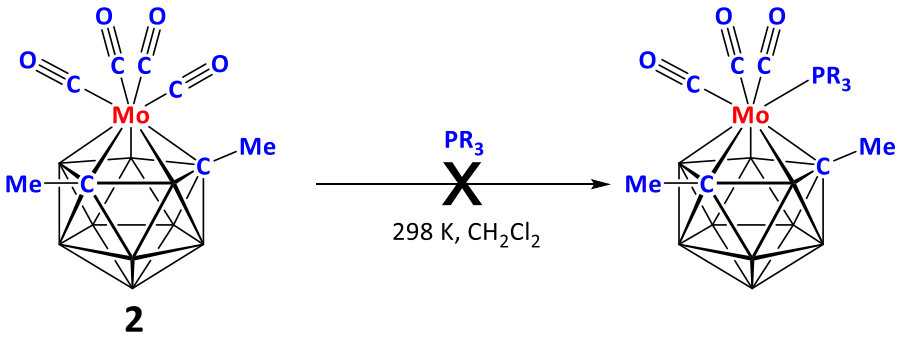

Figure 2.7.5: Attempted synthesis of 1,7-Me_2-2-PR_3-2,2,2-$(CO)_3$-*closo*-2,1,7-$MoC_2B_9H_9$, where PR_3=PCy_3 and P(*o*-tolyl)$_3$.

The second approach envisaged to avoid carbonyl stealing was to instead use a tridentate ligand which would not be susceptible to ligand stealing. To this end, attempts were made to synthesise 1,2-$Me_2$3,3,3-[9]aneS_3-3-CO-*closo*-3,1,2-$MoC_2B_9H_9$, which could then undergo reaction with Me_3NO to produce *hypercloso* [9]aneS_3Mo$Me_2C_2B_9H_9$. However, this was unsuccessful as no molybdenum fragment inserted into the cage, as shown in figure 2.7.6.

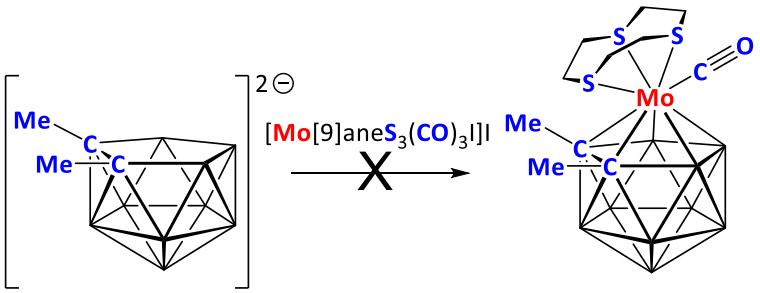

Figure 2.7.6: Attempted synthesis of 1,2-Me_2-3,3,3-[9]aneS_3-3-CO-*closo*-3,1,2-$MoC_2B_9H_9$.

Avoiding carbonyl stealing within the field of metallacarboranes of the group six metals is complicated by the near ubiquity of carbonyl ligands in both molybdacarboranes and tungstacarboranes, a problem that arises from the limited number of metal reagents available in this area of chemistry, of which all are derived from $Mo(CO)_6$ and $W(CO)_6$. One solution to this would be to use ruthenium, a group eight metal from which many reagents can be obtained that do not contain carbonyl ligands. This approach is developed in chapters 3 and 4.

2.8 References

1 M. F. Hawthorne, D. C. Young, T. D. Andrews, D. V. Howe, R. L. Pilling, A. D. Pitts, M. Reintjes, L. F. Warren and P. A. Wegner, *J. Am. Chem. Soc.*, 1968, **90**, 879.

2 J. H. Kim, M. Lamrani, J. W. Hwang and Y. Do, *Inorg. Chim. Acta*, 1998, **283**, 145.

3 R. N. Grimes, *Carboranes*, Elsevier, London, UK, 2nd edn., 2011.

4 N. Carr, D. F. Mullica, E. L. Sappenfield, F. G. A. Stone and M. J. Went, *Organometallics*, 1993, **12**, 4350.

5 M. A. Curtis, E. J. Houser, M. Sabat and R. N. Grimes, *Inorg. Chem.*, 1998, **37**, 102.

6 A. P. M. Robertson, A. Reckziegel, J. J. Jones, G. M. Rosair and A. J. Welch, *Eur. J. Inorg. Chem.*, 2017, **2017**, 4581.

7 S. J. Dossett, S. Li and F. G. A. Stone, *J. Chem. Soc., Dalton Trans.*, 1993, 1585.

8 A. Franken, T. D. McGrath and F. G. A. Stone, *Organometallics*, 2008, **27**, 908.

9 T. E. Barder, *J. Am. Chem. Soc.*, 2006, **128**, 898.

10 M. L. Buil, M. A. Esteruelas, K. Garcés and E. Oñate, *Organometallics*, 2009, **28**, 5691.

11 G.-C. Wang, H. H. Y. Sung, F.-R. Dai, W.-H. Chiu, W.-Y. Wong, I. D. Williams and W.-H. Leung, *Inorg. Chem.*, 2013, **52**, 2556.

12 P. Legzdins and D. T. Martin, *Organometallics*, 1983, **2**, 1785.

13 M. A. Laguna, D. Ellis, G. M. Rosair and A. J. Welch, *Inorg. Chim. Acta*, 2003, **347**, 161.

14 R. G. Hayter, *J. Organomet. Chem.*, 1968, **13**, C1.

15 G. B. Dunks, M. M. McKown and M. F. Hawthorne, *J. Am. Chem. Soc.*, 1971, **93**, 2541.

16 D. F. Dustin, G. B. Dunks and M. F. Hawthorne, *J. Am. Chem. Soc.*, 1973, **95**, 1109.

17 N. M. M. Wilson, D. Ellis, A. S. F. Boyd, B. T. Giles, S. A. Macgregor, G. M. Rosair and A. J. Welch, *Chem. Commun.*, 2002, 464.

18 S. Li, D. F. Mullica and F. G. A. Stone, *J. Organomet. Chem.*, 1994, **467**, 95.

19 D. M. P. Mingos, M. I. Forsyth and A. J. Welch, *J. Chem. Soc. Dalton Trans.*, 1978, 1363.

20 P. D. Abram, D. Ellis, G. M. Rosair and A. J. Welch, *Chem. Commun.*, 2009, 5403.

21 S. Li and F. G. A. Stone, *Polyhedron*, 1993, **12**, 1689.

22 P. K. Baker, S. J. Coles, M. C. Durrant, S. D. Harris, D. L. Hughes, M. B.

Hursthouse and R. L. Richards, *J. Chem. Soc., Dalton Trans.*, 1996, 4003.

3.0 Towards *Hypercloso* Ruthenacarboranes

3.1 Introduction to Ruthenacarboranes

Ruthenacarboranes are a relatively well-explored area of metallacarborane chemistry, with well over 100 such species being reported in the literature. These possess between six and fifteen vertices and contain a wide range of ligands, including aromatic ligands, such as derivatives of Cp and benzene, as well as a significant variety of X and L type ligands. Unlike molybdacarboranes or tungstacarboranes, a large number of ruthenacarboranes are reported that do not contain carbonyl ligands.

The first fifteen vertex metallacarborane discovered was the ruthenacarborane 1-(*p*-cymene)-8,14-$(CH_2)_3$-*closo*-1,8,14-$RuC_2B_{12}H_{12}$, reported by Welch and co-workers.[1] This species was unexpectedly produced in 67% yield from heating the fourteen vertex species 1,2,8-(*p*-cymene)-2,8-$(CH_2)_3$-*closo*-1,2,8-$RuC_2B_{11}H_{11}$ in refluxing toluene for 48 hours, as shown in figure 3.1.1.

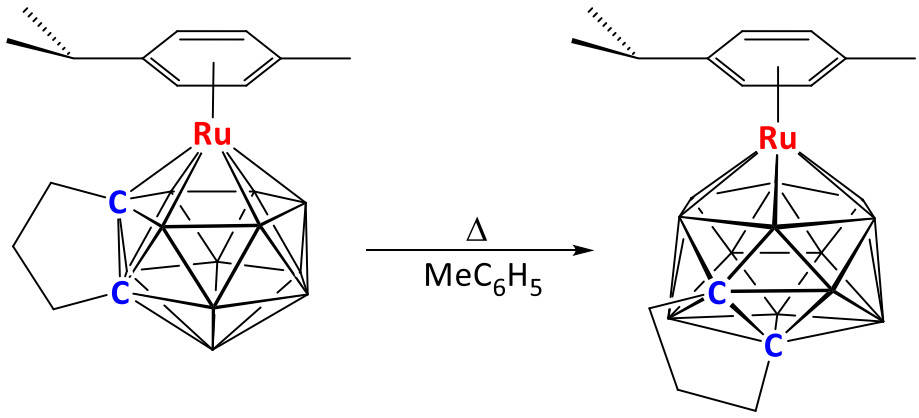

Figure 3.1.1: Synthesis of 1-(*p*-cymene)-8,14-$(CH_2)_3$-*closo*-1,8,14-$RuC_2B_{12}H_{12}$.

In addition to ruthenacarboranes containing *exo*-polyhedral ligands, a small number of ruthenacarborane sandwich compounds are found within the literature, comparable to FeSAN and CoSAN, noted in 1.6.[2] However, the direct, twelve vertex analogue to FeSAN is not known. Instead, only a single analogue of RuSAN based on two C_2B_9 cage units is reported. This species, shown in figure 3.1.2, has a SMe_2 unit attached to B8 on each

cage. It should be noted that the SMe_2 group bonds to boron through a dative bond. This increases the overall electron count of the cluster by one electron vs a vertex with a covalent bond to an *exo*-polyhedral substituent, as is the case with hydrogen atoms or alkyl/aryl groups.

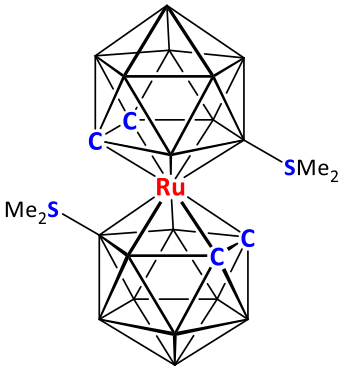

Figure 3.1.2: 3,3-Ru(8-SMe_2-*closo*-1,2-$C_2B_9H_{10})_2$.

In addition to a large number of *closo* ruthenacarboranes where the metal atom is incorporated as a vertex in the cage, there is also a smaller but still significant number of ruthenacarboranes in the literature where the ruthenium atom instead lies *exo* to the cage. This can occur for both *closo* and *nido* species, as shown in figures 3.1.3 and 3.1.4.[3,4] In the case of a ruthenium atom bound *exo* to the cage of a *nido* species, these species are frequently referred to as *exo-nido* species.[4,5] The *exo-nido* ruthenacarborane shown in figure 3.1.4, 5,6,10-[$Cl(Ph_3P)_2Ru$]-5,6,10-μ-$(H)_3$-10-H-7,8-$C_2B_9H_8$, exists as a zwitterion, with a cationic ruthenium centre and an anionic carborane cage. Additionally, said species contains an additional proton in an *endo* position on boron atom ten.

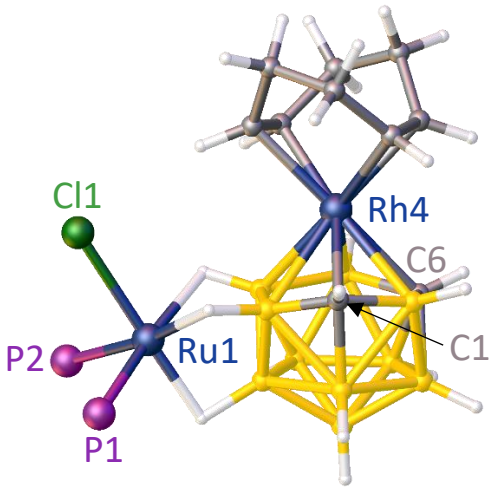

Figure 3.1.3: Structure of 3,7,8-[Cl(PPh$_3$)$_2$Ru]-3,7,8-μ-(H)$_3$-4-(COD)-*closo*-4,1,6-RhC$_2$B$_{10}$H$_9$, where ruthenium lies *exo* to the cage (phenyl units omitted for clarity).[3]

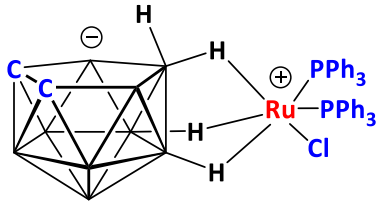

Figure 3.1.4: Structure of the *exo-nido* metallacarborane 5,6,10-[Cl(Ph$_3$P)$_2$Ru]-5,6,10-μ-(H)$_3$-10-H-7,8-C$_2$B$_9$H$_8$ in the solid state.[4]

It should be noted that the *exo-nido* species 5,6,10-[Cl(Ph$_3$P)$_2$Ru]-5,6,10-μ-(H)$_3$-10-H-7,8-C$_2$B$_9$H$_8$ and derivatives thereof are fluxional in solution at room temperature, as shown in figure 3.1.5.[4] In solution, one of the Ru-H-B bonds is cleaved and replaced with a direct Ru-B bond. The H atom then migrates onto the ruthenium atom. As there are three Ru-H-B bonds which can be broken, two of which are equivalent, this gives rise to two isomers, the symmetric and the asymmetric isomer, which exist in equilibrium. This fluxionality gives rise to complicated $^{11}B\{^1H\}$, $^1H\{^{11}B\}$ and $^{31}P\{^1H\}$ NMR spectra.

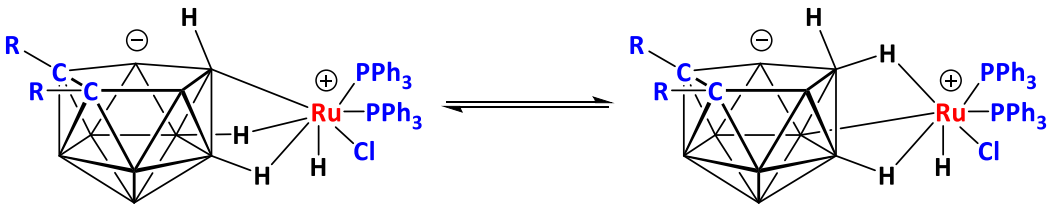

Figure 3.1.5: The symmetric (left) and asymmetric (right) isomers of the generic *exo-nido* species in solution (R =Me or H).

3.2 *Hypercloso* Ruthenacarboranes

Ruthenium is one of the metal atoms most frequently found incorporated in *hypercloso* metallacarboranes. *Hypercloso* ruthenacarboranes frequently contain either aromatic ligands or phosphine ligands. Additionally, *hypercloso* ruthenacarboranes with a range of vertices have been reported, including comparatively rare supraicosahedral (having more than twelve vertices) *hypercloso* metallacarboranes. Examples of *hypercloso* ruthenacarboranes include the ten vertex species $Ph_2P(C_6H_4CH_2CHCH_2)RuMe_2C_2B_7H_7$,[6] shown in figure 3.2.1, and three isomers of $(Cp^*Ru)_2C_2B_{10}H_{12}$, reported by Welch and co-workers,[7] to date the only fourteen vertex *hypercloso* metallacarboranes, one isomer of which is shown in figure 3.2.2.

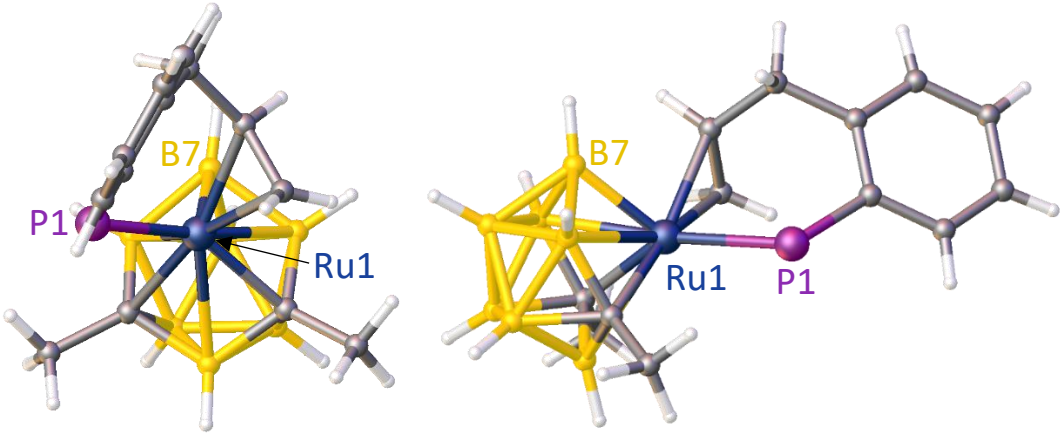

Figure 3.2.1: Structure of $Ph_2P(C_6H_4CH_2CHCH_2)RuMe_2C_2B_7H_7$ seen from two different angles (phenyl units omitted for clarity).[6]

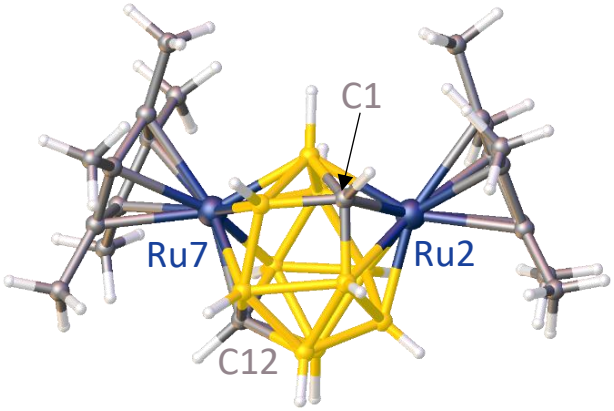

Figure 3.2.2: Structure of 2,7-Cp^*_2-2,7,1,12-$Ru_2C_2B_{10}H_{12}$.[7]

3.3 A New Synthetic Route to *Closo* Ruthenacarboranes

In order to synthesise *hypercloso* ruthenacarboranes *via* ligand manipulation it was first necessary to synthesise *closo* species from which ligands could be abstracted. If monoanionic *closo* species of general formula [1,2-R_2-3-Cl-3,3-$(PPh_3)_2$-*closo*-3,1,2-$RuC_2B_9H_9]^-$ (where R=Me or H) could be synthesised then Cl^- could subsequently be abstracted using $Ag[BF_4]$, as shown in figure 3.3.1.

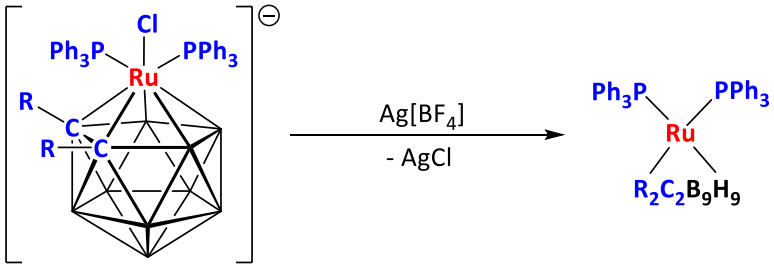

Figure 3.3.1: Proposed synthesis of generic *hypercloso* species $(PPh_3)_2RuR_2C_2B_9H_9$ (R=Me or H).

One such *closo* starting material has been reported by Chizhevsky and co-workers, $[NEt_4][3\text{-}Cl\text{-}3,3\text{-}(PPh_3)_2\text{-}closo\text{-}3,1,2\text{-}RuC_2B_9H_{11}]$ ($[NEt_4]$**VI**).[8] However, the synthesis of this species utilises $Ru(PPh_3)_3HCl$, to which the most common synthetic route involves heating the reaction mixture to reflux under a pressure of hydrogen gas.[9] This was considered too hazardous to attempt. An alternative synthesis is reported by He and co-workers, but this route was found to be unreliable.[10]

An alternative synthetic route to species of general formula [1,2-R_2-3-Cl-3,3-$(PPh_3)_2$-*closo*-3,1,2-$RuC_2B_9H_9]^-$ was therefore required. It was proposed that such species could be synthesised from *exo-nido* species of general formula 5,6,10-$[Cl(Ph_3P)_2Ru]$-5,6,10-μ-$(H)_3$-7,8-R_2-10-H-7,8-$C_2B_9H_6$ by removing the *endo* proton from the open face. This would then generate $[5,6,10\text{-}(Cl\{Ph_3P\}_2Ru)\text{-}5,6,10\text{-}\mu\text{-}(H)_3\text{-}7,8\text{-}R_2\text{-}7,8\text{-}C_2B_9H_6]^-$, a species which is monoanionic overall but that contains a cationic ruthenium centre and a dianionic carborane, as shown in figure 3.3.2. As the π orbitals of the cage would then be available to the ruthenium atom, it was suggested that this would then allow the $\{Cl(PPh_3)_2Ru\}$ fragment to insert into the cage by capping the open face to produce

[1,2-R_2-3-Cl-3,3-$(PPh_3)_2$-*closo*-3,1,2-$RuC_2B_9H_9]^-$, as shown in figure 3.3.2. This process is further aided by electrostatic attraction between the cationic ruthenium centre and the dianionic carborane cage.

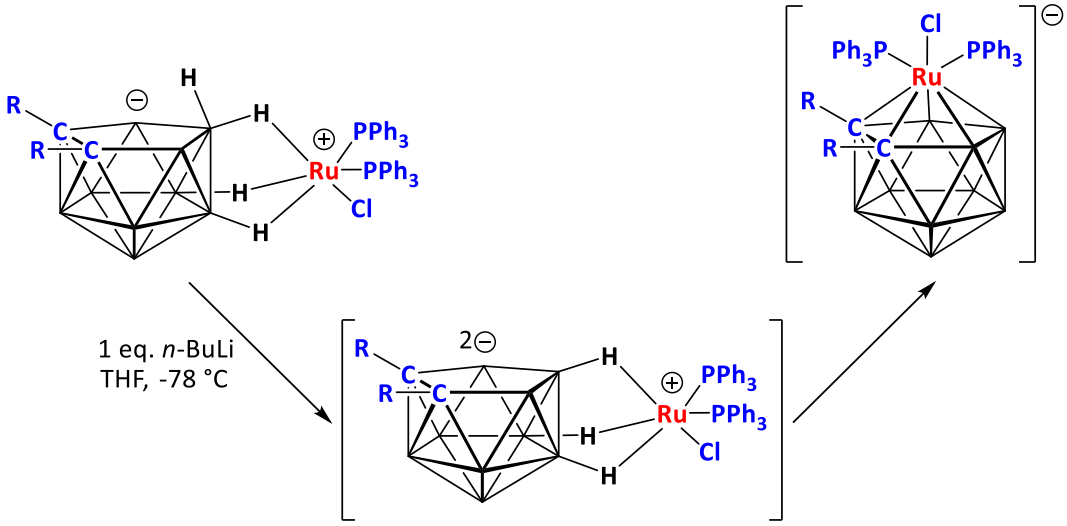

Figure 3.3.2: Postulated synthesis of [1,2-R_2-3-Cl-3,3-$(PPh_3)_2$-*closo*-3,1,2-$RuC_2B_9H_9]^-$ *via* deprotonation of 5,6,10-[$Cl(Ph_3P)_2Ru$]-5,6,10-μ-$(H)_3$-7,8-R_2-10-H-7,8-$C_2B_9H_6$ (R=Me or H).

This hypothesis was tested by reacting 5,6,10-[$Cl(Ph_3P)_2Ru$]-5,6,10-μ-$(H)_3$-10-H-7,8-$C_2B_9H_8$ (**V**), prepared by literature methods,[4] with *n*-BuLi, as shown in figure 3.3.3. This generated the literature species [3-Cl-3,3-$(PPh_3)_2$-*closo*-3,1,2-$RuC_2B_9H_{11}]^-$ (**VI**), as confirmed by $^{11}B\{^1H\}$ NMR spectroscopy.[8] It was also found that **VI** was extremely air-sensitive, a phenomenon not commented on by Chizhevsky and co-workers.

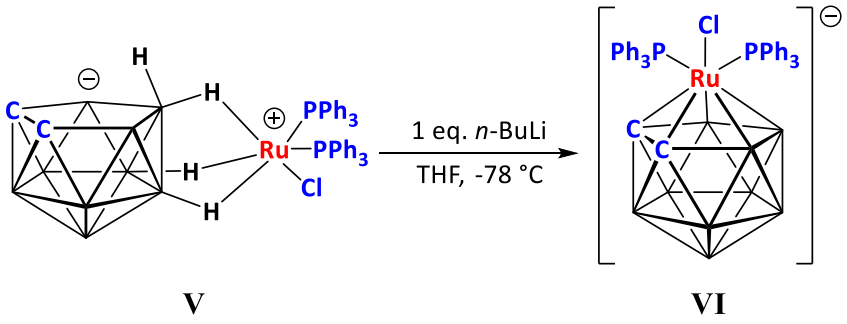

Figure 3.3.3: Synthesis of [3-Cl-3,3-$(PPh_3)_2$-*closo*-3,1,2-$RuC_2B_9H_{11}]^-$ (**VI**).

Based on the air-sensitive nature of **VI**, the decision was made that this species and any analogous species should be synthesised and used *in situ* in order to prevent decomposition. In such cases the solvent would have to be removed *in vacuo* and replaced with CH_2Cl_2, a non-coordinating solvent, before abstracting Cl^- with $Ag[BF_4]$ to produce a generic *hypercloso* species of formula $(PPh_3)_2RuR_2C_2B_9H_9$, as shown in figure 3.3.4.

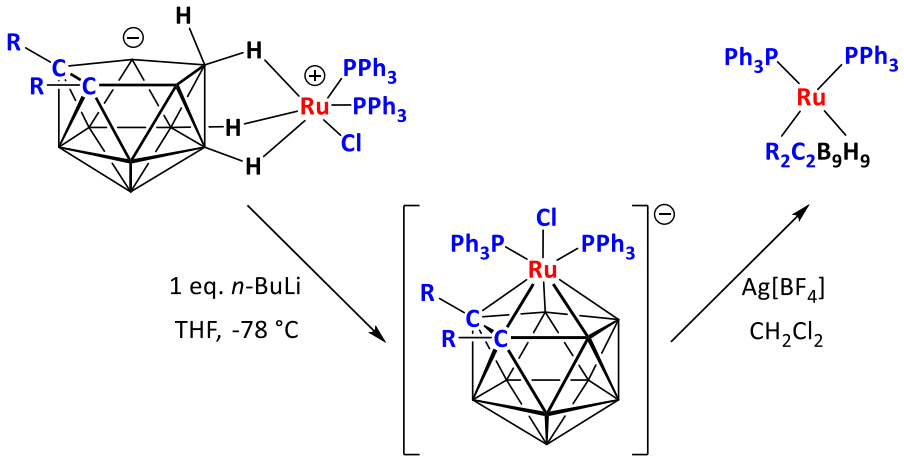

Figure 3.3.4: Proposed synthesis of generic *hypercloso* species $(PPh_3)_2RuR_2C_2B_9H_9$ *via* generation and *in situ* reaction of $[1,2\text{-}R_2\text{-}3\text{-}Cl\text{-}3,3\text{-}(PPh_3)_2\text{-}closo\text{-}3,1,2\text{-}RuC_2B_9H_9]^-$ with $Ag[BF_4]$ (R=Me or H).

3.4 Synthesis of Mixed-Ligand *Closo* Ruthenacarboranes

Abstraction of Cl^- from a species of general formula [1,2-R_2-3-Cl-3,3-$(PPh_3)_2$-*closo*-3,1,2-$RuC_2B_9H_9$]$^-$ in the absence of any coordinating ligands provides a potential route to *hypercloso* ruthenacarboranes. In addition to this, it would be possible to abstract Cl^- in the presence of an L type ligand. Assuming the combined steric bulk of ligands and the carborane cage is not excessive, this should produce in high yield air-stable *closo* species of general formula 1,2-R_2-3-L-3,3-$(PPh_3)_2$-*closo*-3,1,2-$RuC_2B_9H_9$, as shown in figure 3.4.1. This methodology would provide clear evidence that Cl^- could indeed be abstracted from this family of ruthenacarboranes by Ag[BF_4], thereby generating a vacant coordination site that is then filled by an L type ligand. This approach also offers a new route to a wide range of mixed ligand ruthenacarboranes. There is a limited number of mixed ligand ruthenacarboranes containing phosphine ligands, despite the large number of ruthenacarboranes containing phosphine ligands.

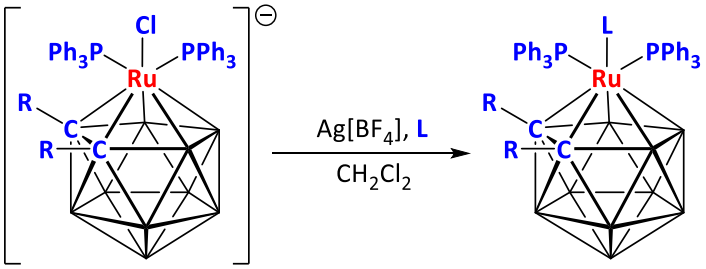

Figure 3.4.1: Synthesis of generic mixed-ligand ruthenacarborane 1,2-R_2-3-L-3,3-$(PPh_3)_2$-*closo*-3,1,2-$RuC_2B_9H_9$ *via* abstraction of chloride in the presence of an L type ligand (R=Me or H).

In order to test this methodology, Li**VI** was prepared and then reacted *in situ* with Ag[BF_4] in the presence of CO gas. It was by this route that the literature species 3,3-$(PPh_3)_2$-3-CO-*closo*-3,1,2-$RuC_2B_9H_{11}$ (**VII**) was synthesised, as shown in figure 3.4.2, as confirmed by $^{11}B\{^1H\}$ and $^{31}P\{^1H\}$ NMR spectroscopy.[11,12]

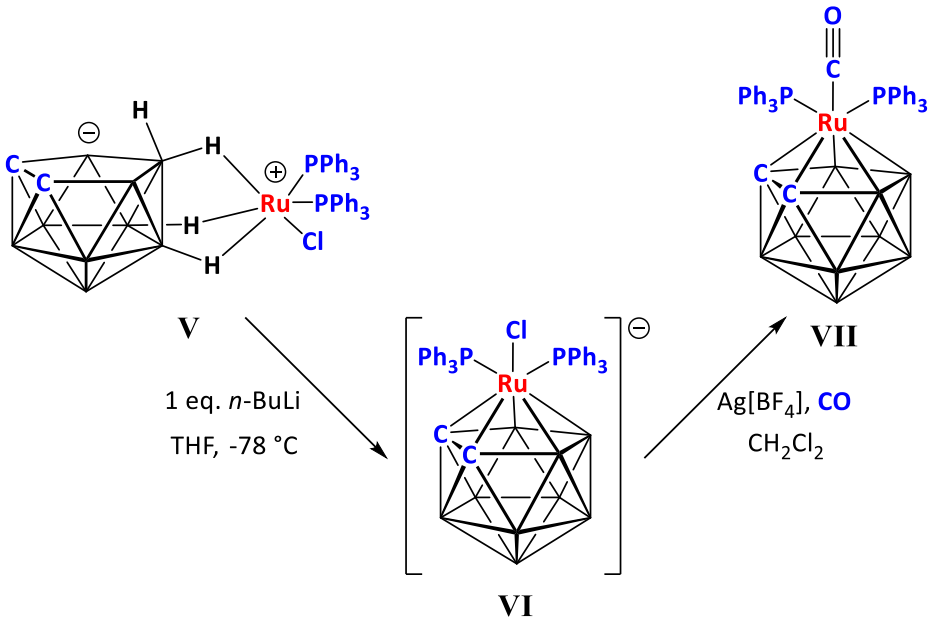

Figure 3.4.2: Synthesis of 3,3-$(PPh_3)_2$-3-CO-*closo*-3,1,2-$RuC_2B_9H_{11}$ (**VII**).

Two new ruthenacarboranes 3,3-$(PPh_3)_2$-3-^{t}BuNC-*closo*-3,1,2-$RuC_2B_9H_{11}$ (**5**) and 3-PPh_3-3,3-$(PMe_3)_2$-*closo*-3,1,2-$RuC_2B_9H_{11}$ (**6**) were synthesised using similar methods, as shown in figure 3.4.3.

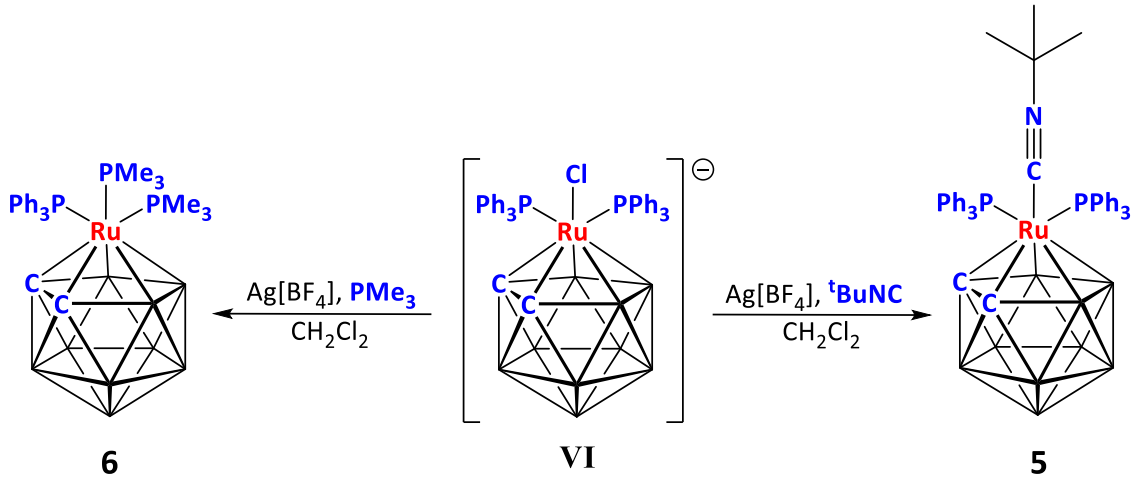

Figure 3.4.3: Synthesis of 3,3-$(PPh_3)_2$-3-^{t}BuNC-*closo*-3,1,2-$RuC_2B_9H_{11}$ (**5**) and 3-PPh_3-3,3-$(PMe_3)_2$-*closo*-3,1,2-$RuC_2B_9H_{11}$ (**6**).

The ^{1}H NMR spectrum of **5** is consistent with the proposed structure, containing two multiplets in the aromatic region relating to the two PPh_3 ligands with a combined integral of 30 and a singlet relating to the ^{t}BuNC ligand with a relative integral of nine. The

spectrum contains a single CH resonance of relative integral two, suggesting that the two CH units are equivalent in solution on the NMR timescale. The $^{31}P\{^{1}H\}$ NMR spectrum obtained indicates the existence of one phosphorus environment, meaning the two PPh_3 ligands must also be equivalent in solution on the NMR timescale. The $^{11}B\{^{1}H\}$ NMR spectrum of **5** could therefore contain up to six signals of relative integral 1:1:1:2:2:2. It instead contains four signals of relative integral 1:1:3:4 (from high frequency to low frequency). This can be explained by overlap of signals within the $^{11}B\{^{1}H\}$ NMR spectrum. Elemental analysis is consistent with the proposed formula.

In the case of **5**, the ^{1}H NMR spectrum indicates that only one ^{t}BuNC ligand has added to the metal centre, as anticipated. However, in the case of **6** the ^{1}H NMR spectrum suggests that two PMe_3 ligands have coordinated to the metal centre, displacing one PPh_3, as the aromatic signal attributable to PPh_3 has a relative integral of 15, whilst the singlet attributable to PMe_3 has a relative integral of 18. This is surprising as only one equivalent of PMe_3 was used and is likely due to steric factors. Both ^{t}BuNC and CO are linear ligands whereas PMe_3 is a conical ligand. Therefore, ^{t}BuNC and CO are small enough add to the ruthenium centre without displacing PPh_3 (in the cases of **5** and **VII**, respectively), whereas the larger, conical PMe_3 is presumably too large to do this without displacing PPh_3. Additionally, elemental analysis is consistent with the proposed formula.

The $^{31}P\{^{1}H\}$ NMR spectrum of **6** indicates the existence of two phosphorus environments, one for the PPh_3 ligand, which is split by two equivalent PMe_3 ligands, producing a triplet, and one for the two equivalent PMe_3 ligands, split by the PPh_3 ligand, producing a doublet. The $^{11}B\{^{1}H\}$ NMR spectrum contains four signals of relative integral 1:1:4:3 (from high frequency to low frequency), a divergence from the anticipated six signals of relative integral 1:1:1:2:2:2 which can be explained by overlap of signals.

The molecular structures of **5** and **6** are shown in figures 3.4.4 and 3.4.5, respectively.

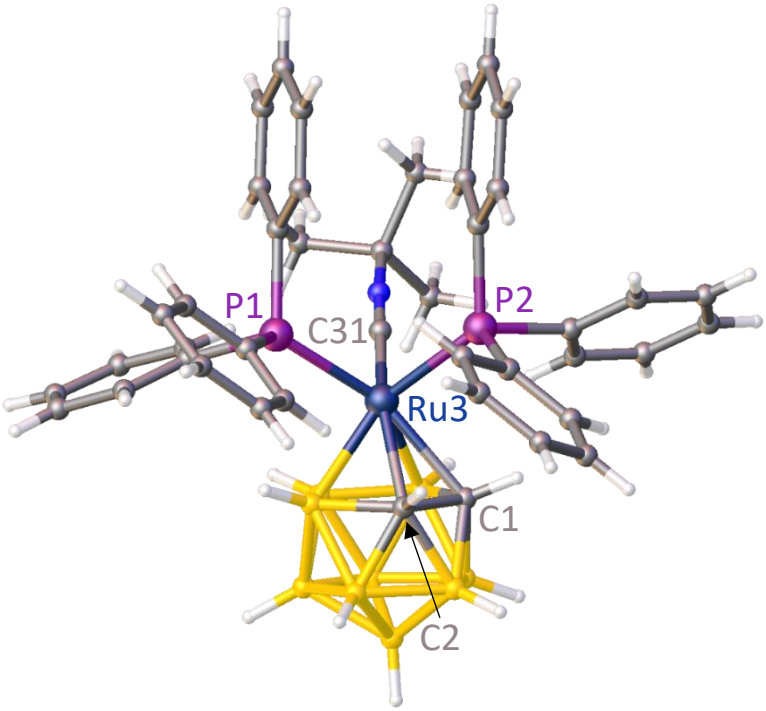

Figure 3.4.4: Structure of 3,3-$(PPh_3)_2$-3-^{t}BuNC-*closo*-3,1,2-$RuC_2B_9H_{11}$ (**5**).

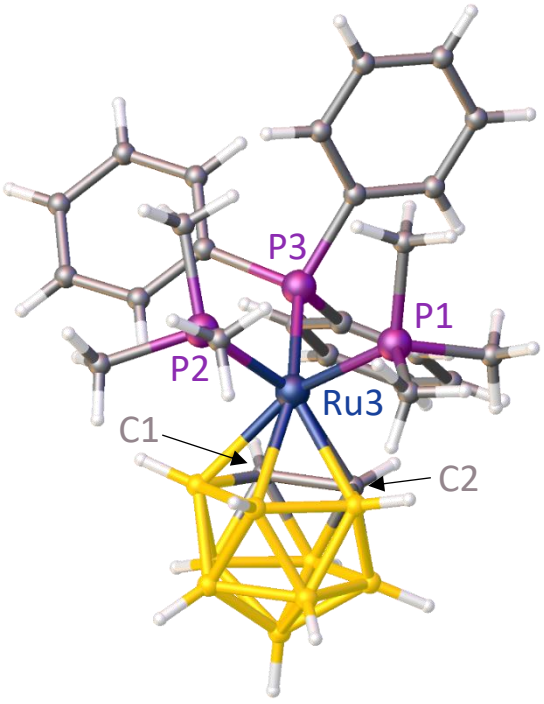

Figure 3.4.5: Structure of 3-PPh_3-3,3-$(PMe_3)_2$-*closo*-3,1,2-$RuC_2B_9H_{11}$ (**6**).

As can be seen from the structure of **5**, one PPh_3 (P2) ligand lies *trans* to cage boron atoms whilst the ^{t}BuNC ligand and the other PPh_3 (P1) ligand lie relatively *trans* to cage carbon atoms. In this case the ^{t}BuNC ligand is slightly more *trans* to the cage carbon atoms than P1. This observation can be quantised using the modulus of the torsion angle (θ) of the ligands relative to the cage carbon atoms. For metallacarboranes, the torsion angle of a given ligand (L) is L-M-X-Y, where M is the metal vertex, X is the centroid of the C_2B_3 face bound to the metal and Y is the centroid of the two carbon atoms (or the lone carbon atom in the open face for 2,1,8-MC_2B_9 isomers). An illustration of this is given for the literature species 3-Cl-3,3-$(PPhMe_2)_2$-*closo*-3,1,2-$CoC_2B_9H_{11}$ in figure 3.4.6.[13] A large |θ| indicates the ligand in question sits *trans* to the two cage carbon atoms, where as a small |θ| indicates the ligand sits *cis* to the cage carbon atoms. These two ligands will be relatively strongly and relatively weakly bound to the metal, respectively, as explained in section 2.4.

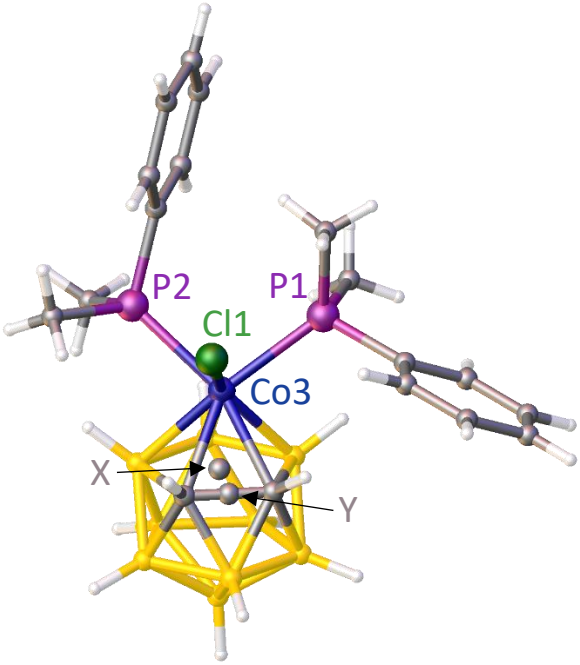

Figure 3.4.6: Structure of 3-Cl-3,3-$(PPhMe_2)_2$-*closo*-3,1,2-$C_2B_9H_{11}$ with C1C2B3B7B8 centroid (X) and C1C2 centroid (Y) displayed.[13]

In the case of **5** the |θ| of P1 is 116.92(4)°, smaller than that of the ^{t}BuNC ligand at 131.84(8)°. The fact that it is a PPh_3 (P2) ligand which lies *trans* to the cage boron atoms [|θ| of 15.94(8)°] suggests that ^{t}BuNC is a stronger ligand than PPh_3, a hypothesis given further support by the fact that the ^{t}BuNC ligand is more *trans* to the cage carbon atoms

than the other PPh_3 ligand (P1). The distance between Ru3 and P1 is significantly shorter than that between Ru3 and P2, at 2.3356(4) Å and 2.3569(4) Å, respectively. This is to be expected, as P1 has a larger |θ| and is therefore more strongly bound. The torsion angles of the three ligands are as expected for a metallacarborane with two ligands with relatively strong STEs and one with a relatively weak STE, in that the strong ligand is almost perfectly *trans* to one of the cage carbon atoms (C2) whilst the two weak ligands have very different values for |θ|.[14] A comparison of the bond lengths and torsion angles of the three ligands is given in table 3.4.1.

Ligand	Torsion angle (θ)	Ru-L bond length (Å)
^{t}BuNC	131.84(8)°	1.9303(16)
PPh_3 (P1)	-116.92(4)°	2.3356(4)
PPh_3 (P2)	15.94(8)°	2.3569(4)

Table 3.4.1: Torsion angles and Ru-L lengths of ligands in **5**.

The molecular structure of **6** confirms that one PPh_3 ligand has been displaced, as was inferred from the ^{1}H and $^{31}P\{^{1}H\}$ NMR spectra. Both of the PMe_3 groups have large |θ| values, 103.50(9)° and 144.36(8)° for P1 and P2, respectively. Conversely, the PPh_3 (P3) ligand is *trans* to cage boron atoms and has a much lower |θ| accordingly, at 19.92(10)°, as shown in table 3.4.2. This suggests that PMe_3 is a stronger ligand than PPh_3. However, despite P2 having a significantly larger |θ| than P1, the Ru3-P2 bond length is actually slightly longer than that between Ru3 and P1, at 2.3376(6) Å and 2.3366(6) Å, respectively. However, this difference is not statistically significant. The orientation of the ligands in **6** is typical of a metallacarborane containing two ligands with strong STEs and one ligand with a weak STE in that the PPh_3 ligand has |θ| of between 0° and 15° whilst the two stronger PMe_3 ligands have |θ| values that are approximately 40° apart.[14]

Ligand	Torsion angle (θ)
PMe_3 (P1)	-103.50(9)°
PMe_3 (P2)	144.36(8)°
PPh_3 (P3)	19.92(10)°

Table 3.4.2: Torsion angles of ligands in **6**.

3.5 Attempts to Synthesise *Hypercloso* $(PPh_3)_2RuC_2B_9H_{11}$

The fact that steric factors caused the displacement of one PPh_3 ligand in the synthesis of **6** has positive implications with regards to the objective of synthesising a *hypercloso* species of formula $(PPh_3)_2RuR_2C_2B_9H_9$. This is because it suggests that said species would have significant steric protection around the ruthenium centre. Towards this end, a reaction between **VI** and $Ag[BF_4]$ was carried out in the absence of any donor ligand with the intention of making a *hypercloso* species of formula $(PPh_3)_2RuC_2B_9H_{11}$. In order to prevent coordination to the vacant site on the ruthenium generated by abstraction of Cl^- it was necessary to carry out the reaction with $Ag[BF_4]$ in a non-coordinating solvent, CH_2Cl_2 in this case. The intended synthesis is shown in figure 3.5.1.

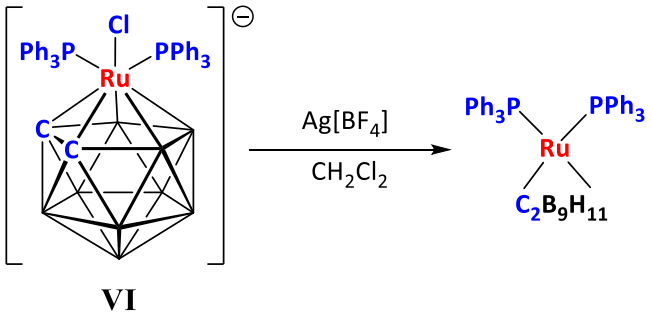

VI

Figure 3.5.1: Proposed synthesis of *hypercloso* $(PPh_3)_2RuC_2B_9H_{11}$.

However, this reaction does not cleanly produce the desired species. Instead, a wide range of species were formed, a fact reflected by the complexity of the resultant preparative TLC plates, shown in figure 3.5.2, on which over ten bands were present. Some components were found to be unstable and decomposed before they could be isolated. Other bands were found to be impossible to purify, as they consisted of bands that overlapped with other bands, often with a degree of streaking. Attempts to isolate various components were further complicated by the fact that each band was produced in very low yield with some components being produced in trace amounts too small for spectroscopic or crystallographic analysis. Additionally, not all components were found by $^{11}B\{^1H\}$ NMR spectroscopy to contain boron.

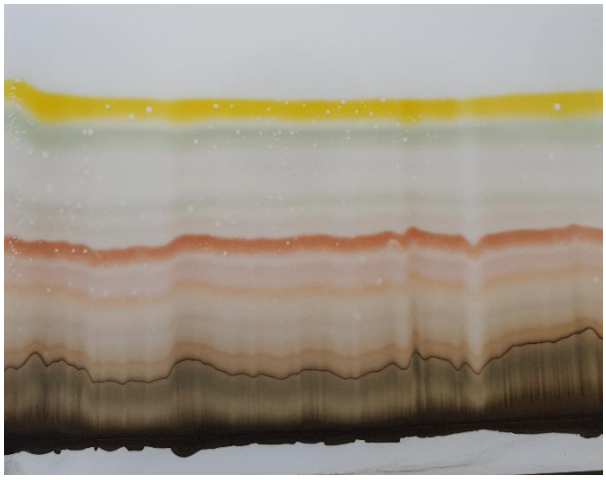

Figure 3.5.2: Preparative TLC plate from reaction of **VI** and $Ag[BF_4]$.

One of the bands (**7**) that was isolated contains an unusually high frequency shift in the $^{11}B\{^1H\}$ NMR spectrum, displayed in figure 3.5.3, a feature characteristic of *hypercloso* species. However, the $^{11}B\{^1H\}$ NMR spectrum contains at least eleven resonances, which is inconsistent with the desired compound, $(PPh_3)_2RuC_2B_9H_{11}$. Additionally, the combined integrals of the signals produced are equal to approximately 18 (when the signal at 61.3 ppm is referenced as one), as opposed to the maximum of nine that would be expected. Both of these observations suggest that the species in question is not the desired one but instead is a species that contains more than one C_2B_9 cage.

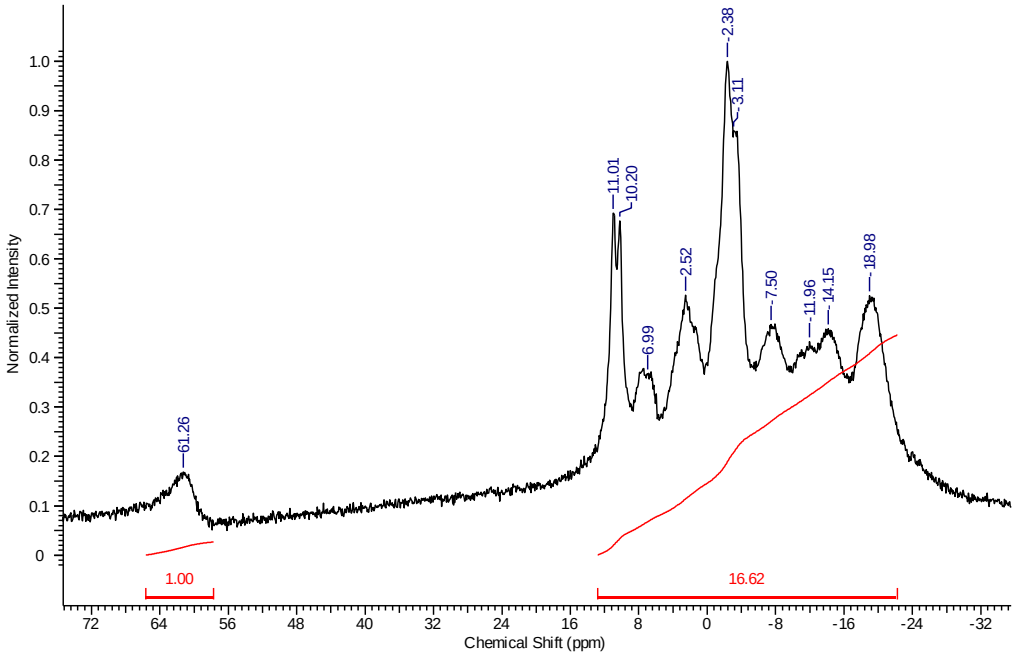

Figure 3.5.3: $^{11}B\{^1H\}$ NMR spectrum of **7**.

The ^{1}H NMR spectrum contains four distinct CH resonances, as identified by the characteristic broad singlet produced, of relative integral 1:1:1:1. Additionally, the $^{1}H\{^{11}B\}$ NMR spectrum contains twelve BH resonances, which have a combined integral of more than nine. Both of these observations also suggest the presence of more than one cage, with the ^{1}H NMR spectrum suggesting the presence of two inequivalent cages specifically. The $^{1}H\{^{11}B\}$ NMR spectrum contains a signal at -8.39 ppm which is not present in the ^{1}H NMR spectrum, indicating a hydridic BH, interpreted as being caused by a M-H-B interaction. Furthermore, the aromatic region of the ^{1}H NMR spectrum contains a multiplet which has a relative integral of 30 when each CH signal is assigned an integral of one, suggesting there is only one molecule of PPh_3 present per cage. The $^{31}P\{^{1}H\}$ NMR spectrum contains two signals, suggesting the phosphines are inequivalent. Elemental analysis of **7** is also inconsistent with the desired compound, with the observed percentage of carbon being over 10% lower than would be expected. It is not possible to deduce the structure of **7** from the spectroscopic data obtained alone. However, repeated efforts to crystallise this species from CH_2Cl_2/petrol and C_6H_5F/petrol were unsuccessful. A suggestion as to the structure of **7** is given in section 3.6.

A further two bands were isolated and characterised by ^{1}H, $^{11}B\{^{1}H\}$ and $^{31}P\{^{1}H\}$ NMR spectroscopy. The first, **8**, was found to produce similar spectra to **7**. The $^{11}B\{^{1}H\}$ NMR spectrum produced, shown in figure 3.5.4, contains remarkable similarities to that of **7**, also shown in figure 3.5.4, including a broad singlet at high frequency (58.6 ppm). A more striking similarity is that both spectra contain overlapping resonances from *ca.* 10 to -20 ppm which are extremely similar in appearance. Additionally, the combined integrals of signals in the $^{11}B\{^{1}H\}$ NMR spectrum combine to more than nine when the high frequency resonance is assigned a relative integral of one, suggesting the presence of more than one cage.

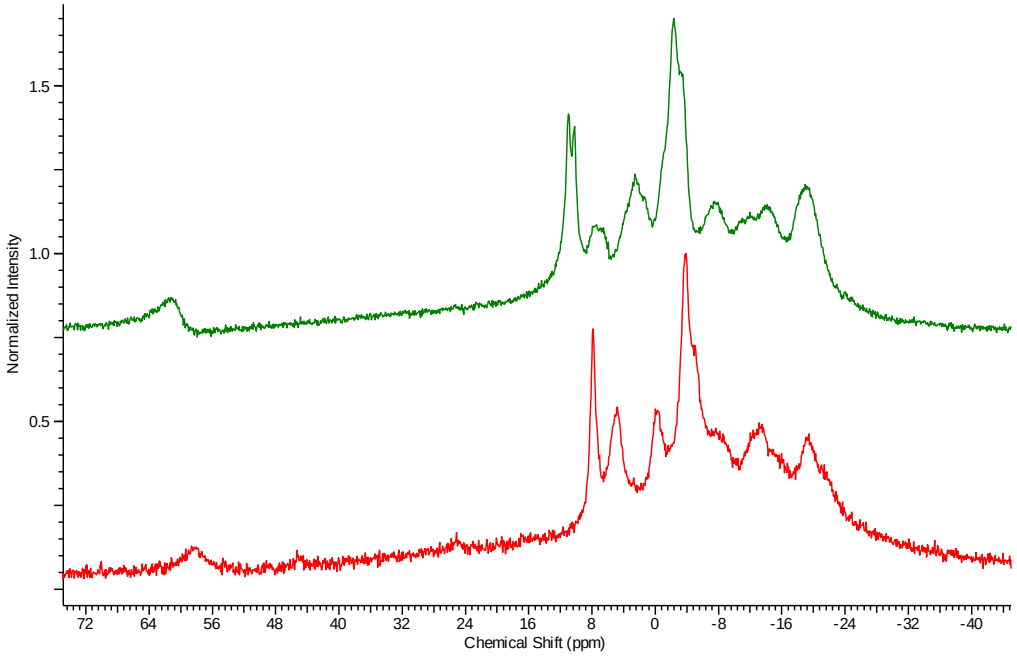

Figure 3.5.4: Overlaid $^{11}B\{^{1}H\}$ NMR spectra of **7** and **8** in green and red, respectively.

There are also commonalities in the ^{1}H NMR spectra of **8** and **7**, as both contain four distinct CH resonances and a multiplet in the aromatic region with a relative integral of 30. This suggests that, like **7**, **8** contains one PPh_3 ligand per cage and more than one cage. The $^{31}P\{^{1}H\}$ spectrum of **8** also contains similarities to that of **7**, containing two singlets, both of which are within 1 ppm of the analogous signals produced by **7**. However, **8** was found to decompose over time and could therefore not be crystallised, inhibiting determination of the molecular structure of said species.

The final component to be isolated, **9**, was also found to produce similar spectra to **7** and **8**. The $^{11}B\{^{1}H\}$ NMR spectrum of **9**, shown in figure 3.5.5, contains similarities to that of **7** and **8**, including a high frequency signal (at 54.9 ppm) and a collection of overlapping signals that are of similar appearance and have similar chemical shifts to analogous envelopes found in the $^{11}B\{^{1}H\}$ NMR spectra of **7** and **8**. However, **9** also has two additional relatively high frequency shifts, at 15.8 and 25.1 ppm. The fact that the combined integrals of the signals produced combine to approximately eighteen (when the signal at 54.9 ppm is assigned a relative integral of one) once again suggests the presence of two inequivalent cages.

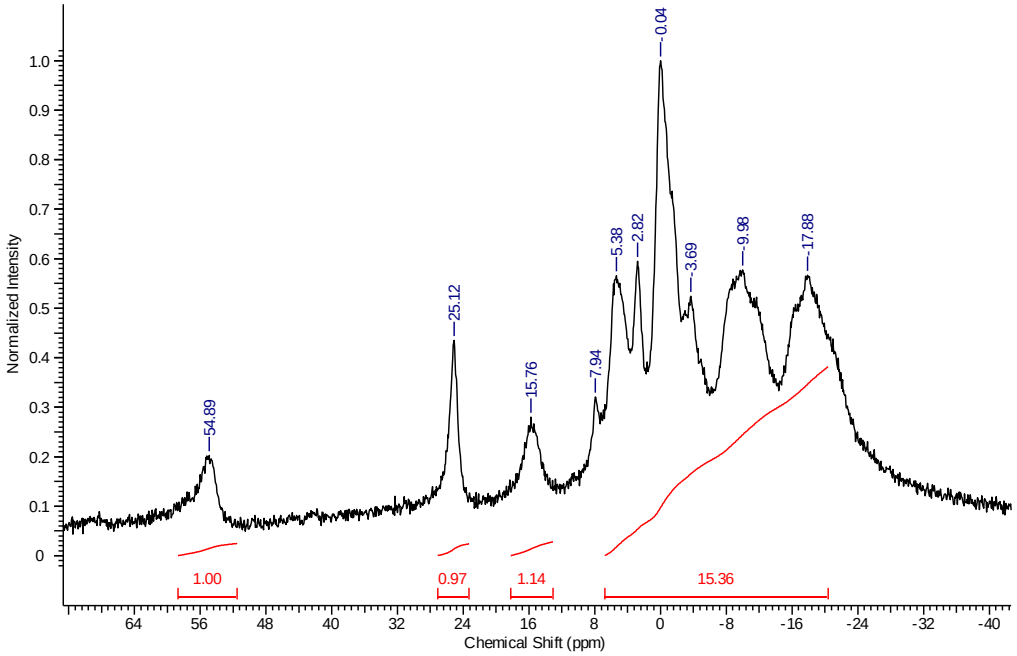

Figure 3.5.5: $^{11}B\{^{1}H\}$ NMR spectrum of **9**.

In addition, like the ^{1}H NMR spectra of **7** and **8**, the ^{1}H NMR spectrum of **9** contains four distinct CH resonances, of relative integral 1:1:1:1, which once again suggests that two inequivalent cages are present. The sum of the combined integrals of the signals generated by aromatic groups is equal to 30, suggesting that there is one PPh_3 molecule present per cage. Finally, the $^{31}P\{^{1}H\}$ NMR spectrum contains two singlet resonances with similar chemical shifts to those of **7** and **8**. However, the structure of **9** was not able to be crystallographically determined as crystals could not be grown despite repeated efforts at crystallisation from CH_2Cl_2/petrol and C_6H_5F/petrol, something made more difficult by the trace amount of material obtained. Compound **9** was found to decompose in THF. Despite this, a reasonable suggestion as to the structures of **7**, **8** and **9** is given in 3.6.

3.6 Attempts to Synthesise *Hypercloso* $(PPh_3)_2RuMe_2C_2B_9H_9$

Repeated attempts to crystallise **7** and **9** were unsuccessful despite the stability of both compounds. It was hypothesised that if an analogous species containing different functional groups on the cage carbon atoms could be isolated then it may be possible to crystallise said species, allowing subsequent crystallographic determination of the molecular structure. This could then provide suggestions as to the molecular structures of **7**, **8** and **9**. To this end the literature species 5,6,10-$[Cl(Ph_3P)_2Ru]$-5,6,10-μ-$(H)_3$-7,8-Me_2-10-H-7,8-$C_2B_9H_6$ (**VIII**)[4] was synthesised before undergoing sequential reaction with *n*-BuLi and $Ag[BF_4]$, as shown in figure 3.6.1.

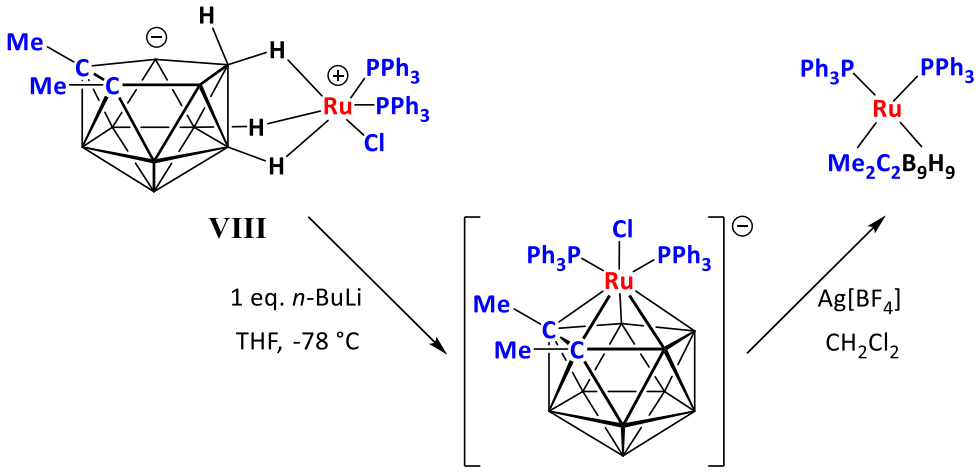

Figure 3.6.1: Proposed synthesis of $(PPh_3)_2RuMe_2C_2B_9H_9$.

The reaction produced a complex product mixture containing a large number of components. The TLC plates produced were similar in appearance to the plates generated by the reaction of **VI** and $Ag[BF_4]$ in that they were very complex, containing over ten bands. However, many components either decomposed, were found by $^{11}B\{^1H\}$ NMR spectroscopy not to contain boron or were impossible to purify from other components with similar R_f values. Some components were produced in trace amounts too small to acquire spectroscopic data from which any reasonable inferences about their structure could be made. Small amounts of regenerated **VIII** were also isolated.

However, one of the bands that was isolated (**10**) was found to contain a relatively high frequency shift in its $^{11}B\{^1H\}$ NMR spectrum, a property characteristic of *hypercloso*

species, at 35.7 ppm. Unlike those of **7**, **8** and **9**, the $^{11}B\{^{1}H\}$ NMR spectrum of **10** does not contain evidence for more than one cage, as the spectrum only contains four signals. The ^{1}H NMR spectrum also does not contain evidence for the presence of more than one cage, with only two signals for the methyl groups of relative integral 1:1. However, the ^{1}H NMR spectrum is inconsistent with the desired compound, $(PPh_3)_2RuMe_2C_2B_9H_9$, as if the two inequivalent methyl signals are each assigned relative integrals of three then the aromatic signals present have a combined relative integral of 15, which is insufficient to be consistent with the proposed structure. A limited amount of information can be gained from the $^{31}P\{^{1}H\}$ NMR spectrum, which contains only a single resonance. Similarly to the $^{1}H\{^{11}B\}$ NMR spectrum of **7**, the $^{1}H\{^{11}B\}$ NMR spectrum of **10** contains a low frequency shift, at -3.77 ppm. This signal does not appear in the ^{1}H NMR spectrum, consistent with this signal arising from a M-H-B interaction. However, unlike the $^{1}H\{^{11}B\}$ NMR spectrum of **7**, the $^{1}H\{^{11}B\}$ NMR spectrum of **10** only contains five BH signals which have a combined integral of sixteen when the aromatic region is assigned a relative integral of 30. It is suspected that the remaining two BH signals cannot be located as they overlap with the residual water peak present. Therefore, the $^{11}B\{^{1}H\}$, ^{1}H and $^{1}H\{^{11}B\}$ NMR spectra of **10** do not contain evidence for the presence of more than one cage.

Attempts to crystallise **10** from CH_2Cl_2/petrol were successful, although this required repeated attempts and even then produced relatively small crystals. The molecular structure of **10** was determined and revealed to be [7,8′-*exo*-(Ru{PPh_3}$_2$)-7,8′-μ-$(H)_2$-*commo*-3,3′-Ru(1,2-Me_2-1,2-$C_2B_9H_8$)(1′,2′-Me_2-1′,2′-$C_2B_9H_8$)], a species which in the solid state contains two inequivalent cages, as shown in figure 3.6.2. The observed structure in the solid state is not suggested by the ^{1}H, $^{1}H\{^{11}B\}$, ^{11}B and $^{31}P\{^{1}H\}$ NMR spectra.

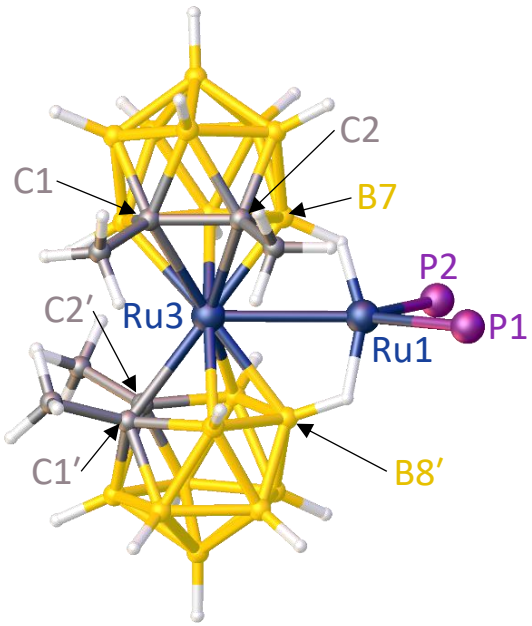

Figure 3.6.2: Structure of [7,8′-*exo*-(Ru{PPh$_3$}$_2$)-7,8′-μ-(H)$_2$-*commo*-3,3′-Ru(1,2-Me$_2$-1,2-C$_2$B$_9$H$_8$)(1′,2′-Me$_2$-1′,2′-C$_2$B$_9$H$_8$)] (**10**) (phenyl units omitted for clarity).

Compound **10** is an unusual species. Firstly, it is only the second known RuSAN analogue based on two C_2B_9 cage units whose structure has been crystallographically determined. Secondly, it is a bis-carborane sandwich compound that contains an additional metal centre *exo* to the cage, an uncommon category of species. The distance between the two Ru atoms is 2.7643(16) Å, well within the range of Ru-Ru bonds reported in the literature, some examples of which are given in table 3.6.1.[15–17] The molecule can therefore be considered to have a Ru-Ru bond. Only two other crystallographically-determined metallacarborane sandwich complexes containing a metal-metal bond have been reported, [(Me$_2$C$_2$B$_4$H$_4$)$_2$Fe]Fe[(OMe)$_2$C$_2$H$_4$] and [({SiMe$_3$}$_2$C$_2$B$_4$H$_4$)$_2$Mn]Mn[(NMe$_2$)$_2$C$_2$H$_4$], both of which consist of two seven vertex cages.[18,19] The former compound is referred to by Grimes as a "wedged" complex, as it contains an atom (the *exo*-polyhedral Fe atom) in a wedging position in the crevice between the two carborane cages. This is a term applicable to **10** as Ru1 is also in a wedging position. To the best of our knowledge **10** is the first twelve vertex metallacarborane sandwich compound containing a metal-metal bond. Other twelve vertex metallacarborane sandwich compounds containing an additional metal atom *exo* to the cluster, such as [4,8,8′-*exo*-(CuPPh$_3$)-4,8,8′-μ-(H)$_3$-*commo*-3,3′-Co(1,2-C$_2$B$_9$H$_9$)(1′,2′-C$_2$B$_9$H$_{10}$)], reported by Chizhevsky and co-workers, do not contain a metal-metal bond; in this case as the authors conclude that the Co-Cu distance is too large, at 2.888 Å.[20]

Species	Ru-Ru bond length (Å)
10	2.7644(16)
$Cp_2Ru_2(\mu\text{-}CO)_2(CO)_2$	2.7412(4)
$[NBu_4][Ru_2(acac)_4Cl_2]$	2.3007(6)
$Ru_3(CO)_{12}$	2.8512(5), 2.8518 (5), 2.8596(5)

Table 3.6.1: A comparison of Ru-Ru bonds in **10** and a range of literature compounds (acac = $CH_3COCHCOCH_3$).[15–17]

The electron count of both Ru3 and Ru1 can be rationalised by conceptualising **10** as consisting of a $[(1,2\text{-}Me_2\text{-}1,2\text{-}C_2B_9H_9)_2Ru]^{2-}$ fragment and a $\{Ru(PPh_3)\}^{2+}$ fragment. This considers the RuSAN core in terms comparable to that of $[(1,2\text{-}C_2B_9H_{11})_2Fe]^{2-}$, a species which is directly comparable as both Fe and Ru are group eight metals. Under this model, Ru3 has eighteen electrons, a valence electron count of eight plus four electrons from each carboranyl ligand as well as an additional two from the dianionic charge, as shown in table 3.6.2. The other ruthenium atom, Ru1, has an electron count of sixteen, as shown in table 3.6.3, as it loses two from the dicationic charge but receives four from the two PPh_3 ligands, two each from two Ru-H-B interactions and two from a dative Ru3→Ru1 bond.

	Number of electrons available	Cumulative electron count
Valence electrons	8	8
$2xMe_2C_2B_9H_9$	2x4=8	16
Dianionic charge	2	18

Table 3.6.2: Electron counting for Ru3 of **10**.

	Number of electrons available	Cumulative electron count
Valence electrons	8	8
2xPPh_3	2x2=4	12
2xRu-H-B	2x2=4	16
Dicationic charge	-2	14
Ru3→Ru1 bond	2	16

Table 3.6.3: Electron counting for Ru1 of **10**.

The $RuMe_2C_2B_9H_9$ cages in **10** are *closo* in both structure and electron count. Results from the synthesis of compounds **VII**, **5** and **6** confirm that Cl^- can be abstracted from **VI** using $Ag[BF_4]$. This strongly implies that *hypercloso* $(PPh_3)_2RuMe_2C_2B_9H_9$ is indeed being formed but is not stable. This is believed to be because either the process of going from a species which has a *hypercloso* electron count but a *closo* structure to one which has both a *hypercloso* electron count and structure is unfavourable or that the latter species is simply unstable. Instead a complex product mixture is generated, of which one component is **10**. One explanation for why **10** is generated instead of the desired species is that heteroboranes have a strong preference for *closo* electron counts over *hypercloso* electron counts, an idea supported by the relative dearth of *hypercloso* metallacarboranes known.

A number of things must happen in order for **10** to be generated. Starting from the assumed *hypercloso* species $(PPh_3)_2RuMe_2C_2B_9H_9$, one cage must eject a $\{Ru(PPh_3)_2\}$ fragment, in order to generate a wedging unit which can bond *exo*. This also produces a carborane with an open face that can then bond to the ruthenium atom of another cage in order to form a RuSAN analogue. However, in order for this to happen, the second ruthenium atom must lose both of its phosphine ligands. Both the ejection of a metal fragment from a metallacarborane and the loss of both phosphine ligands from the other ruthenium centre are highly unusual phenomena. It is unclear whether this is a concerted process or a process which occurs in steps, the order of which would also be unclear.

As well as noting that **10** is an unusual species, it also should be observed that there are discrepancies between the solid state molecular structure and the observed ^{1}H, $^{1}H\{^{11}B\}$, $^{11}B\{^{1}H\}$ and $^{31}P\{^{1}H\}$ NMR spectra. As can be seen from the molecular structure of **10** (figure 3.6.2), the molecule has no symmetry. Therefore, in the solid state all 18 boron atoms and all four methyl groups are in different environments, a phenomenon not observed in the $^{11}B\{^{1}H\}$, ^{1}H and $^{1}H\{^{11}B\}$ NMR spectra, all of which contain no evidence to suggest that **10** contains two inequivalent cages. In the case of the $^{11}B\{^{1}H\}$ NMR spectrum one plausible explanation is that the signals overlap, a phenomenon common in the $^{11}B\{^{1}H\}$ NMR spectra of metallacarboranes due to the broadness of the resonances and the limited chemical shift range such species produce.

However, in the case of the ^{1}H NMR spectrum it is more difficult to reconcile the observed lack of symmetry in the solid state with the two sharp singlets observed for the methyl groups, with relative integrals of 1:1, as opposed to the four signals anticipated, as it is impossible to rationalise this discrepancy through simple overlap of resonances due to the sharpness of the signals. Additionally, the $^{31}P\{^{1}H\}$ NMR spectrum contains a single resonance, which is inconsistent with the molecular structure in which the two phosphines are inequivalent. Instead, a potential explanation for these observations is that the molecule is fluxional in solution. This process involves the *exo* $\{Ru(PPh_3)_2\}$ fragment exchanging from being bound to the RuSAN core by one set of Ru-H-B bonds, as is the case in the solid state, as shown in figure 3.6.3, to an alternative pair of Ru-H-B bonds, as is shown figure 3.6.4.

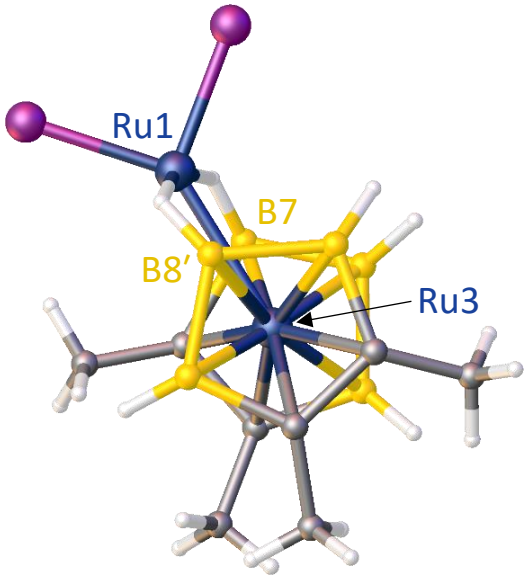

Figure 3.6.3: Molecular structure of **10**, with phenyl units and {BH} units 5-6, 9-12, 5′-6′ and 9′-12′ omitted for clarity.

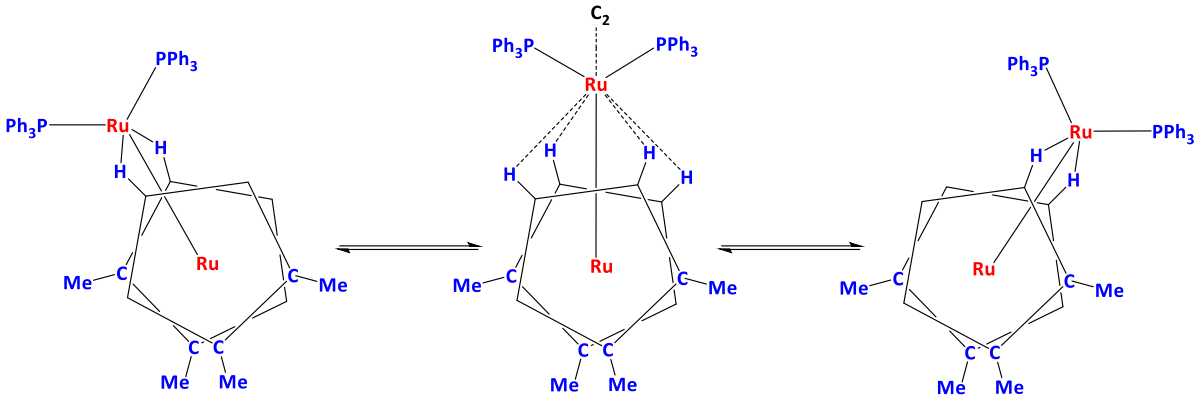

Figure 3.6.4: Proposed mechanism of fluxionality in **10**.

It should be observed that the two pairs of Ru-H-B interactions shown in figure 3.6.4 are equivalent. Under this model, the discrepancies between the crystallographic data and ^{1}H, $^{1}H\{^{11}B\}$, $^{11}B\{^{1}H\}$ and $^{31}P\{^{1}H\}$ NMR spectra are explained by **10** having time-averaged C_2 symmetry in solution.

The molecular structure of **10** allows for some reasonable suggestions as to the structures of **7**, **8** and **9**, given that the latter three species have many common spectroscopic features with **10**. Compounds **7** and **10** contain evidence for Ru-H-B interactions in their $^{1}H\{^{11}B\}$ NMR spectra, whilst all four species contain a single high frequency resonance in their $^{11}B\{^{1}H\}$ NMR spectra. Much of the spectroscopic data obtained for compounds **7**, **8** and **9** are consistent with some sort of RuSAN analogue with an additional *exo* bound $\{Ru(PPh_3)_2\}$ fragment, similar to that of **10**, but in which the *exo* bound $\{Ru(PPh_3)_2\}$ fragment is not fluxional in solution on the NMR timescale. Firstly, the $^{11}B\{^{1}H\}$ and ^{1}H NMR spectra of **7**, **8** and **9** all suggest the presence of two $C_2B_9H_{11}$ cages being present. The ^{1}H NMR spectra of **7**, **8** and **9** also indicate that there is only one molecule of PPh_3 present per cage, which is also consistent with the structure of these species being somewhat analogous with that of **10**. Additionally, the $^{31}P\{^{1}H\}$ NMR spectra of all three species contain two distinct resonances, which is also to be expected for such a species. Finally, elemental analysis of **7** is consistent with the general formula $(PPh_3)_2Ru_2(C_2B_9H_{11})_2$ (Anal. calcd. for $C_{40}H_{52}B_{18}P_2Ru_2$: C, 48.5; H, 5.29: Found, C, 48.1; H, 5.84%). However, the exact molecular structures of **7**, **8** and **9** and the structural differences between them are impossible to infer given the limited spectroscopic information available.

3.7 Chapter Summary

A new synthetic route to ruthenacarboranes of general formula [1,2-R_2-3-Cl-3,3-$(PPh_3)_2$-*closo*-3,1,2-$RuC_2B_9H_9$]$^-$ *via* removal of the *endo* proton from the open face of the appropriate *exo-nido* precursor was discovered, as shown in figure 3.7.1.

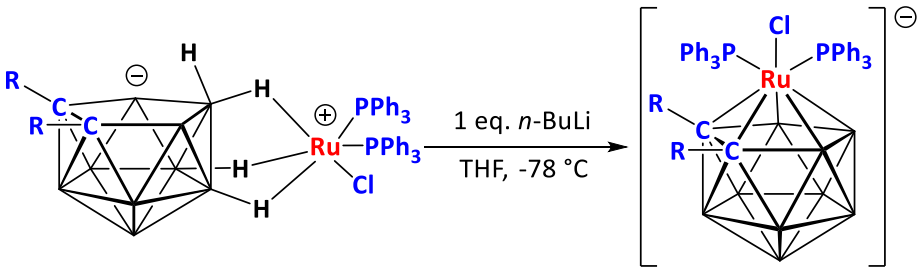

Figure 3.7.1: Synthesis of formula [1,2-R_2-3-Cl-3,3-$(PPh_3)_2$-*closo*-3,1,2-$RuC_2B_9H_9$]$^-$.

Additionally, a new synthetic route to mixed ligand ruthenacarboranes was developed and used to synthesise the literature species 3,3-$(PPh_3)_2$-3-CO-*closo*-3,1,2-$RuC_2B_9H_{11}$ (**VII**) as well as the two new ruthenacarboranes, **5** and **6**, as shown in figure 3.7.2.

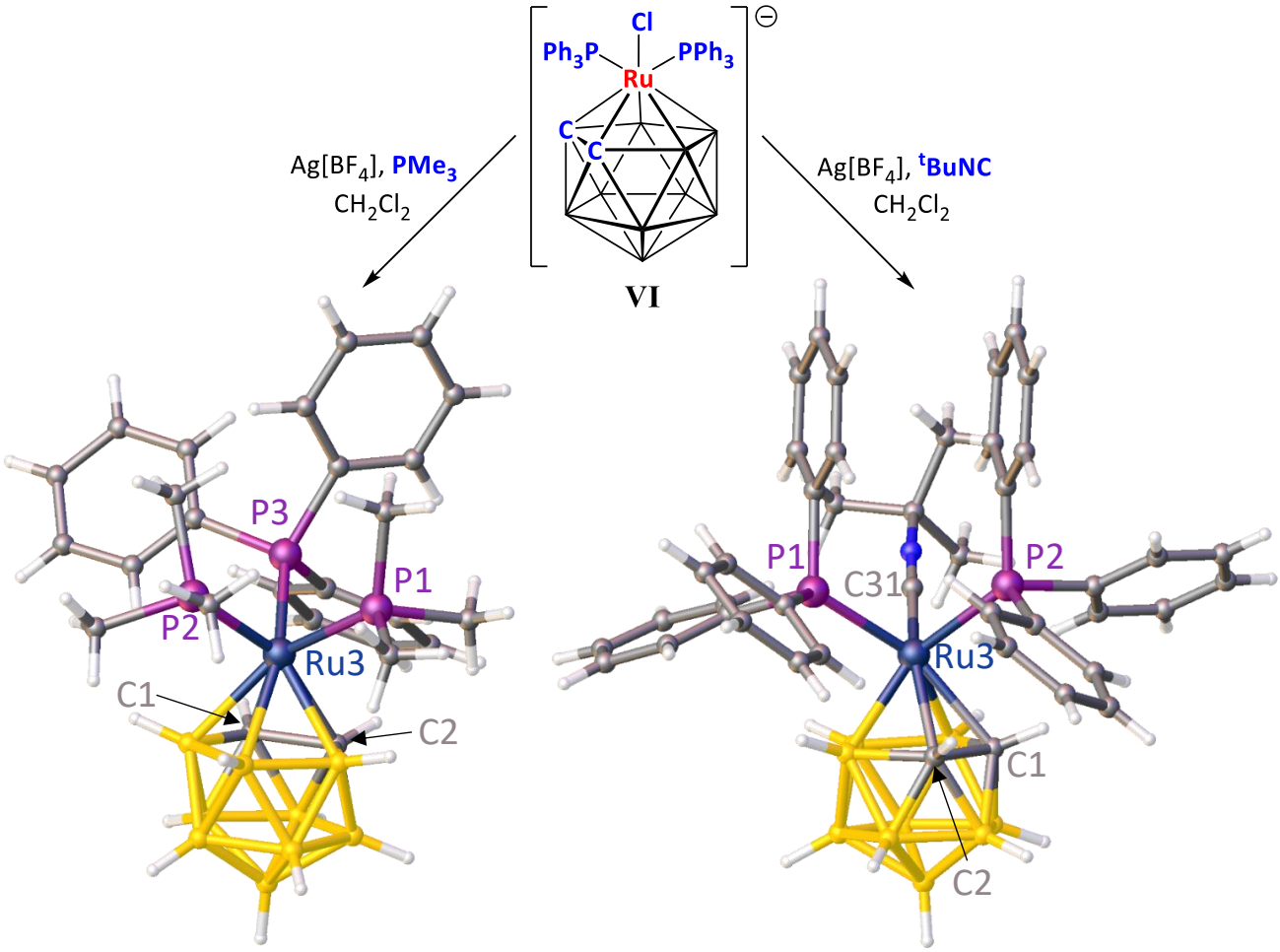

Figure 3.7.2: Synthesis and molecular structures of **5** (right) and **6** (left).

Neither of the sequential reactions of **V**/**VIII** with *n*-BuLi and Ag[BF_4], shown in figures 3.7.3 and 3.7.4, cleanly produced the desired *hypercloso* species. Instead, **10**, shown in figure 3.7.5, was isolated from the latter reaction.

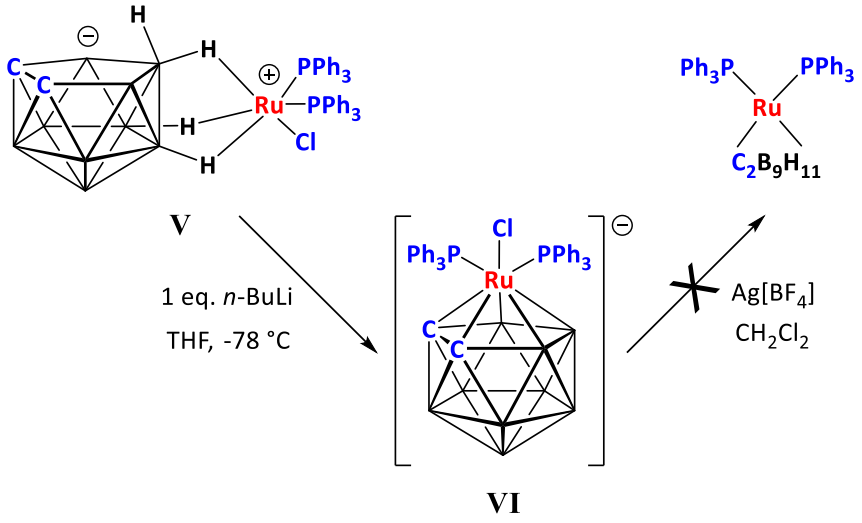

Figure 3.7.3: Attempted synthesis of $(PPh_3)_2RuC_2B_9H_{11}$.

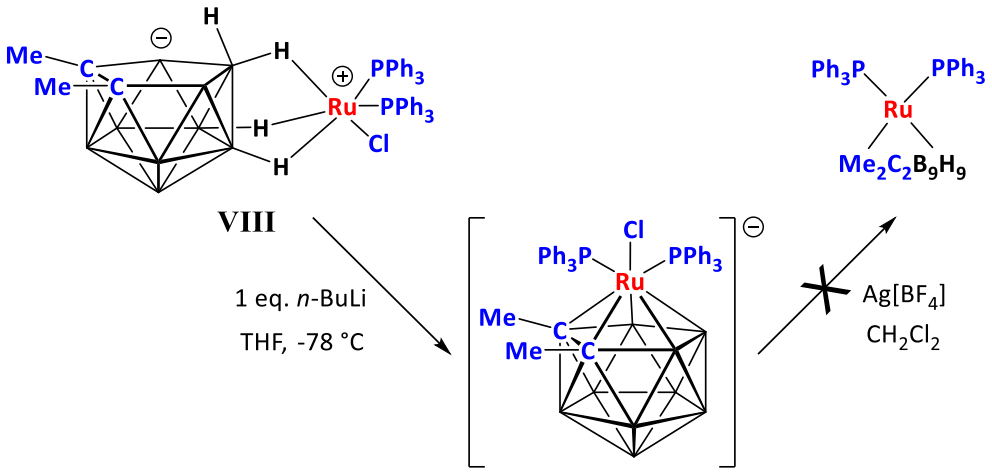

Figure 3.7.4: Attempted synthesis of $(PPh_3)_2RuMe_2C_2B_9H_9$.

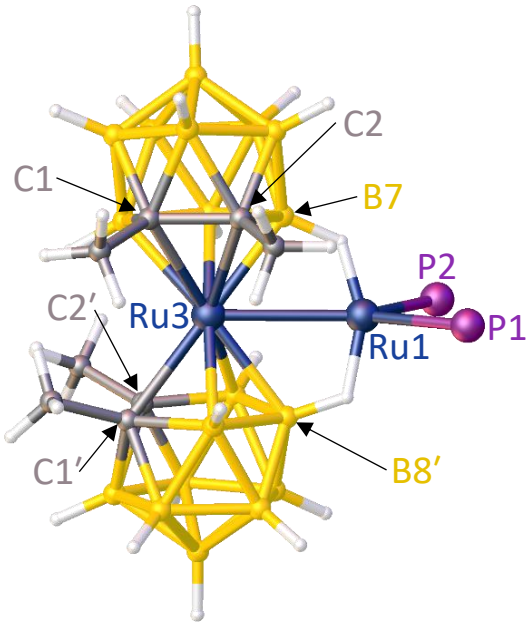

Figure 3.7.5: Molecular structure of **10**.

Compound **10** is a highly unusual species. It is the second crystallographically determined RuSAN analogue known. Additionally, **10** is a metallacarborane sandwich compound with an additional metal centre bound *exo* to the cage via a metal-metal bond, a category of species of which only two seven vertex examples are known within the literature, making **10** the first twelve vertex species of such a kind. The structure of **10** is not suggested by the ^{1}H, $^{1}H\{^{11}B\}$, $^{11}B\{^{1}H\}$ and $^{31}P\{^{1}H\}$ NMR spectra, all of which contain no evidence for the presence of more than one cage. This discrepancy is explained by a

fluxional process in solution in which the *exo* bound ruthenium moves from one pair of Ru-H-B bonds to a different but equivalent pair, meaning that the molecule has time-averaged C_2 symmetry in solution on the NMR timescale.

The structure of **10** provides clues as to the structures of **7**, **8** and **9**, which are not clear from the spectroscopic data available alone. All four species have some common spectroscopic features, such as an unusually high frequency shift in their $^{11}B\{^1H\}$ NMR spectra and the fact that the combined relative integral of the aromatic signals in the ^1H NMR spectra indicate the presence of only one PPh_3 unit per cage. Additionally, many of the spectroscopic properties of **7**, **8** and **9** are consistent with a species which is analogous to **10** but in which the *exo*-polyhedral $\{Ru(PPh_3)_2\}$ fragment is not fluxional.

Ultimately attempts to isolate *hypercloso* ruthenacarboranes were unsuccessful and no evidence for either of the desired species was observed. The fact that **10** was formed suggests that either the *hypercloso* species formed was unstable or that the mechanism of forming the desired *hypercloso* species is unfavourable. In light of these studies, it was considered that it would be advantageous to develop methods to ease the transition from a species with a *hypercloso* electron count but a *closo* structure to a species with a *hypercloso* electron count and structure. This is explored in chapter 4.

3.8 References

1 R. D. McIntosh, D. Ellis, G. M. Rosair and A. J. Welch, *Angew. Chemie - Int. Ed.*, 2006, **45**, 4313.

2 R. Núñez, O. Tutusaus, F. Teixidor, C. Viñas, R. Sillanpää and R. Kivekäs, *Chem. - A Eur. J.*, 2005, **11**, 5637.

3 B. E. Hodson, T. D. McGrath and F. G. A. Stone, *Organometallics*, 2005, **24**, 1638.

4 I. T. Chizhevsky, I. A. Lobanova, V. I. Bregadze, P. V. Petrovskii, A. V. P. Antonovich, A. I. Yanovskii and Yu. T. Struchkov, *Mendeleev Commun.*, 1991, **1**, 47.

5 I. D. Grishin, K. S. Agafonova, A. Y. Kostyukovich, D. I. D'yachihin, I. A. Godovikov, F. M. Dolgushin, D. F. Grishin and I. T. Chizhevsky, *Russ. Chem. Bull.*, 2016, **65**, 1574.

6 C. W. Jung, R. T. Baker, C. B. Knobler and M. F. Hawthorne, *J. Am. Chem. Soc.*, 1980, **102**, 5782.

7 A. P. M. Robertson, N. A. Beattie, G. Scott, W. Y. Man, J. J. Jones, S. A. Macgregor, G. M. Rosair and A. J. Welch, *Angew. Chemie - Int. Ed.*, 2016, **55**, 8706.

8 I. T. Chizhevsky, I. A. Lobanova, P. V Petrovskii, V. I. Bregadze, F. M. Dolgushin, A. I. Yanovsky, Yu. T. Struchkov, A. L. Chistyakov, I. V. Stankevich, C. B. Knobler and M. F. Hawthorne, *Organometallics*, 1999, **18**, 726.

9 R. A. Schunn and E. R. Wonchoba, *Inorg. Synth.*, 1972, **13**, 131.

10 C. J. Yue, Y. Liu and R. He, *J. Mol. Catal. A Chem.*, 2006, **259**, 17.

11 E. H. S. Wong and M. F. Hawthorne, *Inorg. Chem.*, 1978, **17**, 2863.

12 D. D. Ellis, S. M. Couchman, J. C. Jeffery, J. M. Malget and F. G. A. Stone, *Inorg. Chem.*, 1999, **38**, 2981.

13 S. L. Hendershot, J. C. Jeffery, P. A. Jelliss, D. F. Mullica, E. L. Sappenfield and F. G. A. Stone, *Inorg. Chem*, 1996, **35**, 6561.

14 A. J. Welch, *Crystals*, 2017, **7**, 234.

15 T. Straub, M. Haukka and T. A. Pakkanen, *J. Organomet. Chem.*, 2000, **612**, 106.

16 Y. Hiraoka, T. Ikeue, H. Sakiyama, F. Guégan, D. Luneau, B. Gillon, I. Hiromitsu, D. Yoshioka, M. Mikuriya, Y. Kataoka and M. Handa, *Dalton Trans.*, 2015, **44**, 13439.

17 M. R. Churchill, F. J. Hollander and J. P. Hutchinson, *Inorg. Chem.*, 1977, **16**, 2655.

18 R. N. Grimes, R. B. Maynard, E. Sinn, G. A. Brewer and G. J. Long, *J. Am. Chem. Soc.*, 1982, **104**, 5987.

19 N. S. Hosmane, Y. Wang, A. R. Oki, H. Zhang and J. A. Maguire, *Organometallics*, 1996, **15**, 626.

20 E. V. Balagurova, I. V Pisareva, I. A. Godovikov, A. F. Smol'yakov, F. M. Dolgushin and I. T. Chizhevsky, *Russ. Chem. Bull.*, 2013, **62**, 548.

4.0 Pseudocloso Ruthenacarboranes

4.1 Exploiting Steric Interactions To Synthesise *Hypercloso* Ruthenacarboranes

When attempting to generate a *hypercloso* species of general formula $(PPh_3)_2RuR_2C_2B_9H_9$ *via* ligand abstraction from a species of general formula [1,2-R_2-3-Cl-3,3-$(PPh_3)_2$-*closo*-3,1,2-$RuC_2B_9H_9$]$^-$ the product will at first have a *hypercloso* electron count but still retain a *closo* structure. What is predicted to happen at that point is that the molecule will undergo a structural rearrangement in the form of a diamond square diamond (DSD) transition to assume a *hypercloso* geometry, as shown in figure 4.1.1 (see section 1.4.1). This involves the connectivity between the two cage carbon atoms breaking, followed by Ru and the boron atom (B6) of the lower belt moving towards each other and forming a connectivity.

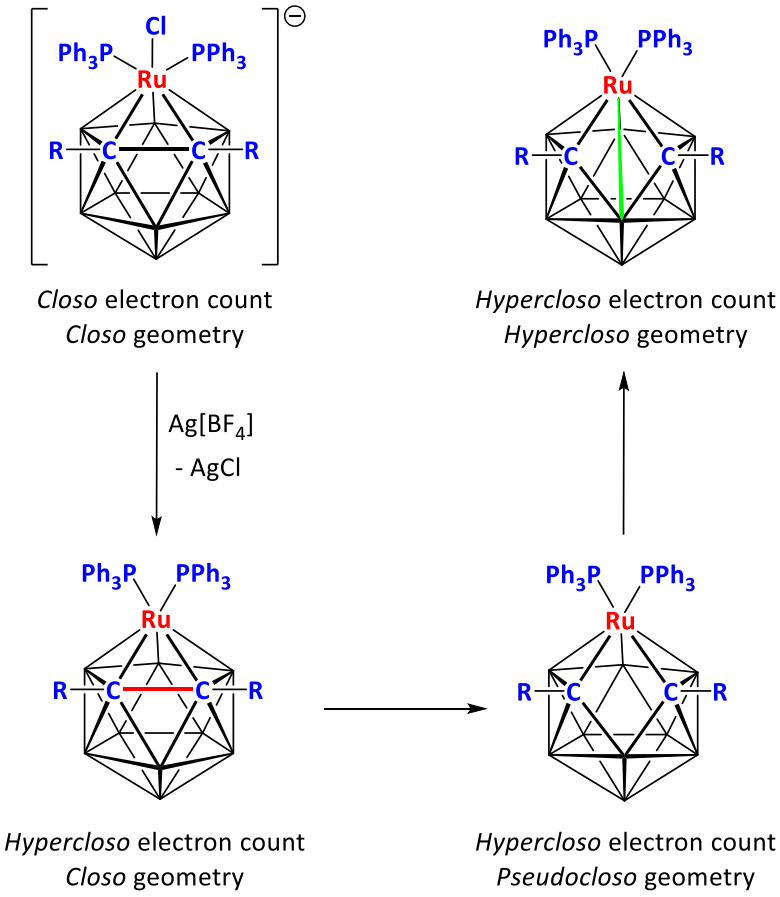

Figure 4.1.1: Anticipated change from *closo* to *hypercloso* structure (where R=non-sterically demanding groups, e.g. H, Me).

One strategy to synthesising *hypercloso* species by this route would be to find a way to encourage this process, therefore directing the products towards *hypercloso* structures and away from some of the unexpected outcomes seen in chapters 2 and 3. This could be achieved by attaching sterically demanding functional groups to the cage carbon atoms which force the monoanionic starting material to assume a *pseudocloso* geometry. The consequence of this is that upon abstraction of Cl^- the resultant species has a *hypercloso* electron count and a *pseudocloso* geometry, as shown in figure 4.1.2. The resultant species would be at pre-organised at the square stage of the DSD rearrangement.

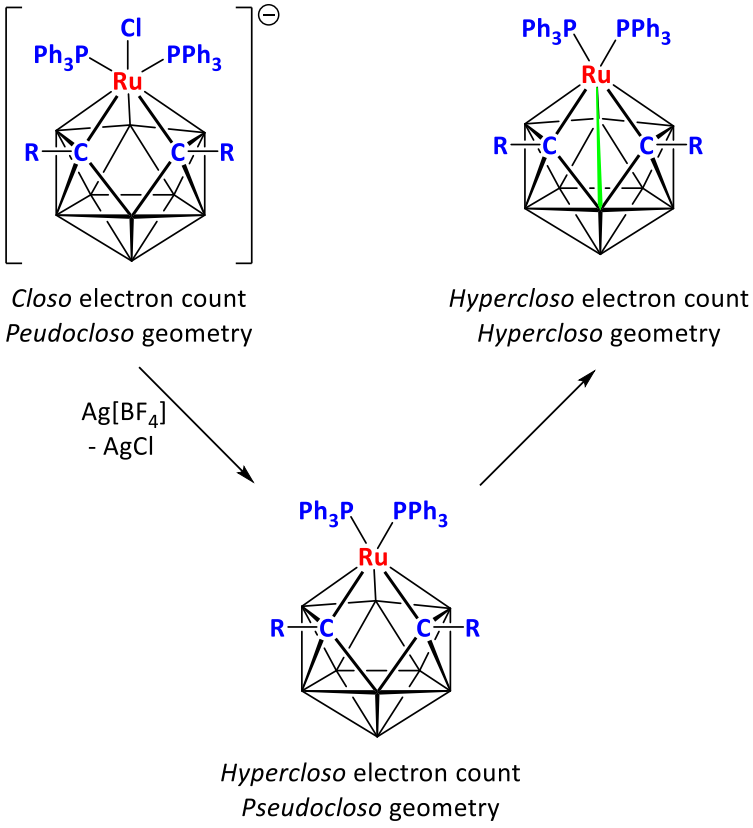

Figure 4.1.2: Anticipated change from *pseudocloso* to *hypercloso* structure (where R=sterically demanding functional groups, e.g. ^{t}Bu, Ph).

As noted in 1.4.3, making C-substituted carboranes *via* reaction of $[C_2B_{10}H_{10}]^{2-}$ and organohalides is only effective for primary alkyl halides, limiting the number of sterically encumbered carboranes that can be generated by this route. An alternative synthesis which is open to a wider range of functional groups is to instead react acetylenes with a decaborane-Lewis base adduct, as shown in figure 4.1.3. However, even this approach

has some limitations, as it cannot be used to insert extremely sterically demanding acetylenes, such as ^{t}BuCC^{t}Bu.

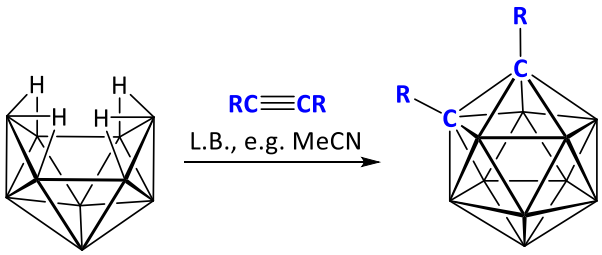

Figure 4.1.3: Synthesis of C,C disubstituted carboranes from $B_{10}H_{14}$.

4.2 ^{t}BuMe-Functionalised Ruthenacarboranes

Research was directed towards carboranes containing tertiary butyl groups, a commonly encountered sterically demanding functional group. These have an advantage as acetylenes containing tertiary butyl groups are available commercially at reasonable expense. As noted in 4.1, no known route to 1,2-^{t}Bu$_2$-*closo*-1,2-$C_2B_{10}H_{10}$ exists but 1-^{t}Bu-*closo*-1,2-$C_2B_{10}H_{11}$ (**IX**) is a known species.[1] It was hypothesised that if **IX** could be alkylated then the combined steric bulk of the two functional groups may be enough to force the cage carbon atoms to separate in any ruthenacarborane made subsequently. To this end 1-^{t}Bu-2-Me-*closo*-1,2-$C_2B_{10}H_{10}$ (**11**) was synthesised *via* the route shown in figure 4.2.1.

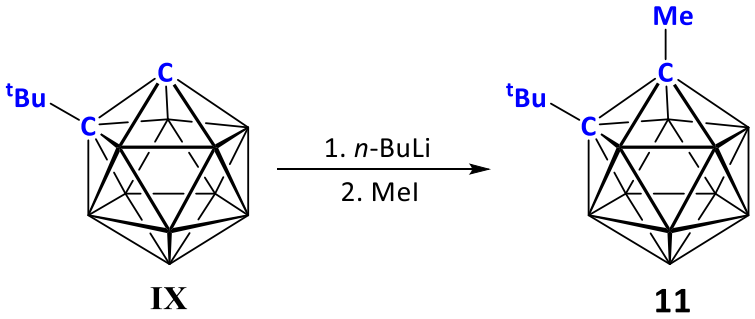

Figure 4.2.1: Synthesis of 1-^{t}Bu-2-Me-*closo*-1,2-$C_2B_{10}H_{10}$ (**11**).

The ^{1}H NMR spectrum of **11** contains one singlet with a relative integral of three which relates to the cage methyl group and one singlet with a relative integral of nine which relates to the tertiary butyl group, indicating that all three CH_3 groups of the ^{t}Bu group are equivalent in solution on the NMR timescale. The molecule has mirror symmetry about a plane through C1, C2, B9 and B12, and could therefore produce an ^{11}B{^{1}H} NMR spectrum with up to six signals of relative integrals 1:1:2:2:2:2. Instead, the ^{11}B{^{1}H} NMR spectrum contains five signals of relative integrals 1:1:2:2:4 (from high frequency to low frequency). This can be explained by simple overlap of two signals of relative integral two. The mass spectrum contains a signal at *m/z* = 214 relating to the molecular ion as well as two signals at 199 and 157 which relate to loss of a methyl and tertiary butyl group, respectively. Elemental analysis is consistent with the proposed product. The

molecular structure of **11** was crystallographically determined and is shown in figure 4.2.2.

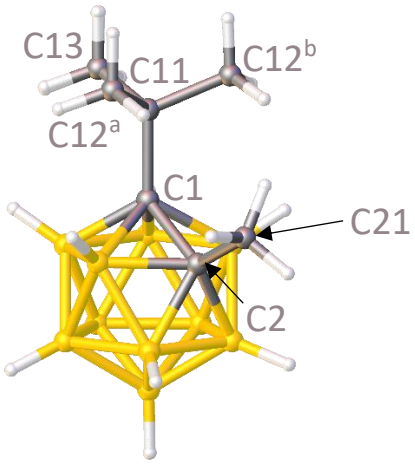

Figure 4.2.2: Structure of 1-^{t}Bu-2-Me-*closo*-1,2-$C_2B_{10}H_{10}$ (**11**).

Compound **11** has crystallographic C_s symmetry as a mirror plane runs through C1, C2, B9 and B12. The C1-C11 bond is significantly longer than that between C2 and the methyl carbon (C21), with bonds lengths of 1.583(2) Å and 1.520(2) Å, respectively. The Cambridge Structural Database (CSD)[2] contains a number of heteroboranes containing carbon bound ^{t}Bu groups. Of these, the relevant bond length in **11** is within the range encountered but is towards the upper limit of said range, likely because of steric interactions between the ^{t}Bu and Me groups, as can be seen in a space filling diagram of **11**, shown in figure 4.2.3. This steric interaction can also be inferred from the C1-C2 bond length in **11** [1.7111(19) Å], which is within the range of lengths encountered for comparable species but is towards the upper limit of said range. This value is much greater than the C1-C2 bond length in 1,2-Me_2-*closo*-1,2-$C_2B_{10}H_{10}$, which is 1.566(12) Å.

Additionally, this steric interaction is implied by the C2-C1-C11 and C1-C2-C21 bond angles, which stand at 122.04(14)° and 121.81(13)°, respectively. These bond angles are larger than the analogous bond angles in 1-^{t}Bu-*closo*-1,2-$C_2B_{10}H_{11}$ (**IX**) and 1,2-Me_2-*closo*-1,2-$C_2B_{10}H_{10}$, 119.2(8)° and 118.3(7)°, respectively. The fact that said bond angles in **11** are greater than those found in comparable species is a result of steric repulsion between the ^{t}Bu and Me groups. As can be seen from figures 4.2.2 and 4.2.3, the ^{t}Bu group is positioned in such a way as that the C21 methyl group is between two of the ^{t}Bu

group's CH_3 groups. Once a metal fragment is inserted into the cage the additional steric bulk associated with said fragment could force the ^{t}Bu and Me groups into a position which increases the amount of steric interaction between the two. This has positive implications with regards to the goal of synthesising a *hypercloso* species through a *pseudocloso* intermediate.

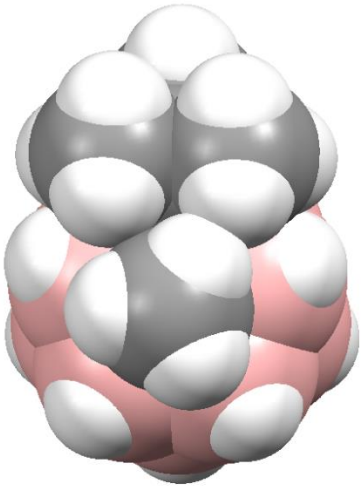

Figure 4.2.3: Space filling diagram of **11**.

Compound **11** was then decapitated *via* the route shown in figure 4.2.4 to give [7-^{t}Bu-8-Me-*nido*-7,8-$C_2B_9H_{10}$]$^-$ (**12**).

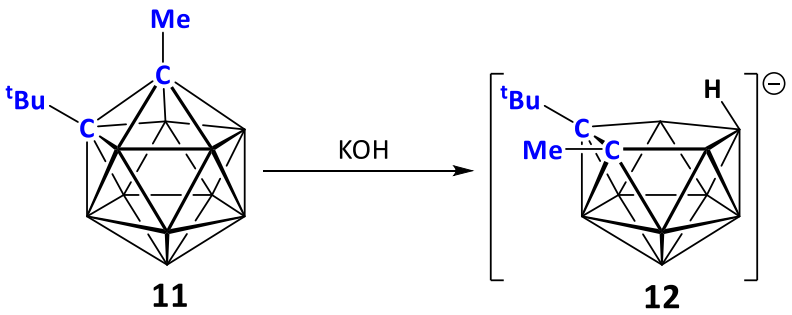

Figure 4.2.4: Synthesis of [7-^{t}Bu-8-Me-*nido*-7,8-$C_2B_9H_{10}$]$^-$ (**12**).

The ^{1}H NMR spectrum of **12** contains a single resonance relating to the ^{t}Bu group, indicating that all three CH_3 groups are equivalent in solution on the NMR timescale. The ^{1}H{^{11}B} NMR spectrum contains a broad singlet at -2.41 ppm that relates to the *endo* H attached to the open face. The molecule has no symmetry and this is reflected in the

$^{11}B\{^{1}H\}$ NMR spectrum, which contains eight resonances of relative integral 1:1:1:1:2:1:1:1 (from high frequency to low frequency), with two signals of relative integral one overlapping to produce the signal of relative integral two. Elemental analysis is consistent with the proposed species. From **12** 5,6,10-[Cl(Ph_3P)$_2$Ru]-5,6,10-μ-(H)$_3$-7-^{t}Bu-8-Me-10-H-7,8-$C_2B_9H_6$ (**13**) was synthesised *via* the route shown in figure 4.2.5.

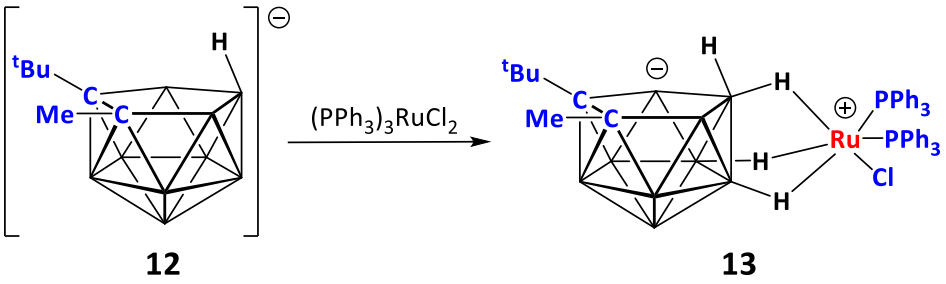

Figure 4.2.5: Synthesis of 5,6,10-[Cl(Ph_3P)$_2$Ru]-5,6,10-μ-(H)$_3$-7-^{t}Bu-8-Me-10-H-7,8-$C_2B_9H_6$ (**13**).

The $^{11}B\{^{1}H\}$ and $^{31}P\{^{1}H\}$ NMR spectra of **13** are different from previously reported *exo-nido* species of general formula 5,6,10-[Cl(Ph_3P)$_2$Ru]-5,6,10-μ-(H)$_3$-7,8-R$_2$-10-H-7,8-$C_2B_9H_6$ (where R=H or Me). This is despite the fact that **13** is electronically similar to **VIII**, in that it contains two alkyl groups attached to the cage carbon atoms. This difference is therefore hypothesised to be because of the lack of symmetry in **13**, whereas **V** and **VIII** contain a mirror plane. The $^{31}P\{^{1}H\}$ NMR spectrum contains six resonances, whereas the $^{31}P\{^{1}H\}$ NMR spectra of **V** and **VIII** both contains three resonances, arranged in such a way as to appear like triplet. Like those of **V** and **VIII**, the $^{11}B\{^{1}H\}$ NMR spectrum of **13** contains two broad singlets at *ca.* 5 and -10 ppm followed by a collection of sharp singlets from *ca.* -15 to -45 ppm. However, the $^{11}B\{^{1}H\}$ NMR spectrum of **13** is also more complex than those of **V** and **VIII**, as it contains a larger number of these sharp singlets than the $^{11}B\{^{1}H\}$ NMR spectra of the latter two species. A comparison of the $^{11}B\{^{1}H\}$ NMR spectra of **13** and **V** is given in figure 4.2.6. Like that of **V** and **VIII**, the signals in the $^{11}B\{^{1}H\}$ NMR spectrum of **13** cannot be assigned relative integrals as the fact that the species is fluxional in solution means that multiple isomers are present.[3]

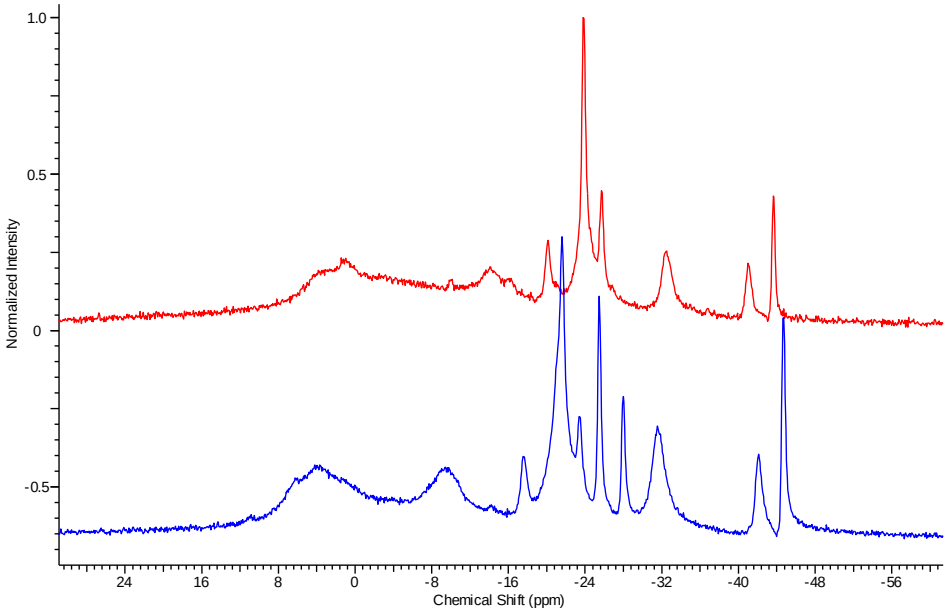

Figure 4.2.6: $^{11}B\{^{1}H\}$ NMR spectra of **13** (blue) and **V** (red) in C_6D_6.

Compound **13** then underwent sequential reaction with *n*-BuLi and $Ag[BF_4]$ in the presence of ^{t}BuNC. This was carried out for a number of reasons. Firstly, this reaction would demonstrate whether or not the *exo* $\{(PPh_3)_2RuCl\}$ fragment could cap the open face of the deprotonated carborane despite the increased steric bulk of **13** over **V** and **VIII**. Secondly, examination of the anticipated product from this reaction, 1-^{t}Bu-2-Me-3,3-$(PPh_3)_2$-3-^{t}BuNC-*pseudocloso*-3,1,2-$RuC_2B_9H_9$, would allow determination of the degree of steric interaction between the two cage alkyl groups. This would be useful in regards to the ultimate goal of synthesising a *hypercloso* species whose formation is aided by cage carbon separation. The reaction was found not to give the anticipated product but to instead give 1-^{t}Bu-2-Me-3-PPh_3-3,3-$(^{t}BuNC)_2$-*closo*-3,1,2-$RuC_2B_9H_9$ (**14**), as shown in figure 4.2.7. Once again, no attempts were made to isolate the monoanionic intermediate, Li[1-^{t}Bu-2-Me-3-Cl-3,3-$(PPh_3)_2$-*closo*-3,1,2-$RuC_2B_9H_9$], as it was assumed this species would be extremely sensitive to oxygen and moisture.

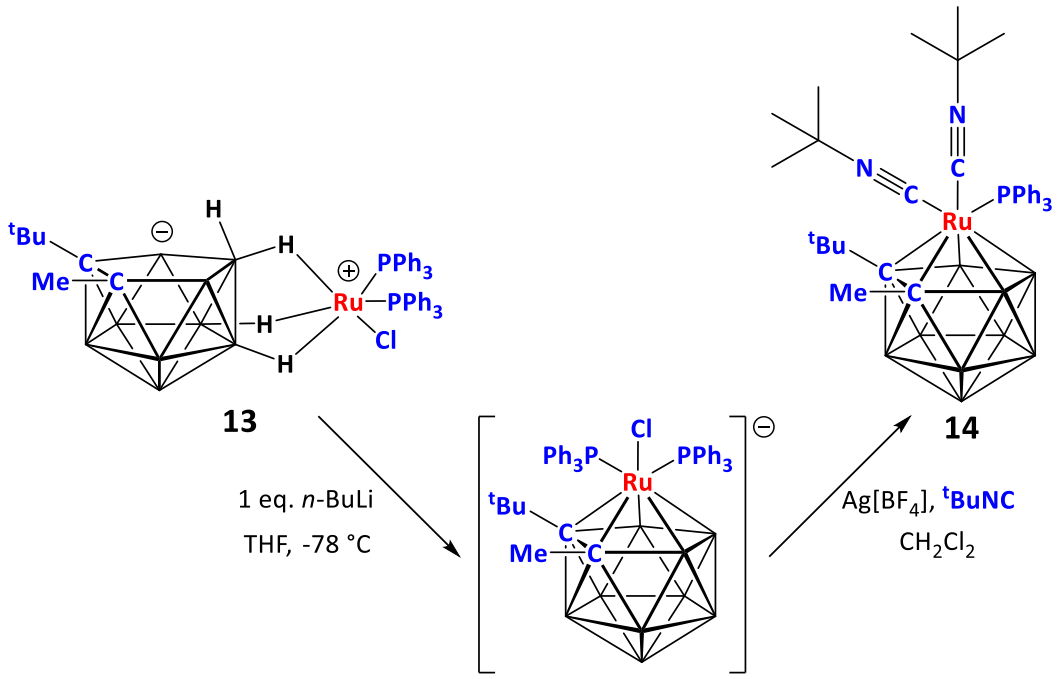

Figure 4.2.7: Synthesis of 1-^{t}Bu-2-Me-3-PPh$_3$-3,3-(^{t}BuNC)$_2$-*closo*-3,1,2-RuC$_2$B$_9$H$_9$ (**14**).

That one PPh$_3$ ligand has been displaced in favour of a second ^{t}BuNC ligand is apparent from the ^{1}H NMR spectrum of **14**, which contains three sharp singlets at 1.43, 1.28 and 1.25 ppm, all of which have relative integrals of nine and are representative of ^{t}Bu groups, one from the cage ^{t}Bu group and two from two inequivalent ^{t}BuNC ligands. The combined signals in the aromatic region have a combined integral of fifteen, which is also consistent with a single PPh$_3$ ligand being present. The ^{31}P{^{1}H} NMR spectrum contains a single resonance relating to the lone PPh$_3$ ligand. As well as containing two resonances with a combined integral of five, the ^{11}B{^{1}H} NMR spectrum also contains four resonances of relative integral one, one more than encountered for symmetrical metallacarboranes.

Additionally, the fact that the weighted average ^{11}B NMR chemical shift <δ(^{11}B)> is -8.8 ppm suggests that the molecule does not have a *pseudocloso* structure but instead has a *closo* structure. This is because *pseudocloso* metallacarboranes of the type MR$_2$C$_2$B$_9$H$_9$ have <δ(^{11}B)> of *ca.* +5 ppm, as exemplified by a number of species produced by Welch and co-workers.[4] In contrast, *closo* metallacarboranes tend to have lower frequency <δ(^{11}B)> values, often *ca.* -10 ppm, as exemplified by **5** and **6**, which

have values of -12.0 and -12.8 ppm, respectively. This suggestion is confirmed by the molecular structure of **14**, shown in figure 4.2.8.

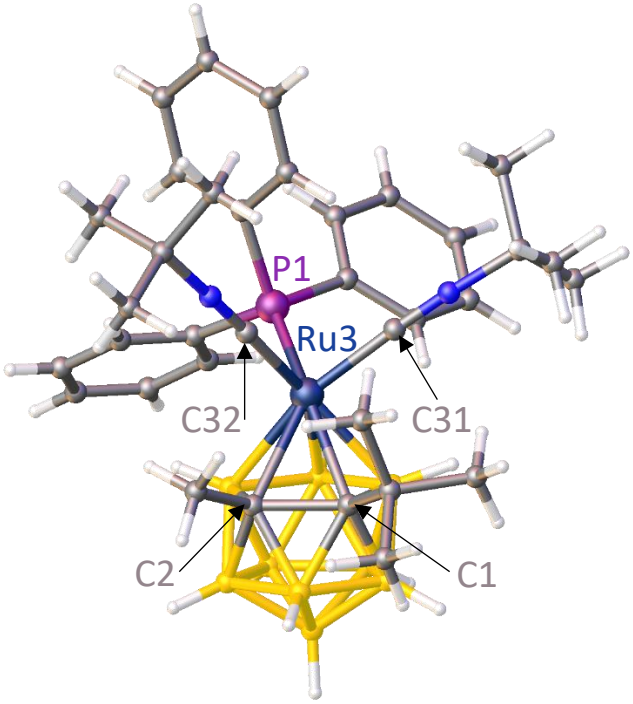

Figure 4.2.8: Structure of 1-^{t}Bu-2-Me-3-PPh_3-3,3-(^{t}BuNC)$_2$-*closo*-3,1,2-$RuC_2B_9H_9$ (**14**).

The PPh_3 ligand in **14** lies *trans* to the cage carbon atoms [|θ| of 155.38(7)°], whilst the two ^{t}BuNC ligands lie *trans* to the cage boron atoms, with C32 [|θ| of 36.58(12)°] positioned more *trans* to the cage boron atoms than C31 [|θ| of 89.92(11)°]. This can be explained by steric interactions, as the bulky PPh_3 ligand in **14** sits almost perfectly *trans* to C1, suggesting that the PPh_3 has arranged itself in such a way as to minimise steric interaction with the ^{t}Bu group. Consequently, the linear ^{t}BuNC ligands are positioned *cis* to the carbon atoms.

However, the most important detail to note from figure 4.2.8 is that it confirms that **14** does not have a *pseudocloso* structure, meaning that the functional groups attached to the cage carbon atoms do not exert sufficient steric pressure on each other to force such a geometry. This fact is reflected in the length of the connectivity between the two cage carbon atoms (C1 and C2), which is 1.692(3) Å, a value which is slightly longer than commonly found for *closo* metallacarboranes but much shorter than that found in *pseudocloso* species of the type $MR_2C_2B_9H_9$.[2] For example, this value is only slightly

longer than the connectivity between the two cage carbon atoms in a related species, 3,3-$(PPh_3)_2$-3-^{t}BuNC-*closo*-3,1,2-$RuC_2B_9H_{11}$ (**5**), which is 1.633(2) Å. Curiously, the connectivity in **14** is actually somewhat shorter than the analogous connectivity in **11**, which is 1.711(2) Å, a small but statistically significant difference. This is surprising as it would be expected that the steric bulk associated with the {(^{t}BuNC)$_2$PPh$_3$Ru} fragment would force the ^{t}Bu and Me groups into a position in which they would have increased steric interaction with each other, lengthening the C1-C2 bond.

4.3 Attempts to Synthesise *Hypercloso* $(PPh_3)_2Ru^tBuMeC_2B_9H_9$

The fact that **14** does not assume a *pseudocloso* structure reduces the chance that *hypercloso* $(PPh_3)_2Ru^tBuMeC_2B_9H_9$ can be synthesised by exploiting the advantages presented by an intermediate with a *pseudocloso* geometry. However, this observation has not eliminated such a possibility. Therefore, a reaction between **13** and *n*-BuLi followed by treatment with $Ag[BF_4]$ in the absence of any potential donor ligands was carried out with the possibility of synthesising *hypercloso* $(PPh_3)_2Ru^tBuMeC_2B_9H_9$, as shown in figure 4.3.1.

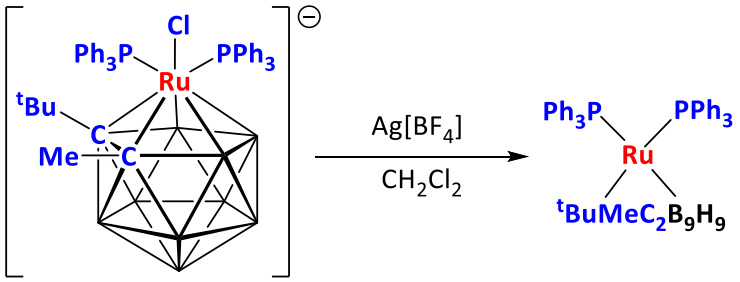

Figure 4.3.1: Proposed synthesis of *hypercloso* $(PPh_3)_2Ru^tBuMeC_2B_9H_9$.

Similar to analogous reactions of **V** and **VIII**, this reaction produced an extremely complex product mixture. Once again, many of the components were either found by $^{11}B\{^1H\}$ NMR spectroscopy not to contain boron, were isolated in trace amounts that did not enable sufficient characterisation or were found to decompose. However, one component (**15**) was isolated and found to contain an unusually high frequency shift in its $^{11}B\{^1H\}$ NMR spectrum. The ^1H NMR spectrum of **15** contains three signals which only have a combined integral of fifteen when the signals generated by the Me and ^{t}Bu group are assigned relative integrals of three and nine, respectively. This is indicative that only one molecule of PPh_3 is present per cage. Additionally, the $^1H\{^{11}B\}$ NMR spectrum contains a low frequency shift that is not present in the ^1H NMR spectrum, at -2.95 ppm, indicative of hydridic BH. The fact that **15** contains a high frequency resonance in its $^{11}B\{^1H\}$ NMR spectrum, a low frequency shift in its $^1H\{^{11}B\}$ NMR spectrum and has only one PPh_3 ligand per cage strongly suggests that **15** may be a "wedged" species similar to compounds **7**, **8**, **9** and **10**. In such a case **15** would contain two cages and an *exo*-polyhedral $\{(PPh_3)_2Ru\}$ fragment bound by Ru-H-B interactions.

Similar to **10**, the $^{11}B\{^{1}H\}$ and $^{1}H\{^{11}B\}$ NMR spectra of **15** do not contain evidence for more than one cage, as both contain a range of signals that integrate to nine. This can be explained either by **15** being a symmetrical wedged species in which the two cages are equivalent or by a degree of fluxionality in solution on the NMR timescale. This latter suggestion is supported by the $^{31}P\{^{1}H\}$ NMR spectrum of **15**, which contains a single broad singlet, which may be indicative of the two PPh_3 groups undergoing slow exchange in solution. Attempts to crystallise **15** were unsuccessful as the compound was found to slowly decompose in solution.

A second component (**16**) was isolated and was found to have an $^{11}B\{^{1}H\}$ NMR spectrum that resembles that of **13**, but with the signals shifted to higher frequency, as shown in figure 4.3.2. The spectrum contains the same mixture of broad signals at higher frequencies and sharper signals at lower frequencies characteristic of *exo-nido* ruthenacarboranes such as **13**, **V** and **VIII**.

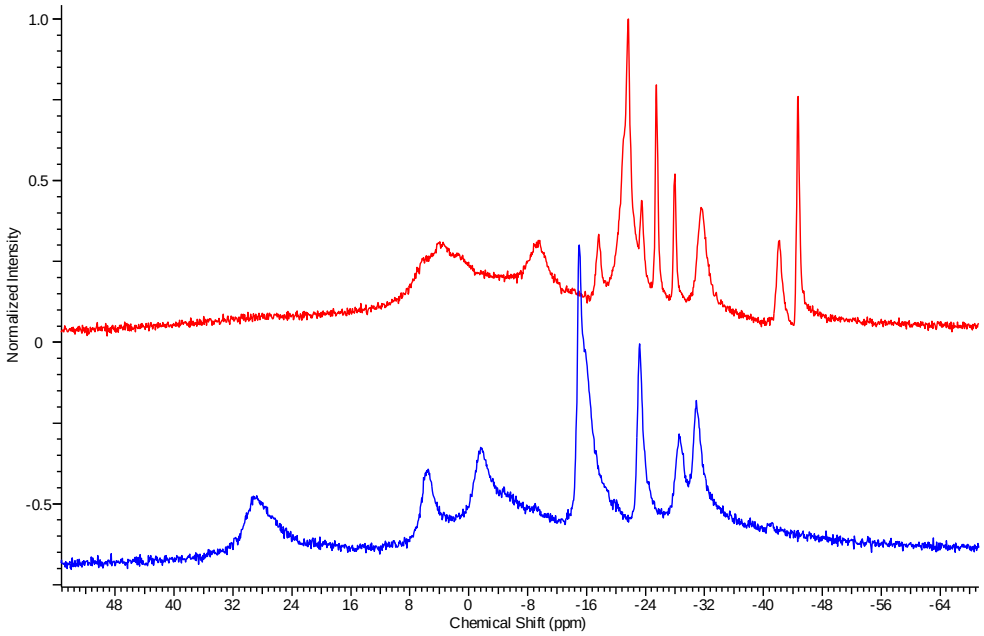

Figure 4.3.2: Comparison of $^{11}B\{^{1}H\}$ NMR spectra of **16** (blue) and **13** (red).

Additionally, the $^{1}H\{^{11}B\}$ NMR spectrum of **16** contains a number of low frequency resonances not present in the ^{1}H NMR spectrum, including one extremely low frequency resonance at -16.12 ppm. These are indicative of hydridic BHs and are characteristic of *exo-nido* ruthenacarboranes, including **13**. A comparison of the $^{1}H\{^{11}B\}$ NMR spectra of **13** and **16** is shown in figure 4.3.3. These observations suggest that **16** is some sort of

exo-nido ruthenacarborane. The $^{31}P\{^{1}H\}$ NMR spectrum contains two doublets with a mutual coupling constant of 31.71 Hz, indicating that there are two P atoms coupled to each other, most likely as a $\{(PPh_3)_2Ru\}$ fragment. This is also consistent with **16** being some sort of *exo-nido* species.

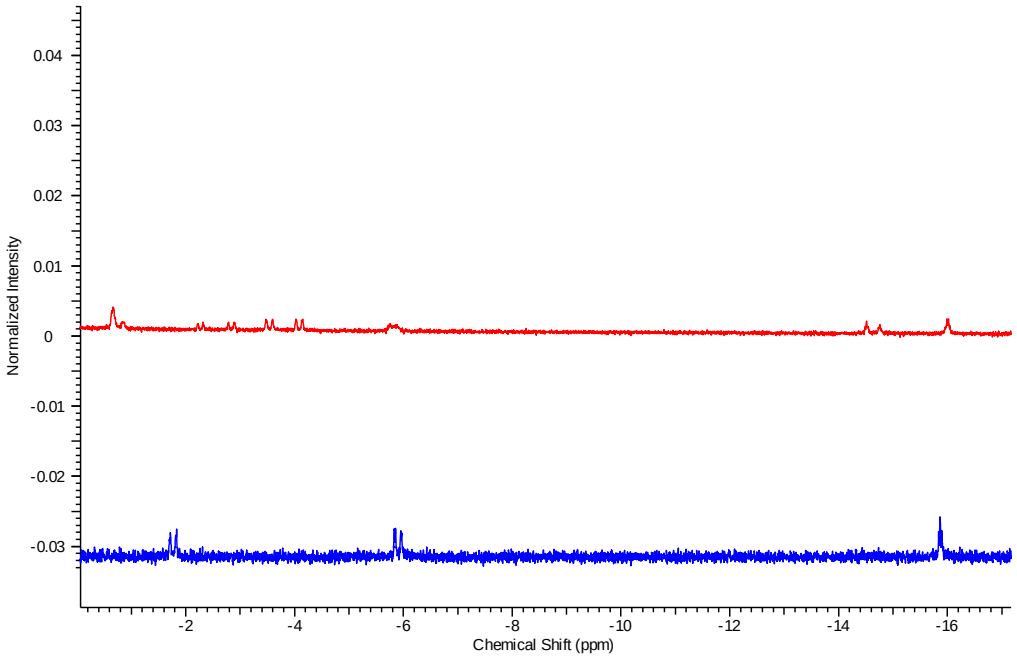

Figure 4.3.3: Comparison of $^{1}H\{^{11}B\}$ NMR spectra of **16** (blue) and **13** (red).

One possible suggestion for the structure of **16** is shown in figure 4.3.4. In this situation the fact that the H atom bound to Ru is not seen in the ^{1}H NMR spectrum is explained by said H atom exchanging with the H atoms of the three Ru-H-B interactions. Additionally, this model explains the relative lack of complexity seen in the $^{1}H\{^{11}B\}$, $^{11}B\{^{1}H\}$ and $^{31}P\{^{1}H\}$ NMR spectra of **16** when compared to that of **13**. This is because the complexity in the latter case is the result of the presence of different isomers existing in solution due to H atoms from the Ru-H-B interactions migrating to the ruthenium atom. In the proposed structure such a process does not occur as there is already a H atom bound to the Ru atom. The suggestion that there are not multiple isomers of **16** in solution is further supported by the fact that the $^{11}B\{^{1}H\}$ NMR spectrum can be integrated to give a total of nine, as shown in figure 4.3.5, something not true of *exo-nido* species such as **13**, **V** and **VIII** due to the aforementioned isomers existing in solution.

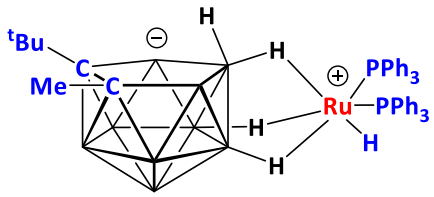

16

Figure 4.3.4: Proposed structure of **16**.

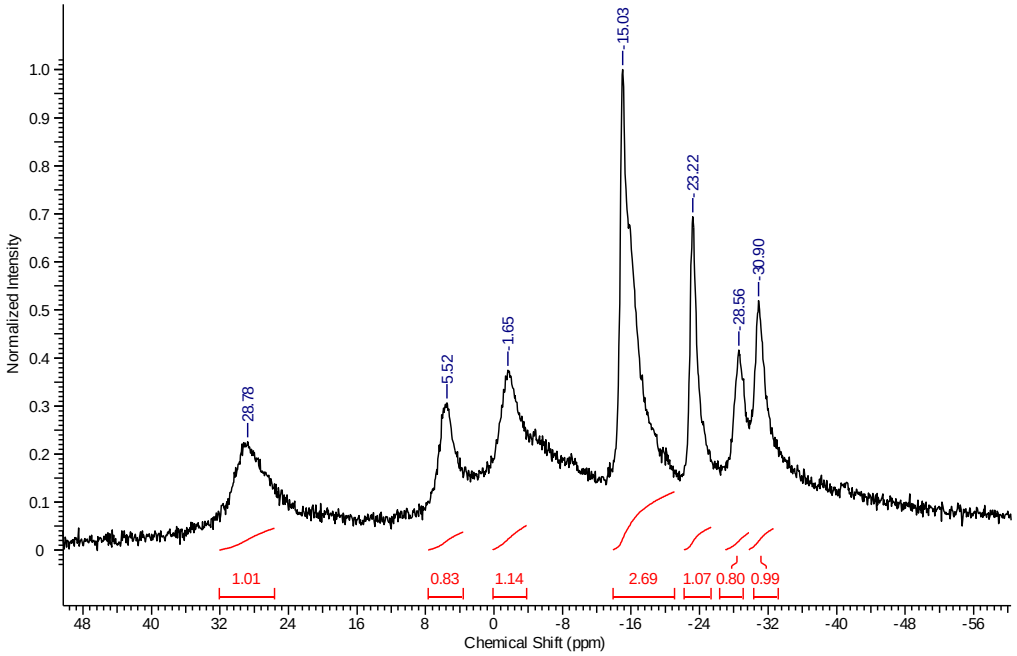

Figure 4.3.5: $^{11}B\{^{1}H\}$ NMR spectrum of **16**.

4.4 Synthesis of *Pseudocloso* Ruthenacarboranes

5,6,10-[Cl(Ph$_3$P)$_2$Ru]-5,6,10-μ-(H)$_3$-7,8-Ph$_2$-10-H-7,8-C$_2$B$_9$H$_6$ (**17**) was synthesised *via* the route shown in figure 4.4.1. Compound **17** was unknown at the time but has subsequently been reported by Chizhevsky and co-workers who synthesised this species concurrently with us.[5]

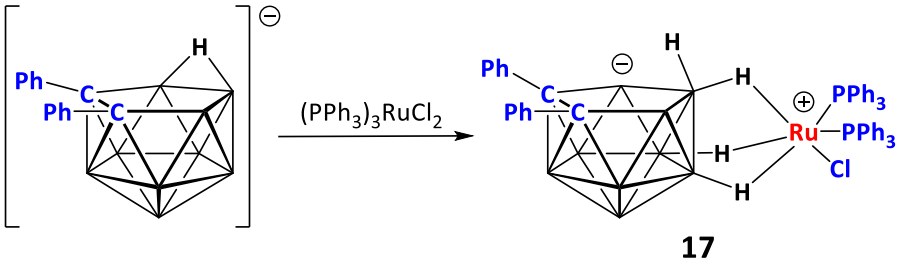

Figure 4.4.1: Synthesis of 5,6,10-[Cl(Ph$_3$P)$_2$Ru]-5,6,10-μ-(H)$_3$-7,8-Ph$_2$-10-H-7,8-C$_2$B$_9$H$_6$ (**17**).

The ^{11}B{^{1}H} NMR spectrum of **17** is complex and also very similar to the ^{11}B{^{1}H} NMR spectra of **V** and **VIII**, the spectrum of the former of which is compared to that of **17** in figure 4.4.2. This is a strong indication that **17** is fluxional by the same mechanism as **V** and **VIII** (see section 3.1). The ^{1}H{^{11}B} NMR spectrum of **17** contains a series of resonances at low frequency, which is something also true of the relevant spectra of **V** and **VIII**. The ^{31}P{^{1}H} NMR spectrum of **17** is also very similar to that of **V** and **VIII**, in that it contains three signals arranged as an apparent triplet. Both elemental analysis and mass spectrometry are consistent with the proposed formula, with the mass spectrum containing the molecular ion and two peaks at *m/z* 911 and 684, relating to loss of chloride and PPh$_3$, respectively. The crystal structure of **17**, previously unreported, was also determined, and the structure of a single molecule is shown in figure 4.4.3.

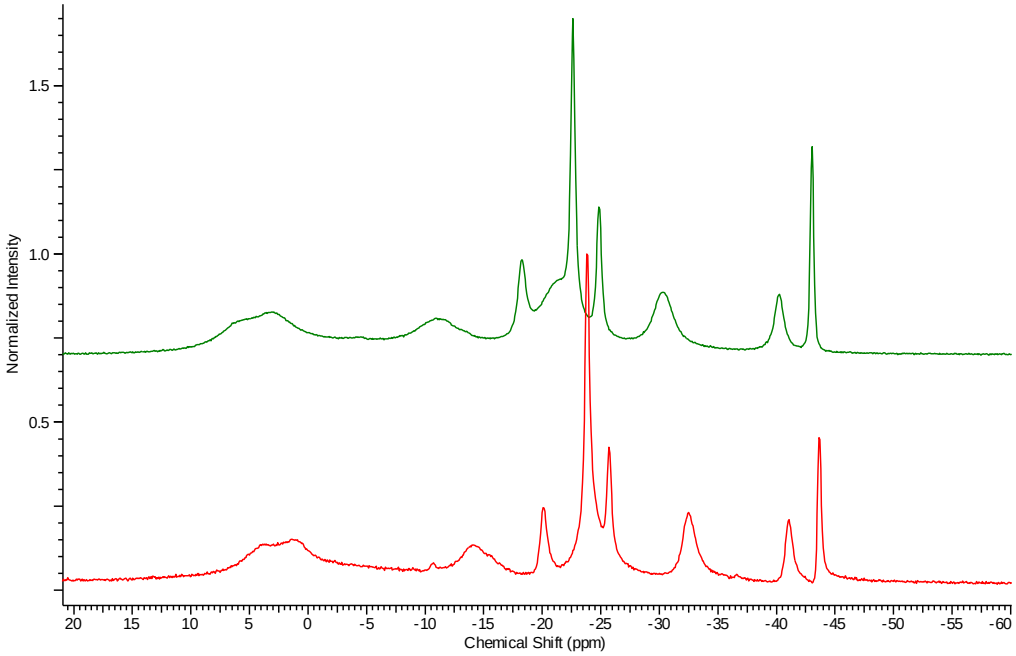

Figure 4.4.2: Comparison of $^{11}B\{^{1}H\}$ NMR spectra in C_6D_6 of **V** (red) and **17** (green).

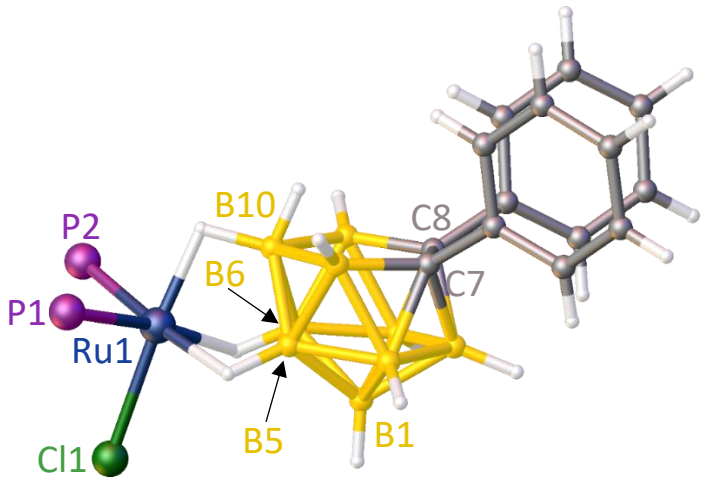

Figure 4.4.3: Structure of 5,6,10-[Cl(Ph_3P)$_2$Ru]-5,6,10-μ-(H)$_3$-7,8-Ph_2-10-H-7,8-$C_2B_9H_6$ (**17**) (phenyl units of PPh_3 ligands omitted for clarity).

The molecular structure of **17** has a number of features in common with those of **V**, **VIII** and **13**. These include the fact that the ruthenium atom is bound through B-H-Ru interactions from {BH} units 5, 6 and 10 as well as the orientation of the *exo*-polyhedral ligands bound to the Ru, specifically the fact that the Cl ligand is *trans* to the open face of the carborane. In the solid state the structure has only effective mirror symmetry along a plane that runs through B1, B10 and Ru1, as the *exo*-polyhedral ligands bound to Ru1

are not positioned in total accord with this mirror plane. The orientation of each cage-bound phenyl ring can be quantised using the modulus of the average of the C_{cage}-C_{cage}-C_{ipso}-C_{ortho} torsion angles (κ). If κ=0° then the plane of the phenyl ring is perpendicular to the C_{cage}-C_{cage} vector whilst if κ=90° then the C_{cage}-C_{cage} vector is contained within the plane of the phenyl ring. In the case of **17**, κ is equal to 5.5(4)° for the Ph group on C7 and 5.7(4)° for that on C8. This is indicative of the fact that the cage Ph groups lie parallel to each other in order to minimise steric interaction between the two.

Compound **17** then underwent sequential deprotonation and halide abstraction with the goal of synthesising the *hypercloso* species $(PPh_3)_2RuPh_2C_2B_9H_9$, as shown in figure 4.4.4. It is assumed that the intermediate species, [1,2-Ph_2-3-Cl-3,3-$(PPh_3)_2$-*pseudocloso*-3,1,2-$RuC_2B_9H_9$]$^-$, would have a *pseudocloso* geometry and that this would aid the generation of such a species. This is because the steric bulk associated with the {$(PPh_3)_2$RuCl} fragment should force the cage phenyl units into a position where they have high κ values and clash sterically with each other, forcing the cage carbon atoms apart. An example of this is given in section 1.3 for the literature species 1,2-Ph_2-3,3,3-[9]aneS_3-*pseudocloso*-3,1,2-$RuC_2B_9H_9$, which has κ values of 53.4° and 53.9°.

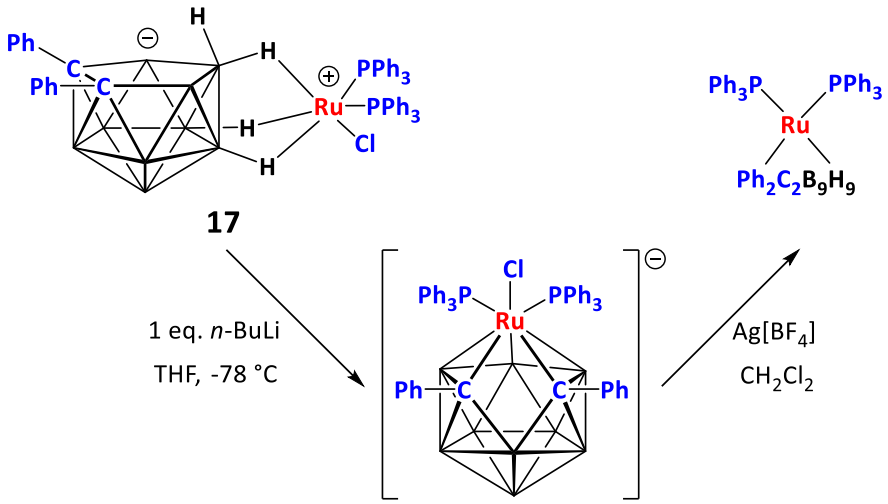

Figure 4.4.4: Proposed synthesis of $(PPh_3)_2RuPh_2C_2B_9H_9$.

No attempts were made to isolate [1,2-Ph_2-3-Cl-3,3-$(PPh_3)_2$-*pseudocloso*-3,1,2-$RuC_2B_9H_9$]$^-$, as it was assumed based on the properties of **VI** that this species would be extremely air-sensitive. Instead, indirect evidence of the existence of [1,2-Ph_2-3-Cl-3,3-

$(PPh_3)_2$-*pseudocloso*-3,1,2-$RuC_2B_9H_9]^-$ was sought through generating this species *in situ* before reacting it with $Ag[BF_4]$ in the presence of an L type ligand. This should then produce air-stable species of generic formula 1,2-Ph_2-3-L-3,3-$(PPh_3)_2$-*pseudocloso*-3,1,2-$RuC_2B_9H_9$.

To this end the sequential reaction of **17** with *n*-BuLi followed by $Ag[BF_4]$ and ^{t}BuNC was carried out with the intention of synthesising 1,2-Ph_2-3,3-$(PPh_3)_2$-3-^{t}BuNC-*pseudocloso*-3,1,2-$RuC_2B_9H_9$, as shown in figure 4.4.5. This would demonstrate that the $\{(PPh_3)_2RuCl\}$ fragment could successfully insert into the cage once the *endo* proton was removed from **17**. This is not to be taken for granted, as the additional steric bulk of the phenyl units could prevent this from occurring. This would also demonstrate that Cl^- could be abstracted from the resultant species.

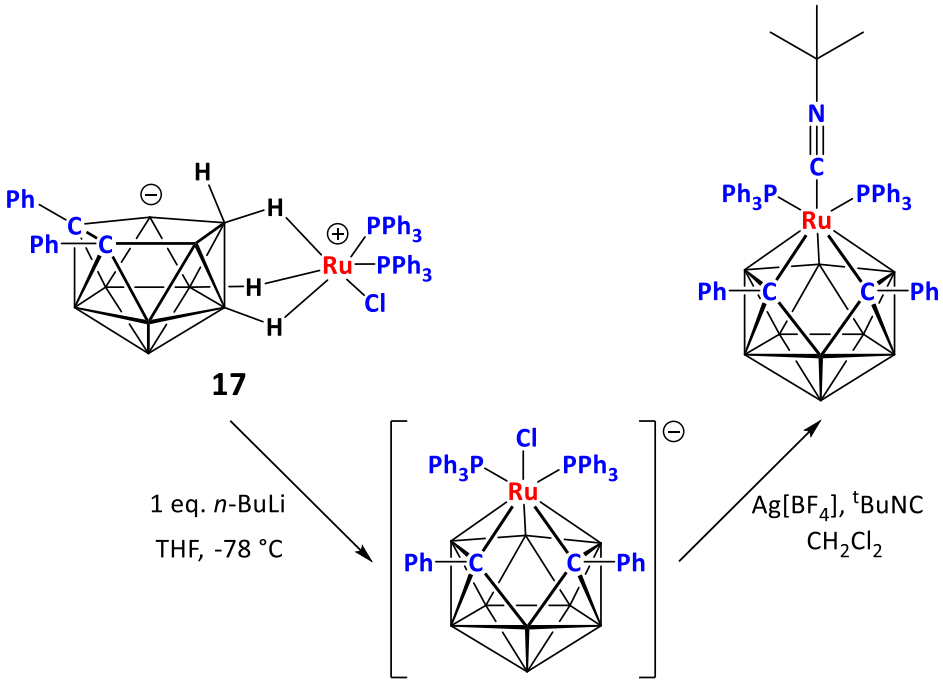

Figure 4.4.5: Proposed synthesis of 1,2-Ph_2-3,3-$(PPh_3)_2$-3-^{t}BuNC-*pseudocloso*-3,1,2-$RuC_2B_9H_9$.

However, the reaction was found not to give the anticipated product, but to instead give 1,2-Ph_2-3-PPh_3-3,3-$(^t$BuNC$)_2$-*pseudocloso*-3,1,2-$RuC_2B_9H_9$ (**18**). This can be discerned from the ^{1}H NMR spectrum, in which the combined integrals of the signals in the aromatic region are equal to 25, indicating that only one PPh_3 ligand is present, in addition to a broad singlet attributable to the two ^{t}BuNC ligands, with a relative integral of 18. This

broad singlet can be seen to split into two separate singlets when cooled to 203 K in CD_2Cl_2, each with a relative integral of nine, indicating that the two ^{t}BuNC ligands are inequivalent in solution at 203 K on the NMR timescale, as can be seen in figure 4.4.6. The fact that the singlet is broad at 298 K indicates a degree of fluxionality (slow exchange) on the NMR timescale at this temperature. The $^{11}B\{^1H\}$ NMR spectrum of **18** at 298 K contains 6 signals of relative integral 1:1:1:2:2:2, as would be expected for such a species. There is a single signal in the $^{31}P\{^1H\}$ NMR spectrum relating to the single PPh_3 group and elemental analysis is consistent with the proposed formula of **18**. The mass spectrum contains a signal at *m/z* 814 that corresponds to M^+ as well as three signals at 731, 648, 386 that relate to sequential loss of one ^{t}BuNC ligand, a second ^{t}BuNC ligand and PPh_3, respectively.

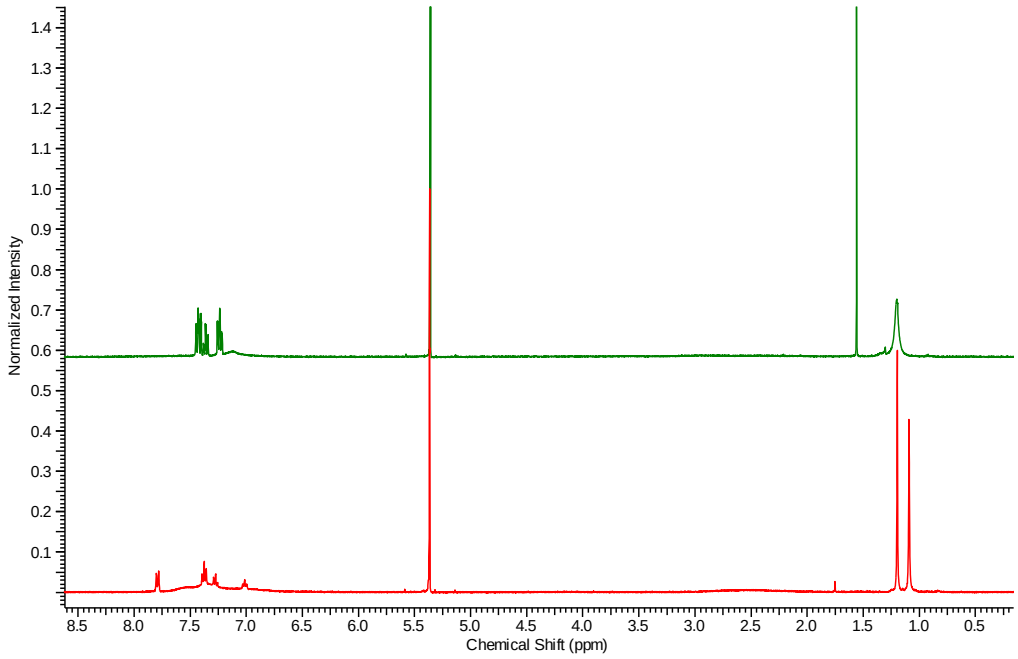

Figure 4.4.6: ^1H NMR spectra of **18** in CD_2Cl_2 at 298 K (green) and 203K (red).

The $^{11}B\{^1H\}$ NMR spectrum of **18** suggests that it has a *pseudocloso* structure, as the weighted average ^{11}B NMR chemical shift $<\delta(^{11}B)>$ of **18** is 5.67 ppm. This is indicative of a *pseudocloso* species, as *pseudocloso* metallacarboranes based on the type $MPh_2C_2B_9H_9$ have $<\delta(^{11}B)>$ of *ca.* +5 ppm.[4] The molecular structure of **18**, shown in figure 4.4.7, confirms that a PPh_3 ligand has been displaced by ^{t}BuNC and that the species does indeed have a *pseudocloso* structure.

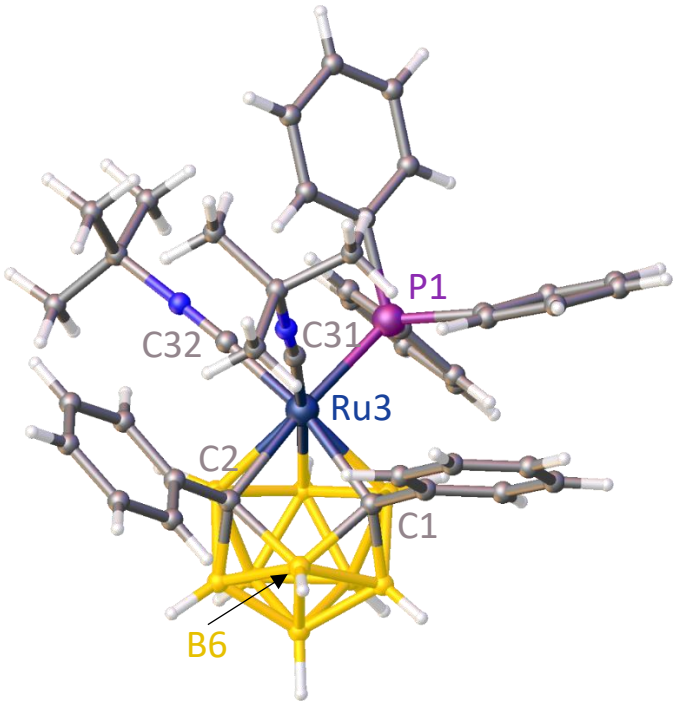

Figure 4.4.7: Structure of 1,2-Ph_2-3-PPh_3-3,3-(^{t}BuNC)$_2$-*pseudocloso*-3,1,2-$RuC_2B_9H_9$ (**18**).

The PPh_3 ligand of **18** is *trans* to C2, with a |θ| of 127.94(19)°. One of the ^{t}BuNC ligands (C32) is *trans* to C1, with a |θ| of 125.2(3)°, whilst the other (C31) is *cis* to the cage carbon atoms, with a |θ| of 2.49(18)°. This is to be contrasted with the structure of 3,3-(PPh_3)$_2$-3-^{t}BuNC-*closo*-3,1,2-$RuC_2B_9H_{11}$ (**5**), in which it is a PPh_3 ligand which is *cis* to the cage carbon atoms. This difference can be explained by steric factors, as the larger, conical PPh_3 ligand in **18** avoids steric interactions with the cage phenyl units. There is a statistically significant difference between the Ru-C bond lengths to the two ^{t}BuNC ligands, with the Ru-C bond of the ligand *trans* to C1 (C32) being shorter than that of C31, at 1.955(5) Å and 2.001(6) Å, respectively, as the ^{t}BuNC *trans* to the cage carbon atom is more strongly bound.

It should be observed that the two cage carbon atoms in **18** have been forced apart by the bulky phenyl units, the carbon-carbon distance now being 2.521(7) Å, as compared to 1.633(2) Å in compound **5**. This is because the Ph groups have been forced into a situation in which they sterically clash with each other, a fact reflected in the torsion angle (κ) values, which are 86.6(5)° and 30.8(6)° for the Ph groups on C1 and C2, respectively. The greater κ value for C1 is a result of the fact that it is *cis* to the more sterically

demanding, conical PPh_3 ligand, whilst C2 is *cis* to the linear ^{t}BuNC ligands. The fact that the κ values in **18** are much greater than those of **17** are a result of the fact that the cage phenyl units cannot position themselves parallel to each other due to the steric bulk of the ligands attached to the metal.

The structure of **18** is typical of that of *pseudocloso* species in that not only have the carbon atoms separated but additionally the boron vertex of the lower belt between the carbon vertices (B6) has moved towards the ruthenium vertex, moving out from the plane of the other four boron atoms in the lower belt (B5, B9, B11 and B12) by 0.341(10) Å, as shown in figure 4.4.8. This has positive implications for attempts to synthesise $(PPh_3)_2RuPh_2C_2B_9H_9$, as the distance between Ru3 and B6 has decreased, implying that it would be easier to form a connectivity between the two. The Ru3-B6 distance is 3.021(6) Å, as compared to 3.5879(19) Å for **5**.

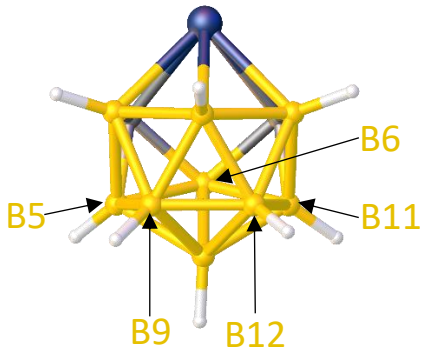

Figure 4.4.8: Structure of **18**, displaying B6 being out of the plane of the other four boron vertices of the lower belt (cage phenyl units, PPh_3 and ^{t}BuNC ligands omitted for clarity).

The fact that two ^{t}BuNC ligands have added in the case of **18**, compared to **5**, where only one ^{t}BuNC added, suggests that this has occurred because of the additional steric bulk of the phenyl units attached to the cage. This has positive implications for attempts to synthesise $(PPh_3)_2RuPh_2C_2B_9H_9$, as it might suggest there is a significant amount of steric protection around the ruthenium atom which could prevent ligand stealing or other ways of the ruthenium acquiring a third ligand (and therefore acquiring a *closo* electron count). In order to further investigate the degree of steric congestion around the ruthenium vertex the reaction was repeated using CO instead of ^{t}BuNC, as shown in figure 4.4.9. It should

be noted that this reaction was carried out in collaboration with Laura English, an undergraduate student who I supervised in the laboratory.

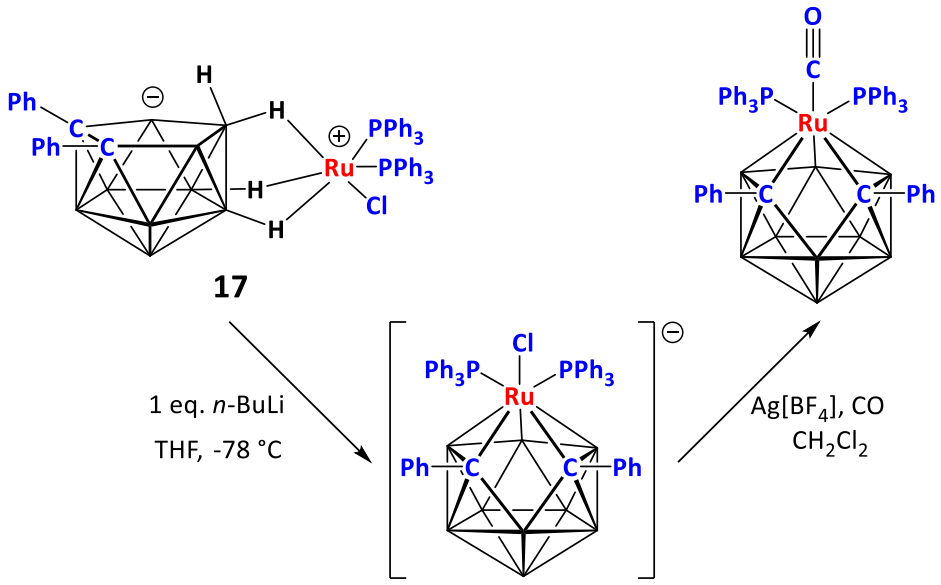

Figure 4.4.9: Proposed synthesis of 1,2-Ph_2-3,3-$(PPh_3)_2$-3-CO-*pseudocloso*-3,1,2-$RuC_2B_9H_9$.

It is not clear from the ^1H NMR spectrum of the product (**19**) alone whether one or two CO ligands have added to the ruthenium centre. This is because all of the signals in said spectrum are generated by protons of the phenyl units, meaning that there is no NMR handle to compare the aromatic region to, as would be the case for a ruthenacarborane with either methyl groups or protons attached to the cage carbon atoms. The result of this is that the spectrum only contains two multiplets in the aromatic region. However, the $^1H\{^{11}B\}$ NMR spectrum contains five signals which when assigned a combined relative integral of nine allow the signals in the aromatic region to be assigned a combined relative integral of 25. This suggests that two CO ligands have added to the metal centre, displacing a PPh_3 ligand, implying the formula of the product is 1,2-Ph_2-3-(PPh_3)-3,3-$(CO)_2$-*pseudocloso*-3,1,2-$RuC_2B_9H_9$ (**19**). Mass spectrometry and elemental analysis are also consistent with the proposed formula. Additionally, IR spectroscopy suggests the presence of two carbonyl bands, as the spectrum contains two CO stretching frequencies, indicative of a symmetric and antisymmetric stretch of a $\{Ru(CO)_2\}$ fragment. The $^{31}P\{^1H\}$ NMR spectrum contains a single resonance. The $^{11}B\{^1H\}$ NMR spectrum of **19** suggests that it has a *pseudocloso* structure, as $<\delta(^{11}B)>$ of **19** is 4.36 ppm. This is

confirmed by the molecular structure of **19**, shown in figure 4.4.10, which also confirms that a PPh_3 has indeed been displaced.

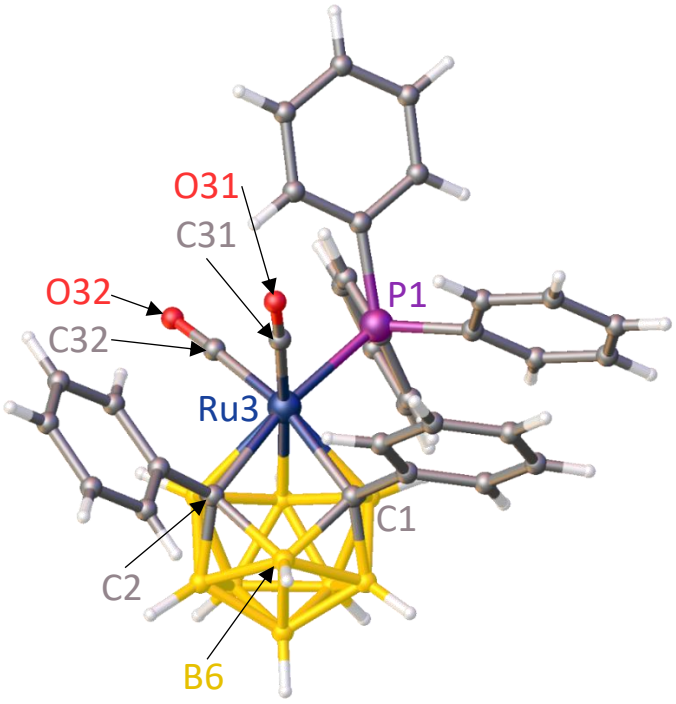

Figure 4.4.10: Structure of 1,2-Ph_2-3-(PPh_3)-3,3-$(CO)_2$-*pseudocloso*-3,1,2-$RuC_2B_9H_9$ (**19**).

The molecular structure of **19** confirms that it has a *pseudocloso* structure, as can be observed from the separation of the cage carbon atoms [C1-C2 distance = 2.457(3) Å] and the reduction in distance between Ru3-B6 relative to a *closo* species [Ru3-B6 distance = 3.094(2) Å]. One CO ligand (C31) in **19** is *cis* to the cage carbon atoms, with a |θ| of 4.11(13)°, whilst the other CO (C32) is *trans* to C1, with a |θ| of 131.77(10)°. The PPh_3 ligand is *trans* to C2, with a |θ| of 123.96(8)°. That it is a CO ligand that is *trans* to the cage boron atoms is to be contrasted with the molecular structure of 3,3-(PPh_3)$_2$-3-CO-*closo*-3,1,2-$RuC_2B_9H_{11}$ (**VII**), reported by Stone and co-workers, in which the CO ligand sits *trans* to the cage carbon atoms.[6] As was the case with **18**, this likely reflects steric factors, as the larger conical PPh_3 ligand is positioned away from the phenyl units of the cage. There are significant differences in both the C-Ru and C-O bond lengths of the CO ligands in **19**. The C-Ru bond length of C32 is shorter than that of C31, at 1.8976(19) Å and 1.953(2) Å, respectively. This is because C32 is *trans* to a cage carbon atom whilst C31 is *cis* to the cage carbon atoms. Similarly, the C-O bond length of C32 is longer than that of C31, at 1.140(2) Å and 1.125(2) Å, respectively. This is because the stronger C-Ru

bond of C32 is accompanied by greater population of the C-O π* antibonding orbital, lengthening the bond more than that of C31-O31. It should be noted that though this difference in C-O bond lengths is statistically significant, it is not very large.

4.5 Synthesis of "Symbiotic" Ruthenacarboranes

The fact that the expected species, 1,2-Ph_2-3,3-$(PPh_3)_2$-3-CO-*pseudocloso*-3,1,2-$RuC_2B_9H_9$, was not generated is an indication that the ruthenium centre is so sterically crowded that even CO, the smallest possible L type ligand, cannot add to it without significant steric consequences. This has positive implications with regards to the synthesis of the desired *hypercloso* species, $(PPh_3)_2RuPh_2C_2B_9H_9$, as it implies the ruthenium centre would have a very large degree of steric protection. To this end, **17** underwent sequential reaction with *n*-BuLi and $Ag[BF_4]$ with the intention of synthesising the *hypercloso* species $(PPh_3)_2RuPh_2C_2B_9H_9$, as shown in figure 4.5.1.

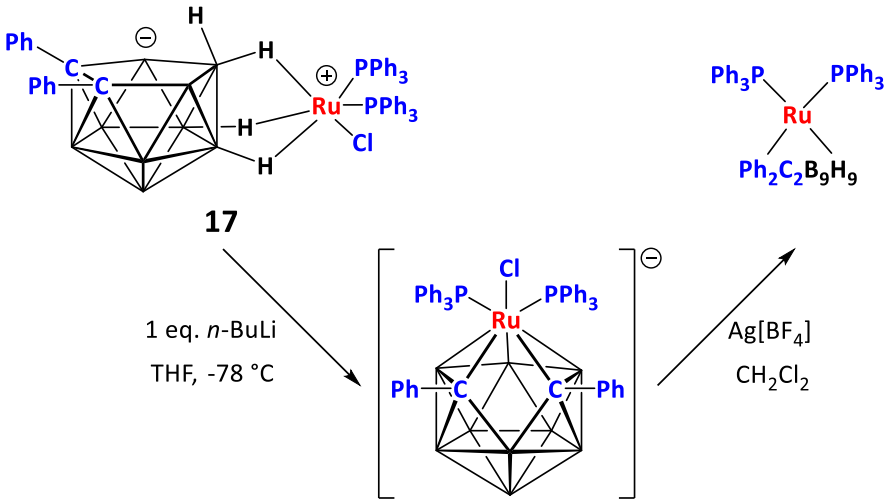

Figure 4.5.1: Proposed synthesis of $(PPh_3)_2RuPh_2C_2B_9H_9$.

The reaction did not cleanly produce the desired product, instead affording a highly complex product mixture. This was reflected in the complexity of the resultant preparative-TLC plates, which contain a number of bands of different colours, similar to those produced by the sequential reactions of **V**/**VIII**/**13** with *n*-BuLi and $Ag[BF_4]$. Several of the bands were found to either decompose or to be inseparable from other components with similar R_f values. Additionally, several bands were either produced in trace amounts too small to obtain reliable spectroscopic data or were found by $^{11}B\{^1H\}$ NMR spectroscopy no to contain boron.

The most abundant component (**20**) was an orange band with an R_f of 0.62. Intriguingly, this component was found by $^{31}P\{^1H\}$ NMR spectroscopy not to contain phosphorus. In addition, the $^{11}B\{^1H\}$ NMR spectrum, shown in figure 4.5.2, contains at least twelve distinct resonances, indicating the presence of more than one cage. These observations discount any possibility that **20** is $(PPh_3)_2RuPh_2C_2B_9H_9$. Additionally, the ^1H NMR spectrum of **20**, shown in figure 4.5.3, contains fourteen distinct signals attributable to aromatic protons, many of which are at lower frequencies than is usual, with a combined relative integral of 20. As there are no PPh_3 ligands present, all of these signals must be generated by phenyl units attached to cage carbon atoms. This therefore also suggests the presence of two inequivalent cages. The fact that many of the signals in the ^1H NMR spectrum which are attributable to aromatic protons are at unusually low frequencies suggests that there may be a metal bound to one or more of the phenyl units attached to the cage carbon atoms.

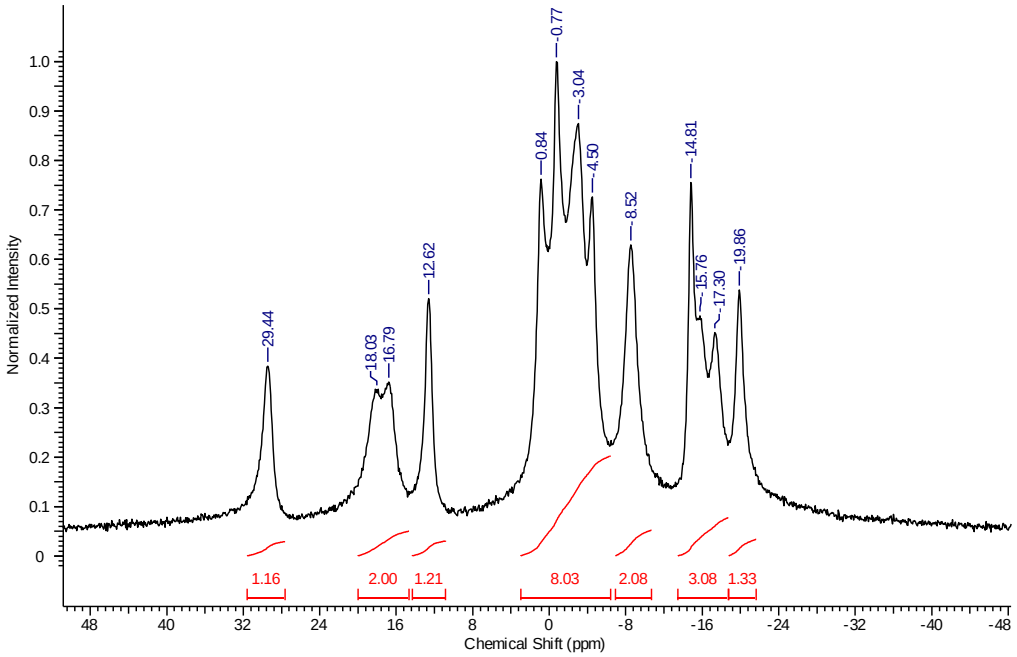

Figure 4.5.2: $^{11}B\{^1H\}$ NMR spectrum of **20**.

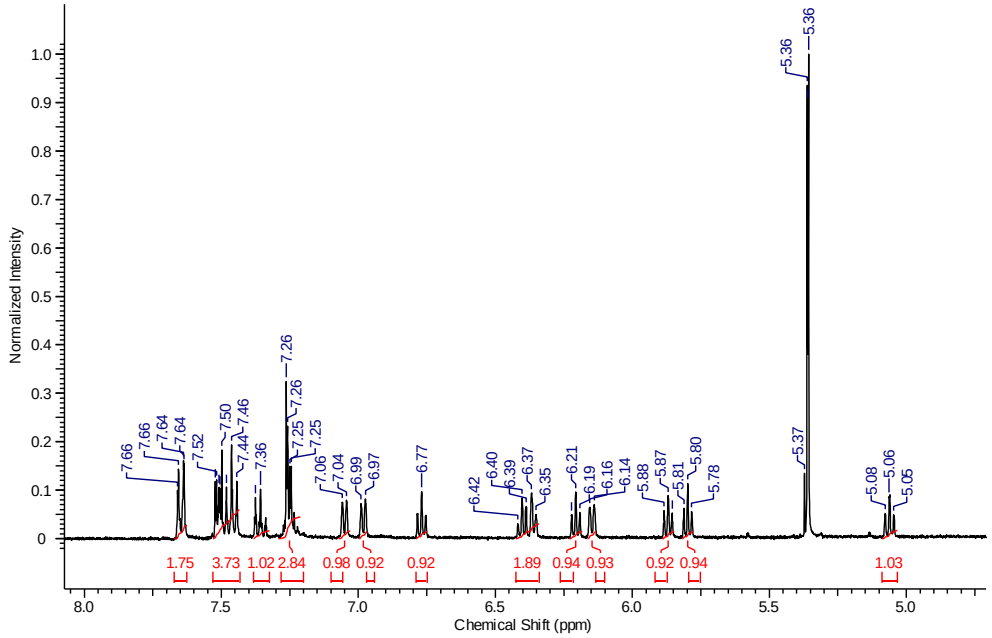

Figure 4.5.3: ^{1}H NMR spectrum of **20** (signal at 5.36 represents CD_2Cl_2).

Elemental analysis is consistent with the empirical formula $C_{14}H_{19}B_9Ru$. The most prominent envelope in the mass spectrum is centred on *m/z* 771.3, which is consistent with M^+ for $C_{28}H_{38}B_{18}Ru_2$, suggesting that the structure of **14** is likely $(C_{14}H_{19}B_9Ru)_2$. Additionally, the $^{11}B\{^{1}H\}$ and ^{1}H spectra are consistent with the proposed formula as both suggest that there are two inequivalent cages present. This information combined with the suggestion from the ^{1}H NMR spectrum that there may be a metal atom bound to one or more of the cage phenyl units suggests that the structure of the species could be one in which both ruthenium atoms have a phenyl unit of the other cage bound η^6 to them. This is supported by the lack of other available ligands for the ruthenium to bind to given the loss of PPh_3. This hypothesis was confirmed by crystallographic analysis of **20**, revealed to be [{1,2-Ph_2-*pseudocloso*-3,1,2-$RuC_2B_9H_9$}{1′,8′-Ph_2-*closo*-2′,1′,8′-$RuC_2B_9H_9$}], as shown in figure 4.5.4.

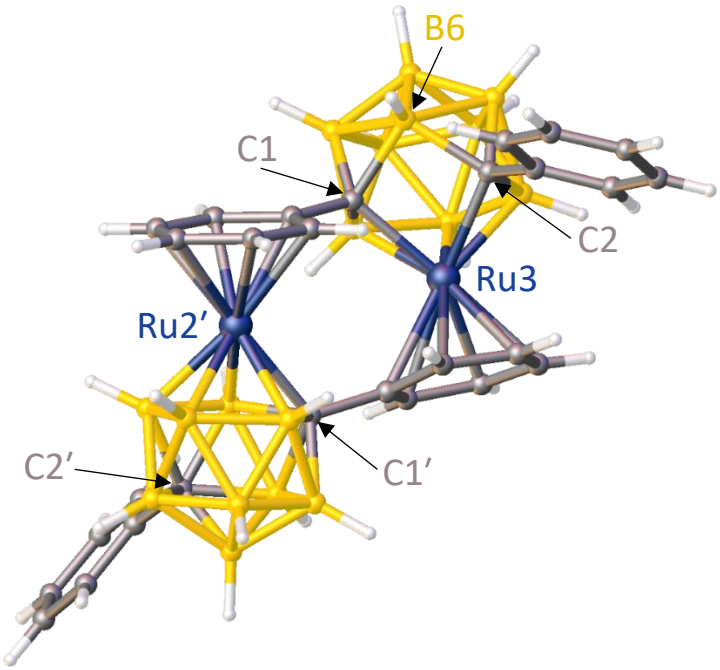

Figure 4.5.4: Structure of [{1,2-Ph_2-*pseudocloso*-3,1,2-$RuC_2B_9H_9$}{1′,8′-Ph_2-*closo*-2′,1′,8′-$RuC_2B_9H_9$}] (**20**).

Compound **20** is a highly unusual species. Each ruthenium atom has lost both PPh_3 ligands, as was also the case for Ru3 in **10**, and instead has a phenyl unit of a second carborane cage bound η^6 to it. The loss of all *exo*-polyhedral ligands is unusual and it is unclear by what mechanism this process proceeds. In this case the ruthenium vertex of each cage achieves an electron count of 18 only through bonding to the phenyl ring of the other cage and as a result the two cages are bound together. This also allows each {PhRu} fragment to act as a one-vertex, two-electron fragment, meaning that both cages have *closo* electron counts. As each cage can only achieve a *closo* electron count through bonding to the other cage, this species has been referred to as a "symbiotic" compound when the work was published,[7] a term borrowed from biology (the definition of symbiosis within biology is a close, often mutually beneficial, relationship between two different species). Compound **20** demonstrates a unique way in which the target species $(PPh_3)_2RuPh_2C_2B_9H_9$ avoids having a *hypercloso* electron count. Compound **20** is almost unique in the literature, with only one such comparable compound known, [{$(MeC_6H_4)Rh(C_2B_9H_9C_6H_4Me)Rh(C_8H_{12})$}$_2$], reported by Chizhevsky and co-workers.[8]

As can be seen from figure 4.5.4, **20** does indeed contain two inequivalent $C_2B_9H_9$ cage units, as predicted from the $^{11}B\{^1H\}$ and ^1H NMR spectra. In this case one cage (primed) has isomerised and is now the 2,1,8-C_2B_9 isomer and therefore *closo*, whilst the other (unprimed) is the 3,1,2-$C_2B_9H_9$ isomer and therefore *pseudocloso*. The two phenyl units of the 3,1,2-C_2B_9 cage have been forced into a position where they clash with each other, a fact reflected in the high κ values, 79.25(5)° and 56.6(5)° for the phenyl units bound to C1 and C2, respectively. As a result the structure of the *pseudocloso* cage is distorted, as can be seen from the locations of the vertices C1, C2 and B6. The two cage carbon atoms have separated, with a distance between the two of 2.491(4) Å, whilst B6 and Ru3 have moved towards one another, with a distance between the two of 2.933(4) Å, in a fashion similar to that seen in **18** and **19**.

There is an apparent relationship between the Ru-C_{Ph} bond lengths and the position of the C_{Ph} atoms relative to the cage carbon atom(s) of the ligating face of the cage. Ru-C_{Ph} bonds of C_{Ph} atoms which are more *trans* to cage carbon atoms are generally shorter than those more *cis* to cage carbon atoms. This is to be expected, as the cage boron atoms exert a stronger STE than the cage carbon atoms. This observation can be quantised by comparing the Ru-C_{ph} bond lengths with |θ|, as shown in charts 4.5.1 and 4.5.2.

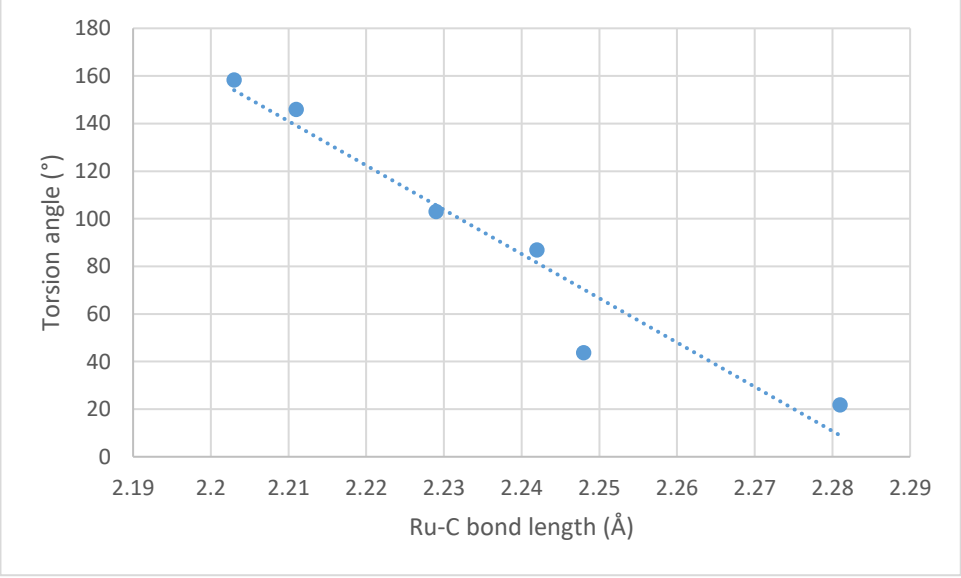

Chart 4.5.1: The relationship between Ru-C_{Ph} bond lengths and C_{Ph}-Ru-X-C1′ torsion angles (|θ|) for the phenyl unit bound to the 2,1,8-C_2B_9 cage, {1′,8′-Ph_2-*closo*-2′,1′,8′-$RuC_2B_9H_9$}, where X is the centroid of the CB_4 face bound to the metal.

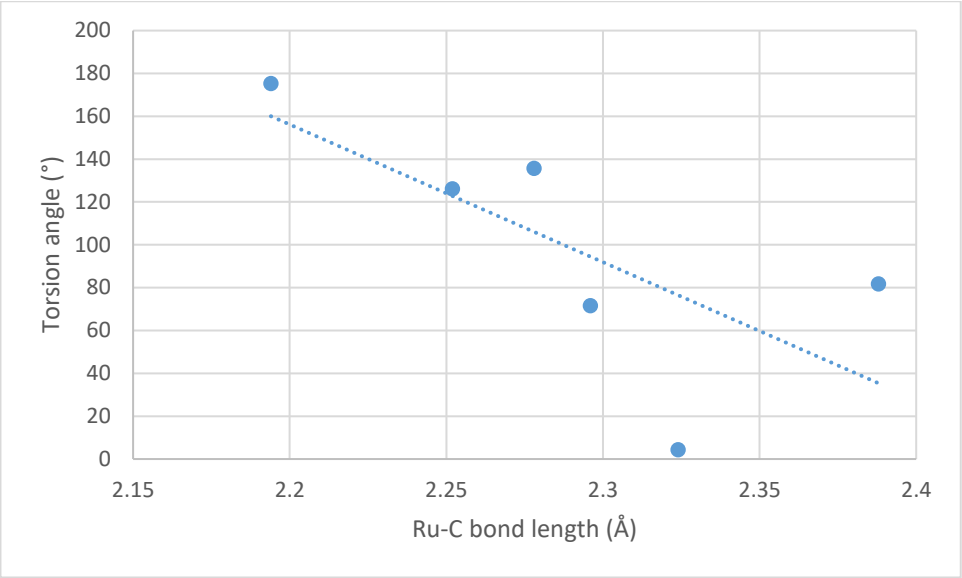

Chart 4.5.2: The relationship between Ru-C_{Ph} bond lengths and C_{Ph}-Ru-X-Y torsion angles (|θ|) for the phenyl unit bound to the 3,1,2-C_2B_9 cage, {1,2-Ph_2-*pseudocloso*-3,1,2-$RuC_2B_9H_9$}, where X is the centroid of the C_2B_3 face bound to the metal and Y is the C1-C2 centroid.

One further component (**21**) was isolated from the reaction mixture and was found to have some spectral similarities with **20**, including that **21** was found by $^{31}P\{^1H\}$ NMR spectroscopy not to contain phosphorus. The ^1H NMR spectrum of **21** contains well over 20 signals attributable to cage phenyl units, suggesting that more than two carborane cages are present. Additionally, the spectrum contains a series of resonances attributable to cage phenyl units found at lower frequency than normal, as shown in figure 4.5.5, similar to those in the ^1H NMR spectrum of **20**. As with the case of **20**, this suggests that some of the cage phenyl units in **21** are bound to Ru atoms. There are thirteen such resonances, with a combined integral of fourteen, suggesting that **21** contains more than two phenyl units bound to Ru atoms. Likewise, the $^{11}B\{^1H\}$ NMR spectrum of **21** is complex, containing at least fourteen resonances which integrate to over eighteen when the distinct singlets present are assigned the minimum possible value of one, suggesting the presence of more than two cages.

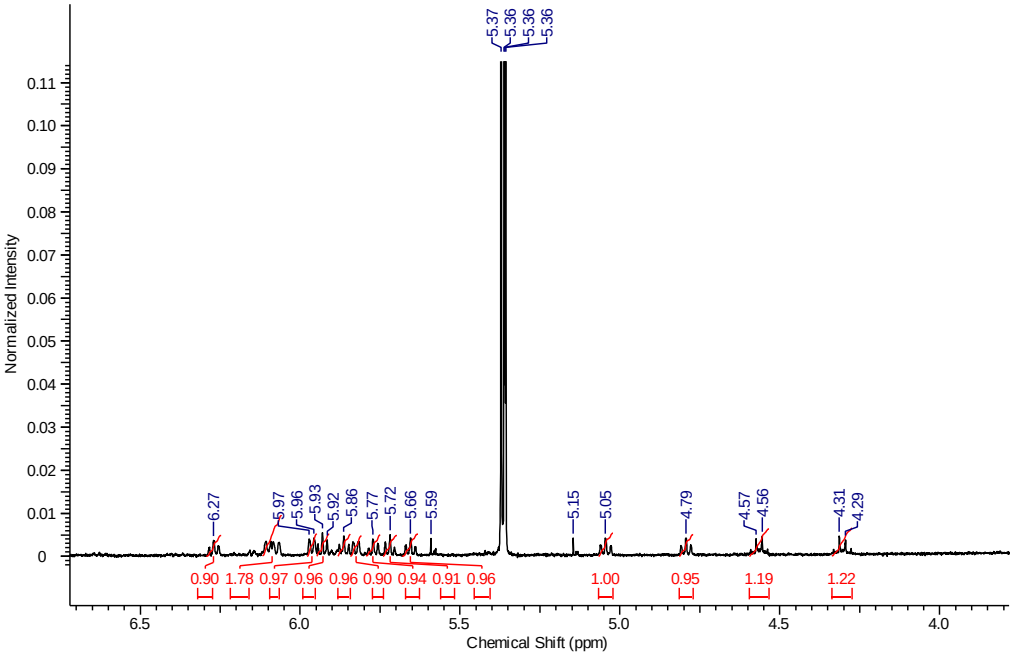

Figure 4.5.5: Section of the ^{1}H NMR spectrum of **21**.

The molecular structure of **21** was determined and shown to be the trimeric "symbiotic" compound [{1,2-Ph_2-*pseudocloso*-3,1,2-$RuC_2B_9H_9$}{1′,8′-Ph_2-*closo*-2′,1′,8′-$RuC_2B_9H_9$}{1″,8″-Ph_2-*closo*-2″,1″,8″-$RuC_2B_9H_9$}], displayed in figure 4.5.6.

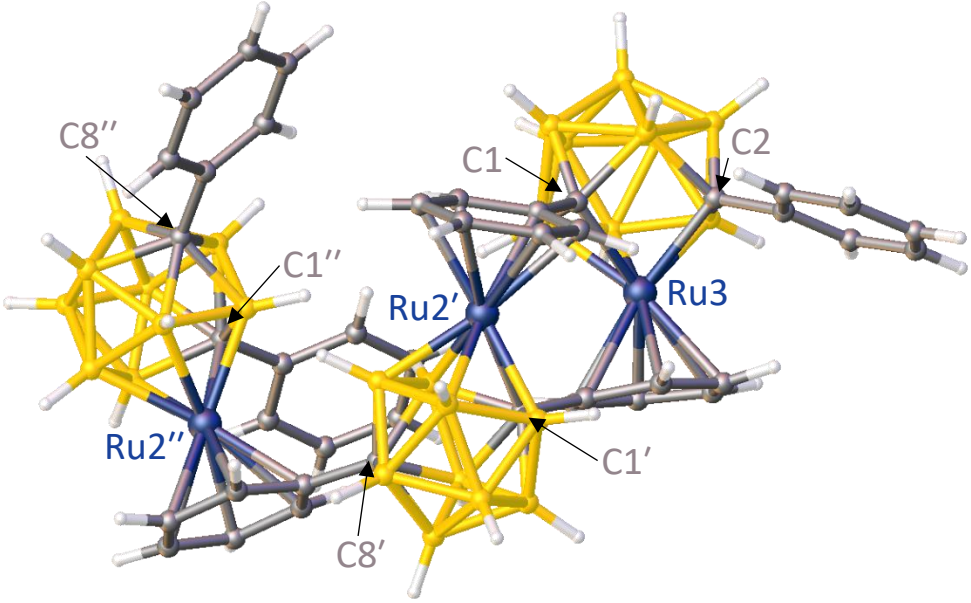

Figure 4.5.6: Structure of [{1,2-Ph_2-*pseudocloso*-3,1,2-$RuC_2B_9H_9$}{1′,8′-Ph_2-*closo*-2′,1′,8′-$RuC_2B_9H_9$}{1″,8″-Ph_2-*closo*-2″,1″,8″-$RuC_2B_9H_9$}] (**21**).

Compound **21** is directly related to **20** by addition of a third $RuPh_2C_2B_9H_9$ unit, {1″,8″-Ph_2-*closo*-2″,1″,8″-$RuC_2B_9H_9$}, which bounds to the phenyl ring attached to C8′ of {1′,8′-Ph_2-*closo*-2′,1′,8′-$RuC_2B_9H_9$}. This implies that **21** is formed *via* addition of third $RuPh_2C_2B_9H_9$ unit to a pre-existing molecule of **20**. This suggests that the desired *hypercloso* species $(PPh_3)_2RuPh_2C_2B_9H_9$ is initially being formed as it is presumably this species which adds to a pre-existing molecule of **20**, displacing both PPh_3 ligands in the process. Additionally, the existence of **21** implies that the addition of further $RuPh_2C_2B_9H_9$ units to **21** is a possibility, a process which would produce polymeric or oligomeric ruthenacarboranes.

As was the case in **20**, the Ph groups of the *pseudocloso* 3,1,2-RuC_2B_9 cage have been forced into a position where they have high κ values [81.54(30)° and 60.2(3)° for the Ph groups bound to C1 and C2, respectively] and consequently sterically clash with each other, reflected in the separation of the cage carbon atoms [C1-C2 distance = 2.492(3) Å] and relatively short Ru3-B6 distance [2.946(3) Å].The *pseudocloso* distortion of the 3,1,2-RuC_2B_9 cage in **21** is therefore very similar in magnitude to that in **20**. Like **20**, compound **21** is a highly unusual species. Once again, in order for **21** to be formed all three ruthenium vertices must have lost both of their PPh_3 ligands, an unusual process. Whilst one other example of a dimeric "symbiotic" species is known, **21** is unique.

4.6 Chapter Summary

The goal of the research contained within this chapter was to synthesise *hypercloso* species of general formula $(PPh_3)_2RuR_2C_2B_9H_9$ by abstraction of chloride from species of generic formula $[1,2\text{-}R_2\text{-}3\text{-}Cl\text{-}3,3\text{-}(PPh)_2\text{-}pseudocloso\text{-}3,1,2\text{-}RuC_2B_9H_9]^-$. It was hypothesised that starting from a ruthenacarborane with a *pseudocloso* structure would ease the transition to a *hypercloso* structure as this would aid the anticipated change in geometry associated with such a transition, as shown in figure 4.6.1.

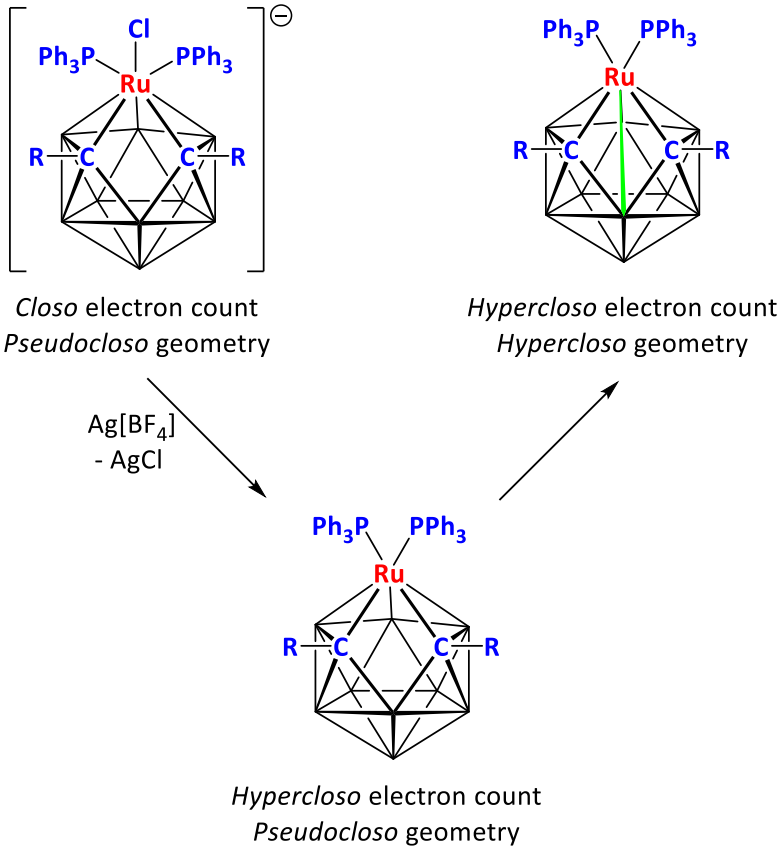

Figure 4.6.1: Anticipated change from *pseudocloso* to *hypercloso* structure (where R=sterically demanding functional groups, e.g. ^{t}Bu, Ph).

A series of new carboranes and ruthenacarboranes containing C substituted ^{t}Bu and Me groups, **11**, **12** and **13**, was synthesised, as shown in figure 4.6.2.

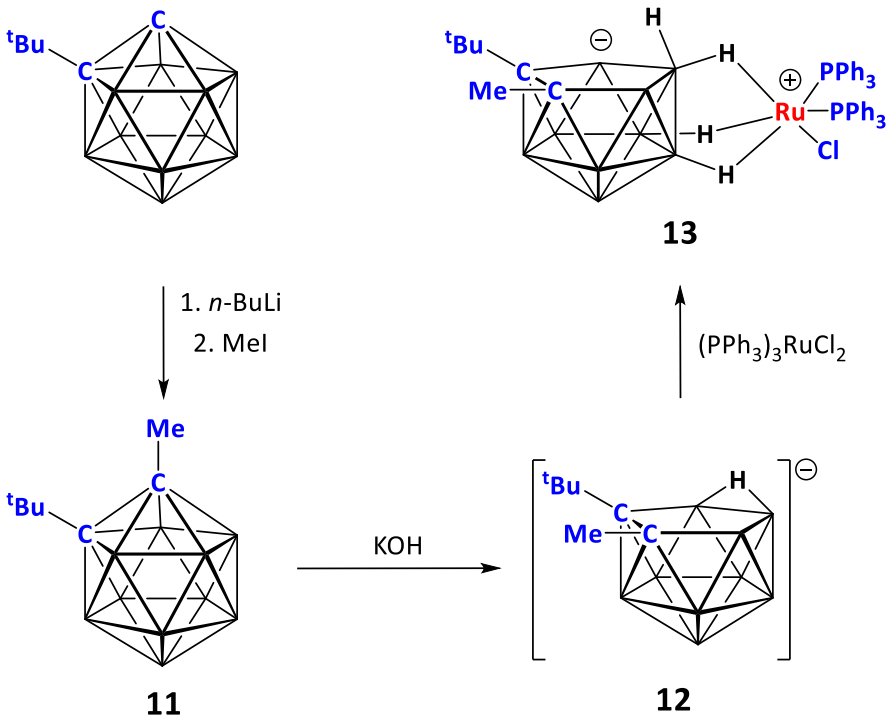

Figure 4.6.2: Synthesis of **11**, **12** and **13**.

Compound **13** then underwent sequential reaction with *n*-BuLi and $Ag[BF_4]$ in the presence of ^{t}BuNC to produce **14**, as shown in figure 4.6.3. However, **14** does not have a *pseudocloso* structure, suggesting that ^{t}BuMe substituted 3,1,2-$RuC_2B_9H_9$ ruthenacarboranes do not have enough steric bulk to force such a change.

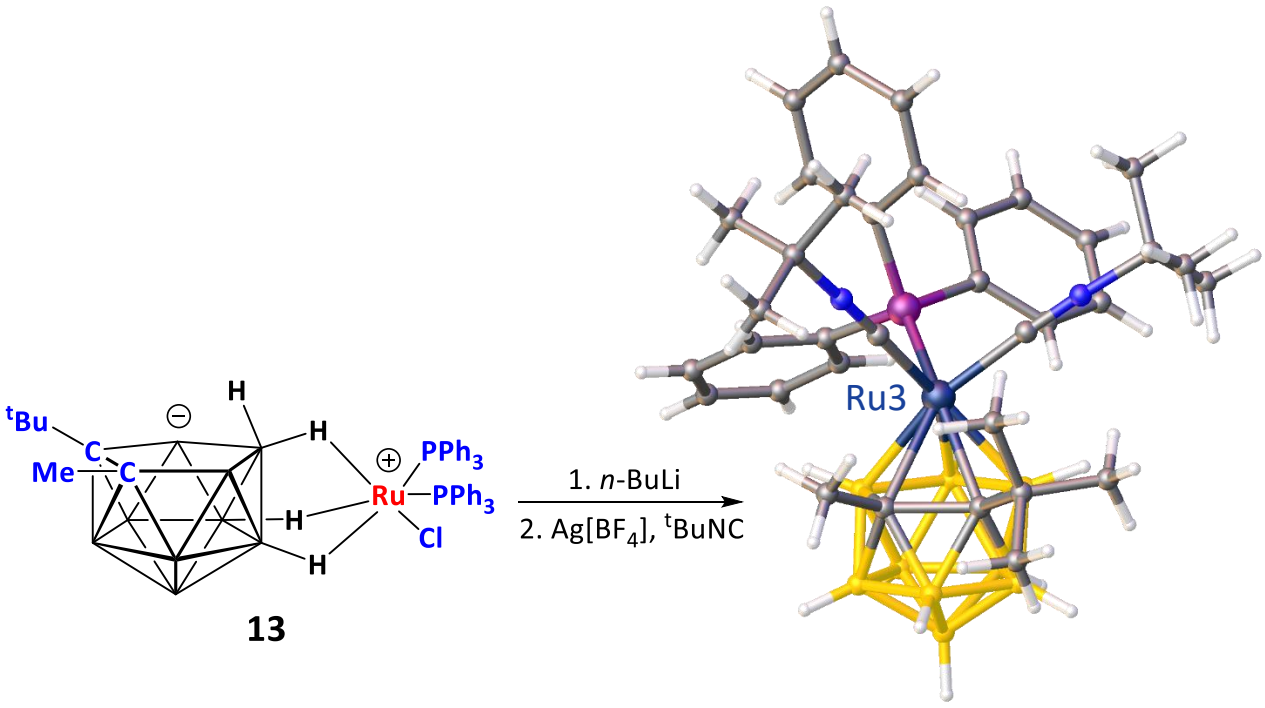

Figure 4.6.3: Synthesis and structure of **14**

Nonetheless, a sequential reaction of **13** with *n*-BuLi and $Ag[BF_4]$ in the absence of any donating ligands was carried out. As was the case with similar reactions of **V** and **VIII**, this was found to produce a highly complex product mixture from which two components were isolated. The first of these, **15**, is suspected to be a "wedged" species similar to **7**, **8**, **9** and **10**, as it possesses many similar spectroscopic properties to these species. This includes the fact that the ^{1}H NMR spectrum suggests the presence of only one PPh_3 ligand per cage, evidence for a Ru-H-B interaction in the $^{1}H\{^{11}B\}$ NMR spectrum and an unusually high frequency resonance in its $^{11}B\{^{1}H\}$ NMR spectrum. The second of these components, **16**, is suspected to be an *exo-nido* species similar to **V**, **VIII**, **13** and **17**, but where the chloride ligand has been replaced by a hydride. The $^{1}H\{^{11}B\}$ NMR spectrum of **16** contains several low frequency signals, including an unusually low frequency resonance at -16.12 ppm. These signals are typical of *exo-nido* ruthenacarboranes. A comparison of the $^{1}H\{^{11}B\}$ NMR spectra of **16** and **13** is given in figure 4.6.4.

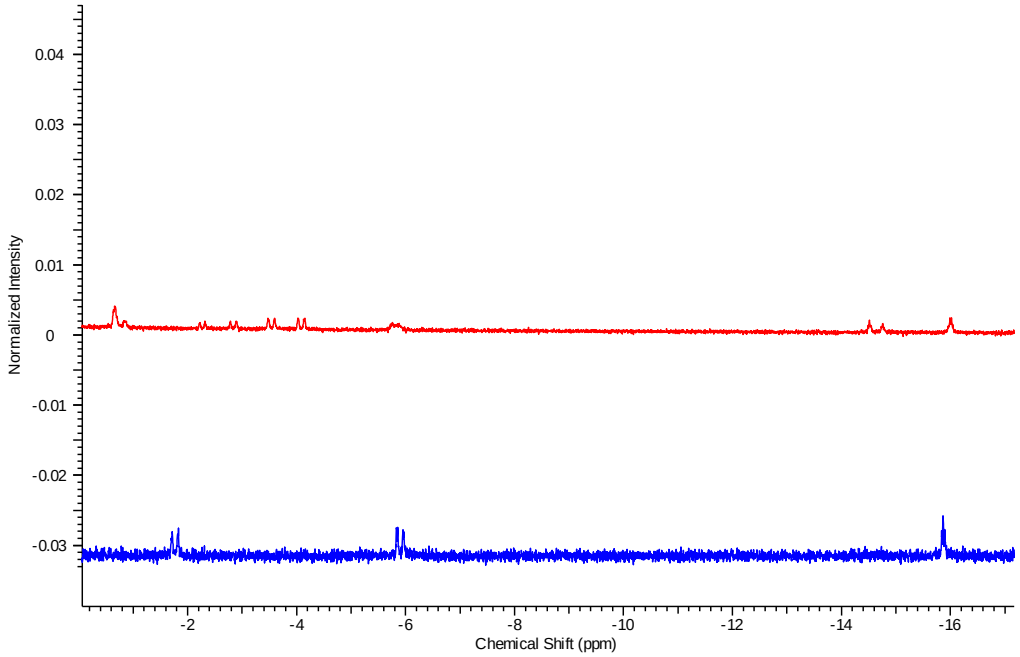

Figure 4.6.4: $^{1}H\{^{11}B\}$ NMR spectra of **16** (blue) and **13** (red).

The structure of **14** suggests that ^{t}BuMe is an insufficiently sterically demanding combination of groups to achieve the desired *pseudocloso* geometry. Instead efforts were directed towards synthesising *hypercloso* $(PPh_3)_2RuPh_2C_2B_9H_9$. To this end **17** was synthesised *via* the route shown in figure 4.6.5. It should be noted that this species was synthesised independently by Chizhevsky and co-workers.[5]

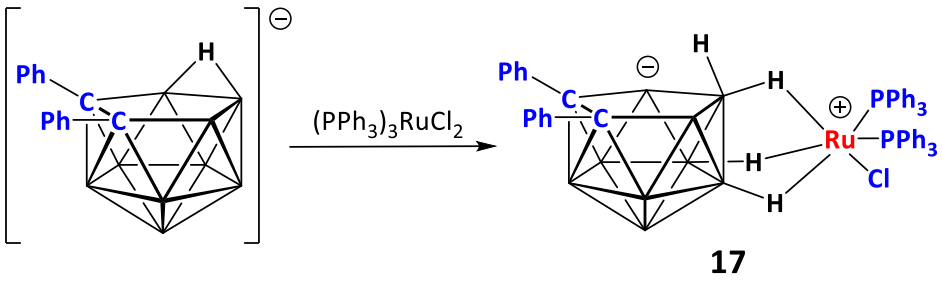

Figure 4.6.5: Synthesis of **17**.

Two new *pseudocloso* ruthenacarboranes were then synthesised *via* sequential reaction of **17** with *n*-BuLi followed by $Ag[BF_4]$ and $^tBuNC/CO$ to give **18** and **19**, respectively, as shown in figure 4.6.6.

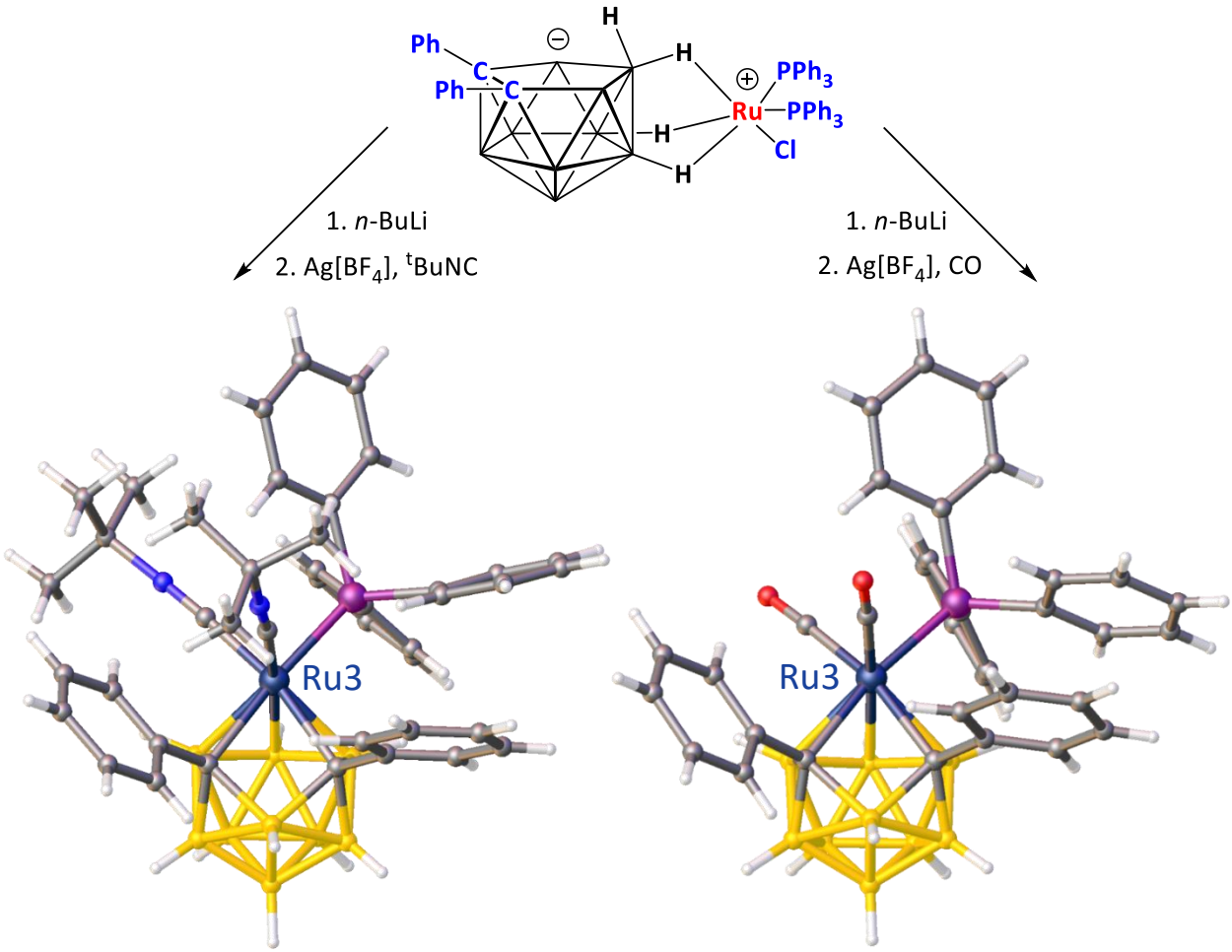

Figure 4.6.6: Synthesis and structures of **18** (left) and **19** (right).

The fact that both species have *pseudocloso* geometries implies that the presumed intermediate, $[1,2\text{-}Ph_2\text{-}3\text{-}Cl\text{-}3,3\text{-}(PPh_3)_2\text{-}3,1,2\text{-}RuC_2B_9H_9]^-$, likely also has a *pseudocloso* geometry, a positive implication for generating *hypercloso* $(PPh_3)_2RuPh_2C_2B_9H_9$. To this

end, a reaction between **17** and *n*-BuLi and Ag[BF_4] was then carried out in the absence of any donor ligands. However, this reaction was found to produce a highly complex product mixture from which the "symbiotic" compounds **20** and **21** were isolated, the molecular structures of which are shown in figures 4.6.7 and 4.6.8.

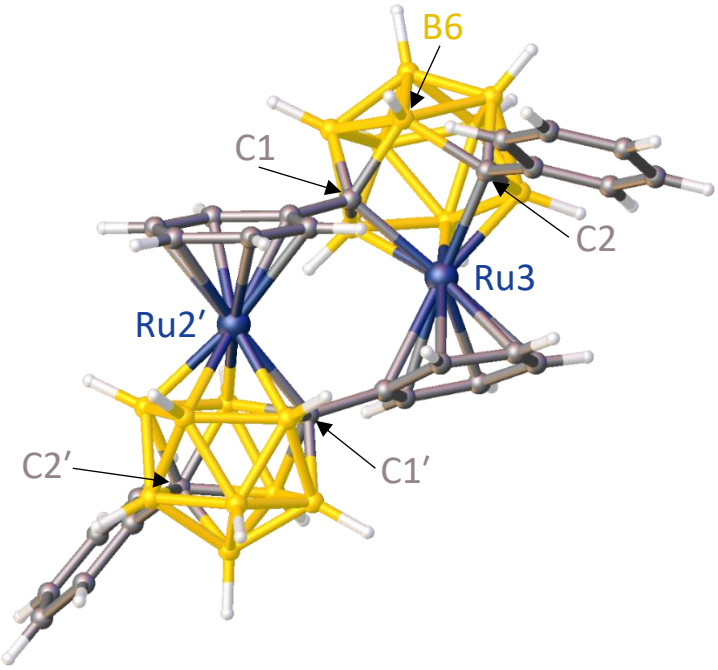

Figure 4.6.7: Structure of [{1,2-Ph_2-*pseudocloso*-3,1,2-$RuC_2B_9H_9$}{1′,8′-Ph_2-*closo*-2′,1′,8′-$RuC_2B_9H_9$}] (**20**).

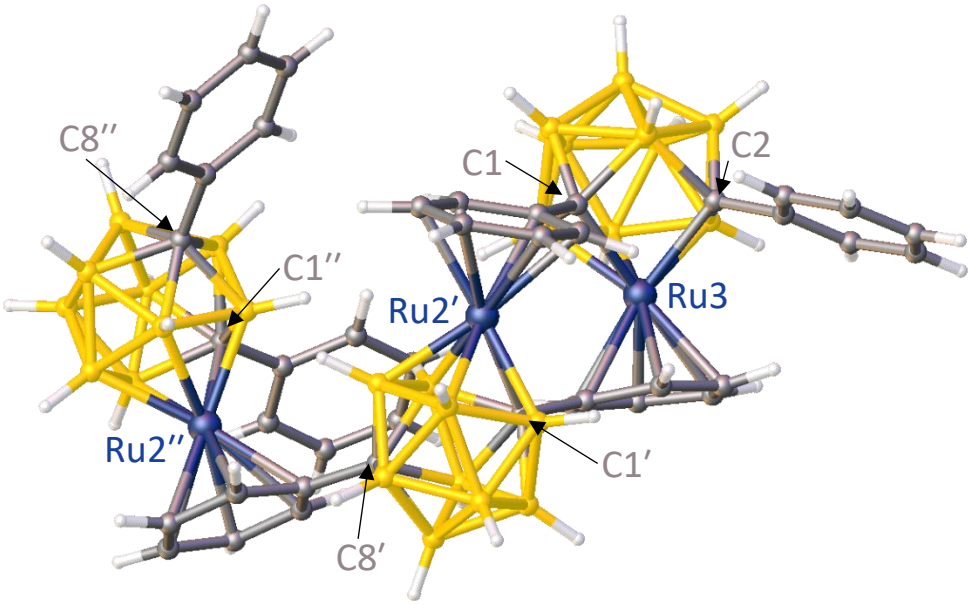

Figure 4.6.8: Structure of [{1,2-Ph_2-*pseudocloso*-3,1,2-$RuC_2B_9H_9$}{1′,8′-Ph_2-*closo*-2′,1′,8′-$RuC_2B_9H_9$}{1″,8″-Ph_2-*closo*-2″,1″,8″-$RuC_2B_9H_9$}] (**21**).

Ultimately, attempts to synthesise *hypercloso* metallacarboranes were once again unsuccessful, although the desired *hypercloso* species $(PPh_3)_2RuPh_2C_2B_9H_9$ is likely initially being formed as it is presumably this species which adds to a pre-existing molecule of **20** in order to form **21**. However, a number of interesting compounds were nonetheless isolated, including **20** and **21**, to the former of which there is only one comparable structure within the literature. Compound **21**, a trimeric, "symbiotic" species, is novel and has no literature precedent.

4.7 References

1 M. Tsuji, *J. Org. Chem.*, 2003, **68**, 9589.

2 C. R. Groom, I. J. Bruno, M. P. Lightfoot and S. C. Ward, *Acta Cryst.*, 2016, **B72**, 171.

3 I. T. Chizhevsky, I. A. Lobanova, V. I. Bregadze, P. V. Petrovskii, A. V. P. Antonovich, A. I. Yanovskii and Yu. T. Struchkov, *Mendeleev Commun.*, 1991, **1**, 47.

4 P. T. Brain, M. Bühl, J. Cowie, Z. G. Lewis and A. J. Welch, *J. Chem. Soc., Dalton Trans.*, 1996, **3**, 231.

5 A. Y. Kostyukovich, D. I. D'yachihin, I. D. Grishin, I. A. Godovikov, A. F. Smol'yakov, F. M. Dolgushin, D. F. Grishin, I. T. Chizhevsky and E. V. Balagurova, *Mendeleev Commun.*, 2017, **27**, 392.

6 D. D. Ellis, S. M. Couchman, J. C. Jeffery, J. M. Malget and F. G. A. Stone, *Inorg. Chem.*, 1999, **38**, 2981.

7 J. J. Jones, L. E. English, A. P. M. Robertson, G. M. Rosair and A. J. Welch, *J. Organomet. Chem.*, 2018, **865**, 65.

8 L. S. Alekseev, F. M. Dolgushin, A. A. Korlyukov, I. A. Godovikov, E. V. Vorontsov and I. T. Chizhevsky, *Organometallics*, 2007, **26**, 3868.

5.0 Conclusions and Future Work

Repeated attempts to synthesise *hypercloso* metallacarboranes have instead produced highly unusual species and phenomena. Many of the observations made suggest that the desired *hypercloso* species is initially generated but that said species then finds a way to restore a *closo* electron count through some otherwise unusual process. Examples of carbonyl stealing, the formation of "wedged" species and synthesis of "symbiotic" compounds have all been observed. Presumably this is either because the structural rearrangement required to go from a *closo* structure to a *hypercloso* structure is unfavourable or simply that the resultant *hypercloso* species is unstable.

A reaction between $[NEt_4]$**3** and $Ag[BF_4]$ designed to produce *hypercloso* $(CO)_3MoMe_2C_2B_9H_9$ instead unexpectedly regenerated **2**, as shown in figure 5.1. This is postulated to have occurred *via* carbonyl stealing, as described in 2.4. In this process the transient species "$(CO)_3MoMe_2C_2B_9H_9$" is generated but then reacts with another molecule of itself to regenerate **2**, as well as one molecule of "$(CO)_2MoMe_2C_2B_9H_9$" which would presumably undergo rapid decomposition.

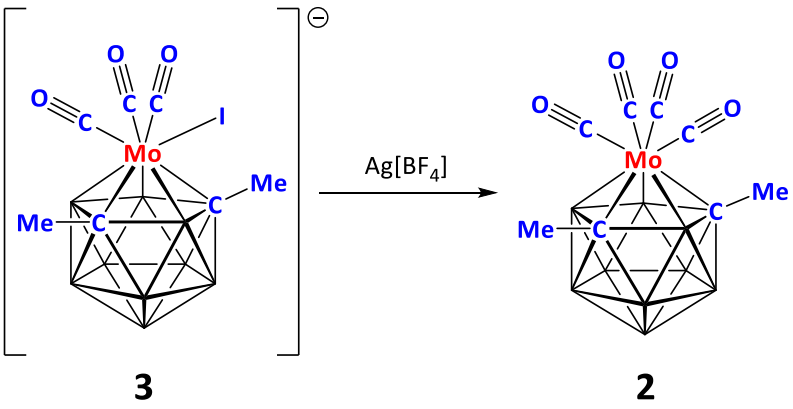

Figure 5.1: Regeneration of **2** *via* carbonyl stealing.

Similarly, the reaction between $[NEt_4]$**IV** and $Ag[BF_4]$ produced a species consistent with **4**, as shown in figure 5.2, a species previously unknown. This is also postulated to be caused by carbonyl stealing. The EIMS, $^{11}B\{^1H\}$ and ^1H NMR spectra are consistent with the proposed structure. Data obtained from the reaction of **1** and Me_3NO and the photolysis of **II** are also consistent with carbonyl stealing.

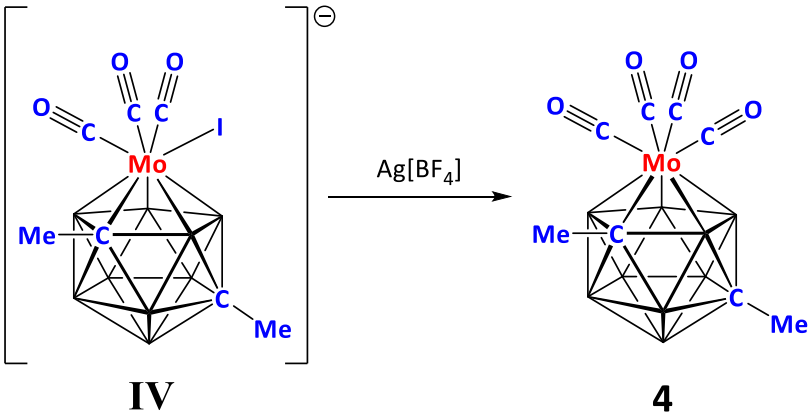

Figure 5.2: Postulated synthesis of **4** *via* carbonyl stealing.

Given recurrent evidence for carbonyl stealing and the near ubiquity of carbonyl ligands in tungstacarboranes and molybdacarboranes efforts were instead directed towards trying to synthesise *hypercloso* ruthenacarboranes. In this case the methodology would be to abstract Cl^- using $Ag[BF_4]$ from species of generic formula [1,2-R_2-3-Cl-3,3-$(PPh_3)_2$-*closo*-3,1,2-$RuC_2B_9H_9$]$^-$, as shown in figure 5.3. Towards this end a new route to species of generic formula [1,2-R_2-3-Cl-3,3-$(PPh_3)_2$-*closo*-3,1,2-$RuC_2B_9H_9$]$^-$ *via* removal of the *endo* proton from the open face of an appropriate *exo-nido* precursor was devised, as shown in figure 5.4.

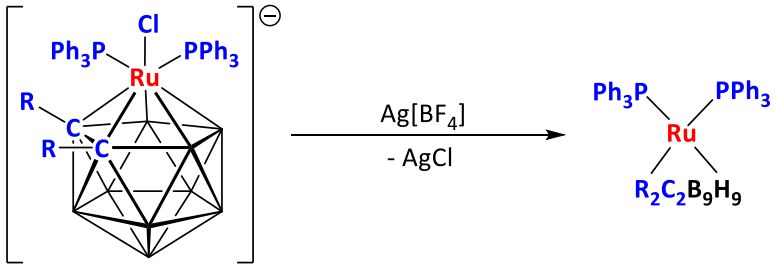

Figure 5.3: Proposed synthesis of generic *hypercloso* species $(PPh_3)_2RuR_2C_2B_9H_9$.

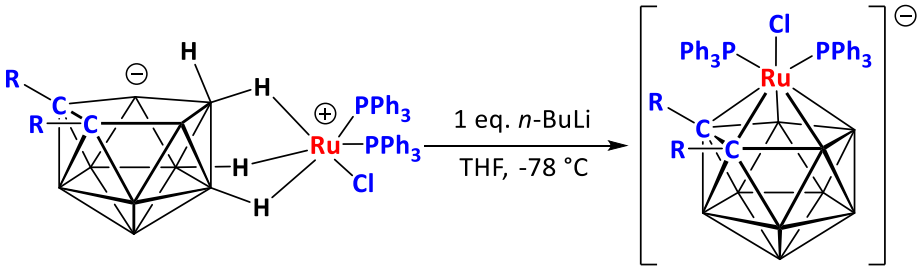

Figure 5.4: Synthesis of [1,2-R_2-3-Cl-3,3-$(PPh_3)_2$-*closo*-3,1,2-$RuC_2B_9H_9$]$^-$.

The same methodology shown in figure 5.3 was used to synthesise a diverse family of mixed ligand ruthenacarboranes (**VII**, **5**, **6**, **14**, **18** and **19**) of generic formula 1-R-2-R′-3-L-3,3-L′$_2$-*closo/pseudocloso*-3,1,2-$RuC_2B_9H_9$ (where either L or L′ is PPh_3 and the other is an L type ligand whilst R and R′ are either H, Me, Ph or ^{t}Bu) by carrying out the reaction in the presence of an L type ligand. Steric interactions meant that this sometimes resulted in the displacement of one molecule of PPh_3 by a second equivalent of L. Representative examples for the synthesis of **5** and **6** are shown in figure 5.5.

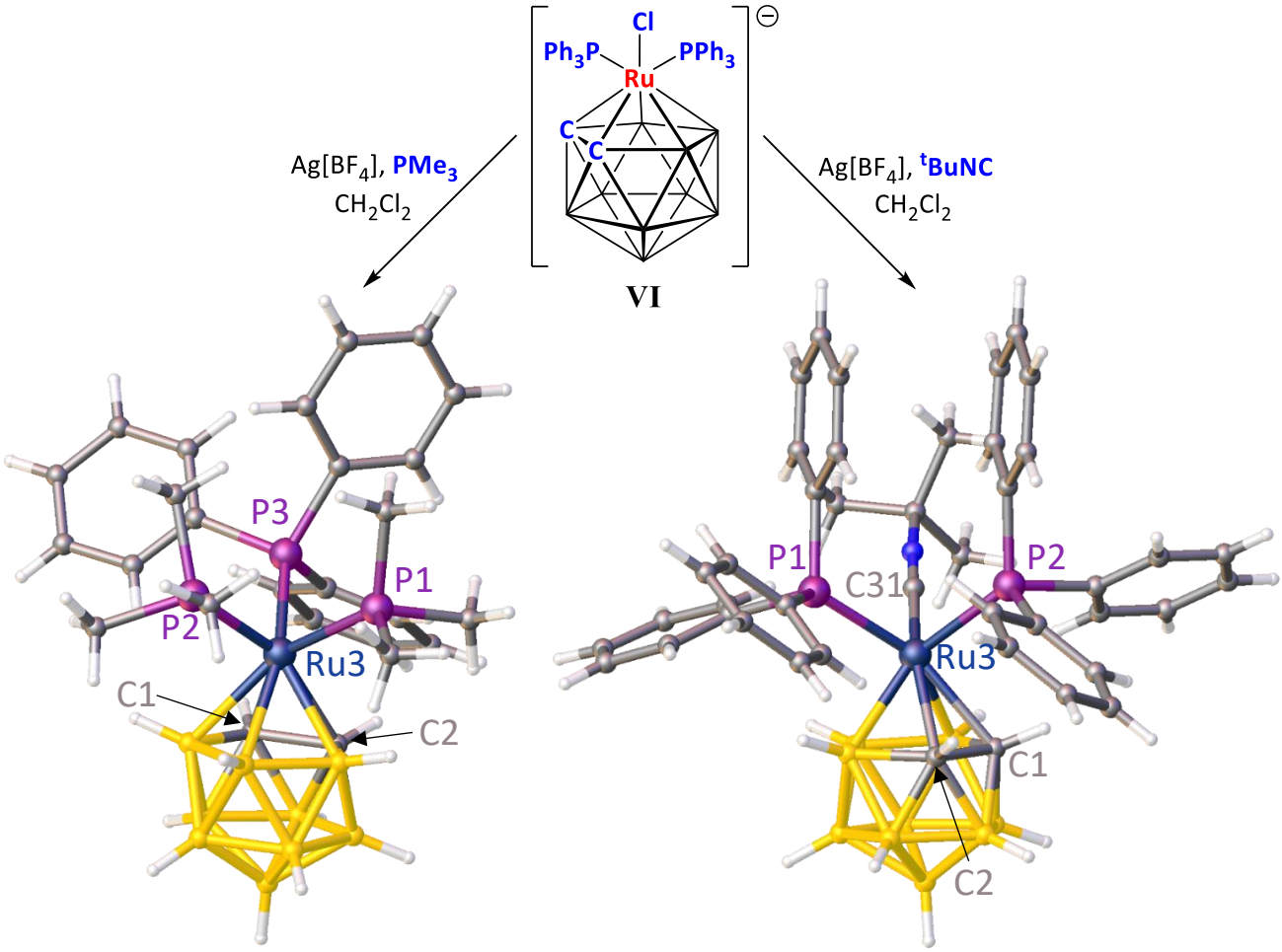

Figure 5.5: Synthesis and molecular structures of **5** (right) and **6** (left).

Abstraction of chloride from species of generic formula [1-R-2-R′-3-Cl-3,3-$(PPh)_2$-*closo*-3,1,2-$RuC_2B_9H_9$]$^-$ (where R and R′ are H, Me or ^{t}Bu) did not produce the desired *hypercloso* species but instead produced highly complex product mixtures. From these mixtures a number of species (**7**, **8**, **9**, **10** and **15**) were isolated which are consistent with RuSAN analogues containing an additional {$(PPh_3)_2$Ru} unit bound *exo* to the cage in a "wedging" position. The molecular structure of **10** is shown in figure 5.6.

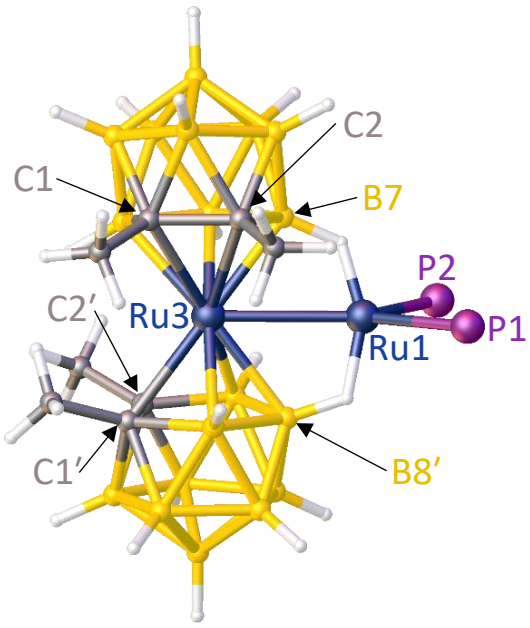

Figure 5.6: Molecular structure of **10**.

In order to encourage the formation of *hypercloso* ruthenacarboranes sterically demanding groups were utilised with the hope that the resulting *pseudocloso* intermediate would aid the anticipated structural change by pre-positioning the resultant species at the square stage of the DSD rearrangement, as noted in section 4.1. To this end a reaction between **17** and *n*-BuLi followed by Ag[BF_4] was carried out. This reaction instead produced a complex product mixture from which the two "symbiotic" species **20** and **21** were isolated, the molecular structures of which are shown in figures 5.7 and 5.8.

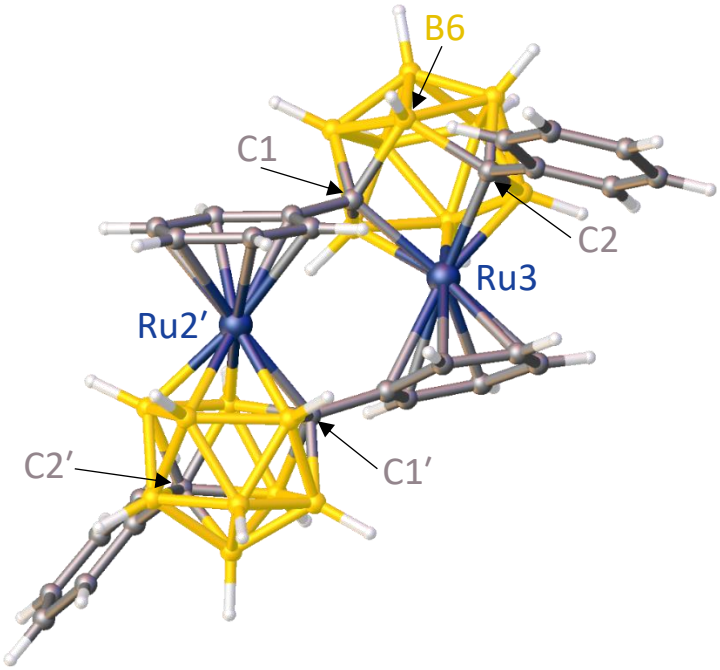

Figure 5.7: Structure of [{1,2-Ph_2-*pseudocloso*-3,1,2-$RuC_2B_9H_9$}{1′,8′-Ph_2-*closo*-2′,1′,8′-$RuC_2B_9H_9$}] (**20**).

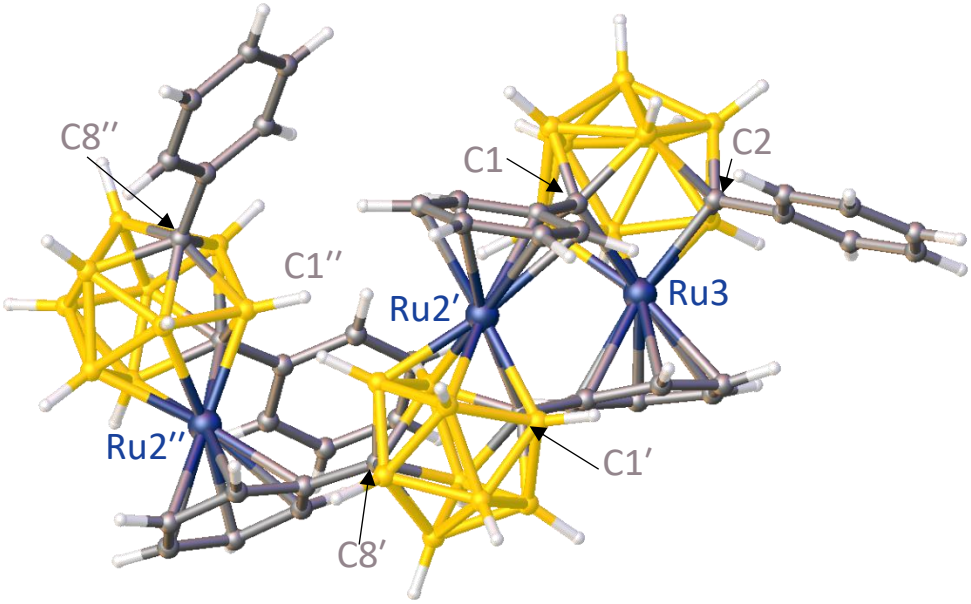

Figure 5.8: Structure of [{1,2-Ph_2-*pseudocloso*-3,1,2-$RuC_2B_9H_9$}{1′,8′-Ph_2-*closo*-2′,1′,8′-$RuC_2B_9H_9$}{1″,8″-Ph_2-*closo*-2″,1″,8″-$RuC_2B_9H_9$}] (**21**).

Compound **21** is presumably generated when a molecule of the transient *hypercloso* species $(PPh_3)_2RuPh_2C_2B_9H_9$ reacts with a pre-existing molecule of **20**. This supports the suggestion that the desired *hypercloso* is indeed being formed but that it is unfavourable for it to undergo the required structural rearrangement or that the resultant species is simply unstable.

5.1 Future Work

The production of **20** suggests that if a reaction were carried out between a species of generic formula [1,2-R_2-3-Cl-3,3-$(PPh_3)_2$-*closo*-3,1,2-$RuC_2B_9H_9$]$^-$ and Ag[BF_4] in the presence of an aromatic ligand then that this could provide an interesting new route to a diverse family of *closo* arene ruthenacarboranes, as shown in figure 5.1.1 for a reaction between **VI**, Ag[BF_4] and toluene. Although a number of *closo* arene ruthenacarboranes are known no general route to them is yet reported.

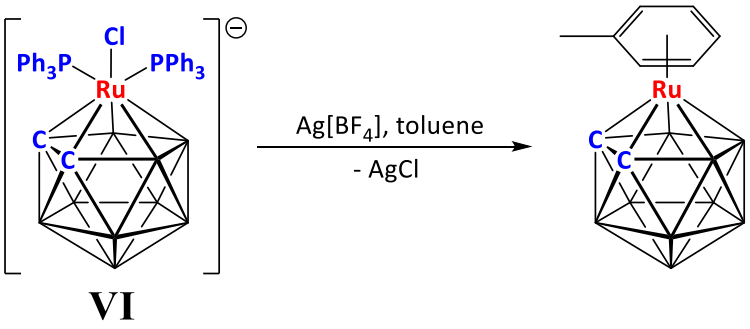

VI

Figure 5.1.1: Proposed synthesis of 3-(MeC_6H_5)-*closo*-3,1,2-$RuC_2B_9H_{11}$.

Additionally, the production of **21** suggests that further symbiotic ruthenacarboranes containing additional cage units may be able to be synthesised by similar routes. For example, if a reaction between **17** and BuLi/Ag[BF_4] in the presence of **21** were carried out this could produce a quadrameric species of formula $(RuPh_2C_2B_9H_9)_4$, as shown in figure 5.1.2. Repetition of this process could potentially afford novel oligomeric ruthenacarboranes. Alternatively, a reaction between **17** and BuLi/Ag[BF_4] in the presence of **20** may produce **21** in higher yields.

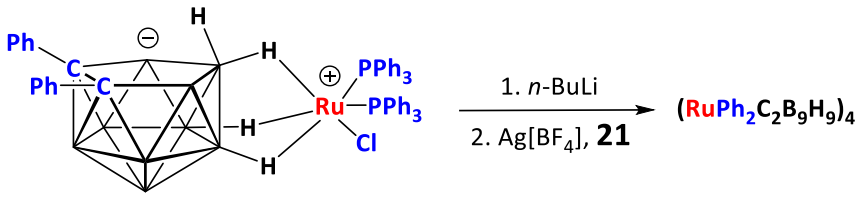

17

Figure 5.1.2: Proposed synthesis of $(RuPh_2C_2B_9H_9)_4$.

The goal of synthesising *hypercloso* ruthenacarboranes through a *pseudocloso* intermediate was unsuccessful for the reaction between **17** and *n*-BuLi/Ag[BF_4] because the Ph units of the cage could provide electrons to neighbouring ruthenium centres, allowing the restoration of a *closo* electron count. However, if the Ph groups could be replaced by a functional group which is chemically inert and sterically demanding then no such problems would occur. Therefore, for example, a reaction between [1,2-Cy_2-3-Cl-3,3-$(PPh_3)_2$-*pseudocloso*-3,1,2-$RuC_2B_9H_9$]$^-$ and Ag[BF_4] could produce *hypercloso* $(PPh_3)_2RuCy_2C_2B_9H_9$, as shown in figure 5.1.3. Alternatively, two $SiMe_3$ groups could be utilised as although ^{t}BuCC^{t}Bu is too sterically demanding to successfully insert into decaborane, the fact that C-Si bonds tend to be longer than alkyl C-C bonds may reduce steric encumbrance, enabling $(Me)_3SiCCSi(Me)_3$ to insert. It should be noted that 1,2-$(SiMe_3)_2$-1,2-$C_2B_{10}H_{10}$ is a known species but no route to said species is provided by the authors.[1]

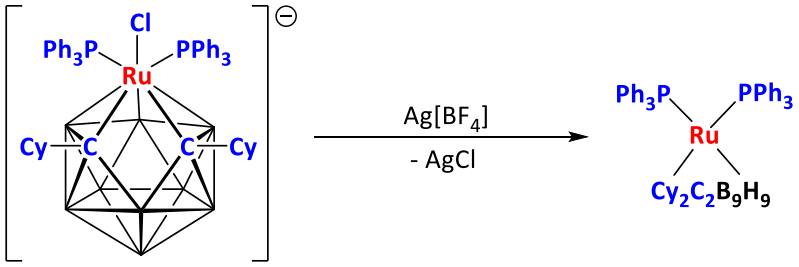

Figure 5.1.3: Proposed synthesis of *hypercloso* $(PPh_3)_2RuCy_2C_2B_9H_9$.

Work by Chizhevsky and co-workers report a diverse family of *exo-nido* osmacarboranes.[2,3] As osmium is, like ruthenium, a group eight metal this means that if an osmacarborane of general formula $L_2OsR_2C_2B_nH_n$ could be synthesised then said species would have a *hypercloso* electron count. Chizhevsky and co-workers report a family of *exo-nido* osmacarboranes which are directly analogous to the *exo-nido* ruthenacarboranes utilised in chapters three and four, of general formula 5,6,10-$[Cl(Ph_3P)_2Os]$-5,6,10-μ-$(H)_3$-7,8-R_2-10-H-7,8-$C_2B_9H_6$.[2] Sequential reaction of said species with *n*-BuLi and Ag[BF_4] could generate *hypercloso* species of generic formula $(PPh_3)_2OsR_2C_2B_9H_9$, as shown in figure 5.1.4

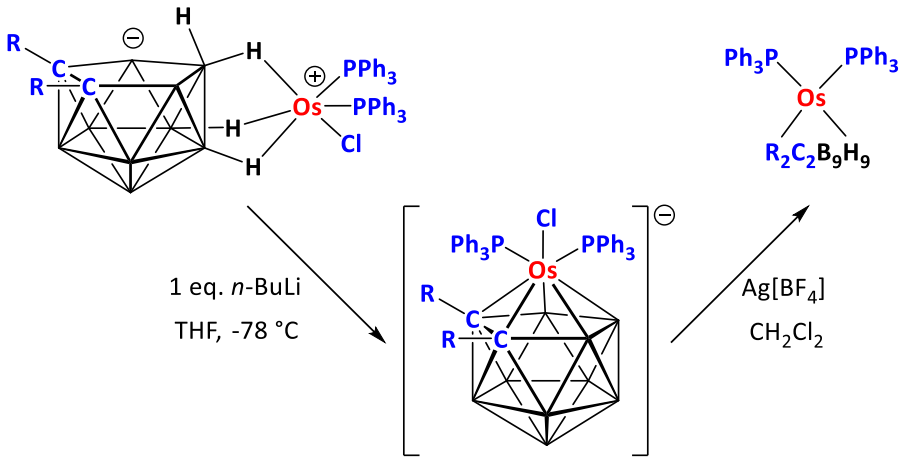

Figure 5.1.4: Proposed synthesis of $(PPh_3)_2OsMe_2C_2B_9H_9$ *via* sequential reaction of 5,6,10-$[Cl(Ph_3P)_2Os]$-5,6,10-μ-$(H)_3$-7,8-R_2-10-H-7,8-$C_2B_9H_6$ with *n*-BuLi and $Ag[BF_4]$.

Alternatively, a family of *exo-nido* ruthenacarboranes of general formula 5,6,10-$[Cl(Ph_3P)_2Ru]$-5,6,10-μ-$(H)_3$-7,9-R_2-10-H-7,9-$C_2B_9H_6$ could be synthesised from K[7,9-R_2-7,9-$C_2B_9H_{10}$], as shown in figure 5.1.5. There is literature precedent for such an approach, as work by Chizhevsky and co-workers has used an analogous route to succesfully synthesise a series of osmacarboranes of general formula 10,11-$[HCl(Ph_3P)_2Os]$-10,11-μ-$(H)_2$-7-R-7,9-$C_2B_9H_8$ (where R=Ph or H). Sequential reaction of said ruthenacarboranes with *n*-BuLi and $Ag[BF_4]$ could then generate *hypercloso* ruthenacarboranes. The fact that any functional groups attached to the cage carbon atoms would be separated from each other may mean that steric interactions inhibit the coordination of an *exo* bound metal fragment, as was seen in the case of the "wedged" species **10**, instead producing *hypercloso* ruthencarboranes. Alternatively, if cage carbon bound phenyl groups were utilised then symbiotic ruthenacarboranes analogous to **20** and **21** would likely be synthesised which could have interesting molecular structures.

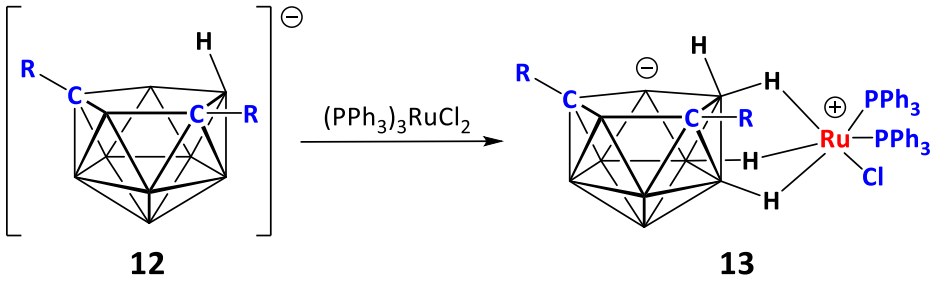

Figure 5.1.5: Proposed synthesis of generic ruthenacarborane 5,6,10-$[Cl(Ph_3P)_2Ru]$-5,6,10-μ-$(H)_3$-7,9-R_2-10-H-7,9-$C_2B_9H_6$.

5.2 References

1 R. M. Salinger and C. L. Frye, *Inorg. Chem.,* 1965, **4**, 1815.

2 G. D. KolomnikovaP. V. PetrovskiiP. V. SorokinF. M. DolgushinA. I. YanovskyI. T. Chizhevsky, *Russ. Chem. Bull.*, 2001, **50**, 706.

3 E. V. Balagurova, D. N. Cheredilin, G. D. Kolomnikova, O. L. Tok, F. M. Dolgushin, A. I. Yanovsky, and I. T. Chizhevsky, *J. Am. Chem. Soc*., 2007, **129**, 3745.

6.0 Experimental

6.1 General Experimental

6.1.1 Synthesis, Spectroscopy and Spectrometry

All experiments were carried out under dry, deoxygenated N_2 using standard Schlenk line techniques although some subsequent manipulations were performed in the open laboratory. Some reagents were stored and weighed out in an MBRAUN UNIlab Plus glovebox. Tetrahydrofuran (THF), diethyl ether and 40:60 petroleum ether (petrol) were freshly distilled under N_2 from sodium wire immediately prior to use. CH_2Cl_2 and MeCN were distilled under N_2 from CaH_2 prior to use. All solvents were degassed *via* three freeze-pump-thaw cycles before use. Deuterated solvents were stored over 3 Å molecular sieves. Column chromatography was carried out using 60 Å silica and preparative TLC was carried out on 20x20 cm silica Kieselgel F_{254} glass plates.

NMR spectra were recorded at 400.1 MHz (^{1}H), 128.4 MHz (^{11}B) and 162.0 MHz (^{31}P) on a Bruker AVIII-400 spectrometer in $CDCl_3$ at 298 K unless otherwise stated. Elemental analysis was recorded using an Exeter CE-440 elemental analyser. Electron impact mass spectrometry (EIMS) was carried out using a Finnigan (Thermo) LCQ Classic ion trap mass spectrometer at the University of Edinburgh. Infrared (IR) spectra were recorded in the solid state using a Thermo Scientific Nicolet iS5 FTIR spectrometer with a iD7 Diamond ATR accessory.

Unless otherwise states, all reagents were purchased from commercial suppliers such as Sigma-Aldrich, Alfa-Aesar and Fluorochem and were used as received. Exceptions to this include $C_2B_{10}H_{12}$, purchased from Katchem. $Mo(CO)_2(MeCN)_2(C_3H_5)Br$,[1] [BTMA][4,4-$(CO)_2$-4-$(C_3H_5)$-*closo*-4,1,6-$MoC_2B_{10}H_{12}$],[2] [PNP][1,6-$Me_2$-4,4-$(CO)_2$-4-$(C_3H_5)$-*closo*-4,1,6-$MoC_2B_{10}H_{10}$] ([PNP]**III**),[3] 5,6,10-[$Cl(Ph_3P)_2Ru$]-5,6,10-μ-$(H)_3$-10-H-7,8-$C_2B_9H_8$ (**V**),[4] 5,6,10-[$Cl(Ph_3P)_2Ru$]-5,6,10-μ-$(H)_3$-7,8-Me_2-10-H-7,8-$C_2B_9H_6$ (**VIII**),[4] $Ru(PPh_3)_3Cl_2$[5] and 1-^{t}Bu-*closo*-1,2-$C_2B_{10}H_{11}$ (**IX**)[6] were prepared *via* literature routes.

6.1.2 Crystallography

All crystals were grown from slow diffusion of petrol and a CH_2Cl_2 solution of the appropriate compound at -20 °C unless otherwise stated. Crystals were mounted in inert oil and cooled by a cryostream on the diffractometer. Structures were solved and refined by Dr. G. M. Rosair of Heriot-Watt University. Using OLEX2,[7] structures were solved utilising SHELXS[8] or SHELXT[9] and refined by full-matrix least-squares using SHELXL.[8] Where appropriate, CH vertices were distinguished from BH vertices using VCD[10,11] and BHD[11,12] methods. H atoms bound to cage B atoms were allowed to refine positionally whilst other H atoms were constrained to idealised geometries with C_{phenyl}-H 0.95 Å, C_{phenyl}-H (η-bound to Ru) 1.00 Å, C_{methyl}-H 0.98 Å and $C_{secondary}$-H 0.99 Å. All H displacement parameters were constrained to be 1.2 x U_{eq} (bound B or C) except Me H atoms 1.5 x U_{eq} (C_{methyl}). The diffractometer used in each experiment are specified within the tables found in appendix A.

6.2 Attempts to Synthesise *Hypercloso* Molybdacarboranes

6.2.1 Improved synthesis of $Mo(CO)_2(MeCN)_2(C_3H_5)Br$ (I)

MeCN (30 mL) was added to $Mo(CO)_6$ (6 g, 22.7 mmol), producing a suspension. To this allyl bromide (7.86 mL, 90.9 mmol, *ca.* four equivalents) was added and the resulting suspension heated to reflux for 16 hours, by the end of which an orange-yellow precipitate had formed. The solution was then cooled to -10 ˚C, leading to the formation of a greater mass of precipitate. The solvent was then removed using a filter cannula and the resultant orange-yellow solid washed with petrol (3x15 mL). $Mo(CO)_2(MeCN)_2(C_3H_5)Br$ (**I**) (6.382 g, 18.0 mmol, 79.1% yield) was collected as a semi-crystalline orange-yellow solid and was characterised by ^1H NMR and IR spectroscopy, producing data consistent with those reported in the literature.[1]

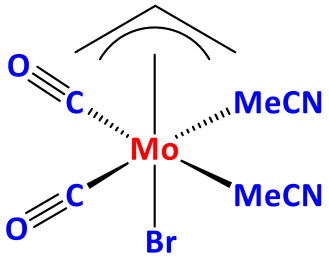

6.2.2 Synthesis of 4,4,4,4-$(CO)_4$-*closo*-4,1,6-$MoC_2B_{10}H_{12}$ (1)

[BTMA][4,4-$(CO)_2$-4-(C_3H_5)-*closo*-4,1,6-$MoC_2B_{10}H_{12}$] (0.810 g, 1.66 mmol) was dissolved in CH_2Cl_2 (40 mL) to give a yellow solution. This was then cooled to -78 ˚C and saturated with carbon monoxide gas. To this $HBF_4{\cdot}Et_2O$ (0.31 ml, 2.6 mmol) was added and the resulting solution was stirred at -78 ˚C for 15 minutes, allowed to warm to room temperature and then allowed to stir for a further hour. The solvent was then removed *in vacuo* from the resulting yellow solution to give a sandy brown-yellow solid. A 50:50 mixture of CH_2Cl_2:petrol (75 mL) was added and the resulting suspension was filtered through celite. The filtrate was reduced in volume before being purified by cold column chromatography at -40 ˚C using 40:60 CH_2Cl_2:petrol as the eluent to produce 4,4,4,4-$(CO)_4$-*closo*-4,1,6-$MoC_2B_{10}H_{12}$ (**1**) (0.310 g, 0.880 mmol, 53.0% yield) as a yellow solid.

NMR: ^{1}H NMR, δ 4.38 (s, 2H, CH)

^{11}B{^{1}H} NMR, δ 10.5 (1B), 5.6 (1B), 2.52 (2B), 1.2 (2B), -6.3 (1B), -8.3 (3B).

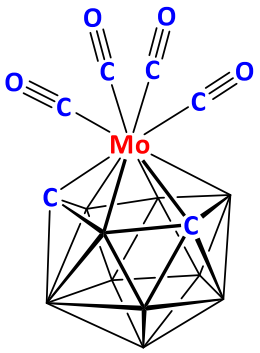

6.2.3 Reaction between 1 and Me_3NO

Compound **1** (205 mg, 0.582 mmol) was dissolved in CH_2Cl_2 (20 mL) to give a yellow solution before Me_3NO (44 mg, 0.586 mmol) was added. This immediately gave rise to a red-brown solution which was allowed to stir for thirty minutes before the solvent was removed *in vacuo* to give a brown paste. This was revealed by $^{11}B\{^1H\}$ NMR spectroscopy to contain **1**.

ATR-IR: ν_{max} 2530 (B-H), 2067 (CO), 2045 (CO), 1998 (CO) cm^{-1}.

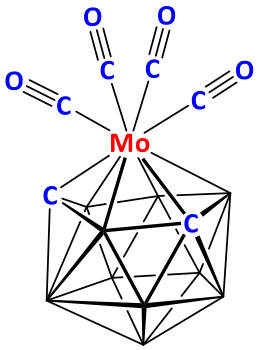

6.2.4 Synthesis of 1,7-Me_2-2,2,2,2-$(CO)_4$-*closo*-2,1,7-$MoC_2B_9H_9$ (2)

[PNP][4,4-$(CO)_2$-4-(C_3H_5)-1,6-Me_2-*closo*-4,1,6-$MoC_2B_{10}H_{10}$] ([PNP]**III**) (2.472 g, 2.74 mmol) was dissolved in CH_2Cl_2 (24 mL) and the resulting yellow solution saturated with CO before being cooled to -78 ˚C. $HBF_4{\cdot}Et_2O$ (0.51 mL, 3.73 mmol, 1.36 equivalents) was then added and the mixture stirred at -78 ˚C for 30 minutes, before being allowed to warm to room temperature and stir for an additional 30 minutes, over which time a brown solution formed. The solvent was then removed *in vacuo* and the resultant brown solid was washed with a 50:50 mixture of CH_2Cl_2:petrol. The washings were then dried *in vacuo* before being purified via cold column chromatography, using 40:60 CH_2Cl_2:petrol as the eluent. This gave rise to a yellow band which was found to be 1,7-Me_2-2,2,2,2-$(CO)_4$-*closo*-2,1,7-$MoC_2B_9H_9$ (**2**) (103 mg, 0.280 mmol, 10.2%) as a yellow solid.

NMR: ^{1}H NMR, δ 1.45 (s, 6H, CH_3).

^{1}H{^{11}B} NMR, δ 3.81 (broad s, 1H, BH), 3.49 (broad s, 1H, BH), 2.59 (broad s, 2H, BH), 2.33 (broad s, 2H, BH), 2.27 (broad s, 1H, BH), 2.06 (broad s, 2H, BH), 1.45 (s, 6H, CH_3).

^{11}B{^{1}H} NMR, δ 6.6 (1B), -4.4 (2B), -5.8 (1B), -7.1 (2B), -9.0 (2B), -12.0 (1B).

EIMS: *m/z* 368 (M^+), 353 (M-CH_3), 325 (M-CH_3, -CO), 312 (M-2×CO), 297 (M-CH_3, -2×CO), 284 (M-3×CO), 269 (M-CH_3, -3×CO), 256 (M-4×CO).

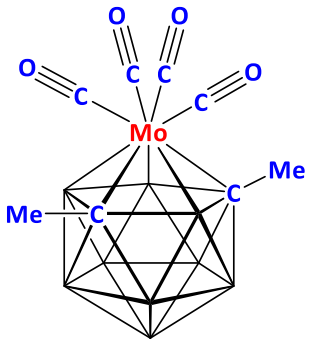

6.2.5 Synthesis of [NEt_4][1,7-Me_2-2-I-2,2,2-$(CO)_3$-*closo*-2,1,7-$MoC_2B_9H_9$] (3)

Compound **2** (68 mg, 0.184 mmol) was dissolved in CH_2Cl_2 (15 mL) and [NEt_4]I (47 mg, 0.183 mmol) added. The resultant orange-red solution was stirred for 16 hours before the solvent was removed *in vacuo* to produce the highly air-sensitive species [NEt_4][1,7-Me_2-2-I-2,2,2-$(CO)_3$-*closo*-2,1,7-$MoC_2B_9H_9$] ([NEt_4]**3**) (108 mg, 0.181 mmol, 98.2%) as an orange solid.

NMR: ^{1}H NMR (CD_2Cl_2), δ 3.30 (q, 8H, NCH_2), 1.59 (s, 6H, CH_3), 1.40 (t, 12H, NCH_2CH_3).

^{11}B{^{1}H} NMR (CD_2Cl_2), δ -4.6 (3B), -8.1 (3B), -10.8 (2B), -12.3 (1B).

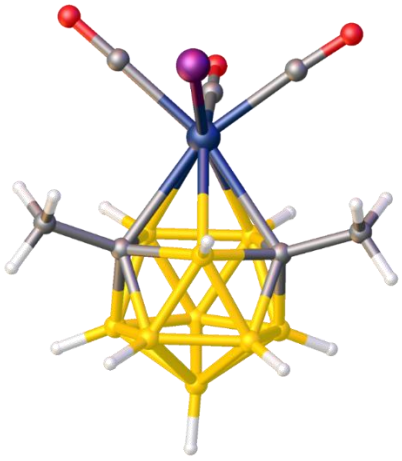

6.2.6 Dehalogenation of [NEt$_4$]3

[NEt$_4$]**3** (40 mg, 0.0669 mmol) was dissolved in CH_2Cl_2 (10 mL) before being frozen at -196 ˚C. Ag[BF_4] (25 mg, 0.128 mmol) was added before the vessel was evacuated and then refilled with nitrogen. The reaction mixture was then allowed to warm to room temperature and stir for 16 hours, producing a brown suspension. The suspension was filtered through celite before the solvent was removed *in vacuo* to produce a yellow solid which was identified by $^{11}B\{^1H\}$ NMR spectroscopy as regenerated 1,7-Me_2-2,2,2,2-$(CO)_4$-*closo*-2,1,7-$MoC_2B_9H_9$ (**2**) (10 mg, 0.027 mmol, 40.6%).

6.2.7 Synthesis of [NEt$_4$][1,8-Me$_2$-2,2,2-(CO)$_3$-2-I-*closo*-2,1,8-MoC$_2$B$_9$H$_9$] ([NEt$_4$]IV)

The anion [1,8-Me$_2$-2,2,2-(CO)$_3$-2-I-*closo*-2,1,8-MoC$_2$B$_9$H$_9$]$^-$ (**IV**) has been previously prepared as the PNP salt by Stone and co-workers by a different route, although it has previously not been crystallographically characterised.

1,2-Me$_2$-3,3,3,3-(CO)$_4$-*closo*-3,1,2-MoC$_2$B$_9$H$_9$ (150 mg, 0.407 mmol) was dissolved in THF (12 mL) before [NEt$_4$]I (105 mg, 0.408 mmol) was added. The reagents were then heated to reflux for three hours, producing a red solution. The solution was allowed to cool to room temperature and the solvent removed *in vacuo*. The resulting red oil was then purified *via* column chromatography at -40 ˚C using CH_2Cl_2 as the eluent. This produced an orange-red band which was found to be [NEt$_4$][1,8-Me$_2$-2,2,2-(CO)$_3$-2-I-*closo*-2,1,8-MoC$_2$B$_9$H$_9$] ([NEt$_4$]**IV**) (55 mg, 0.092 mmol, 22.6%).

NMR: ^{1}H NMR (CD_2Cl_2), δ 3.21 (q, 8H, N CH_2), 2.44 (s, 3H, CH_3), 2.31 (s, 3H, CH_3), 1.24 (t, 12H, CH_2CH_3).

^{11}B{^{1}H} NMR (CD_2Cl_2), δ -0.1 (1B), -4.5 (3B), -5.7 (1B), -6.7 (2B), -8.4 (2B).

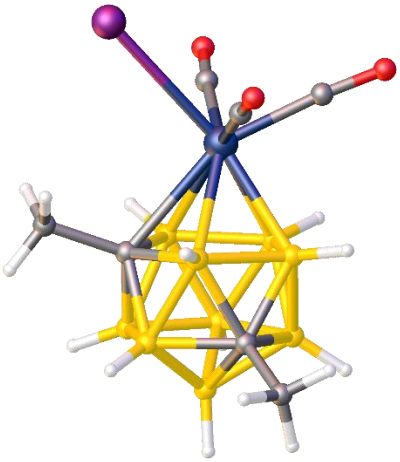

v

6.2.8 Synthesis of 1,8-Me_2-2,2,2,2-$(CO)_4$-*closo*-2,1,8-$MoC_2B_9H_9$ (4)

[NEt_4]**IV** (55 mg, 0.092 mmol) was dissolved in CH_2Cl_2 (12 mL). The resulting solution was then frozen at -196 ˚C and Ag[BF_4] (18 mg, 0.093 mmol) was added, before the vessel was evacuate and refilled with nitrogen. The reaction mixture was then allowed to warm to room temperature and stir for one hour, over which time the mixture changed from an orange-red colour to a brown-yellow colour. The mixture was then filtered through celite before being reduced *in vacuo*. The mixture was purified by cold column chromatography at -40 ˚C using 30:70 CH_2Cl_2:petrol as eluent. This afforded a yellow band from which the solvent was removed *in vacuo* to give a yellow solid, postulated to be 1,8-Me_2-2,2,2,2-$(CO)_4$-*closo*-2,1,8-$MoC_2B_9H_9$ (**4**).

NMR: ^{1}H NMR (C_6D_6), δ 1.48 (s, 3H, CH_3), 1.14 (s, 3H, CH_3).

^{11}B{^{1}H} NMR (C_6D_6), δ 5.7 (1B), -0.5 (1B), -3.5 (2B), -5.2 (2B), -6.9 (1B), -9.5 (1B), -10.6 (1B).

EIMS: *m/z* 368 (M^+), 340 (M-CO), 312 (M-2×CO), 284 (M-3×CO), 256 (M-4×CO).

CHN: $C_8H_{15}B_9MoO_4$ requires C, 26.08; H, 4.10. Found: C, 26.40; H, 4.59%.

6.3 Towards *Hypercloso* Ruthenacarboranes

6.3.1 Synthesis of Li[3-Cl-3,3-$(PPh_3)_2$-*closo*-3,1,2-$RuC_2B_9H_{11}$] (Li[VI])

5,6,10-[$Cl(Ph_3P)_2Ru$]-5,6,10-μ-$(H)_3$-10-H-7,8-$C_2B_9H_8$ (**V**) (100 mg, 0.126 mmol) was dissolved in THF (10 mL) and the resulting red solution cooled to -78 ˚C. *n*-BuLi (0.05 mL of a 2.5 mol dm^{-3} solution in hexanes, 0.126 mmol) was then added, giving rise to a dark red solution. This was then allowed to warm to room temperature and stir for 30 minutes before 1 mL of the solution was transferred to a separate vessel and the solvent removed *in vacuo*, producing a dark red paste. CD_3CN (0.8 mL) was then added and the resulting red solution transferred to a J. Youngs NMR tube.

NMR: $^{11}B\{^1H\}$ NMR (CD_3CN), δ -1.5 (1B), -5.8 (2B), -8.4 (1B), -10.9 (1B), -12.3 (2B), -25.4 (2B).

$^{31}P\{^1H\}$ NMR (CD_3CN), δ 45.27 (s).

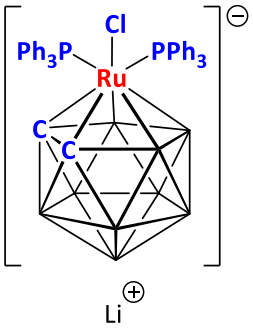

6.3.2 Synthesis of 3,3-$(PPh_3)_2$-3-CO-*closo*-3,1,2-$RuC_2B_9H_{11}$ (VII)

5,6,10-$[Cl(Ph_3P)_2Ru]$-5,6,10-μ-$(H)_3$-10-H-7,8-$C_2B_9H_8$ (**V**) (199 mg, 0.250 mmol) was dissolved in THF (20 mL) before *n*-BuLi (0.1 mL of a 2.5 M solution in hexanes, 0.50 mmol) was added at -78 ˚C, producing a dark red solution. The reaction mixture was then allowed to warm to and stir at room temperature for 30 minutes before the solvent was removed *in vacuo* and replaced with CH_2Cl_2 (15 mL). The resulting solution was then saturated with CO gas before being frozen at -196 ˚C. $Ag[BF_4]$ (54 mg, 0.276 mmol, 1.1 equivalents) was then added and the reaction mixture allowed to warm to room temperature before being stirred for 16 hours, producing a dark brown suspension. The solvent was then removed *in vacuo* and the resultant dark brown paste extracted into CH_2Cl_2 and filtered through celite before being purified using column chromatography, using 30:70 CH_2Cl_2:petrol as the eluent. This produced a yellow band which was found to be 3,3-$(PPh_3)_2$-3-CO-*closo*-3,1,2-$RuC_2B_9H_{11}$ (**VII**) (108 mg, 0.137 mmol, 55.0% yield).

NMR: $^{11}B\{^1H\}$ NMR (CD_2Cl_2), δ 1.7 (1B), -2.4 (1B), -8.2 (4B), -20.4 (3B).

$^{31}P\{^1H\}$ NMR (CD_2Cl_2), δ 40.48 (s).

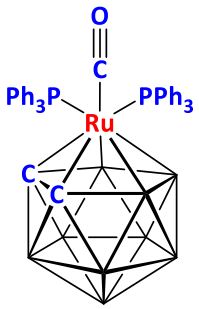

6.3.3 Synthesis of 3,3-$(PPh_3)_2$-3-^{t}BuNC-*closo*-3,1,2-$RuC_2B_9H_{11}$ (5)

Compound **V** (199 mg, 0.25 mmol) was dissolved in THF (20 mL) and the resulting red solution cooled to -78 ˚C before *n*-BuLi (0.10 mL of a 2.5 mol dm^{-3} solution in hexanes, 0.25 mmol) was added, immediately giving rise to a dark red solution. To this ^{t}BuNC (21 mg, 0.25 mmol, 0.03 mL) was added, causing the solution to take on an orange-red colour. The solution was then transferred *via* cannula into a vessel containing $Ag[BF_4]$ (49 mg, 0.25 mmol) and allowed to stir for one hour, over which time the resulting suspension assumed a yellow colour. The solvent was then removed *in vacuo* to produce a brown-yellow paste which was redissolved in CH_2Cl_2, filtered through celite and reduced in volume *in vacuo*. The resulting mixture was purified by column chromatography, using 50:50 CH_2Cl_2:petrol as the eluent and giving rise to a yellow band which was found to be 3,3-$(PPh_3)_2$-3-^{t}BuNC-*closo*-3,1,2-$RuC_2B_9H_{11}$ (**5**) (44 mg, 0.052 mmol, 20.9% yield).

NMR: ^{1}H NMR (CD_2Cl_2), δ 7.40-7.25 (m, 18H, C_6H_5), 7.23-7.13 (m, 12H, C_6H_5), 2.11 (broad s, 2H, CH), 1.65 (s, 9H, CH_3).

^{11}B{^{1}H} NMR (CD_2Cl_2), δ -0.5 (1B), -3.0 (1B), -9.5 (4B), -22.3 (3B).

^{31}P{^{1}H} NMR (CD_2Cl_2), δ 42.20 (s).

CHN: $C_{43}H_{50}B_9NP_2Ru$ requires C, 61.4; H, 5.99; N, 1.67. Found: C, 61.9; H, 6.04; N, 1.59%.

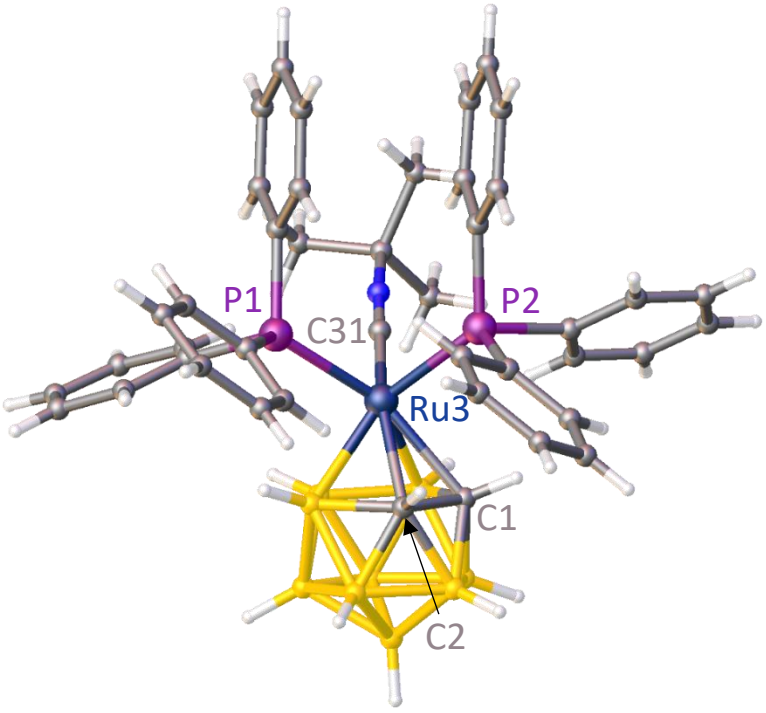

6.3.4 Synthesis of 3,3-$(PMe_3)_2$-3-PPh_3-*closo*-3,1,2-$RuC_2B_9H_{11}$ (6)

Compound **V** (199 mg, 0.25 mmol) was dissolved in THF (20 mL) and the resulting red solution cooled to -78 ˚C before *n*-BuLi (0.10 mL of a 2.5 mol dm^{-3} solution in hexanes, 0.25 mmol) was added, immediately giving rise to a dark red solution. This was then allowed to warm to room temperature and stir for 30 minutes. PMe_3 (0.25 mL of a 1.0 mol dm^{-3} solution in THF, 0.25 mmol) was added and the resulting solution then transferred *via* cannula into a vessel containing $Ag[BF_4]$ (49 mg, 0.25 mmol), creating a brown-yellow suspension which was allowed to stir for 16 hours. The solvent was then removed *in vacuo* before the resulting green-brown paste was redissolved in CH_2Cl_2 and passed through a silica plug. This produced a yellow filtrate, which was concentrated *in vacuo* and then purified by column chromatography using 50:50 CH_2Cl_2:petrol as the eluent. A yellow band was collected and the solvent was removed *in vacuo* to produce 3-PPh_3-3,3-$(PMe_3)_2$-*closo*-3,1,2-$RuC_2B_9H_{11}$ (**6**) (71 mg, 0.110 mmol, 43.8% yield).

NMR: ^{1}H NMR (CD_2Cl_2), δ 7.77-7.32 (m, 15H, C_6H_5), 1.83 (broad s, 2H, CH), 1.55-1.48 (m, 18H, CH_3).

^{11}B{^{1}H} NMR (CD_2Cl_2), δ -1.9 (s, 1B), -6.1 (s, 1B), -7.0 to -12.0 (overlapping resonances with maxima at -9.0 and -10.3, 4B), -23.0 (s, 3B).

^{31}P{^{1}H} NMR (CD_2Cl_2), δ 45.56 (t, {$^2J_{PP}$ 35.67 Hz}), -1.61 (d, {$^2J_{PP}$ 35.67 Hz}).

CHN: $C_{26}H_{44}B_9P_3Ru$ requires C, 45.2; H, 7.25. Found: C, 44.6; H, 6.44%.

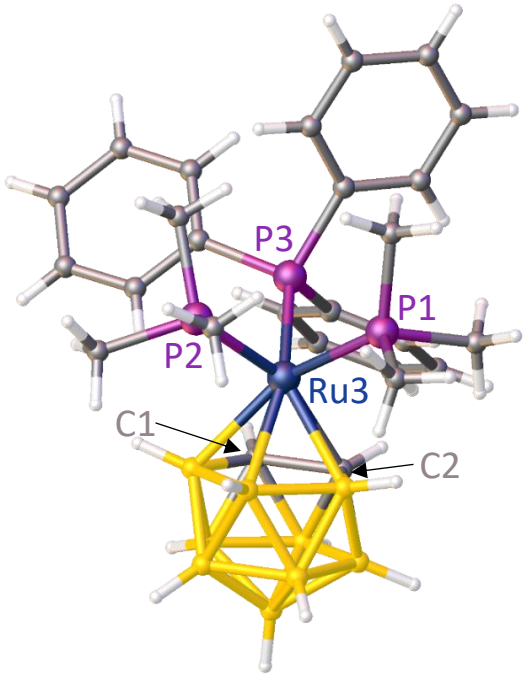

6.3.5 Deprotonation and dehalogenation of 5,6,10-[Cl(Ph$_3$P)$_2$Ru]-5,6,10-μ-(H)$_3$-10-H-7,8-C$_2$B$_9$H$_8$ (V)

Compound **V** (1.200 g, 1.51 mmol) was dissolved in THF (35 mL) and the resulting red solution cooled to -78 ˚C before *n*-BuLi (0.6 mL of a 2.5 mol dm^{-3} solution in hexanes, 1.51 mmol) was added, immediately giving rise to a dark red solution. This was then allowed to warm to room temperature before being allowed to stir for 20 minutes. The solvent was then removed *in vacuo* and replaced with CH_2Cl_2 (40 mL). The resulting solution was then transferred *via* cannula into a vessel containing Ag[BF_4] (294 mg, 1.51 mmol), creating a dark brown suspension which was allowed to stir for 16 hours. The solvent was then removed *in vacuo* before the resulting dark brown solid material was redissolved in CH_2Cl_2 and filtered through celite. The filtrate was then concentrated *in vacuo* before the resulting dark brown solution was purified *via* preparative TLC using 40:60 CH_2Cl_2:petrol as the eluent. This give rise to an extremely complex set of TLC plates with multiple bands of various colours. Three such bands were isolated and found by $^{11}B\{^1H\}$ NMR spectroscopy to contain boron. One such red-orange band (**7**) (R_f=0.42) was isolated and found to be have data consistent with the "wedge" species [($C_2B_9H_{11}$)$_2$Ru]-*exo*-Ru(PPh_3)$_2$ (51 mg). Two further bands (**8** and **9**, yellow: R_f=0.61: 29 mg and brown: R_f=0.30: 17 mg, respectively) were isolated and found to produce $^{11}B\{^1H\}$, ^1H and $^{31}P\{^1H\}$ NMR spectra similar to that of **7**.

Compound 7

NMR: ^{1}H NMR (CD_2Cl_2), δ 8.04-7.13 (m, 30H, C_6H_5), 5.69 (s, 1H, CH), 4.17 (s, 1H, CH), 2.33 (s, 1H, CH), 2.29 (s, 1H, CH).

^{1}H {^{11}B} NMR (CD_2Cl_2), δ 8.04-7.13 (m, 30H, C_6H_5), 5.69 (s, 1H, CH), 4.17 (s, 1H, CH), 3.71 (s, 1H, BH), 3.42 (s, 1H, BH), 2.71 (s, 1H, BH), 2.48 (s, 1H, BH), 2.30 to 2.24 (overlapping resonances with maxima at 2.33, 2.29 and 2.26, 4H, mixture of 2 CHs and 2 BHs), 2.06 (s, 2H, BH), 1.94 (s, 1H, BH), 1.79 (s, 3H, BH), 1.70 (s, 2H, BH), 1.38 (s, 1H, BH), 0.71 (s, 1H, BH), -8.39 (s, 1H, BH).

^{11}B{^{1}H} NMR (CD_2Cl_2), δ 61.3 (broad s, 1B), 11.9 to -22.0 (overlapping resonances with maxima at 11.0, 10.2, 7.0, 2.5, -2.4, -3.1, -7.5, -12.0, -14.2 and -19.0, 17B).

^{31}P{^{1}H} NMR (CD_2Cl_2), δ 46.5 (s), 30.1(s).

CHN: $C_{38}H_{41}B_9P_2Ru$ requires C, 60.2; H, 5.45. $C_{40}H_{52}B_{18}P_2Ru_2$ requires C, 48.5; H, 5.29. Found: C, 48.1; H, 5.84%.

Compound 8

NMR: ^{1}H NMR (CD_2Cl_2), δ 8.04-7.09 (m, 30H, C_6H_5), 5.86 (s, 1H, CH), 3.84 (s, 1H, CH), 2.58 (s, 1H, CH), 2.09 (s, 1H, CH).

^{11}B{^{1}H} NMR (CD_2Cl_2), δ 58.6 (broad s, 1B), 8.9 to 3.7 (overlapping resonances with maxima at 7.9 and 4.8, 3B), 1.2 to -22.1 (overlapping resonances with maxima at 0.0, -3.9, -5.0, -7.9, -13.1 and -19.4, 14B).

^{31}P{^{1}H} NMR (CD_2Cl_2), δ 47.17 (s), 29.67 (s).

Compound 9

NMR: ^{1}H NMR (CD_2Cl_2), δ 8.00-7.24 (m, 30H, C_6H_5), 4.41 (s, 1H, CH), 3.57 (s, 1H, CH), 2.45 (s, 1H, CH), 2.15 (s, 1H, CH).

^{11}B{^{1}H} NMR (CD_2Cl_2), δ 54.9 (1B), 25.1 (1B), 15.8 (1B), 8.8 to -23.3 (overlapping resonances with maxima at 7.9, 5.4, 2.8, 0.0, -3.69, -10.0 and 17.9, 15B).

^{31}P{^{1}H} NMR (CD_2Cl_2), δ 44.92 (s), 34.70 (s).

6.3.6 Deprotonation and dehalogenation of 5,6,10-[Cl(Ph$_3$P)$_2$Ru]-5,6,10-μ-(H)$_3$-7,8-Me$_2$-10-H-7,8-C$_2$B$_9$H$_6$ (VIII). Synthesis of [7,8′-*exo*-(Ru{PPh$_3$}$_2$)-7,8′-μ-(H)$_2$-*commo*-3,3′-Ru(1,2-Me$_2$-1,2-C$_2$B$_9$H$_8$)(1′,2′-Me$_2$-1′,2′-C$_2$B$_9$H$_8$)] (10).

5,6,10-[Cl(Ph$_3$P)$_2$Ru]-5,6,10-μ-(H)$_3$-7,8-Me$_2$-10-H-7,8-C$_2$B$_9$H$_6$ (**VIII**) (565 mg, 0.69 mmol) was dissolved in THF (20 mL) and the resulting red solution cooled to -78 ˚C before *n*-BuLi (0.27 mL of a 2.5 mol dm^{-3} solution in hexanes, 0.69 mmol) was added, immediately giving rise to an extremely dark solution. This was then warmed to room temperature before being allowed to stir for 30 minutes. The solvent was then removed *in vacuo* and replaced with CH_2Cl_2 (20 mL). The resulting solution was then transferred *via* cannula into a vessel containing Ag[BF$_4$] (147 mg, 0.76 mmol), creating a dark brown suspension which was allowed to stir for 16 hours. The solvent was then removed *in vacuo* before the resulting dark brown solid material was redissolved in CH_2Cl_2 and filtered through celite. The filtrate was then concentrated *in vacuo* before the resulting dark brown solution was purified *via* preparative TLC using 40:60 CH_2Cl_2:petrol as the eluent. This give rise to an extremely complex set of TLC plates with several bands of various colours. One such green band (R_f=0.38) was isolated and found to be the "wedge" species [7,8′-*exo*-(Ru{PPh$_3$}$_2$)-7,8′-μ-(H)$_2$-*commo*-3,3′-Ru(1,2-Me$_2$-1,2-C$_2$B$_9$H$_8$)(1′,2′-Me$_2$-1′,2′-C$_2$B$_9$H$_8$)] (**10**) (28 mg, 0.027 mmol, 3.9% yield).

NMR: ^{1}H NMR, δ 7.61-7.33 (m, 15H, C$_6$H$_5$), 7.29-6.94 (m, 15H, C$_6$H$_5$), 1.81 (s, 6H, CH$_3$), 1.30 (s, 6H, CH$_3$).

^{1}H{^{11}B} NMR, δ 7.61-7.33 (m, 15H, C$_6$H$_5$), 7.29-6.94 (m, 15H, C$_6$H$_5$), 3.20 (s, 2H, BH), 2.51 (s, 3H, BH), 2.06 (s, 6H, BH), 1.81 (s, 6H, CH$_3$), 1.30 (s, 6H, CH$_3$), 0.76 (s, 3H, BH), -3.77 (s, 2H, BH).

^{11}B{^{1}H} NMR, δ 35.7 (2B), 10.3 to -18.8 (overlapping resonances with maxima at -5.4, -7.1 and -10.6, 16B).

^{31}P{^{1}H} NMR, δ 68.33 (s).

CHN: C$_{44}$H$_{60}$B$_{18}$P$_2$Ru$_2$ requires C, 50.4; H, 5.77. Found: C, 51.0; H 5.84%.

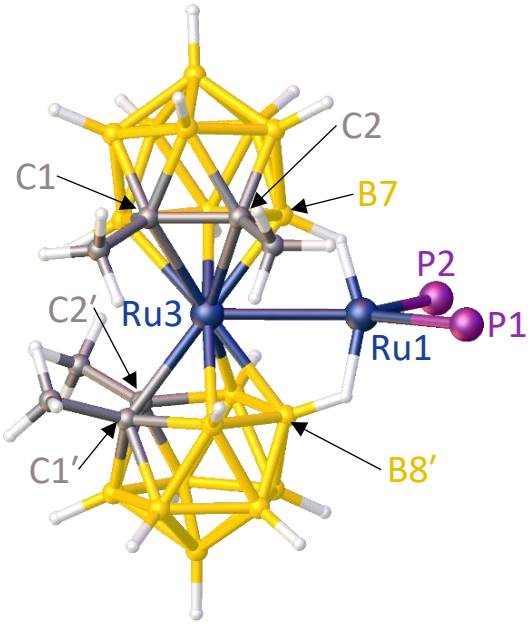

Phenyl units omitted for clarity.

6.4 *Pseudocloso* Ruthenacarboranes

6.4.1 Synthesis of 1-^{t}Bu-2-Me-*closo*-1,2-$C_2B_{10}H_{10}$ (11)

1-^{t}Bu-*closo*-1,2-$C_2B_{10}H_{11}$ (**IX**) (1.04 g, 5.19 mmol) was dissolved in THF (30 mL). *n*-BuLi (2.7 mL of a 2.5 mol dm^{-3} solution in hexanes, 6.75 mmol, 1.3 equivalents) was then added at 0°C and the solution allowed to warm to room temperature and stir for 30 minutes, giving rise to a cloudy suspension. Methyl iodide (0.42 mL, 6.75 mmol, 1.3 equivalents) was then added and the reaction mixture heated to reflux for one hour. The resulting clear, orange solution was allowed to cool to room temperature before the solvent was removed *in vacuo*. The resulting oily solid was dissolved in Et_2O (30 mL) and deionised water (30 mL) added. The organic layer was then extracted, dried over $MgSO_4$, filtered and the solvent removed *in vacuo* to give 1-^{t}Bu-2-Me-*closo*-1,2-$C_2B_{10}H_{10}$ (**11**) (1.02 g, 4.77 mmol, 92% yield) as a white solid.

NMR: ^{1}H NMR, δ 2.20 (s, 3H, Me), 1.38 (s, 9H, ^{t}Bu).

^{11}B{^{1}H} NMR, δ -3.1 (1B), -4.9 (1B), -8.4 (2B), -9.8 (2B), -10.6 (4B).

EIMS: *m/z* 214 (M^+), 199 (M^+-CH_3), 157 (M^+-C_4H_9).

CHN: $C_7H_{22}B_{10}$ requires C 39.2, H 10.34; found C 39.4, H 10.64%.

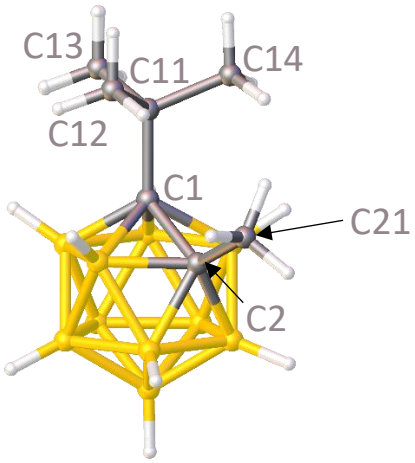

6.4.2 Synthesis of K[7-^{t}Bu-8-Me-*nido*-7,8-$C_2B_9H_{10}$] (12)

1-^{t}Bu-2-Me-*closo*-1,2-$C_2B_{10}H_{10}$ (**11**) (1.02 g, 4.77 mmol) was dissolved in ethanol (30 mL), KOH (0.802 g, 14.3 mmol, 3 equivalents) added and the resulting suspension heated to reflux for 120 hours. This was then allowed to cool to room temperature before CO_2 was bubbled through it, resulting in a precipitate of K_2CO_3, which was then removed *via* filtration. The filtrate was then evaporated *in vacuo* and the resulting solid dissolved in THF (10 mL). The resulting solution was then slowly added, with stirring, to petrol (250 mL). The precipitate was collected and dried *in vacuo* to give K[7-^{t}Bu-8-Me-*nido*-7,8-$C_2B_9H_{10}$] (**12**) (0.930 g, 3.83 mmol, 80.3% yield) as a white solid.

NMR: ^{1}H NMR (CD_3COCD_3), δ 1.56 (s, 3H, Me), 1.10 (s, 9H, ^{t}Bu).

^{1}H{^{11}B} NMR (CD_3COCD_3), δ 2.84 (broad s, 2H, BH), 1.56 (s, 3H, Me), 2.04 (s, 1H, BH), 1.87 (broad s, 1H, BH), 1.58 (s, 3H, BH), 1.10 (s, 9H, ^{t}Bu), 0.52 (broad s, 1H, BH), 0.00 (broad s, 1H, BH), -2.41 (broad s, 1H, B-H-B).

^{11}B{^{1}H} NMR (CD_3COCD_3), δ -7.0 (1B), -10.8 (1B), -12.7 (1B), -14.7 (1B), -19.2 (2B), -20.7 (1B), -35.2 (1B), -36.8 (1B).

CHN: $C_7H_{22}B_{10}K$ requires C 34.7, H 9.14; found: C 34.8, H 9.05%.

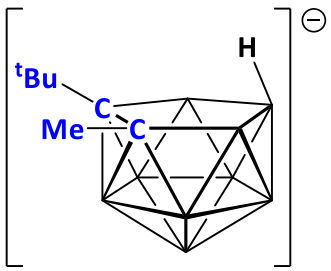

6.4.3 Synthesis of 5,6,10-[Cl(Ph$_3$P)$_2$Ru]-5,6,10-μ-(H)$_3$-7-^{t}Bu-8-Me-10-H-7,8-C$_2$B$_9$H$_6$] (13)

K[7-^{t}Bu-8-Me-*nido*-7,8-C$_2$B$_9$H$_{10}$] (**12**) (0.379 g, 1.564 mmol) was dissolved in THF (15 mL) and the resulting solution transferred *via* cannula into a vessel containing Ru(PPh$_3$)$_3$Cl$_2$ (1.65 g, 1.721 mmol, 1.1 equivalents). The resulting dark brown solution was stirred for 16 hours before the solvent was removed *in vacuo* to give a dark brown solid, which was then dissolved in CH_2Cl_2 (30 mL) and filtered through celite. An aqueous extraction was then carried out and the organic layer separated, dried over $MgSO_4$ and filtered. The resulting brown solution was reduced in volume and purified *via* column chromatography, using pure CH_2Cl_2 as the eluent. This produced an orange band, which was dried *in vacuo* to give 5,6,10-[Cl(Ph$_3$P)$_2$Ru]-5,6,10-μ-(H)$_3$-7-^{t}Bu-8-Me-10-H-7,8-C$_2$B$_9$H$_6$ (**13**) (0.855 g, 0.9889 mmol, 63.2% yield) as an orange-red solid.

NMR: ^{1}H NMR (C$_6$D$_6$), δ 7.68-7.34 (m, 12 H), 6.96-6.78 (m, 18H), 1.73 (s, 1H, Me), 1.71 (s, 2H, Me), 1.11 (s, 3H, ^{t}Bu), 1.08 (s, 6H, ^{t}Bu).

^{1}H{^{11}B} NMR (C$_6$D$_6$), δ 7.68-7.34 (m, 12 H), 6.96-6.78 (m, 18H), 3.80 (broad s, BH), 2.85 (broad s, BH), 2.71 (broad s, BH), 2.60 (broad s, BH), 2.53 (broad s, BH), 2.42 (broad s, BH), 2.36 (broad s, BH), 2.30 (broad s, BH), 2.24 (broad s, BH), 1.73 (s, 1H, Me), 1.71 (s, 2H, Me), 1.11 (s, 3H, ^{t}Bu), 1.08 (s, 6H, ^{t}Bu), 0.64 (broad s, BH), 0.48 (broad s, BH), -0.86 (broad s, BH), -1.03 (broad s, BH), -2.48 (broad s, BH), -3.05 (broad s, BH), -3.74 (broad s, BH), -4.29 (broad s, BH), -6.01 (broad s, BH), -14.71 (broad s, BH), -14.96 (broad s, BH), -16.20 (broad s, BH).

^{11}B{^{1}H} NMR (C$_6$D$_6$), δ 3.9 (broad), -9.4 (broad), -17.6, -21.6, -23.4, -25.4, -28.0, -31.6, -42.1, -44.7.

^{31}P{^{1}H} NMR (C$_6$D$_6$), δ 55.25 (d), 53.05 (apparent d), 51.01 (apparent d), 49.04 (m), 46.06 (m), 45.53 (m).

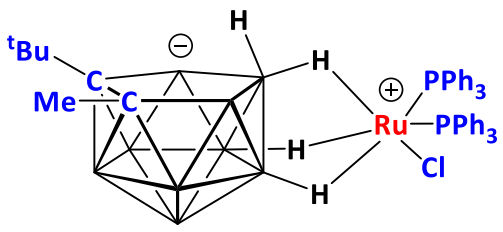

6.4.4 1-^{t}Bu-2-Me-3-PPh$_3$-3,3-(^{t}BuNC)$_2$-*closo*-3,1,2-RuC$_2$B$_9$H$_9$ (14)

5,6,10-[Cl(Ph$_3$P)$_2$Ru]-5,6,10-μ-(H)$_3$-7-^{t}Bu-8-Me-10-H-7,8-C$_2$B$_9$H$_6$ (**13**) (265 mg, 0.307 mmol) was dissolved in THF (25 mL) and *n*-BuLi (0.12 mL of a 2.5 mol dm^{-3} solution in hexanes, 0.307 mmol) was added at 0°C. This was then allowed to warm to and stir at room temperature for 30 minutes to give a very dark solution. The solvent was removed *in vacuo* to give a dark solid, which was then dissolved in CH_2Cl_2 (20 mL). The resulting dark solution was transferred *via* cannula onto a mixture of Ag[BF_4] (71.6 mg, 0.368 mmol, 1.2 equivalents) and ^{t}BuNC (0.035 mL, 0.307 mmol). This was then stirred for 30 minutes to give a yellow-brown suspension before the solvent was removed *in vacuo* to give a dark brown solid. The solid material was then dissolved in CH_2Cl_2 and filtered through celite to give a yellow-brown solution, which was reduced in volume. The crude solution was then purified using preparative TLC, using 60:40 CH_2Cl_2:petrol as the eluent. This produced plates with a number of bands, including a yellow band at R_f=0.50, found to be 1-^{t}Bu-2-Me-3-PPh$_3$-3,3-(^{t}BuNC)$_2$-*closo*-3,1,2-RuC$_2$B$_9$H$_9$ (**14**) (91 mg, 0.125 mmol, 41% yield) as a yellow solid.

NMR: ^{1}H NMR, δ 7.69-7.62 (m, 6H, C$_6$H$_5$), 7.44-7.33 (m, 9H, C$_6$H$_5$), 2.17 (s, 3H, Me), 1.43 (s, 9H, ^{t}Bu) 1.28 (m, 9H, ^{t}Bu), 1.25 (m, 9H, ^{t}Bu).

^{11}B{^{1}H} NMR, δ 11.9 (1H), 9.0 (1H), 1.1 (2H), -2.2 (3H), -7.6 (1H), -17.7 (1H).

^{31}P{^{1}H} NMR, δ 47.19 (s).

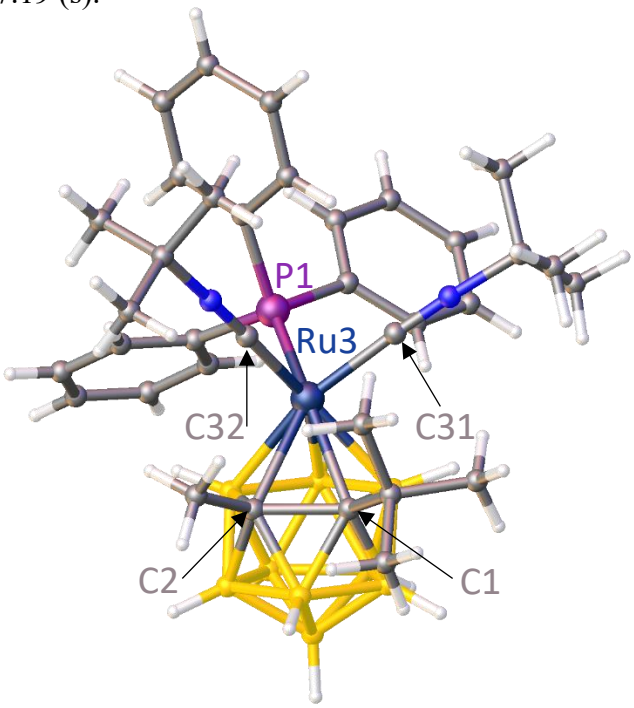

6.4.5 Deprotonation and dehalogenation of 5,6,10-[Cl(Ph$_3$P)$_2$Ru]-5,6,10-μ-(H)$_3$-7-^{t}Bu-8-Me-10-H-7,8-$C_2B_9H_6$ (13). Synthesis of compounds 15 and 16.

Compound **13** (216 mg, 0.250 mmol) was dissolved in THF (20 mL) and *n*-BuLi (0.1 mL of a 2.5 mol dm^{-3} solution in hexanes, 0.250 mmol) was added at 0°C. This was then allowed to warm to and stir at room temperature for thirty minutes, producing a very dark solution. The solvent was then removed *in vacuo* before being replaced with CH_2Cl_2 (20 mL). The resulting dark solution was transferred *via* cannula into a vessel containing Ag[BF_4] (58 mg, 0.300 mmol) and the resulting suspension allowed to stir overnight. The solvent was then removed *in vacuo* to produce a dark brown solid which was then extracted into CH_2Cl_2 and filtered through celite. The resulting dark solution was then reduced in volume and purified *via* preparative TLC using 40:60 CH_2Cl_2:petrol as the eluent. This gave rise to an extremely complex set of plates containing over ten bands, of which components **15** (R_f=0.51) and **16** (R_f=0.27) were isolated as orange solids.

Compound 15

NMR: ^{1}H NMR, δ 7.46 (t, 6H, C_6H_5), 7.27 (t, 12H, C_6H_5), 7.22-7.15 (m, 12H, C_6H_5), 2.38 (s, 6H, Me), 1.31 (s, 18H, ^{t}Bu).

^{1}H{^{11}B} NMR, δ 7.46 (t, 6H, C_6H_5), 7.27 (t, 12H, C_6H_5), 7.22-7.15 (m, 12H, C_6H_5), 4.46 (s, 2H, BH), 3.26 (s, 2H, BH), 2.91 (s, 2H, BH), 2.69 (s, 2H, BH), 2.62 (s, 2H, BH), 2.53 (s, 2H, BH), 2.38 (s, 6H, Me), 2.29 (s, 2H, BH), 0.95 (s, 2H, BH), -2.95 (s, 2H, BH).

^{11}B{^{1}H} NMR, δ 42.5 (2B), 17.3 (2B), 8.4 (2B), 2.4 (2B), -1.1 (4B), -2.7 to -7.2 (overlapping resonances with maxima at -3.8 and -4.9, 4B) -19.2 (2B).

^{31}P{^{1}H} NMR, δ 11.80 (broad s).

Compound 16

NMR: ^{1}H NMR, δ 7.61-7.53 (m, 6H, C_6H_5), 7.36-7.26 (m, 12H, C_6H_5), 7.25-7.18 (m, 6H, C_6H_5), 7.17-7.10 (m, 6H, C_6H_5), 1.54 (s, 3H, Me), 1.29 (s, 9H, ^{t}Bu).

^{1}H{^{11}B} NMR, δ 7.61-7.53 (m, 6H, C_6H_5), 7.36-7.26 (m, 12H, C_6H_5), 7.25-7.18 (m, 6H, C_6H_5), 7.17-7.10 (m, 6H, C_6H_5), 3.15 (s, 1H, BH), 2.39 (s, 1H, BH), 2.19 (s, 1H, BH),

1.95 (s, 1H, BH), 1.72 (s, 1H, BH), 1.54 (s, 3H, Me), 1.29 (s, 9H, ^{t}Bu), -1.98 (d, 1H, BH), -6.10 (d, 2H, BH), -16.07 (apparent t, 1H, BH).

^{11}B{^{1}H} NMR, δ 28.8 (1B), 5.5 (1B), -1.7 (1B) -15.0 (3B), -23.2 (1B), -28.6 (1B), -30.9 (1B).

^{31}P{^{1}H} NMR, δ 51.80 (d, {$^{2}J_{PP}$ 31.71 Hz}), 41.36 (d, {$^{2}J_{PP}$ 31.71 Hz}).

6.4.6 Synthesis of 5,6,10-[Cl(Ph$_3$P)$_2$Ru]-5,6,10-μ-(H)$_3$-7,8-Ph$_2$-10-H-7,8-C$_2$B$_9$H$_6$ (17)

K[7,8-Ph$_2$-7,8-C$_2$B$_9$H$_{10}$] (0.500 g, 1.54 mmol) was dissolved in THF (40 mL) and the resulting orange-red solution transferred *via* cannula into a vessel containing solid Ru(PPh$_3$)$_3$Cl$_2$ (1.624 g, 1.1 equivalents, 1.69 mmol). This was then stirred at room temperature for three hours to give a dark brown solution. The solvent was then removed *in vacuo* to give a dark brown solid, which was then dissolved in CH_2Cl_2 (30 mL) and filtered through celite before the solvent was removed *in vacuo*. The resulting dark brown solid was then purified by column chromatography. Initially pure petrol was used as the eluent, before incrementally transitioning to 60:40 CH_2Cl_2:petrol (*via* 20:80 and 40:60 CH_2Cl_2:petrol). This produced a red band which was collected and the solvent removed *in vacuo* to give 5,6,10-[Cl(Ph$_3$P)$_2$Ru]-5,6,10-μ-(H)$_3$-7,8-Ph$_2$-10-H-7,8-C$_2$B$_9$H$_6$ (**17**) (1.138 g, 1.20 mmol, 78.1% yield) as a red solid.

NMR: ^{1}H NMR (C$_6$D$_6$), δ 7.65-7.55 (m, 6H, C$_6$H$_5$), 7.54-7.47 (t, 6H, C$_6$H$_5$), 7.13-7.06 (m, 3H, C$_6$H$_5$), 6.95-6.81 (m, 18H, C$_6$H$_5$), 6.77-6.62 (m, 6H, C$_6$H$_5$).

^{1}H{^{11}B} NMR (C$_6$D$_6$), δ δ 7.65-7.55 (m, 6H, C$_6$H$_5$), 7.54-7.47 (t, 6H, C$_6$H$_5$), 7.13-7.06 (m, 3H, C$_6$H$_5$), 6.95-6.81 (m, 18H, C$_6$H$_5$), 6.77-6.62 (m, 6H, C$_6$H$_5$), 4.10 (broad s, BH), 3.60 (broad s, BH), 3.48 (broad s, BH), 3.07-2.97 (overlapping resonances with maxima at 3.04 and 3.00, broad s, BH), 2.78 (broad s, BH), 2.67 (broad s, BH), 2.62-2.53 (overlapping resonances with maxima at 2.58 and 2.56, broad s, BH), -0.09 (d, BH), -2.61 (d, BH), -3.81 (d, BH), -5.72 (m, BH), -15.18 (t, BH), -16.03 (q, BH).

^{11}B{^{1}H} NMR (C$_6$D$_6$), δ 5.7 (broad), 3.6 (broad), -11.1 (broad), -18.3, -22.6 (with shoulder at 21.3), -24.8, -30.3, -40.2, -43.1.

^{31}P{^{1}H} NMR (C$_6$D$_6$), δ 53.14 (d), 49.2 (s), 46.34 (broad).

EIMS: *m/z* 947 (M^+), 911 (M^+-Cl), 684 (M^+-PPh$_3$).

CHN: C$_{50}$H$_{50}$B$_9$ClP$_2$Ru requires C, 63.4; H, 5.32. Found: C, 63.6; H, 5.47%.

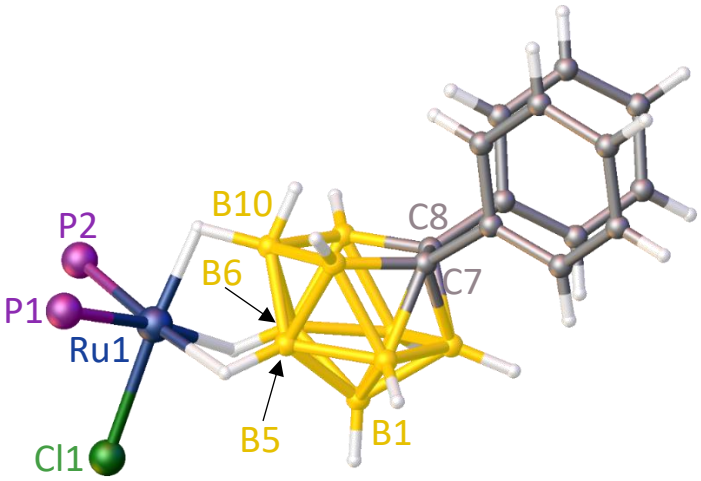
P2
P1
Ru1
Cl1
B10
B6
B5
B1
C8
C7

6.4.7 Synthesis of 1,2-Ph_2-3-(^{t}BuNC)$_2$-3-PPh_3-*pseudocloso*-3,1,2-$RuC_2B_9H_9$ (18)

5,6,10-[Cl(Ph_3P)$_2$Ru]-5,6,10-μ-(H)$_3$-7,8-Ph_2-10-H-7,8-$C_2B_9H_6$ (**17**) (210 mg, 0.222 mmol) was dissolved in THF (18 mL) and *n*-BuLi (0.09 mL of a 2.5 mol dm^{-3} solution in hexanes, 0.225 mmol) was added at 0°C. This was then stirred for 30 minutes to give an extremely dark solution. The solvent was removed *in vacuo* to give a dark solid, which was then dissolved in CH_2Cl_2 (20 mL). The resulting dark solution was transferred *via* cannula onto a mixture of ^{t}BuNC (0.03 mL, 0.266 mmol, 1.16 equivalents) and Ag[BF_4] (45 mg, 0.231 mmol) and stirred for 30 minutes to give a dark brown suspension before the solvent was removed *in vacuo* to give a dark brown solid. The solid material was then dissolved in CH_2Cl_2 and filtered through celite to give a yellow-brown solution, which was reduced in volume. The crude solution was then purified using column chromatography, using 50:50 CH_2Cl_2:petrol as the eluent. This produced a yellow band, from which the solvent was removed *in vacuo* to give 1,2-Ph_2-3-(^{t}BuNC)$_2$-3-PPh_3-1,2-Ph_2-*pseudocloso*-3,1,2-$RuC_2B_9H_9$ (**18**) (62 mg, 0.076 mmol, 34.3 % yield) as an orange-yellow solid.

NMR: ^{1}H NMR, δ 7.41-7.35 (m, 10H, C_6H_5), 7.35-7.30 (m, 5H, C_6H_5), 7.23-7.18 (m, 10H, C_6H_5), 1.17 (s, br, 18H, ^{t}Bu).

^{1}H NMR (CD_2Cl_2, 203 K), δ 7.80 to 6.71 (m, 25H, C_6H_5), 1.20 (s, 9H, ^{t}Bu), 1.09 (s, 9H, ^{t}Bu).

^{11}B{^{1}H} NMR, δ 23.6 (1B), 15.1 (1B), 12.7 (2B), 4.5 (2B), -0.6 (2B), -19.9 (1B).

^{31}P{^{1}H} NMR, δ 41.2 (s).

EIMS: *m/z* 814 (M^+), 731 (M^+-^{t}BuNC), 648 (M^+-2x^{t}BuNC), 386 (M^+-2x^{t}BuNC, PPh_3).

CHN: $C_{42}H_{52}B_9N_2PRu$ requires C 62.0, H 6.44, N 3.44; found C 62.5, H 5.94, N 2.73%.

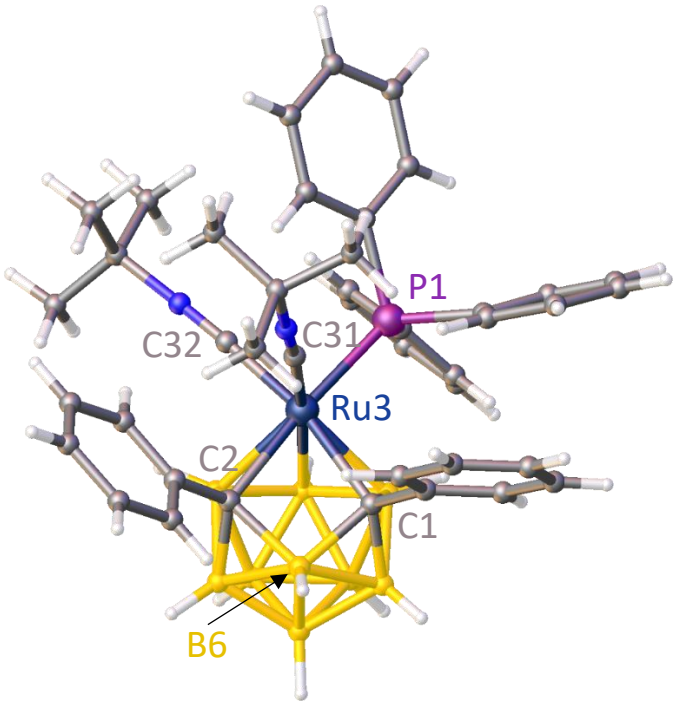
P1
C32
C31
Ru3
C2
C1
B6

6.4.8 Synthesis of 1,2-Ph_2-3-PPh_3-3,3-$(CO)_2$-*pseudocloso*-3,1,2-$RuC_2B_9H_9$ (**19**)

Compound **17** (299 mg, 0.316 mmol) was dissolved in THF (30 mL) and cooled to -78 ˚C before *n*-BuLi was added (0.13 mL of a 2.5 mol dm^{-3} solution in hexanes, 0.325 mmol,), immediately giving rise to an extremely dark solution. This was then stirred for thirty minutes before being frozen at -196 ˚C. $Ag[BF_4]$ (74 mg, 0.379 mmol) was then added and the vessel filled with carbon monoxide gas, a supply of which was maintained as the reaction mixture was allowed to warm to room temperature. The carbon monoxide supply was then removed and the resultant yellow suspension was allowed to stir for 16 hours. The reaction mixture was then filtered through celite before all volatiles were removed *in vacuo*. The resulting material was redissolved in CH_2Cl_2 and filtered through celite before being reduced in volume. The resulting yellow solution was chromatographed using preparative TLC plates, using 50:50 CH_2Cl_2:petrol as the eluent. This gave rise to a yellow band (R_f=0.80) which was found to be 1,2-Ph_2-3-PPh_3-3,3-$(CO)_2$-*pseudocloso*-3,1,2-$RuC_2B_9H_9$ (**19**) (55 mg, 0.078 mmol, 25%). The molecular structure of **19** was determined using crystals grown from slow diffusion of THF/petrol at -20 °C.

NMR: ^{1}H NMR, δ 7.47-7.31 (m, 19H, C_6H_5), 7.21-7.11 (m, 6H, C_6H_5).

^{1}H{^{11}B} NMR, δ 7.47-7.31 (m, 19H, C_6H_5), 7.21-7.11 (m, 6H, C_6H_5), 4.62 (broad s, 1H, BH), 3.04 and 3.01 (overlapping broad resonances, 3H, BH), 2.78 (broad s, 4H, BH), 2.15 (broad s, 1H, BH).

^{11}B{^{1}H} NMR, δ 17.8 (2B), 7.1 (2B), 3.7 (2B), 0.1 (2B), -18.0 (1B).

^{31}P{^{1}H} NMR, δ 38.8 (s).

CHN: $C_{34}H_{34}B_9O_2PRu$ requires C 58.0, H 4.87; found C 57.8, H 5.41%.

ATR-IR: ν_{max} 2534 (B-H), 2049 (CO), 2002 (CO) cm^{-1}.

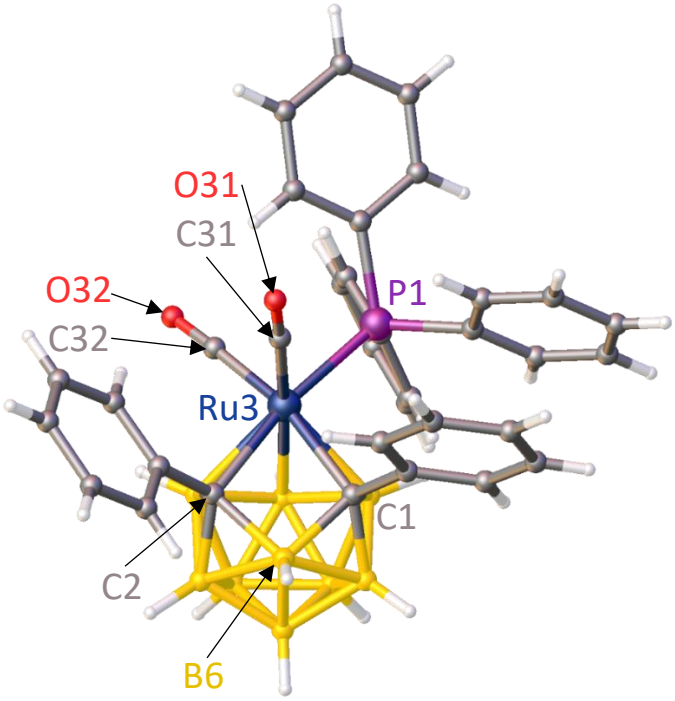
O31
C31
O32
C32
P1
Ru3
C1
C2
B6

6.4.9 Deprotonation and dehalogenation of 5,6,10-[Cl(Ph$_3$P)$_2$Ru]-5,6,10-μ-(H)$_3$-7,8-Ph$_2$-10-H-7,8-C$_2$B$_9$H$_6$] (17). Synthesis of [{1,2-Ph$_2$-*pseudocloso*-3,1,2-RuC$_2$B$_9$H$_9$}{1′,8′-Ph$_2$-*closo*-2′,1′,8′-RuC$_2$B$_9$H$_9$}] (20) and [{1,2-Ph$_2$-*pseudocloso*-3,1,2-RuC$_2$B$_9$H$_9$}{1′,8′-Ph$_2$-*closo*-2′,1′,8′-RuC$_2$B$_9$H$_9$}{1″,8″-Ph$_2$-*closo*-2″,1″,8″-RuC$_2$B$_9$H$_9$}] (21).

Compound **17** (500 mg, 0.528 mmol) was dissolved in THF (25 mL) and *n*-BuLi (0.21 mL of a 2.5 mol dm^{-3} solution in hexanes, 0.525 mmol) was added at 0°C. This was then stirred for 30 minutes to give an extremely dark solution. The solvent was removed *in vacuo* to give a dark solid, which was then dissolved in CH_2Cl_2 (20 mL). The resulting dark solution was transferred *via* cannula onto Ag[BF_4] (140 mg, 0.719 mmol) and stirred for 30 minutes to give a dark brown suspension before the solvent was removed *in vacuo* to give a dark brown solid. The solid material was then dissolved in CH_2Cl_2 and filtered through celite to give a dark brown solution, which was reduced in volume. The crude solution was then purified *via* preparative thin layer chromatography, using 50:50 CH_2Cl_2:petrol as the eluent. As the crude mixture contained a number of products, this gave rise to a complicated plate with several bands. The most prominent band (R_f=0.58) was found to be [{1,2-Ph$_2$-*pseudocloso*-3,1,2-RuC$_2$B$_9$H$_9$}{1′,8′-Ph$_2$-*closo*-2′,1′,8′-RuC$_2$B$_9$H$_9$}] (**20**) (25 mg, 6.1 % yield) an orange solid. A second red-orange band (R_f=0.33) was isolated and found to be [{1,2-Ph$_2$-*pseudocloso*-3,1,2-RuC$_2$B$_9$H$_9$}{1′,8′-Ph$_2$-*closo*-2′,1′,8′-RuC$_2$B$_9$H$_9$}{1″,8″-Ph$_2$-*closo*-2″,1″,8″-RuC$_2$B$_9$H$_9$}] (**21**), produced in trace yields.

Compound 20

NMR: ^{1}H NMR (CD_2Cl_2), δ 7.68-7.62 (m, 2H, C_6H_5), 7.54-7.49 (m, 2H, C_6H_5), 7.49-7.43 (m, 2H, C_6H_5), 7.38-7.33 (m, 1H, C_6H_5), 7.29-7.20 (m, 3H, C_6H_5), 7.05 (d, 1H, C_6H_5), 6.98 (d, 1H, C_6H_5), 6.77 (t, 1H, C_6H_5), 6.43-6.34 (m, 2H, C_6H_5), 6.21 (t, 1H, C_6H_5), 6.15 (d, 1H, C_6H_5), 5.87 (t, 1H, C_6H_5), 5.80 (t, 1H, C_6H_5), 5.09-5.04 (m, 1H, C_6H_5).

^{11}B{^{1}H} NMR (CD_2Cl_2), δ 29.4 (1B), 20.1 to 14.5 (overlapping resonances with maxima at 18.0 and 16.8, 2B), 12.6 (1B), 3.0 to -6.4 (overlapping resonances with

maxima at 0.8, -0.8, -3.0 and -4.5, 8B), -8.5 (2B), -13.5 to -18.7 (overlapping resonances with maxima at -14.8 and -17.3, 3B), -19.9 (1B).

EIMS: envelope centred *m/z* 771.3 (M^+).

CHN: $C_{28}H_{38}B_{18}Ru_2$ requires C 43.6, H 4.97; found C 43.9, H 5.09%.

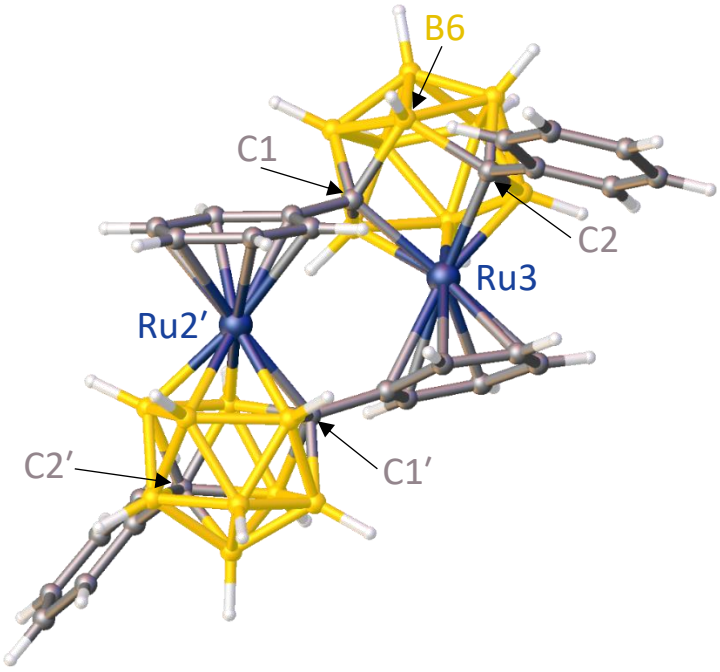

[{1,2-Ph_2-*pseudocloso*-3,1,2-$RuC_2B_9H_9$}{1′,8′-Ph_2-*closo*-2′,1′,8′-$RuC_2B_9H_9$}] (**20**)

Compound 21

NMR: ^{1}H NMR (CD_2Cl_2), δ 7.71-7.67 (m, 2H, C_6H_5), 7.63-7.60 (m, 2H, C_6H_5), 7.43 (t, 2H, C_6H_5), 6.85-6.82 (m, 1H, C_6H_5), 6.72-6.67 (m, 1H, C_6H_5), 6.25-6.21 (m, 1H, C_6H_5), 6.11-6.07 (m, 1H, C_6H_5), 6.02-5.98 (m, 1H, C_6H_5), 5.94-5.91 (m, 1H, C_6H_5), 5.89-5.85 (m, 1H, C_6H_5), 5.83-5.78 (m, 2H, C_6H_5), 5.76-5.73 (m, 1H, C_6H_5), 5.67-5.63 (m, 2H, C_6H_5), 5.01-4.96 (m, 1H, C_6H_5), 4.72-4.67 (m, 1H, C_6H_5).

^{11}B{^{1}H} NMR (CD_2Cl_2), δ 29.8 (1B), 17.9 (1B), 13.2 (1B), 4.3 to -11.5 (overlapping resonances with maxima at 1.4, -0.6, -2.1 and -8.1, 15B), -12.7 (1B), -13.8 to -24.0 (overlapping resonances with maxima at -15.1, -16.7, -19.3 and -22.9, 8B).

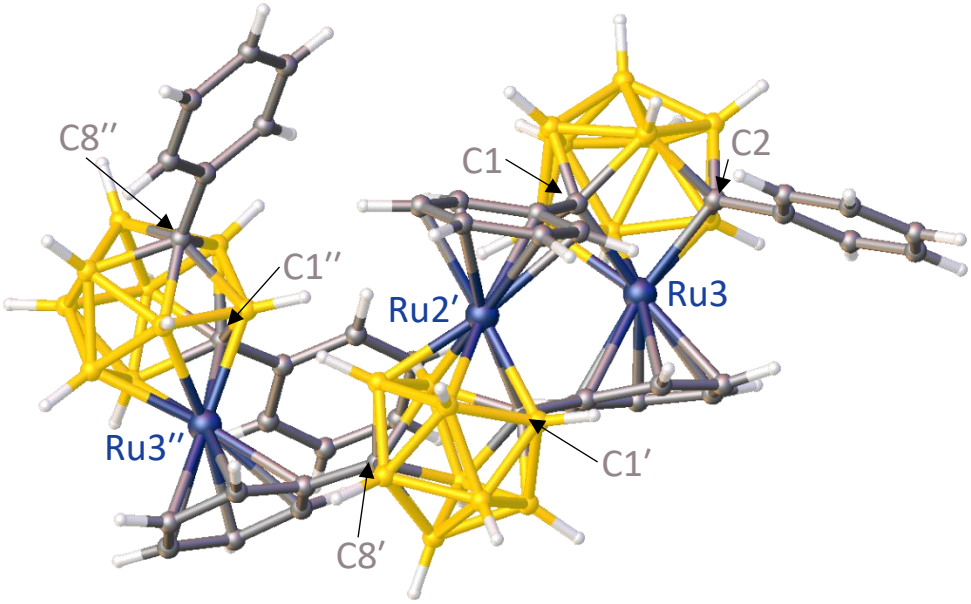

Structure of [{1,2-Ph_2-*pseudocloso*-3,1,2-$RuC_2B_9H_9$}{1′,8′-Ph_2-*closo*-2′,1′,8′-$RuC_2B_9H_9$}{1″,8″-Ph_2-*closo*-2″,1″,8″-$RuC_2B_9H_9$}] (**21**).

6.5 References

1 R. G. Hayter, *J. Organomet. Chem.*, 1968, **13**, C1.

2 M. A. Laguna, D. Ellis, G. M. Rosair and A. J. Welch, *Inorg. Chim. Acta*, 2003, **347**, 161.

3 S. Li, D. F. Mullica and F. G. A. Stone, *J. Organomet. Chem.*, 1994, **467**, 95.

4 I. T. Chizhevsky, I. A. Lobanova, V. I. Bregadze, P. V. Petrovskii, A. V. P. Antonovich, A. I. Yanovskii and Yu. T. Struchkov, *Mendeleev Commun.*, 1991, **1**, 47.

5 P. S. Hallman, T. A. Stephenson and G. Wilkinson, *Inorg. Synth.*, 1970, **12**, 237.

6 M. Tsuji, *J. Org. Chem.*, 2003, **68**, 9589.

7 O. V. Dolomanov, L. J. Bourhis, R. J. Gildea, J. A. K. Howard and H. Puschmann, *J. Appl. Crystallogr.*, 2009, **42**, 339–341.

8 G. M. Sheldrick, *Acta Crystallogr. Sect. C Struct. Chem.*, 2015, **71**, 3–8.

9 G. M. Sheldrick, *Acta Crystallogr. Sect. A Found. Crystallogr.*, 2008, **64**, 112–122.

10 A. McAnaw, G. Scott, L. Elrick, G. M. Rosair and A. J. Welch, *Dalton Trans.*, 2013, **42**, 645.

11 A. J. Welch, *Crystals*, 2017, **7**, 234.

12 A. McAnaw, M. E. Lopez, D. Ellis, G. M. Rosair and A. J. Welch, *Dalton Trans.*, 2014, **43**, 5095.

	3	**IV**	**5**
Formula	$C_{15}H_{35}B_9IMoNO_3$	$C_{15}H_{35}B_9IMoNO_3$	$C_{43}H_{50}B_9NP_2Ru$
Diffractometer	Bruker X8 APEX 2	Bruker X8 APEX 2	Bruker X8 APEX 2
Temperature/K	100	100	150
M	597.57	597.57	841.14
Crystal system	monoclinic	monoclinic	triclinic
Space group	$P2_1/c$	$P2_1/n$	P-1
a/Å	15.8048(7)	7.4410(17)	11.5309(3)
b/Å	12.4359(5)	11.025(3)	13.3591(3)
c/Å	13.4966(6)	30.358(6)	16.5849(4)
α/°	90	90	79.4000(10)
β/°	108.967(2)	95.199(15)	88.5330(10)
γ/°	90	90	78.1340(10)
Volume/Å^3	2508.69(19)	2480.3(10)	2457.32(10)
Z	4	4	2
ρ_{calc}/g cm^{-3}	1.582	1.600	1.137
μ/mm^{-1}	1.770	1.790	0.412
F(000)	1184.0	1184.0	868.0
Crystal size/mm^3	0.2 × 0.2 × 0.1	0.54 × 0.38 × 0.06	0.254 × 0.22 × 0.12
Radiation	MoKα (λ = 0.71073)	MoKα (λ = 0.71073)	MoKα (λ = 0.71073)
2θ range for data collection/°	2.724 to 61.288	5.39 to 66.354	6.676 to 56.63
Index ranges	$0 \le h \le 22$, $-17 \le k \le 0$, $-18 \le l \le 18$	$-9 \le h \le 11$, $-14 \le k \le 16$, $-45 \le l \le 43$	$-15 \le h \le 15$, $-17 \le k \le 17$, $-21 \le l \le 22$
Reflections collected	56685	45824	100651
Independent reflections	7639 [R_{int} = 0.0504, R_{sigma} = 0.0460]	8742 [R_{int} = 0.0302, R_{sigma} = 0.0289]	11921 [R_{int} = 0.0402, R_{sigma} = 0.0245]
Data/restraints/parameters	7639/0/339	8742/0/304	11921/0/541
Goodness-of-fit on F^2	1.047	1.040	1.051
Final *R* indexes [I>=2σ (I)]	R_1 = 0.0362, wR_2 = 0.0674	R_1 = 0.0241, wR_2 = 0.0457	R_1 = 0.0270, wR_2 = 0.0739
Final *R* indexes [all data]	R_1 = 0.0513, wR_2 = 0.0721	R_1 = 0.0330, wR_2 = 0.0482	R_1 = 0.0323, wR_2 = 0.0764
Largest diff. peak/hole / e Å^{-3}	0.76/-0.73	0.95/-0.52	0.61/-0.42

	6	**10**	**11**
Formula	$C_{27}H_{46}B_9Cl_2P_3Ru$	$C_{44}H_{58}B_{18}P_2Ru_2$	$C_7H_{22}B_{10}$
Diffractometer	Bruker X8 APEX 2	Rigaku FR-E+	Bruker X8 APEX 2
Temperature/K	100	100	100
M	732.81	1045.56	214.34
Crystal system	monoclinic	triclinic	monoclinic
Space group	$P2_1/n$	$P\bar{1}$	$P2_1/m$
a/Å	15.7898(19)	11.0931(9)	7.5999(17)
b/Å	11.9109(16)	11.3219(8)	10.724(2)
c/Å	19.670(3)	20.1045(11)	8.8344(18)
α/°	90	84.527(5)	90
β/°	111.457(6)	75.039(6)	112.597(10)
γ/°	90	81.647(6)	90
Volume/Å^3	3443.0(8)	2409.1(3)	664.7(3)
Z	4	2	2
ρ_{calc}/g cm^{-3}	1.414	1.441	1.071
μ/mm^{-1}	0.770	0.727	0.048
F(000)	1504.0	1060.0	228.0
Crystal size/mm^3	0.58 × 0.4 × 0.2	0.25 × 0.15 × 0.05	0.28 × 0.24 × 0.06
Radiation	MoKα (λ = 0.71073)	MoKα (λ = 0.71073)	MoKα (λ = 0.71073)
2θ range for data collection/°	2.85 to 64.818	3.642 to 54.968	5.806 to 55.768
Index ranges	$-23 \le h \le 23$, $-17 \le k \le 17$, $-29 \le l \le 23$	$-14 \le h \le 14$, $-14 \le k \le 14$, $-26 \le l \le 26$	$-9 \le h \le 9$, $-14 \le k \le 13$, $-9 \le l \le 11$
Reflections collected	67419	90076	10295
Independent reflections	12225 [R_{int} = 0.0509, R_{sigma} = 0.0413]	11019 [R_{int} = 0.1471, R_{sigma} = 0.0626]	1666 [R_{int} = 0.0604, R_{sigma} = 0.0486]
Data/restraints/parameters	12225/3/418	11019/198/599	1666/0/106
Goodness-of-fit on F^2	1.057	1.155	1.026
Final *R* indexes [$I>=2\sigma(I)$]	R_1 = 0.0337, wR_2 = 0.0824	R_1 = 0.1698, wR_2 = 0.3601	R_1 = 0.0436, wR_2 = 0.1048
Final *R* indexes [all data]	R_1 = 0.0462, wR_2 = 0.0870	R_1 = 0.2022, wR_2 = 0.3772	R_1 = 0.0704, wR_2 = 0.1185
Largest diff. peak/hole / e Å^{-3}	1.11/-0.78	5.04/-4.43	0.30/-0.26

	14	**17**	**18**
Formula	$C_{36.5}H_{57}B_9N_2PRuCl_3$	$C_{51}H_{52}B_9Cl_3P_2Ru$	$C_{42}H_{52}B_9N_2PRu$
Diffractometer	Bruker X8 APEX 2	Bruker X8 APEX 2	Rigaku 007-HF
Temperature/K	100	120	100
M	859.52	1031.57	814.18
Crystal system	monoclinic	monoclinic	tetragonal
Space group	$P2_1/c$	$P2_1/n$	$P4_1$
a/Å	21.2050(9)	11.7427(5)	11.41683(8)
b/Å	10.7895(4)	19.9771(9)	11.41683(8)
c/Å	19.2841(7)	22.2816(8)	31.9871(5)
α/°	90	90.0	90
β/°	100.701(2)	90.735(4)	90
γ/°	90	90.0	90
Volume/Å^3	4335.3(3)	5226.5(4)	4169.32(9)
Z	4	4	4
ρ_{calc}/g cm^{-3}	1.317	1.311	1.297
μ/mm^{-1}	0.612	0.654	3.637
F(000)	1780.0	2112.0	1688.0
Crystal size/mm^3	0.38 × 0.36 × 0.1	0.224 × 0.138 × 0.099	0.1 × 0.015 × 0.01
Radiation	MoKα (λ = 0.71073)	MoKα (λ = 0.71073)	CuKα (λ = 1.54178)
2θ range for data collection/°	4.252 to 64.154	5.408 to 59.502	7.744 to 136.452
Index ranges	$-31 \le h \le 31$, $-16 \le k \le 15$, $-28 \le l \le 28$	$-14 \le h \le 15$, $-27 \le k \le 25$, $-23 \le l \le 31$	$-13 \le h \le 13$, $-13 \le k \le 11$, $-38 \le l \le 31$
Reflections collected	78161	59685	19497
Independent reflections	14920 [R_{int} = 0.0772, R_{sigma} = 0.0668]	13334 [R_{int} = 0.0837, R_{sigma} = 0.0881]	6614 [R_{int} = 0.0505, R_{sigma} = 0.0514]
Data/restraints/parameters	14920/0/470	13334/0/598	6614/1/529
Goodness-of-fit on F^2	0.987	1.060	1.024
Final *R* indexes [I>=2σ (I)]	R_1 = 0.0415, wR_2 = 0.0960	R_1 = 0.0632, wR_2 = 0.1163	R_1 = 0.0382, wR_2 = 0.0918
Final *R* indexes [all data]	R_1 = 0.0681, wR_2 = 0.1053	R_1 = 0.0886, wR_2 = 0.1259	R_1 = 0.0412, wR_2 = 0.0933
Largest diff. peak/hole / e Å^{-3}	0.58/-1.05	0.67/-0.52	0.71/-0.37

	19	**20**	**21**
Formula	$C_{38}H_{42}B_9O_3PRu$	$C_{29}H_{40}B_{18}Cl_2Ru_2$	$C_{44}H_{61}B_{27}Cl_4Ru_3$
Diffractometer	Bruker X8 APEX 2	Bruker X8 APEX 2	Rigaku 007-HF
Temperature/K	100	100	100
M	776.04	856.23	1326.80
Crystal system	monoclinic	monoclinic	triclinic
Space group	$P2_1/c$	$P2_1/n$	*P*-1
a/Å	15.0547(5)	14.1714(9)	13.33989(10)
b/Å	13.6097(5)	14.3879(10)	13.53829(7)
c/Å	18.2327(7)	18.3408(14)	15.12453(9)
α/°	90	90	84.5284(5)
β/°	96.913(2)	104.213(4)	87.0673(6)
γ/°	90	90	83.1449(5)
Volume/Å^3	3708.5(2)	3625.2(4)	2697.41(3)
Z	4	4	2
ρ_{calc}/g cm^{-3}	1.390	1.569	1.634
μ/mm^{-1}	0.504	1.006	8.319
F(000)	1592.0	1704.0	1320.0
Crystal size/mm^3	0.42 × 0.4 × 0.14	0.22 × 0.2 × 0.16	0.099 × 0.045 × 0.04
Radiation	MoKα (λ = 0.71073)	MoKα (λ = 0.71073)	CuKα (λ = 1.54178)
2θ range for data collection/°	5.406 to 64.096	4.582 to 57.718	6.602 to 136.484
Index ranges	$-22 \le h \le 22$, $-20 \le k \le 20$, $-26 \le l \le 27$	$-19 \le h \le 19$, $-19 \le k \le 17$, $-24 \le l \le 23$	$-15 \le h \le 15$, $-16 \le k \le 16$, $-18 \le l \le 18$
Reflections collected	96122	67222	92481
Independent reflections	12831 [R_{int} = 0.0739, R_{sigma} = 0.0510]	9460 [R_{int} = 0.0866, R_{sigma} = 0.0656]	9843 [R_{int} = 0.0415, R_{sigma} = 0.0207]
Data/restraints/parameters	12831/10/506	9460/3/519	9843/0/767
Goodness-of-fit on F^2	1.038	1.053	1.035
Final *R* indexes [I>=2σ (I)]	R_1 = 0.0400, wR_2 = 0.0900	R_1 = 0.0397, wR_2 = 0.0833	R_1 = 0.0228, wR_2 = 0.0598
Final *R* indexes [all data]	R_1 = 0.0578, wR_2 = 0.0972	R_1 = 0.0649, wR_2 = 0.0923	R_1 = 0.0237, wR_2 = 0.0603
Largest diff. peak/hole / e Å^{-3}	0.59/-0.77	0.71/-0.78	0.44/-0.72

Appendix B: Synthesis of *Hypercloso* $(Cp^*Ru)_2Me_2C_2B_9H_9$

The work described within this appendix has been omitted from the results chapters of the thesis on the grounds that it does not involve attempting to generate *hypercloso* species through ligand set manipulation, which is the theme of the entirety of the work contained within said results chapters.

Work by Welch and co-workers yielded three isomers of $(Cp^*Ru)_2C_2B_{10}H_{12}$,[1] the first and to date only examples of fourteen vertex *hypercloso* heteroboranes, from the reaction between $Na_2[C_2B_{10}H_{12}]$ and 0.5 equivalents of $[Cp^*RuCl]_4$. All three isomers have the same novel geometry, containing a four atom trapezoidal face. However, the lack of symmetry in the observed structure inhibits the identification of the cage carbon atoms as the usual methods employed to differentiate cage carbon and cage boron atoms (the BHD and VCD methods) are difficult to apply to low symmetry species. This issue was resolved through computations carried out by the Macgregor group.

Nonetheless, attempts were made to avoid this problem by instead labelling the cage carbon atoms with methyl groups. Towards this end, a reaction between 1,2-Me_2-*closo*-1,2-$C_2B_{10}H_{10}$ (0.203 g, 1.18 mmol) and $Na[C_{10}H_8]$ (2.6 mmol) followed by addition of $[Cp^*RuCl]_4$ (640 mg, 0.59 mmol, 0.5 equivalents) in THF (15 mL) was carried out. The solvent was then removed *in vacuo* and the resulting dark brown paste dissolved in CH_2Cl_2 and passed through a sinter before the resulting solution was reduced in volume. This was then purified *via* preparative TLC using 50:50 CH_2Cl_2:petrol as the eluent. This give rise to an extremely complex set of TLC plates with several bands of various colours. The most abundant of such bands (R_f=0.49) was found to be 2,10-Me_2-4,5-Cp^*_2-*hypercloso*-4,5,2,10-$Ru_2C_2B_9H_9$.

NMR: ^{1}H NMR, δ 2.09 (s, 3H, Me), 1.68 (s, 15H, Cp*), 1.57 (s, 15H, Cp*) and 0.46 (s, 3H, Me).

^{11}B{^{1}H} NMR, δ 119.0 (1B), 33.6 (1B), 14.9 (3B), 11.7 (1B), 7.4 (1B), -5.0 (1B) and -13.4 (1B).

EIMS: *m/z* 633 (M^+).

The ^{1}H NMR spectrum of this compound is unremarkable, containing two signals each of relative integral fifteen for the two Cp* groups and two signals each of relative integral three for the two Me groups. However, the $^{11}B\{^{1}H\}$ NMR spectrum, shown in figure B.1, contains a resonance at 119.0 ppm. This is an extremely high frequency resonance even by the standards of *hypercloso* metallacarboranes.

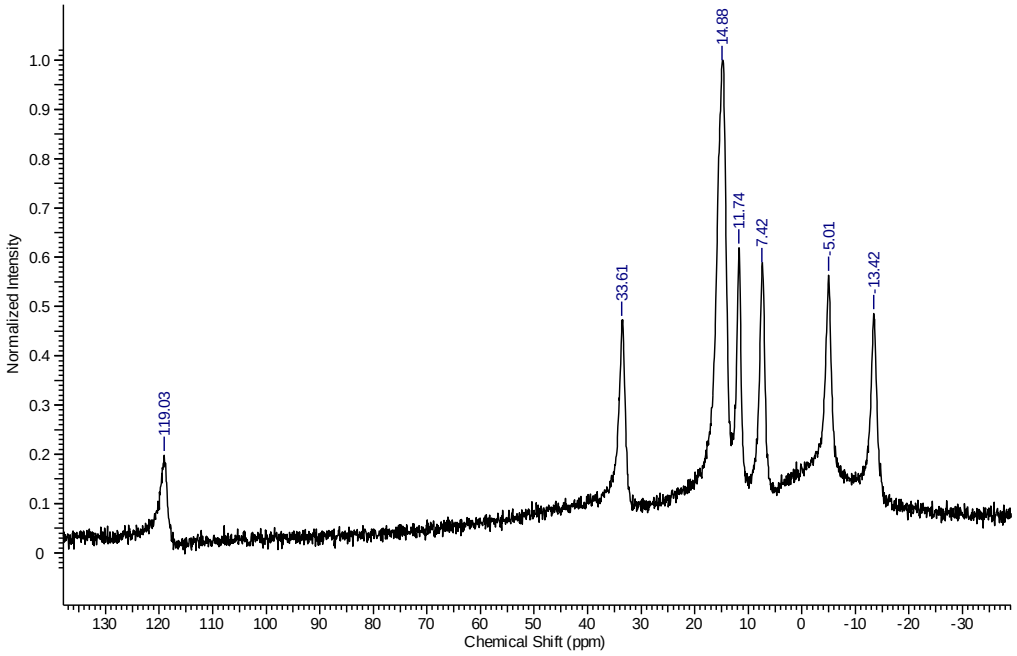

Figure B.1: $^{11}B\{^{1}H\}$ NMR spectrum of 2,10-Me_2-4,5-Cp^*_2-*hypercloso*-4,5,2,10-$Ru_2C_2B_9H_9$.

The molecular structure of 2,10-Me_2-4,5-Cp^*_2-*hypercloso*-4,5,2,10-$Ru_2C_2B_9H_9$ was determined and is shown in figure B.2.

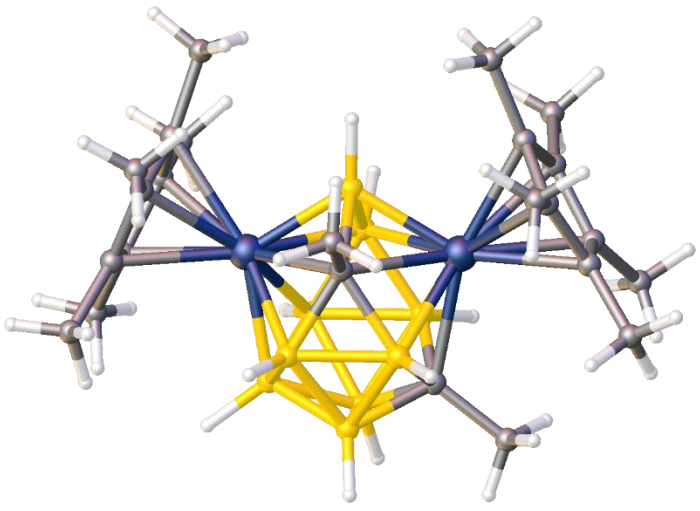

Figure B.2: Molecular structure of 2,10-Me_2-4,5-Cp^*_2-*hypercloso*-4,5,2,10-$Ru_2C_2B_9H_9$.

2,10-Me_2-4,5-Cp^*_2-*hypercloso*-4,5,2,10-$Ru_2C_2B_9H_9$ has a *hypercloso* electron count but has the same geometry as that of a thirteen vertex *closo* species. As noted in section 1.9.1, this is typical of thirteen vertex *hypercloso* species. Nevertheless, 2,10-Me_2-4,5-Cp^*_2-*hypercloso*-4,5,2,10-$Ru_2C_2B_9H_9$ is of interest in that it is the first 4,5,2,10-$M_2C_2B_9$ metallacarborane known. Unfortunately, the desired fourteen vertex *hypercloso* species, $(Cp^*Ru)_2Me_2C_2B_{10}H_{10}$ was not isolated. The EIMS spectrum of the crude reaction mixture suggests that the fourteen vertex species is not present as no signal was observed at *m/z* = 644, corresponding to the molecular ion of such a species. 2,10-Me_2-4,5-Cp^*_2-*hypercloso*-4,5,2,10-$Ru_2C_2B_9H_9$ could only be formed by loss of a {BH} vertex. By what mechanism this proceeds is unclear.

1 A. P. M. Robertson, N. A. Beattie, G. Scott, W. Y. Man, J. J. Jones, S. A. Macgregor, G. M. Rosair and A. J. Welch, *Angew. Chemie - Int. Ed.*, 2016, **55**, 8706.

Metallacarboranes

International Edition: DOI: 10.1002/anie.201602440
German Edition: DOI: 10.1002/ange.201602440

14-Vertex Heteroboranes with 14 Skeletal Electron Pairs: An Experimental and Computational Study

Alasdair P. M. Robertson, Nicholas A. Beattie, Greig Scott, Wing Y. Man, John J. Jones, Stuart A. Macgregor, Georgina M. Rosair, and Alan J. Welch**

Abstract: *Three isomers of $[(Cp^*Ru)_2C_2B_{10}H_{12}]$, the first examples of 14-vertex heteroboranes containing 14-skeletal electron pairs, have been synthesized by the direct electrophilic insertion of a $\{Cp^*Ru^+\}$ fragment into the anion $[4\text{-}Cp^*\text{-}4,1,6\text{-}RuC_2B_{10}H_{12}]^-$. All three compounds have the same unique polyhedral structure having an approximate C_s symmetry and featuring a four-atom trapezoidal face. X-ray diffraction studies could confidently identify only one of the two cage C atoms in each structure. The other C atom position has been established by a combination of i) best fitting of computed and experimental ^{11}B and ^1H NMR chemical shifts, and ii) consideration of the lowest computed energy for series of isomers studied by DFT calculations. In all three isomers, one cage C atom occupies a degree-4 vertex on the short parallel edge of the trapezium.*

The structures of boranes and heteroboranes are usually interpreted in terms of the electron-counting principles, established by Wade and Mingos more than 40 years ago.[1] These rules rationalize families of clusters, such as *closo* structures with $n+1$ skeletal electron pairs (SEPs), *nido* structures with $n+2$ SEPs, and *arachno* structures with $n+3$ SEPs (where n is the number of cluster vertices).

A small but interesting further family of heteroboranes is that in which the members possess only n SEPs, and these species, generally referred to as *hypercloso*, have been the subject of significant interest in the literature.[2] In general these clusters do not have the structures normally encountered for $n+1$ SEP species but rather they are related to them by a single diamond-square-diamond (d-s-d) isomerization.[3] An excellent early example is $[(CpFe)_2C_2B_6H_8]$,[4] a 10-vertex (10-v) 10-SEP species structurally related to the bicapped square antiprismatic 10-v 11-SEP cobalt analogue $[(CpCo)_2C_2B_6H_8]$[5] by a d-s-d rearrangement of the 2-6-10-9 diamond of the latter polyhedron (Figure 1).

A number of these *hypercloso* clusters have been reported by Kennedy et al.[6] who argued that they are actually $n+1$ SEP compounds in which the metal utilizes four, as opposed to the usual three, orbitals in cluster bonding. In this approach the compounds are simply regarded as differently structured *closo* species and, accordingly, the authors used the descriptor *isocloso*. Although MO calculations by Mingos and co-workers support the *hypercloso* view[7] and the fact that Spencer et al. have shown that the simple addition of two electrons to $[hypercloso\text{-}(\eta\text{-}C_6Me_6)RuB_9H_9]$ converts it into $[closo\text{-}(\eta\text{-}C_6Me_6)RuB_9H_9]^{2-}$,[8] the *isocloso* descriptor is still in use in the present day.[6f]

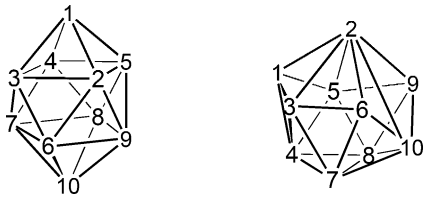

Figure 1. Left: The 10-v 11-SEP bicapped square antiprismatic structure of 2,6-Cp_2-2,6,1,10-$Co_2C_2B_6H_8$. Right: The 10-v 10-SEP structure of 2,10-Cp_2-2,10,1,9-$Fe_2C_2B_6H_8$, featuring a degree-6 metal atom at vertex 2. The two polyhedra are related by applying a d-s-d sequence to the 2-6-10-9 diamond of the left structure.

To date, the small library of *hypercloso* heteroboranes has almost exclusively been composed of clusters with between 9 and 12 vertices, limiting the possibility of an extensive study of such species. The *hypercloso* electron count distorts the cluster from a geometry associated with an $n+1$ SEP species to one in which at least one vertex, usually a transition metal, becomes highly connected. Accordingly we believe that the supraicosahedral area holds promise with respect to a systematic study of *hypercloso* compounds since supraicosahedra necessarily contain highly connected vertices. Currently this field is relatively under-developed, the only confirmed[9] examples of supraicosahedral *hypercloso* metallacarboranes[10] being the 13-v 13-SEP species $[4,5\text{-}Cp^*_2\text{-}4,5,2,3\text{-}Ru_2C_2B_9H_{11}]$ (**I**) and $[4,5\text{-}Cp^*_2\text{-}6\text{-}SMe_2\text{-}4,5,2,3\text{-}Ru_2C_2B_9H_{10}]^+$ (**II**) isolated by Kudinov and co-workers.[11] In this Communication we describe the synthesis of the first 14-v 14-SEP *hypercloso* metallacarboranes and their characterization by a combination of spectroscopic, crystallographic, and computational studies.

The two-electron reduction of $[1,2\text{-}C_2B_{10}H_{12}]$ with Na in THF followed by treatment with $[Cp^*Ru(MeCN)_3]Cl$ and cation metathesis afforded the 13-v 14-SEP ruthenacarborane $[BTMA][4\text{-}Cp^*\text{-}4,1,6\text{-}RuC_2B_{10}H_{12}]$ (**1**) in 76% yield (BTMA = $PhCH_2NMe_3$). Salt **1** was fully characterized spectroscopically and crystallographically (see the Supporting Information).[21] As is common for 4,1,6-MC_2B_{10} species, the anion in **1** is fluxional in solution at room temperature

[*] Dr. A. P. M. Robertson, N. A. Beattie, Dr. G. Scott, Dr. W. Y. Man, J. J. Jones, Prof. S. A. Macgregor, Dr. G. M. Rosair, Prof. A. J. Welch
Institute of Chemical Sciences, Heriot-Watt University
Edinburgh EH14 4AS (UK)
E-mail: s.a.macgregor@hw.ac.uk
a.j.welch@hw.ac.uk

Supporting information (containing the experimental, spectroscopic, crystallographic, and computational details of all new compounds reported herein) and the ORCID identification number(s) for the author(s) of this article can be found under http://dx.doi.org/10.1002/anie.201602440.

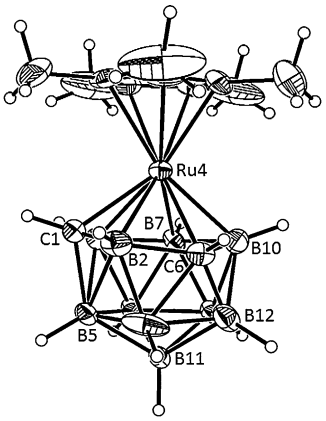

Figure 2. Solid-state structure of the anion of **1**.[21] The structure is partially disordered and only the major component is shown. Selected bond lengths [Å]: Ru4–C1 2.213(4), Ru4–B2 2.301(4), Ru4–C6 2.259(4), Ru4–B10 2.242(3), Ru4–B7 2.267(3), Ru4–B3 2.256(2), Ru4–C(Cp*) 2.192(5)–2.242(5).

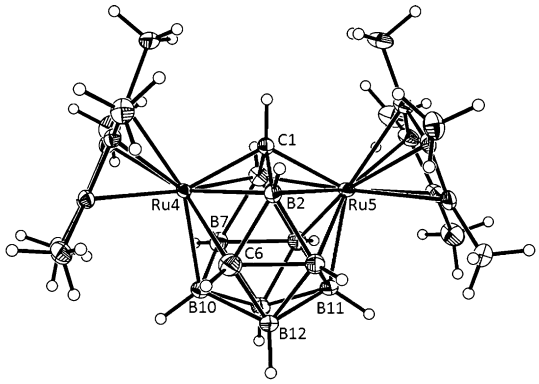

Figure 3. Solid-state structure of compound **2**.[21] Selected bond lengths [Å]: Ru4–C1 2.0254(16), Ru4–B2 2.2788(19), Ru4–C6 2.204(2), Ru4–B10 2.2167(19), Ru4–B7 2.2117(19), Ru4–B3 2.2801(19), Ru5–C1 2.0342(16), Ru5–B2 2.2786(19), Ru5–B9 2.2029(19), Ru5–B11 2.2119(19), Ru5–B8 2.2229(19), Ru5–B3 2.299(2), Ru4–C(Cp*) 2.2308(16)–2.2510(15), Ru5–C(Cp*) 2.2294(16)–2.2469(17).

through a double d-s-d process,[12] with NMR spectra revealing time-averaged C_s symmetry. A perspective view of the anion is shown in Figure 2.

Treatment of **1** in THF with 0.25 equiv $[Cp^*RuCl]_4$ followed by heating to reflux over 16 h produced a complex mixture of products with eight well-defined species clearly visible by thin-layer chromatography (see Plate S1 in the Supporting Information). Four of these species have been successfully characterized by a combination of mass spectrometry, multinuclear NMR spectroscopy, X-ray diffraction, and DFT calculations.

The seventh fastest moving band is an orange compound (**2**) which was assigned as $[(Cp^*Ru)_2C_2B_9H_{11}]$ by mass spectrometry and NMR spectroscopy. Notably, however, NMR spectroscopy indicated this was clearly not the 4,5,2,3-$Ru_2C_2B_9$ species **I** isolated by Kudinov et al. since both the ^1H and ^{11}B NMR spectra reveal no molecular symmetry. Moreover there is no very high-frequency ^{11}B NMR resonance signal in the spectrum of **2** ($\delta_{max} = 31$ ppm in **2**; $\delta_{max} = 97$ ppm in the 4,5,2,3 compound). Instead, there is a high frequency resonance signal in the ^1H NMR spectrum ($\delta = 16.6$ ppm) attributable to the $C_{cage}H$ proton. A crystallographic study (Figure 3) established that **2** is [4,5-Cp^*_2-4,5,1,6-$Ru_2C_2B_9H_{11}$], a 13-v 13-SEP *hypercloso* species and a positional isomer of **I**.[21] We assume that **2** is formed by loss of the {B5H} fragment from the anion of **1** or (possibly more likely) its 4,1,8-RuC_2B_{10} isomer,[13] and capping of the open face thus produced by a $\{Cp^*Ru^+\}$ fragment.

The diruthenacarborane cage in **2** has a docosahedral structure, essentially the same structure as found in 13-v 14-SEP species, and the origin of this superficially unusual result has been traced to the fact that the C_{2v}-symmetric docosahedron necessarily has nondegenerate molecular orbitals.[14] We have shown that the HOMO of the parent borate $[B_{13}H_{13}]^{2-}$ is strongly bonding with respect to the 1-2 and 1-3 edges, and moderately strongly bonding with respect to the 6-9 and 7-8 edges.[15] This allows us to rationalize the facts that the 1-2 and 1-3 distances in **2** are about 0.09–0.10 Å longer, and the 6-9 and 7-8 distances in **2** are about 0.02–0.04 Å longer, than the equivalent distances in crystallographically characterized 13-v 14-SEP 4,5,1,6-$M_2C_2B_9$ species (see the Supporting Information).[15,16]

The fastest moving band (identified as purple compound **3**), the third fastest band (dark green compound **4**), and the sixth fastest moving band (purple compound **5**) were also studied, with elemental analysis and/or mass spectrometry suggesting the formula $[(Cp^*Ru)_2C_2B_{10}H_{12}]$ for all three. The ^1H NMR spectra of **3–5** contain one relatively high frequency $C_{cage}H$ resonance signal ($\delta = 8.6$ to 10.5 ppm) and two resonance signals corresponding to the Cp^* H atoms. The asymmetry of all three compounds is confirmed by their ^{11}B NMR spectra which exhibit ten equal-integral resonance signals for **4** and **5** and nine resonance signals for **3** (one less signal as a result of the overlapping of two signals). In all three compounds, the range of ^{11}B chemical shifts is relatively large, $\delta = 76.0$ to -13.6 ppm for **3**, 54.8 to -22.9 ppm for **4**, and 72.1 to -12.1 ppm for **5**.

Thus compounds **3–5** appear to be the first examples of 14-v 14-SEP *hypercloso* species, presumably formed by direct electrophilic insertion (DEI)[11,16b,17] of a $\{Cp^*Ru^+\}$ fragment into the anion of **1**, and it was clearly of importance to characterize each of them crystallographically. To our initial surprise, compounds **3**, **4**, and **5** are all isomorphous with **2** but the origin of this became clear when the structures were solved. Compounds **3–5**, isomers of each other differing only in the positions of the cage C atoms, share the same basic skeleton, which is shown together with an arbitrary numbering scheme in Figure 4. As in **2**, the carborane central cores in **3–5** are flanked by two large {Cp*Ru} fragments whose Cp* rings are inclined at about 47°. The isomorphism presumably results from the packing of molecules in the crystal being determined by the same overall shape of the molecules and not the relatively minor differences in dipole moment that arise from different C atom positions or the presence (in **3–5**) of one additional BH unit. The 14-vertex cluster has two degree-6 vertices (i.e., 6-connected with respect to the polyhedron, vertices 2 and 7) occupied by the Ru atoms, ten degree-5 vertices, and two degree-4 vertices (1 and 4)

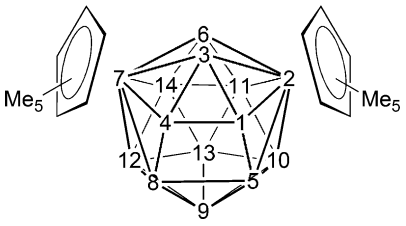

Figure 4. Generalized representation of compounds **3**–**5** and atomic numbering scheme.

occupying the short parallel edge of an approximate trapezium (1-4-8-5). The 1-4 distances are 1.642(4), 1.618(6), and 1.612(4) Å and the 5-8 distances 2.196(6), 2.024(9), and 2.049(5) Å for compounds **3**, **4** and **5**, respectively. The whole molecule has approximate C_s symmetry about the plane containing vertices 3, 6, 9, and 13. To the best of our knowledge this is the first time such a cluster structure has been reported. It is clearly distinct from the bicapped hexagonal antiprism (bha) typical of 14-v 15-SEP species,[17,18] again reflecting the unique structures of *hypercloso* clusters. Formally, a bha structure could be formed from this unique polyhedron by making the 4–5 connection and applying a d-s-d process to the 1-2-10-5 diamond.

It is clearly important to identify which $[(Cp^*Ru)_2C_2B_{10}H_{12}]$ isomer is which for each of compounds **3**–**5** by establishing the positions of the cage C atoms. Analysis of the various NMR spectra confirms that in none of the compounds do both cage C atoms occupy vertices on the approximate mirror plane of symmetry (that is, vertices 3, 6, 9, and 13), nor are they related by that plane of symmetry. Distinguishing between BH and CH vertices in (hetero)carborane structures studied crystallographically is well-known to be challenging, and it is particularly so in the case of compounds **3**–**5**. This arises because 76% of the X-ray scattering power of the molecules is localized in the two peripheral {Cp*Ru} fragments which are effectively symmetry-related, resulting in a degree of pseudo-symmetry overall and comparatively poor definition of the asymmetric $\{C_2B_{10}\}$ fragments.

We have recently described two new approaches, the vertex–centroid distance (VCD)[19] and boron–hydrogen distance (BHD)[17] methods, that are useful in distinguishing cage B and cage C atoms in carboranes and heterocarboranes. Both methods analyze the "Prostructure", the result of refinement in which all B or C vertices are treated as B. The VCD method works by comparing distances from topologically equivalent vertices to the polyhedral centroid, whereas in the BHD method each B–H distance is compared against all others. Although both methods were successfully used to identify the cage C atoms in **1** and **2**, the relatively low symmetry of the polyhedra in compounds **3**–**5** (C_s at best) means that for these compounds the more useful approach is the BHD method. B–H distances in the Prostructures of **3**–**5** are given in the Supporting Information.

The compound in which the clearest indication is given of the position of one of the cage C atoms is compound **4**, which has B12–H12 0.33(6) Å in the Prostructure. The next shortest B–H distance is at vertex 1 (0.73(4) Å). However, although we are fully confident that in **4** one cage C atom is at vertex 12, we have sought further evidence for the position of the second C atom through DFT calculations. Using DFT, the crystallographically determined skeleton was used to build ten isomers [2,7-Cp*-2,7,12,*a*-$Ru_2C_2B_{10}H_{12}$] (with $a = 1, 3, 4, 5, 6, 8, 9, 11, 13$, and 14; $a = 10$ can be disregarded since that would be mirror-symmetric) and each isomer was optimized using the BP86 functional. Following optimization, the ^{1}H and ^{11}B NMR chemical shifts of each isomer were calculated at the B3LYP level and compared with those measured experimentally.[20] In summary, the isomer [2,7-Cp*-2,7,1,12-$Ru_2C_2B_{10}H_{12}$] very clearly gave the best agreement between theory and experiment. Thus linear regression of the computed and experimental ^{11}B NMR shifts yields an R^2 value for the 2,7,1,12 isomer of 0.9954, compared with $R^2 = 0.8676$ for the next-best isomer (2,7,3,12). In terms of ^{1}H NMR shifts, the difference in the sum ($\Delta\Sigma\delta$) of the calculated and actual chemical shifts for the two $C_{cage}H$ resonance signals is only 1.21 ppm for the 2,7,1,12 isomer, compared with 5.01 ppm for the next-best isomer (2,7,4,12). Finally, of all of the ten isomers the lowest free energy computed (BP86-D3 with a correction for the THF solvent) was for the 2,7,1,12 isomer, which had a value 3.5 kcal mol^{-1} below that of the next most stable isomer (2,7,4,12). Thus compound **4** is identified as [2,7-Cp*-2,7,1,12-$Ru_2C_2B_{10}H_{12}$]. The position of the second cage C atom at vertex 1 is, moreover, chemically sensible in that vertex 1 is the degree-4 vertex in the trapezoidal face which subtends an acute angle, B4-C1-B5 = 86.7(4)°, consistent with B4···B5 being an incipient connectivity, 2.220(11) Å. A perspective view of **4** is given in Figure 5.

In the Prostructure of compound **5** there is also one strong indication of a cage carbon atom since the B6–H6 distance is only 0.50(3) Å (the next shortest B–H distance is at vertex 1 and measures 0.96(3) Å). Since vertex 6 lies on the effective mirror plane of the molecule, there are only four possible isomers for compound **5**, [2,7-Cp*-2,7,6,*b*-$Ru_2C_2B_{10}H_{12}$] (with $b = 1$, 5, 11, and 12). DFT calculations strongly suggest that $b = 1$. R^2 is 0.9899 for the 2,7,1,6 isomer compared to 0.8611 for the next-best fit (2,7,6,11). Only one resonance signal

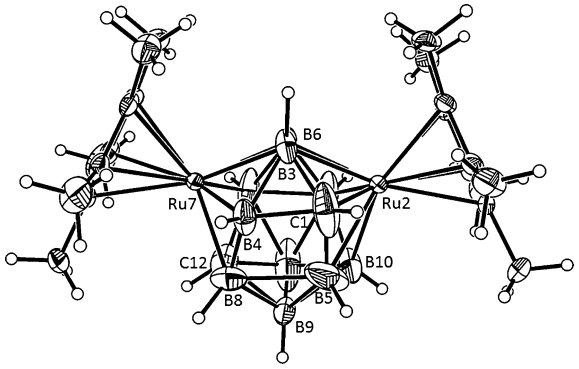

Figure 5. Solid-state structure of compound **4**.[21] Selected bond lengths [Å]: Ru2–C1 2.049(4), Ru2–B5 2.315(7), Ru2–B10 2.127(5), Ru2–B11 2.187(4), Ru2–B6 2.264(4), Ru2–B3 2.258(4), Ru7–B3 2.253(4), Ru7–B4 2.132(4), Ru7–B8 2.197(5), Ru7–C12 2.147(4), Ru7–B14 2.158(4), Ru7–B6 2.265(4), Ru2–C(Cp*) 2.236(3)–2.271(3), Ru7–C(Cp*) 2.243(3)–2.261(3), B4···B5 2.220(11).

attributed to $C_{cage}H$ protons was evident in the ^{1}H NMR spectrum of **5** (see the Supporting Information) but it fits best ($\Delta\delta = 0.61$ ppm) with one of the computed shifts for the 2,7,1,6 isomer (next smallest $\Delta\delta = 4.90$ ppm). Finally, the 2,7,1,6 isomer has the lowest computed free energy of all four isomers considered, being 4.9 kcal mol^{-1} more stable than the next most stable isomer (2,7,5,6). We therefore conclude that compound **5** is [2,7-Cp*-2,7,1,6-$Ru_2C_2B_{10}H_{12}$]. There is partial disorder between the C1 and B4 centers in the crystallographically determined structure of **5** but this does not change the isomer since 2,7,1,6 and 2,7,4,6 are enantiomeric.

For compound **3** the BHD analysis is complicated by three apparently short B–H distances, measuring 0.58(4), 0.74(3), and 0.87(4) Å at vertices 5, 1, and 13 respectively, although the significance of the short B5–H5 distance may be questioned since B5 is disordered over two positions (see the Supporting Information). Nevertheless, for this compound DFT calculations were performed on two sets of isomers, [2,7-Cp*-2,7,5,*c*-$Ru_2C_2B_{10}H_{12}$] (with $c = 1$, 3, 4, 6, 9, 10, 11, 12, 13, and 14), and [2,7-Cp*-2,7,1,*d*-$Ru_2C_2B_{10}H_{12}$] (with $d = 3$, 5, 6, 8, 9, 10, 11, 12, 13, and 14). In the latter case, these calculations gave strong support for the second cage C atom being located at vertex 13. Location of this atom at vertex 13 afforded the best fit between calculated and actual ^{11}B NMR chemical shifts ($R^2 = 0.9939$), the lowest free energy, and the third best fit between calculated and actual ^{1}H NMR chemical shifts ($\Delta\Sigma\delta = 0.93$ ppm). In the former case (that is, with one cage C atom at vertex 5), the situation was anomalous, with the 2,7,3,5 isomer being best in terms of ^{11}B NMR shifts, the 2,7,4,5 isomer best in terms of ^{1}H NMR shifts, and the 2,7,5,13 isomer having the lowest free energy. None of these, however, was either better or lower in value than the corresponding measure for the 2,7,1,13 isomer and therefore we tentatively suggest that compound **3** is [2,7-Cp*-2,7,1,13-$Ru_2C_2B_{10}H_{12}$] based on the available data.

In conclusion, we have prepared the first examples of 14-v 14-SEP (*hypercloso*) heteroboranes and established that they have unique cluster structures. By a combination of spectroscopic, crystallographic, and computational studies, we have determined the isomeric nature of three examples, establishing that in all cases one cage C atom occupies a degree-4 vertex (vertex 1 in our arbitrary numbering scheme shown in Figure 4) on the short parallel edge of a trapezoidal polyhedral face. The formation of multiple isomers by a DEI reaction has precedent[17] and is to be expected since there are likely to be multiple sites on the surface of the *closo* anionic cage where the electrophile can attack, unlike the conventional reduction–metalation synthesis of metallacarboranes in which an open face is presented to the incoming electrophile. Future contributions will develop this theme and expand further the unique chemistry of supraicosahedral *hypercloso* metallacarboranes.

Acknowledgements

We thank the Leverhulme Trust for support of A.P.M.R. and J.J.J. (project RPG-2014-286) and the Engineering and Physical Sciences Research Council both for support of W.Y.M. (project EP/I031545/1) and for DTP studentships supporting N.A.B. and G.S.

Keywords: cage compounds · carboranes · density functional calculations · ruthenium · structure elucidation

[1] a) K. Wade, *J. Chem. Soc. D* **1971**, 792 – 793; b) D. M. P. Mingos, *Nat. (London) Phys. Sci.* **1972**, *236*, 99 – 102.
[2] See, for example: a) R. T. Baker, *Inorg. Chem.* **1986**, *25*, 109 – 111; b) J. D. Kennedy, *Inorg. Chem.* **1986**, *25*, 111 – 112.
[3] a) A. Kaczmarczyk, R. D. Dobrott, W. N. Lipscomb, *Proc. Natl. Acad. Sci. USA* **1962**, *48*, 729 – 733; b) W. N. Lipscomb, *Science* **1966**, *153*, 373 – 378.
[4] K. P. Callahan, W. J. Evans, F. Y. Lo, C. E. Strouse, M. F. Hawthorne, *J. Am. Chem. Soc.* **1975**, *97*, 296 – 302.
[5] E. L. Hoel, C. E. Strouse, M. F. Hawthorne, *Inorg. Chem.* **1974**, *13*, 1388 – 1392.
[6] See, for example: a) J. Bould, N. N. Greenwood, J. D. Kennedy, W. S. McDonald, *J. Chem. Soc. Chem. Commun.* **1982**, 465 – 467; b) J. E. Crook, M. Elrington, N. N. Greenwood, J. D. Kennedy, M. Thornton-Pett, J. D. Woollins, *J. Chem. Soc. Dalton Trans.* **1985**, 2407 – 2415; c) E. J. Ditzel, X. L. R. Fontaine, N. N. Greenwood, J. D. Kennedy, M. Thornton-Pett, *J. Chem. Soc. Chem. Commun.* **1988**, 1262 – 1264; d) J. Bould, N. N. Greenwood, J. D. Kennedy, *J. Chem. Soc. Dalton Trans.* **1990**, 1451 – 1458; e) J. Bould, J. D. Kennedy, M. Thornton-Pett, *J. Chem. Soc. Dalton Trans.* **1992**, 563 – 576; f) J. Bould, R. W. Harrington, W. Clegg, J. D. Kennedy, *J. Organomet. Chem.* **2012**, *721 – 722*, 155 – 163; and references therein.
[7] a) R. L. Johnston, D. M. P. Mingos, *Inorg. Chem.* **1986**, *25*, 3321 – 3323; b) R. L. Johnston, D. M. P. Mingos, P. Sherwood, *New J. Chem.* **1991**, *15*, 831 – 841.
[8] R. Littger, U. Englich, K. Ruhlandt-Senge, J. T. Spencer, *Angew. Chem. Int. Ed.* **2000**, *39*, 1472 – 1474; *Angew. Chem.* **2000**, *112*, 1532 – 1534.
[9] The compound [$(CpFe)_2C_2B_9H_{11}$] (13-v 13-SEP) is proposed to have a 4,5,2,3-$Fe_2C_2B_9$ structure based on spectroscopic data, but no crystallographic study has been reported. C. G. Salentine, M. F. Hawthorne, *Inorg. Chem.* **1978**, *17*, 1498 – 1501.
[10] 15-v 15-SEP and 16-v 16-SEP metallaboranes have been reported. See: a) D. K. Roy, B. Mondal, P. Shankhari, R. S. Anju, K. Geetharani, S. M. Mobin, S. Ghosh, *Inorg. Chem.* **2013**, *52*, 6705 – 6712; b) D. K. Roy, S. K. Bose, R. S. Anju, B. Mondal, V. Ramkumar, S. Ghosh, *Angew. Chem. Int. Ed.* **2013**, *52*, 3222 – 3226; *Angew. Chem.* **2013**, *125*, 3304 – 3308.
[11] a) A. R. Kudinov, D. S. Perekalin, S. S. Rynin, K. A. Lyssenko, G. V. Grintselev-Knyazev, P. V. Petrovskii, *Angew. Chem. Int. Ed.* **2002**, *41*, 4112 – 4114; *Angew. Chem.* **2002**, *114*, 4286 – 4288; b) A. R. Kudinov, M. I. Rybinskaya, D. S. Perekalin, V. I. Meshcheryakov, Yu. A. Zhuravlev, P. V. Petrovskii, A. A. Korlyukov, D. G. Golovanov, K. A. Lyssenko, *Russ. Chem. Bull.* **2004**, *53*, 1958 – 1962.
[12] a) D. F. Dustin, G. B. Dunks, M. F. Hawthorne, *J. Am. Chem. Soc.* **1973**, *95*, 1109 – 1115; b) A. Burke, D. Ellis, D. Ferrer, D. L. Ormsby, G. M. Rosair, A. J. Welch, *Dalton Trans.* **2005**, 1716 – 1721.
[13] D. F. Dustin, M. F. Hawthorne, *J. Am. Chem. Soc.* **1974**, *96*, 3462 – 3467; See also Ref. [16].
[14] M. E. O'Neill, K. Wade, *Polyhedron* **1984**, *3*, 199 – 212.
[15] M. E. Lopez, M. J. Edie, D. Ellis, A. Horneber, S. A. Macgregor, G. M. Rosair, A. J. Welch, *Chem. Commun.* **2007**, 2243 – 2245.

[16] a) W. Y. Man, S. Zlatogorsky, H. Tricas, D. Ellis, G. M. Rosair, A. J. Welch, *Angew. Chem. Int. Ed.* **2014**, *53*, 12222 – 12225; *Angew. Chem.* **2014**, *126*, 12418 – 12421; b) W. Y. Man, D. Ellis, G. M. Rosair, A. J. Welch, *Angew. Chem. Int. Ed.* **2016**, *55*, 4596 – 4599; *Angew. Chem.* **2016**, *128*, 4672 – 4675.

[17] A. McAnaw, M. E. Lopez, D. Ellis, G. M. Rosair, A. J. Welch, *Dalton Trans.* **2014**, *43*, 5095 – 5105.

[18] a) W. J. Evans, M. F. Hawthorne, *J. Chem. Soc. Chem. Commun.* **1974**, 38 – 39; b) W. M. Maxwell, R. Weiss, E. Sinn, R. N. Grimes, *J. Am. Chem. Soc.* **1977**, *99*, 4016 – 4029; c) J. R. Pipal, R. N. Grimes, *Inorg. Chem.* **1978**, *17*, 6 – 10; d) D. Ellis, M. E. Lopez, R. McIntosh, G. M. Rosair, A. J. Welch, *Chem. Commun.* **2005**, 1917 – 1919; e) L. Deng, H.-S. Chan, Z. Xie, *Angew. Chem. Int. Ed.* **2005**, *44*, 2128 – 2131; *Angew. Chem.* **2005**, *117*, 2166 – 2169; f) R. D. McIntosh, D. Ellis, G. M. Rosair, A. J. Welch, *Angew. Chem. Int. Ed.* **2006**, *45*, 4313 – 4316; *Angew. Chem.* **2006**, *118*, 4419 – 4422; g) J. Zhang, L. Deng, H. S. Chan, Z. Xie, *J. Am. Chem. Soc.* **2007**, *129*, 18 – 19; h) A. McAnaw, M. E. Lopez, D. Ellis, G. M. Rosair, A. J. Welch, *Dalton Trans.* **2013**, *42*, 671 – 679.

[19] A. McAnaw, G. Scott, L. Elrick, G. M. Rosair, A. J. Welch, *Dalton Trans.* **2013**, *42*, 645 – 664.

[20] Full computational details including the calculated chemical shifts and test calculations based on the B3LYP-optimized structures are given in the Supporting Information.

[21] CCDC 1458452 – 1458456 contain the supplementary crystallographic data for this paper. These data are provided free of charge by The Cambridge Crystallographic Data Centre.

Received: March 9, 2016
Revised: April 19, 2016
Published online: ■■ ■■, ■■■■

Communications

Metallacarboranes

A. P. M. Robertson, N. A. Beattie, G. Scott, W. Y. Man, J. J. Jones, S. A. Macgregor,* G. M. Rosair, A. J. Welch* ——— ■■■■–■■■■

14-Vertex Heteroboranes with 14 Skeletal Electron Pairs: An Experimental and Computational Study

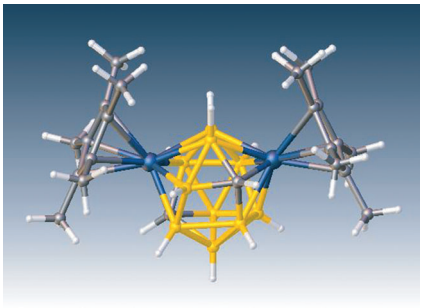

Living on the edge: The first three examples of 14-vertex heteroboranes with 14 skeletal electron pairs have been prepared and characterized by a combination of spectroscopic, crystallographic, and computational techniques. The compounds $[(Cp^*Ru)_2C_2B_{10}H_{12}]$ all share a unique cluster structure featuring a trapezoidal face. Atom colors: C gray, B yellow, Ru blue.

Journal of Organometallic Chemistry 865 (2018) 65–71

Contents lists available at ScienceDirect

Journal of Organometallic Chemistry

journal homepage: www.elsevier.com/locate/jorganchem

Mixed-ligand (triphenylphosphine)ruthenium complexes of diphenylcarborane by ligand manipulation and an asymmetric, bimolecular "symbiotic" cluster

John J. Jones, Laura E. English, Alasdair P.M. Robertson, Georgina M. Rosair, Alan J. Welch*

Institute of Chemical Sciences, Heriot-Watt University, Edinburgh EH14 4AS, UK

ARTICLE INFO

Article history:
Received 14 December 2017
Received in revised form
5 February 2018
Accepted 6 February 2018
Available online 10 February 2018

Dedicated to Professor Narayan Hosmane with very best wishes on the occasion of his 70th birthday.

Keywords:
Diphenylcarborane
Metallacarborane
Synthesis
Crystal structure
Pseudocloso
Hypercloso

ABSTRACT

Deprotonation of [*exo*-5,6,10-{RuCl(PPh$_3$)$_2$}-5,6,10-(μ-H)$_3$-*nido*-7,8-$C_2B_9H_9$] (**1a**) and its *C*,*C*-diphenyl analogue (**1b**) affords the anions [3,3-(PPh$_3$)$_2$-3-Cl-*closo*-3,1,2-$RuC_2B_9H_{11}$]$^-$ (**2a**) and [1,2-Ph$_2$-3,3-(PPh$_3$)$_2$-3-Cl-*closo*-3,1,2-$RuC_2B_9H_9$]$^-$ (**2b**), respectively. Dehalogenation of **2b** in the presence of one equivalent of ^{t}BuNC yields [1,2-Ph$_2$-3,3-(^{t}BuNC)$_2$-3-PPh$_3$-*pseudocloso*-3,1,2-$RuC_2B_9H_9$] (**3**), and if **2b** is dehalogenated in the presence of CO a very similar compound, [1,2-Ph$_2$-3,3-(CO)$_2$-3-PPh$_3$-*pseudocloso*-3,1,2-$RuC_2B_9H_9$] (**4**), is formed. Treatment of **2b** with Ag^+ in the absence of a donor ligand affords, amongst a number of products, the compound [{1,2-Ph$_2$-*pseudocloso*-3,1,2-$RuC_2B_9H_9$}{1′,8′-Ph$_2$-*closo*-2′,1′,8′-$RuC_2B_9H_9$}] (**5**) in which two different {$RuPh_2C_2B_9H_9$} units both achieve electronic and coordinative saturation at their Ru centres by η^6-coordination of a Ph ring on the other cluster in a symbiotic manner. Compounds **1b**, **3**, **4** and **5** were fully characterised, including by crystallographic studies.

1. Introduction

The structures of the vast majority of polyhedral boranes, carboranes and their metal derivatives are governed by the Polyhedral Skeletal Electron Pair Theory [1], relating structure to the number of polyhedral vertices (*n*) and the number of skeletal electron pairs (SEPs) that the cluster possesses. In contrast to the large and well-known families of closo (*n*+1 SEPs), nido (*n*+2 SEPs) and arachno (*n*+3 SEPs) polyhedra, an interesting smaller group is the hypercloso family, having only *n* SEPs. Hypercloso metallacarboranes often have structures based on those of closo analogues but which have undergone a single diamond-square-diamond (d-s-d) rearrangement which typically decreases the degree (connectivity number) of at least one cage C atom whilst increasing the degree of a transition metal vertex. An excellent example of this is afforded by a comparison of the structures of [*closo*-(CpCo)$_2$$C_2B_6H_8$] [2] and [*hypercloso*-(CpFe)$_2$$C_2B_6H_8$] [3], Fig. 1.

In considering deliberate and potentially general synthetic routes to hypercloso metallacarboranes one option would be to introduce either one 1-vertex 0-electron (1-v 0-e) metal fragment or two 1-v 1-e metal fragments into a {$C_2B_xH_{2+x}$} or {$C_2B_xH_xR_2$} framework, and we recently described examples of the latter approach in the synthesis of the first 14-v 14-SEP heteroboranes [4]. An alternative approach is "ligand manipulation" by which we mean the removal of a 2-e ligand from a 1-v 2-e metal fragment in a closo metallacarborane precursor, converting the metal to a 1-v 0-e fragment and the metallacarborane from *n*+1 SEP closo to *n* SEP hypercloso. Within the context of ligand manipulation, however, it is important to consider the nature of the ligands remaining on the metal centre since if these include CO then "carbonyl-stealing" by the putative hypercloso metallacarborane can occur to regenerate a closo metallacarborane [5].

To avoid CO-stealing we have instead focussed on metallacarboranes with halide and phosphine ligands, identifying the anionic ruthenacarborane **2** (Scheme 1) as an attractive potential precursor to hypercloso metallacarboranes by loss of Cl^- on treatment with Ag^+. Moreover, to encourage the anticipated d-s-

* Corresponding author.
E-mail address: a.j.welch@hw.ac.uk (A.J. Welch).

https://doi.org/10.1016/j.jorganchem.2018.02.007
0022-328X/

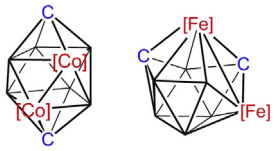

Fig. 1. Left; the bicapped square-antiprismatic structure of the 10-vertex 11-SEP species [*closo*-$(CpCo)_2C_2B_6H_8$], [Co]=CpCo. Right; the structure of the 10-vertex 10-SEP species [*hypercloso*-$(CpFe)_2C_2B_6H_8$], [Fe]=CpFe. Topologically the structure of the ferracarborane is derived from that of the cobaltacarborane by the application of a single diamond-square-diamond rearrangement.

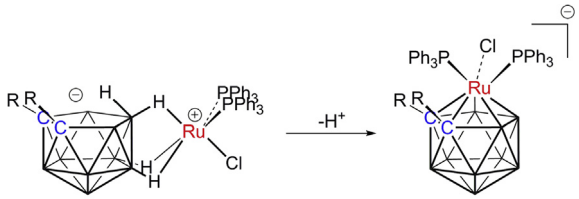

1a R=H, **1b** R=Ph **2a** R=H, **2b** R=Ph

Scheme 1. Deprotonation of the exo-nido species [*exo*-5,6,10-{$RuCl(PPh_3)_2$}-5,6,10-(μ-H)$_3$-*nido*-7,8-$C_2B_9H_9$] (**1a**) and [*exo*-5,6,10-{$RuCl(PPh_3)_2$}-5,6,10-(μ-H)$_3$-7,8-Ph_2-*nido*-7,8-$C_2B_9H_7$] (**1b**) to afford the closo anions [3,3-$(PPh_3)_2$-3-Cl-*closo*-3,1,2-$RuC_2B_9H_{11}]^-$ (**2a**) and [1,2-Ph_2-3,3-$(PPh_3)_2$-3-Cl-*closo*-3,1,2-$RuC_2B_9H_9]^-$ (**2b**) respectively.

d transformation we have focussed initial attention on the *C*,*C*-diphenyl derivative **2b**. This is because it is well-established that *C*,*C*-diphenyl 3,1,2-MC_2B_9 metallacarboranes with a bulky ligand set are prone to adopt structures in which the Ph substituents, forced to lie nearly co-planar by steric congestion, push against each other and stretch the C1–C2 connectivity affording "pseudocloso" geometries [6] which can be considered as half-way-houses in the d-s-d rearrangement of closo to hypercloso. Herein we describe the zwitterionic exo-nido compound **1b** as a precursor to **2b** and the reactions of **2b** with Ag^+ in both the presence and absence of 2-e ligands. Whilst this manuscript was in preparation Kostyukovich et al. independently reported the synthesis of **1b** [7].

2. Results and discussion

Concurrently with Kostyukovich, Chizhevsky and co-workers [7] we prepared [*exo*-5,6,10-{$RuCl(PPh_3)_2$}-5,6,10-(μ-H)$_3$-7,8-Ph_2-*nido*-7,8-$C_2B_9H_7$] (**1b**) from the reaction between K[7,8-Ph_2-*nido*-7,8-$C_2B_9H_{10}$] and $[RuCl_2(PPh_3)_3]$ in THF, achieving a yield of 78%. Our sample is spectroscopically identical to that prepared by our Russian colleagues but, in addition, we also characterised the product crystallographically, and a perspective view of a single molecule is shown in Fig. 2. As discussed for the parent, non *C*,*C*-diphenyl derivative **1a**, these exo-nido compounds exist in solution at room temperature as an equilibrium mixture of symmetric and asymmetric hydrido Ru^{IV} species [8]. In the solid state, however, **1a** has a 5,6,10-(μ-H)$_3$ structure and a formally Ru^{II} exo-nido metal centre [8] and the same is true of **1b**. The Cl ligand is positioned opposite the open face of the carborane affording the structure as a whole approximate C_s molecular symmetry. Bond distances in **1b** are in close accord with those reported for **1a** with the exception of the C7–C8 connectivity, which is ca. 0.1 Å longer in **1b** at 1.646(5) Å presumably as the result of crowding between the *C*-bound Ph rings. In *C*-aryl carboranes and their derivatives it is instructive to define the orientation of the aryl ring in terms of θ, the modulus of the average C_{cage}–C_{cage}–C–C torsion angle [9]; if θ = 90° the plane of the aryl ring contains the C_{cage}–C_{cage} vector and if θ = 0° it stands perpendicular to it. For **1b** θ for Ph on C7 is 5.5(4)° and for Ph on C8 it is 5.7(4)°.

We targeted the exo-nido zwitterion **1b** as a potential precursor to closo **2b** which we intended then to use in halide abstraction reactions. Anion **2b** is currently unknown but the parent species **2a** (as the $[NEt_4]^+$ salt) has been reported from the reaction between $[HNMe_3]$[*nido*-7,8-$C_2B_9H_{12}$] and $[RuH(Cl)(PPh_3)_3]$ in the presence of $[NEt_4]Cl$ [10]. We hypothesised that a potentially simpler route to **2a** (or **2b**) would be removal of the endo-proton of **1a** (or **1b**) resulting in subsequent capitation of the open C_2B_3 face of the carborane by the {$RuCl(PPh_3)_2$} fragment (Scheme 1). To test this hypothesis, compound **1a** in THF at 0 °C was treated with one

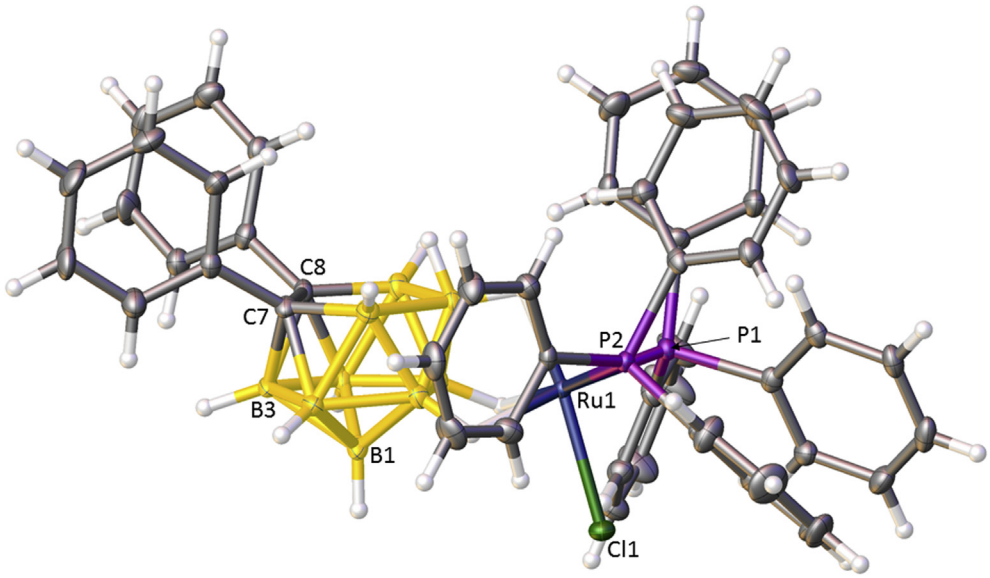

Fig. 2. Perspective view of [*exo*-5,6,10-{$RuCl(PPh_3)_2$}-5,6,10-(μ-H)$_3$-7,8-Ph_2-*nido*-7,8-$C_2B_9H_7$] (**1b**). Displacement ellipsoids are drawn at the 50% probability level except for H atoms. Selected molecular parameters (Å; °): Ru–B5 2.392(4), Ru1–B6 2.391(4), Ru1–B10 2.288(4), Ru1–P1 2.3193(9), Ru1–P2 2.2968(9), Ru1–Cl1 2.3935(8), C7–C8 1.646(5); θ(Ph ring on C7) 5.4(4), θ(Ph ring on C8) 5.7(4).

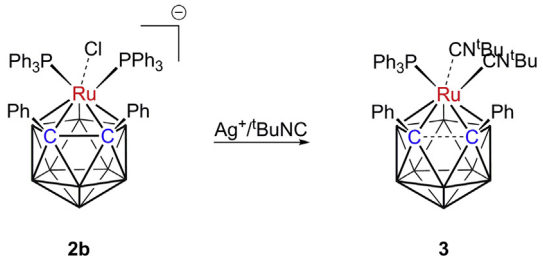

Scheme 2. Dehalogenation of [1,2-Ph_2-3,3-$(PPh_3)_2$-3-Cl-*closo*-3,1,2-$RuC_2B_9H_9$]$^-$ (**2b**) in the presence of ^{t}BuNC yielding [1,2-Ph_2-3,3-(^{t}BuNC)$_2$-3-PPh_3-*pseudocloso*-3,1,2-$RuC_2B_9H_9$] (**3**).

equivalent of ^{n}BuLi and the resultant dark-red product was shown to be identical to [NEt_4]**2a** [10] by $^{11}B\{^1H\}$ spectroscopic analysis. Anion **2a** is, however, highly sensitive to traces of air or moisture, and assuming that **2b** would be similarly reactive we have not attempted to isolate **2b** but rather we have used it directly in subsequent reactions.

Our initial halide abstraction reaction was treatment of Li[**2b**], prepared *in situ* from the deprotonation of **1b** with ^{n}BuLi as described above, with Ag[BF_4] in the presence of one equivalent of ^{t}BuNC. This would serve not only to confirm that loss of Cl^- from anion **2b** was achievable but would also afford a novel route to mixed-ligand $(PPh_3)_yL_zRuC_2B_9$ species [10,11]. We expected that the product of this reaction would have $y = 2$ and $z = 1$ but it was immediately apparent from elemental analysis, mass spectrometric and NMR spectroscopic study of the only isolatable product (following work-up involving column chromatography) that, in fact, $y = 1$ and $z = 2$. Thus the species formed is [1,2-Ph_2-3,3-(^{t}BuNC)$_2$-3-PPh_3-*pseudocloso*-3,1,2-$RuC_2B_9H_9$] (**3**) resulting from replacement of Cl^- by ^{t}BuNC and displacement of one PPh_3 ligand by a second mole of ^{t}BuNC, even though only one equivalent of ^{t}BuNC was used (Scheme 2). The yield is 34% based on **1b** but 68% based on ^{t}BuNC. In the ^{1}H NMR spectrum of **3** a broad singlet at δ 1.17 integrates for 18H (2 × ^{t}BuNC ligands) versus 25H for phenyl protons (1 × PPh_3 ligand +1 × $Ph_2C_2B_9$ ligand). In the $^{11}B\{^1H\}$ NMR spectrum are six resonances between +24 and −20 ppm with integrals in the relative ratio 1:1:2:2:2:1 from high frequency to low frequency, corresponding to time-averaged C_s molecular symmetry. The weighted-average ^{11}B chemical shift, $<\delta(^{11}B)>$, is +5.8 ppm. This is reminiscent of $<\delta(^{11}B)>$ in typical pseudocloso compounds of diphenylcarborane [12] and, indeed, the pseudocloso structure of **3** was confirmed by a crystallographic study as shown in Fig. 3.

In the solid state molecules of **3** are asymmetric with one ^{t}BuNC ligand lying over the square face formed by Ru3, C1, B6 and C2 that is characteristic of pseudocloso metallacarboranes [6]. The diagonals of this face are C1···C2 2.521(7) Å and Ru3···B6 3.021(6) Å. The Ph ring on C1 adopts a θ value of 86.6(5) ° because of the demands of the ligand set on the Ru vertex (and there is evidence for π-π stacking with one Ph ring of the PPh_3 ligand) whilst the Ph ring on C2 is at an intermediate θ value, 30.9°. Dimensions within the Ru3-C-N sequences reflect the relative Structural Trans Effects (STEs) of the cage atoms they lie opposite [13]; Ru3−C31 (trans to B) is significantly longer (and therefore weaker) than Ru3−C32 (trans to C). A reverse pattern exists in the C31−N31 and C32−N32 distances, although the difference here is not statistically significant.

In solution at room temperature compound **3** is clearly fluctional since the ^{11}B NMR spectrum is consistent with mirror symmetry and there is only one resonance for the ^{t}BuNC protons in the ^{1}H NMR spectrum. This is consistent with rotation (or at least significant libration) of the {Ru(PPh_3)(^{t}BuNC)$_2$} fragment about the metal-cage axis. That the ^{t}BuNC resonance is broad, however, implies restricted rotation and we suggest a simple oscillation of ca. 120° that exchanges the positions of the ^{t}BuNC ligands above the RuCBC square face. A ^{1}H NMR spectrum recorded at 203 K shows that this oscillation is frozen out and two sharp singlets are observed for the ^{t}BuNC protons.

We assume that the unexpected loss of a PPh_3 ligand (replaced by ^{t}BuNC) in the synthesis of **3** is a consequence of unacceptable steric crowding in the anticipated product [1,2-Ph_2-3,3-$(PPh_3)_2$-3-^{t}BuNC-3,1,2-$RuC_2B_9H_9$]. Even so, **3** itself is clearly still sterically-crowded, as evidenced by its pseudocloso structure and the restricted rotation of the {Ru(PPh_3)(^{t}BuNC)$_2$} fragment. Consequently our next reaction was to mimic the synthesis of **3** replacing ^{t}BuNC by the smallest L-type ligand, CO.

The reaction of Ag[BF_4] with deprotonated **1b** in an atmosphere of CO (Scheme 3), followed by work-up involving preparative thin-layer chromatography (TLC) afforded [1,2-Ph_2-3,3-$(CO)_2$-3-PPh_3-*pseudocloso*-3,1,2-$RuC_2B_9H_9$] (**4**) as the only isolatable product. The fact that **4** has again lost one PPh_3 ligand and is thus the dicarbonyl compound is readily apparent from

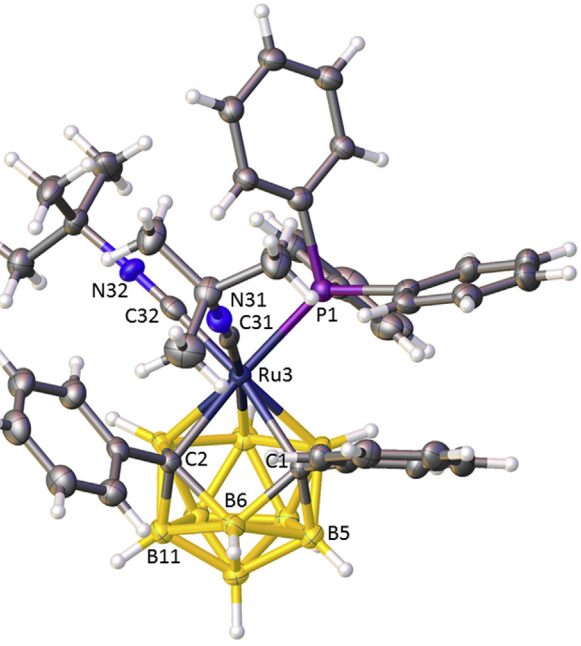

Fig. 3. Perspective view of [1,2-Ph_2-3,3-(^{t}BuNC)$_2$-3-PPh_3-*pseudocloso*-3,1,2-$RuC_2B_9H_9$] (**3**). Displacement ellipsoids as in Fig. 2. Selected molecular parameters (Å; °): Ru3−C1 2.244(5), Ru3−C2 2.222(5), Ru3−B 2.236(6)-2.284(6), Ru3−P1 2.3625(13), Ru3−C31 2.001(6), Ru3−C32 1.955(5), C31−N31 1.157(7), C32−N32 1.163(7), C1···C2 2.521(7), Ru3···B6 3.021(6); Ru3−C1−B6 98.4(3), C1−B6−C2 93.1(4), B6−C2−Ru3 98.5(3), C2−Ru3−C1 68.72(19), θ(Ph ring on C1) 86.6(5), θ(Ph ring on C2) 30.9(6).

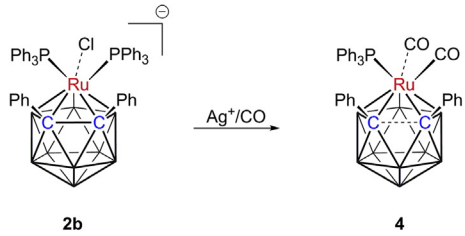

Scheme 3. Dehalogenation of [1,2-Ph_2-3,3-$(PPh_3)_2$-3-Cl-*closo*-3,1,2-$RuC_2B_9H_9$]$^-$ (**2b**) in the presence of CO to afford [1,2-Ph_2-3,3-$(CO)_2$-3-PPh_3-*pseudocloso*-3,1,2-$RuC_2B_9H_9$] (**4**).

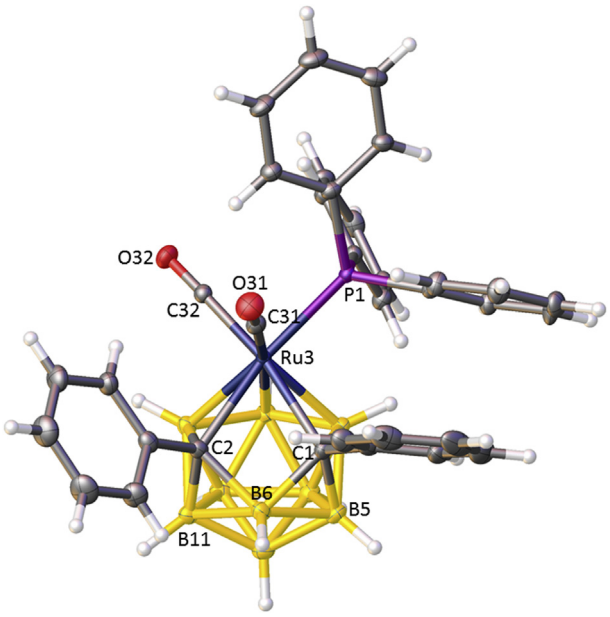

Fig. 4. Perspective view of [1,2-Ph_2-3,3-$(CO)_2$-3-PPh_3-*pseudocloso*-3,1,2-$RuC_2B_9H_9$] (**4**). Displacement ellipsoids as in Fig. 2. Selected molecular parameters (Å; °): Ru3–C1 2.2391(18), Ru3–C2 2.2678(18), Ru3–B 2.251(2)-2.278(2), Ru3–P1 2.3781(5), Ru3–C31 1.953(2), Ru3–C32 1.8976(19), C31–O31 1.125(2), C32–O32 1.140(2), C1···C2 2.457(3), Ru3···B6 3.094(2); Ru3–C1–B6 101.96(11), C1–B6–C2 90.35(13), B6–C2–Ru3 100.17(11), C2–Ru3–C1 66.06(7), θ(Ph ring on C1) 86.7(2), θ(Ph ring on C2) 18.4(2).

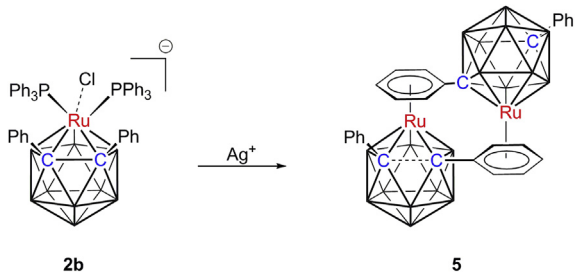

Scheme 4. Dehalogenation of [1,2-Ph_2-3,3-$(PPh_3)_2$-3-Cl-*closo*-3,1,2-$RuC_2B_9H_9$]$^-$ (**2b**) in the absence of a donor ligand yields the symbiotic compound [{1,2-Ph_2-*pseudocloso*-3,1,2-$RuC_2B_9H_9$}{1′,8′-Ph_2-*closo*-2′,1′,8′-$RuC_2B_9H_9$}] (**5**).

elemental analysis, mass spectrometry, IR spectroscopy (symmetric and antisymmetric C-O stretches) and NMR spectroscopy; in the last the $^1H\{^{11}B\}$ spectrum clearly shows evidence for only one PPh_3 ligand relative to the $\{Ph_2C_2B_9H_9\}$ fragment. The $^{11}B\{^1H\}$ NMR spectrum appears as a 2:2:2:2:1 pattern (high frequency to low frequency) between δ +18 and −18 ppm, with $<\delta(^{11}B)>$ +4.4 ppm again implying a pseudocloso structure. This was subsequently confirmed by crystallographic analysis showing that a single molecule of **4** (Fig. 4) is practically identical to that of **3** in which the ^{t}BuNC ligands have been replaced by CO. In detail, however, the Ph ring on C2 is less flattened by the smaller adjacent CO ligands [θ = 18.4(2) °] and so the repulsive interaction with the Ph ring on C1 is reduced and the consequent pseudocloso distortion is somewhat less pronounced. In compound **4** C1···C2 is 2.457(3) Å and Ru3···B6 is 3.094(2) Å, and compared to **3** the Ru3-C1-B6-C2 unit is less deformed into a square, with somewhat wider angles at C1 and C2 and narrower angles at Ru3 and B6. Similarly to **3**, the Ru–CO and C–O distances in **4** reflect the cage atoms to which the CO ligands lie opposite. C32O32 (trans to C) is the stronger bound ligand with significantly shorter Ru–CO and significantly longer C–O bonds than C31O31 (trans to B).

Thus even with the small CO ligand it appears that the species [1,2-Ph_2-3,3-$(PPh_3)_2$-3-CO-3,1,2-$RuC_2B_9H_9$] is too sterically-crowded to be isolated, resulting in displacement of one PPh_3 by CO and the formation of compound **4** (note that the less-crowded non-*C*,*C*-diphenyl analogue, [3,3-$(PPh_3)_2$-3-CO-*closo*-3,1,2-$RuC_2B_9H_{11}$] is a known species [10,11b,d] as is its 2,1,7-isomer [2,2-$(PPh_3)_2$-2-CO-*closo*-2,1,7-$RuC_2B_9H_{11}$] [11a]. One positive implication of this, however, is that the hypothetical hypercloso species [1,2-Ph_2-3,3-$(PPh_3)_2$-3,1,2-$RuC_2B_9H_9$] might be sufficiently sterically-protected at the Ru centre to be isolated; the less-crowded analogous species [2,2-$(PPh_3)_2$-*hypercloso*-2,1,7-$RuC_2B_9H_{11}$] has been reported from thermal dehydrogenation of [2,2-$(PPh_3)_2$-2,2-$(H)_2$-*closo*-2,1,7-$RuC_2B_9H_{11}$] [14,11a] but not characterised crystallographically.

Consequently Li[**2b**] in the non-donor solvent DCM was treated with $Ag[BF_4]$ in the absence of a donor ligand (Scheme 4). Work-up by preparative TLC afforded numerous coloured mobile bands the most abundant of which, an orange band, was collected yielding [{1,2-Ph_2-*pseudocloso*-3,1,2-$RuC_2B_9H_9$}{1′,8′-Ph_2-*closo*-2′,1′,8′-$RuC_2B_9H_9$}] (**5**) as an orange solid. Microanalysis was consistent with the empirical formula $C_{14}H_{19}B_9Ru$ and $^{31}P\{^1H\}$ NMR spectroscopy quickly revealed the absence of phosphine ligands. In the ^1H NMR spectrum is a series of thirteen multiplets from δ 7.7 to 5.0 and in the $^{11}B\{^1H\}$ NMR spectrum are thirteen distinct resonances. Collectively these suggest that the molecular formula must be some multiple of the empirical formula, subsequently confirmed by the mass spectrum which displays a molecular ion corresponding to $(C_{14}H_{19}B_9Ru)_2$.

The nature of compound **5** was revealed by a crystallographic study (Fig. 5). The molecule consists of two $\{RuPh_2C_2B_9H_9\}$ units, one (unprimed) of 3,1,2-RuC_2B_9 architecture and the other (primed) having isomerised to a 2′,1′,8′-RuC_2B_9 architecture. The unprimed cage is pseudocloso due to the high θ values of the Ph rings on C1 and C2; C1···C2 is 2.491(4) Å and Ru3···B6 2.933(4) Å. In contrast the primed cage has a conventional closo distorted icosahedral geometry since there is no steric repulsion between the non-adjacent rings on C1′ and C8′. Most importantly, the Ph ring on C1′ acts as an η^6-ligand to Ru3 whilst the Ph ring on C1 acts in a similar fashion to Ru2′, resulting in 18-e configurations at each metal centre and 13 SEP counts for each 12-vertex ruthenacarborane cage.

This unusual structure demonstrates a unique way in which the target molecule [1,2-Ph_2-3,3-$(PPh_3)_2$-*hypercloso*-3,1,2-$RuC_2B_9H_9$] avoids its inherent electron deficiency – by loss of both PPh_3 ligands and two $\{RuPh_2C_2B_9H_9\}$ units coming together to provide 6-e to the Ru atom of the other cluster via η^6-ligation of a Ph substituent. Borrowing a term from biology, we describe compound **5** as a symbiotic cluster. There is a small number of examples in the literature of compounds in which an aryl substituent on a (hetero) carborane acts as an η^6-ligand to a transition metal atom [15], and even fewer cases in which that metal atom is itself part of a metallacarborane [15c,16]. Of the latter group only one example, $[\{(MeC_6H_4)Rh(C_2B_9H_9C_6H_4Me)Rh(C_8H_{12})\}_2]$ [16b], is a symbiotic species similar to compound **5**.

In conclusion, we have shown that the highly reactive anions **2a** and **2b** can be formed from simple deprotonation of the exo-nido precursors **1a** and **1b**, respectively, and that dehalogenation of **2b** in the presence of only one equivalent of ^{t}BuNC results in loss of a PPh_3 ligand and the formation of the pseudocloso bis(^{t}BuNC) species **3**. Performing the dehalogenation in the

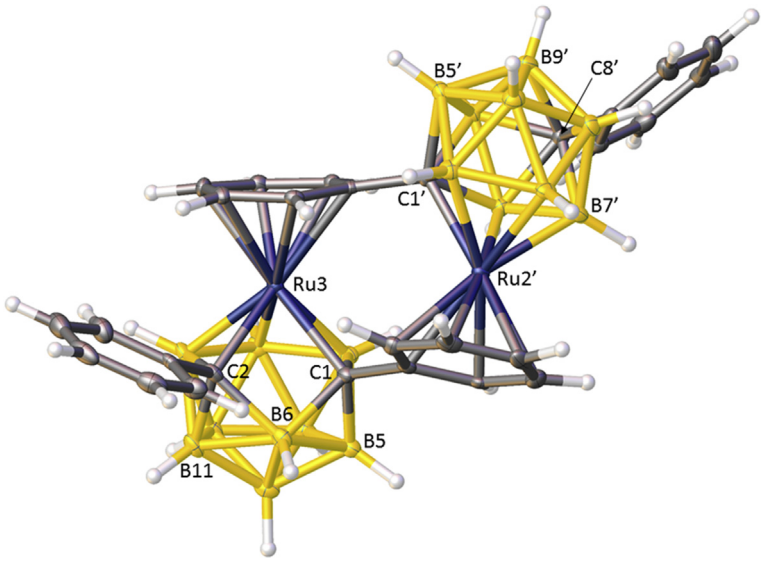

Fig. 5. Perspective view of the symbiotic compound [{1,2-Ph_2-*pseudocloso*-3,1,2-$RuC_2B_9H_9$}{1′,8′-Ph_2-*closo*-2′,1′,8′-$RuC_2B_9H_9$}] (**5**). Displacement ellipsoids as in Fig. 2. Selected molecular parameters (Å; °): Ru3–C1 2.135(3), Ru3–C2 2.147(3), Ru3–B 2.199(4)-2.222(3), Ru3–C (Ph ring on C1′) 2.194(3)-2.388(3), C1···C2 2.491(4), Ru3···B6 2.933(4), Ru2′–C1′ 2.176(3), Ru2′–B 2.149(4)-2.196(4), Ru2′–C (Ph ring on C1) 2.203(3)-2.281(3); Ru3–C1–B6 98.31(18), C1–B6–C2 91.9(2), B6–C2–Ru3 97.46(18), C2–Ru3–C1 71.12(12), θ(Ph ring on C1) 79.3(3), θ(Ph ring on C2) 56.6(3).

presence of CO affords a very similar product (**4**). If **2b** is dehalogenated in the absence of donor ligands, however, one of several products formed is the unusual symbiotic species **5** in which the Ru centres have lost both PPh_3 ligands but achieve electronic saturation from η^6-ligation of a Ph substituent of the complementary cluster. This interesting last result demonstrates how the targeted hypercloso metallacarborane [1,2-Ph_2-3,3-$(PPh_3)_2$-*hypercloso*-3,1,2-$RuC_2B_9H_9$] was able to take advantage of a source of additional electrons and so avoid being hypoelectronic. Current studies are directed towards the synthesis of hypercloso metallacarboranes in which such sources of additional electrons are unavailable.

3. Experimental

3.1. Synthesis

Experiments were performed under dry, oxygen-free, N_2 using standard Schlenk techniques, although subsequent manipulations were sometimes performed in the open laboratory. Solvents were freshly distilled under nitrogen from the appropriate drying agent [THF and 40–60 petroleum ether (petrol) from sodium wire, and CH_2Cl_2 (DCM) from calcium hydride] and were degassed (3 × freeze-pump-thaw cycles) before use. Deuterated solvents for NMR spectroscopy ($CDCl_3$, CD_2Cl_2, CD_3CN) were stored over 4 Å molecular sieves. Preparative TLC employed 20 × 20 cm Kieselgel F_{254} glass plates and column chromatography used 60 Å silica as the stationary phase. Elemental analyses were conducted using an Exeter CE-440 elemental analyser. The IR spectrum was measured on a Nicolet iS5 FT-IR spectrometer. NMR spectra at 400.1 MHz (^{1}H), 162.0 MHz (^{31}P) or 128.4 MHz (^{11}B) were recorded on a Bruker DPX-400 spectrometer from $CDCl_3$ solutions at room temperature unless otherwise noted. Electron impact mass spectrometry (EIMS) was carried out using a Finnigan (Thermo) LCQ Classic ion trap mass spectrometer at the University of Edinburgh. The starting material [*exo*-5,6,10-{RuCl$(PPh_3)_2$}-5,6,10-(μ-H)$_3$-*nido*-7,8-$C_2B_9H_9$] (**1a**) was made by the method of Chizhevsky and co-workers [8] and the *C*,*C*-diphenyl analogue [*exo*-5,6,10-{RuCl$(PPh_3)_2$}-5,6,10-(μ-H)$_3$-7,8-Ph_2-*nido*-7,8-$C_2B_9H_7$] (**1b**) by an analogous method. All other reagents were supplied commercially.

3.1.1. Deprotonation of [exo-5,6,10-{RuCl$(PPh_3)_2$}-5,6,10-(μ-H)$_3$-nido-7,8-$C_2B_9H_9$] (**1a**)

Compound **1a** (0.100 g, 0.126 mmol) was dissolved in THF (12 mL) and ^{n}BuLi (0.05 mL of a 2.5 M solution in hexanes, 0.126 mmol) added at 0 °C. The solution was stirred for 0.5 h to afford a dark red solution. An aliquot (0.5 mL) of this solution was then transferred to a J. Young NMR tube containing CD_3CN (0.2 mL). ^{11}B{^{1}H} NMR; δ −1.5 (1B), −5.8 (1B), −8.4 (1B), −10.9 (1B), −12.3 (2B), −23.3 (1B), −24.5 (2B), essentially identical to the chemical shifts and integrals reported for [3,3-$(PPh_3)_2$-3-Cl-*closo*-3,1,2-$RuC_2B_9H_{11}]^-$ (**2a**) as its $[NEt_4]^+$ salt [10].

3.1.2. [1,2-Ph_2-3,3-(^{t}BuNC)$_2$-3-PPh_3-pseudocloso-3,1,2-$RuC_2B_9H_9$] (**3**)

Compound **1b** (0.210 g, 0.222 mmol) was dissolved in THF (18 mL) and cooled to 0 °C and to this stirred solution was added, dropwise, ^{n}BuLi (0.09 mL of a 2.5 M solution in hexanes, 0.225 mmol). After stirring at room temperature for 0.5 h the dark red solution of Li[**2b**] was transferred by cannula to a second Schlenk tube containing Ag[BF_4] (0.045 g, 0.231 mmol) and ^{t}BuNC (0.03 mL, 0.266 mmol). After stirring for 0.5 h volatiles were removed *in vacuo* to afford a dark brown solid. This was dissolved in DCM (20 mL) and filtered through Celite. The resulting brown solution was then concentrated and purified by column chromatography on silica, eluting with DCM:petrol 1:1. This yielded a yellow mobile band, isolation of which afforded the product [1,2-Ph_2-3,3-(^{t}BuNC)$_2$-3-PPh_3-*pseudocloso*-3,1,2-$RuC_2B_9H_9$] (**3**) as a yellow solid. Yield 0.062 g, 0.076 mmol, 34%. $C_{42}H_{52}B_9N_2PRu$ requires C 62.0, H 6.44, N 3.44; found C 62.5, H 5.94, N 2.73%. ^{1}H NMR; δ 7.41–7.35 (m, 10H, C_6H_5), 7.35–7.30 (m, 5H, C_6H_5), 7.23–7.18 (m, 10H, C_6H_5), 1.17 (br. s, 18H, CH_3). ^{1}H NMR (CD_2Cl_2, 203 K); δ 7.85–6.70 (br. hump with four groups of sharp multiplets superimposed, 15H, C_6H_5), 1.20 (s, 9H, CH_3), 1.09 (s, 9H, CH_3). ^{11}B{^{1}H} NMR; δ 23.6 (1B), 15.1 (1B), 12.7 (2B), 4.5 (2B), −0.6 (2B), −19.9 (1B). ^{31}P{^{1}H} NMR; δ 41.2 (s, PPh_3). EIMS; envelope centred

on *m/z* 814 (M^+).

3.1.3. [1,2-Ph_2-3,3-$(CO)_2$-3-PPh_3-*pseudocloso*-3,1,2-$RuC_2B_9H_9$] (**4**)

A THF (30 mL) solution of Li[**2b**] was prepared by deprotonation of compound **1b** (0.299 g, 0.316 mmol) as described above. This was frozen at −196 °C and to it was added Ag[BF_4] (0.074 g, 0.379 mmol). The Schlenk tube was then charged with an atmosphere of CO and allowed to warm to room temperature with stirring. Finally, CO gas was bubbled through the resultant solution for 16 h resulting in an opaque mustard-yellow solution. This was filtered through Celite, all volatiles removed under vacuum, the solids redissolved in DCM, and the solution filtered again. Preparative TLC eluting with DCM:petrol 1:1 revealed a yellow mobile band (R_f 0.80), isolation of which afforded [1,2-Ph_2-3,3-$(CO)_2$-3-PPh_3-*pseudocloso*-3,1,2-$RuC_2B_9H_9$] (**4**) as a bright-yellow solid. Yield 0.055 g, 0.078 mmol, 25%. $C_{34}H_{34}B_9O_2PRu$ requires C 58.0, H 4.87; $C_{34}H_{34}B_9O_2PRu\cdot C_4H_8O$ requires 58.8, 5.45; found C 57.8, H 5.41%. ATR-IR; ν_{max} 2534 (B-H), 2049 (C-O), 2002 (C-O) cm^{-1}. ^1H NMR δ 7.47–7.31 (m, 19H, C_6H_5), 7.21–7.11 (m, 6H, C_6H_5). $^1H\{^{11}B\}$ NMR δ 7.47–7.30 (m, 19H, C_6H_5), 7.23–7.12 (m, 6H, C_6H_5), 4,62 (br. s, 1H, B*H*), 3.04 and 3.01 (overlapping br. resonances, 2H, 1H, B*H*), 2.78 (br., 4H, B*H*), 2.15 (br. s, 1H, B*H*). $^{11}B\{^1H\}$ NMR; δ 17.8 (2B), 7.1 (2B), 3.7 (2B), 0.1 (2B), −18.0 (1B). $^{31}P\{^1H\}$ NMR; δ 38.8 (s, PPh_3). EIMS; envelopes centred on *m/z* 704 (M^+), 676 (M^+−CO), 648 (M^+−2CO).

3.1.4. [{1,2-Ph_2-*pseudocloso*-3,1,2-$RuC_2B_9H_9$}{1′,8′-Ph_2-*closo*-2′,1′,8′-$RuC_2B_9H_9$}] (**5**)

A THF (25 mL) solution of Li[**2b**] was prepared by deprotonation of compound **1b** (0.500 g, 0.528 mmol) as described above. After stirring for 0.5 h volatiles were removed under vacuum and the solids redissolved in DCM (20 mL), and this solution was transferred by cannula to a second Schlenk tube containing Ag[BF_4] (0.140 g, 0.719 mmol). Stirring for 0.5 h resulted in a dark-brown suspension subsequently filtered through Celite to afford a dark-brown solution. This was concentrated, applied to preparative TLC plates and eluted with DCM:petrol 1:1, revealing ca. ten mobile bands the most abundant of which (R_f 0.62) was collected. From this was isolated [{1,2-Ph_2-*pseudocloso*-3,1,2-$RuC_2B_9H_9$}{1′,8′-Ph_2-*closo*-2′,1′,8′-$RuC_2B_9H_9$}] (**5**) as an orange solid. Yield 0.025 g, 0.032 mmol, 6%. $C_{28}H_{38}B_{18}Ru_2$ requires C 43.6, H 4.97; found C 43.9, H 5.09%. ^1H NMR (CD_2Cl_2); δ 7.67–7.63 (m, 2H, C_6H_5), 7.53–7.43 (m, 4H, C_6H_5), 7.39–7.33 (m, 1H, C_6H_5), 7.28–7.22 (m, 3H, C_6H_5), 7.05 (d, 1H, C_6H_5), 6.98 (d, 1H, C_6H_5), 6.77 (t, 1H, C_6H_5), 6.43–6.34 (m, 2H C_6H_5), 6.21 (app. t, 1H, C_6H_5), 6.15 (d, 1H, C_6H_5), 5.87 (app. t, 1H, C_6H_5), 5.80 (app. t, 1H, C_6H_5), 5.06 (app. t, 1H, C_6H_5). $^{11}B\{^1H\}$ NMR (CD_2Cl_2); δ 29.4 (1B), 18.0 and 16.8 (overlapping resonances, 2B), 12.6 (1B), 3.0 to −6.4 (overlapping resonances with maxima at 0.8, −0.8, −3.0 and −4.5, 8B), −8.5 (2B), −14.8, −15.8 and −17.3 (overlapping resonances, 3B), −19.9 (1B). EIMS; envelope centred on *m/z* 771 (M^+).

3.2. Crystallography

Single crystals of **1b**, **3** and **5** were grown by diffusion of a DCM solution of the compound and petrol at −20 °C, whilst crystals of **4** were afforded by diffusion of a THF solution and petrol, also at −20 °C. Diffraction data were collected on a Rigaku Oxford Diffraction SuperNova diffractometer at 120 K (Cu-K_α *X*-radiation; compound **1b**), a Rigaku FR-E+ diffractometer at 100 K (Mo-K_α; **3**) or a Bruker ×8 APEXII diffractometer at 100 K (Mo-K_α; **4**, **5**) from crystals mounted in inert oil on a cryoloop and cooled in a stream of cold N_2. Using OLEX2 [17] structures were solved using the SHELXS [18] or SHELXT [19] programme and refined by full-matrix least-squares using SHELXL [18]. Compound **4** crystallises with one partially-disordered molecule of THF per molecule of metallacarborane, and **5** with one (also partially disordered) molecule of DCM per molecule of metallacarborane. For **1b** there is also disordered solvent in the lattice but since it proved impossible to model this satisfactorily the intensity contribution of the solvent was removed using the BYPASS procedure [20] implemented in OLEX2. The total electron count of the solvent was 163 e per unit cell (corresponding to four DCM molecules) located in two voids of ca. 477 $Å^3$ each. H atoms bound to cage B atoms were allowed to refine positionally whilst other H atoms were constrained to idealised geometries with C_{phenyl}–H 0.95 Å, C_{phenyl}–H (η-bound

Table 1
Crystallographic data.

	1b·CH_2Cl_2	3	4·C_4H_8O	5·CH_2Cl_2
Formula	$C_{50}H_{50}B_9ClP_2Ru\cdot CH_2Cl_2$	$C_{42}H_{52}B_9N_2PRu$	$C_{34}H_{34}B_9O_2PRu\cdot C_4H_8O$	$C_{28}H_{38}B_{18}Ru_2\cdot CH_2Cl_2$
M	1031.57	814.18	776.04	856.23
Crystal system	monoclinic	tetragonal	monoclinic	monoclinic
Space group	$P2_1/n$	$P4_1$	$P2_1/c$	$P2_1/n$
a/Å	11.7427(5)	11.41683(8)	15.0547(5)	14.1714(9)
b/Å	19.9771(9)	11.41683(8)	13.6097(5)	14.3879(10)
c/Å	22.2816(8)	31.9871(5)	18.2327(7)	18.3408(14)
α/°	90	90	90	90
β/°	90.735(4)	90	96.913(2)	104.213(4)
γ/°	90	90	90	90
U/$Å^3$	5226.5(4)	4169.32(9)	3708.5(2)	3625.2(4)
Z, *Z*′	4, 1	4, 1	4, 1	4, 1
F(000)/e	2112	1688	1592	1704
D_{calc}/Mg m^{-3}	1.311	1.297	1.390	1.569
X-radiation	Mo-K_α	Cu-K_α	Mo-K_α	Mo-K_α
λ/Å	0.71073	1.54178	0.71073	0.71073
μ/mm^{-1}	0.549	3.637	0.504	1.006
θ_{max}/°	29.75	68.23	32.05	28.59
Data measured	59685	19497	96122	67222
Unique data	13334	6614	12831	9460
R_{int}	0.0837	0.0505	0.0739	0.0866
R, wR_2 (obs. data)	0.0632, 0.1163	0.0382, 0.0918	0.0400, 0.0901	0.0397, 0.0833
S	1.060	1.024	1.037	1.053
Variables	598	529	506	519
E_{max}, E_{min}/e $Å^{-3}$	0.67, −0.52	0.71, −0.37	0.59, −0.77	0.71, −0.78
Flack parameter	–	−0.020(8)	–	–

to Ru) 1.00 Å, $C_{secondary}$–H 0.99 Å, $C_{primary}$–H 0.98 Å. All H displacement parameters were constrained to be 1.2 × U_{eq} (bound B or C) except Me H atoms 1.5 × U_{eq} (C_{methyl}). Table 1 contains further experimental details. Structures have been deposited with the Cambridge Crystallographic Data Centre, CCDC 1590018-1590021.

Acknowledgements

We thank the Leverhulme Trust for support of JJJ and APMR (project RPG-2014-286). We also thank Dr G.S. Nichol (University of Edinburgh) for data collection of compound **1b** and the UK National Crystallographic Service for data collection of compound **3**.

Appendix A. Supplementary data

Supplementary data related to this article can be found at https://doi.org/10.1016/j.jorganchem.2018.02.007.

References

[1] (a) K. Wade, J. Chem. Soc. D (1971) 792;
(b) D.M.P. Mingos, Nat. Phys. Sci. (Lond.) 236 (1972) 99.
[2] E.L. Hoel, C.E. Strouse, M.F. Hawthorne, Inorg. Chem. 13 (1974) 1388.
[3] K.P. Callahan, W.J. Evans, F.Y. Lo, C.E. Strouse, M.F. Hawthorne, J. Am. Chem. Soc. 97 (1975) 296.
[4] A.P.M. Robertson, N.A. Beattie, G. Scott, W.Y. Man, J.J. Jones, S.A. Macgregor, G.M. Rosair, A.J. Welch, Angew. Chem. Int. Ed. 55 (2016) 8706.
[5] A.P.M. Robertson, A. Reckziegel, J.J. Jones, G.M. Rosair, A.J. Welch, Eur. J. Inorg. Chem. 2017 (2017) 4581.
[6] (a) Z.G. Lewis, A.J. Welch, J. Organomet. Chem. 430 (1992) C45;
(b) P.T. Brain, M. Bühl, J. Cowie, Z.G. Lewis, A.J. Welch, J. Chem. Soc., Dalton Trans. (1996) 231;
(c) U. Grädler, A.S. Weller, A.J. Welch, D. Reed, J. Chem. Soc., Dalton Trans. (1996) 335;
(d) A.J. Welch, A.S. Weller, Inorg. Chem. 35 (1996) 4548;
(e) M.A. McWhannell, G.M. Rosair, A.J. Welch, F. Teixidor, C. Viñas, J. Organomet. Chem. 573 (1999) 165;
(f) D. Reed, A.J. Welch, J. Cowie, D.J. Donohoe, J.A. Parkinson, Inorg. Chim. Acta. 289 (1999) 125.
[7] A.Yu. Kostyukovich, D.I. D'yachihin, I.D. Grishin, I.A. Godovikov, A.F. Smol'yakov, F.M. Dolgushin, D.F. Grishin, I.T. Chizhevsky, E.V. Balagurova, Mendeleev Commun. 27 (2017) 392.
[8] I.T. Chizhevsky, I.A. Lobanova, V.I. Bregadze, P.V. Petrovskii, V.A. Antonovich, A.V. Polyakov, A.I. Yanovskii, Yu.T. Struchkov, Mendeleev Commun. 1 (1991) 47.
[9] J. Cowie, B.D. Reid, J.M.S. Watmough, A.J. Welch, J. Organomet. Chem. 481 (1994) 283.
[10] I.T. Chizhevsky, I.A. Lobanova, P.V. Petrovskii, V.I. Bregadze, F.M. Dolgushin, A.I. Yanovsky, Yu.T. Struchkov, A.L. Chistyakov, I.V. Stankevich, C.B. Knobler, M.F. Hawthorne, Organometallics 18 (1999) 726.
[11] (a) E.H.S. Wong, M.F. Hawthorne, Inorg. Chem. 17 (1978) 2863;
(b) A.R. Siedle, J. Organomet. Chem. 90 (1975) 249;
(c) S. Anderson, D.F. Mullica, E.L. Sappenfield, F.G.A. Stone, Organometallics 15 (1996) 1676;
(d) D.D. Ellis, S.M. Couchman, J.C. Jeffery, J.M. Malget, F.G.A. Stone, Inorg. Chem. 38 (1999) 2981;
(e) S. Du, D.D. Ellis, P.A. Jelliss, J.A. Kautz, J.M. Malget, F.G.A. Stone, Organometallics 19 (2000) 1983;
(f) D.I. D'yachikhin, F.M. Dolgushin, I.A. Godovikov, I.T. Chizhevsky, Mendeleev Commun. 20 (2010) 174;
(g) S.L. Powley, G.M. Rosair, A.J. Welch, Dalton Trans. 45 (2016) 11742.
[12] Comparison of <δ(^{11}B)> in pseudocloso metallacarboranes containing the {$Ph_2C_2B_9H_9$} ligand and directly analogous closo metallacarboranes containing the {$C_2B_9H_{11}$} ligand reveal values of ca. +5/+6 ppm in the former group and −10/−11 ppm in the latter. See, e.g., ref. [6b].
[13] A.J. Welch, Crystals 7 (2017) 234 and references therein.
[14] E.H.S. Wong, M.F. Hawthorne, J. Chem. Soc., Chem. Commun. (1976) 257.
[15] (a) G.K. Magomedov, A.S. Frenkel, V.N. Kalinin, L.I. Zakharkin, Izvestiya Akad. Nauk SSSR Seriya Khim. (1977) 949;
(b) L.I. Zakharkin, G.G. Zhigareva, Zh. Obshch. Khim. 53 (1983) 953;
(c) J.M. Russell, M. Sabat, R.N. Grimes, Organometallics 21 (2002) 4113;
(d) B.M. Ramachandran, S.M. Trupia, W.E. Geiger, P.J. Carroll, L.G. Sneddon, Organometallics 21 (2002) 5078;
(e) M.J. Ingleson, G. Kociok-Köhn, A.S. Weller, Inorg. Chim. Acta. 358 (2005) 1571;
(f) G.F. Jin, J.-H. Hwang, J.-D. Lee, K.-R. Wee, I.-H. Suh, S.O. Kang, Chem. Commun 49 (2013) 9398.
[16] (a) M. Bluhm, H. Pritzkow, W. Siebert, R.N. Grimes, Angew. Chem. Int. Ed. 39 (2000) 4562;
(b) L.S. Alekseev, F.M. Dolgushin, A.A. Korlyukov, I.A. Godovikov, E.V. Vorontsov, I.T. Chizhevsky, Organometallics 26 (2007) 3868.
[17] O.V. Dolomanov, L.J. Bourhis, R.J. Gildea, J.A.K. Howard, H. Puschmann, J. Appl. Crystallogr. 42 (2009) 339.
[18] G.M. Sheldrick, Acta Crystallogr. A64 (2008) 112.
[19] G.M. Sheldrick, Acta Crystallogr. A71 (2015) 3.
[20] (a) P. van der Sluis, A.L. Spek, Acta Crystallogr. A46 (1990) 194;
(b) A.L. Spek, J. Appl. Crystallogr. 36 (2003) 7.

ChemPubSoc Europe

DOI: 10.1002/ejic.201700492

EurJIC European Journal of Inorganic Chemistry

Full Paper

Molybdacarboranes

CLUSTER ISSUE

Balancing Steric and Electronic Effects in Carbonyl–Phosphine Molybdacarboranes

Alasdair P. M. Robertson,[a] Alexander Reckziegel,[a] John J. Jones,[a] Georgina M. Rosair,[a] and Alan J. Welch*[a]

Abstract: Analysis of the literature structures $[(CO)(PPh_3)_2MC_2B_9H_{11}]$ and $[(CO)_2(PPh_3)MC_2B_9H_{11}]$ suggests that in $[L_3MC_2B_9H_{11}]$ metallacarboranes the *trans* influence of CO is greater than that of PPh_3. Extending this study to the $[L_4MC_2B_9H_{11}]$ system the new molybdacarboranes [3,3,3-$(CO)_3$-3-PPh_3-3,1,2-*closo*-$MoC_2B_9H_{11}$] (**2**), [1,2-Me_2-3,3,3-$(CO)_3$-3-PPh_3-3,1,2-*closo*-$MoC_2B_9H_9$] (**3**) and *trans*-[3,3-$(CO)_2$-3,3-$(PPh_3)_2$-3,1,2-*closo*-$MoC_2B_9H_{11}$] (**4**) were prepared and fully characterised. Consideration of the exopolyhedral ligand orientations (ELO) in **2** confirms that, in terms of *trans* influence, CO > PPh_3 in $[L_4MC_2B_9H_{11}]$ also. The ELO is effectively reversed in **3** through intramolecular steric crowding between the cage CH_3 groups and the PPh_3 ligand. The dicarbonylbis(triphenylphosphine) compound **4** has effective C_s symmetry with one CO ligand *trans* and the other CO ligand *cis* to the cage C–C connectivity. Unexpectedly the Mo–CO bond lengths are equal. DFT calculations on **4** reproduce this unusual result, but suggest that in the less-crowded PH_3 analogue, the Mo–CO bond length *trans* to cage C would be about 0.2 Å shorter than that *trans* to cage B. To test this prediction, the analogous PEt_3 complex was prepared as *cis* and *trans* structural isomers **5** and **6**. The *cis* isomer **5** is quantitatively converted into the *trans* isomer **6** when heated to reflux in THF. In **6** the Mo–CO bond more *trans* to cage C is about 0.2 Å shorter than that which is more *trans* to cage B, in line with the DFT prediction.

Introduction

In the vast majority of metallacarboranes the carborane ligand face to which the metal is bonded contains either one or two carbon atoms, and we have had a long-standing interest in the consequences of this on the bonding of the exopolyhedral ligands. Briefly, in a carborane ligand the frontier molecular orbitals of the carborane are localised on the boron atoms in the open face,[1] causing the cage carbon to have a weaker *trans* influence than the cage boron. In bis(phosphine) metallacarboranes this results in longer M–P distances *trans* to boron[2] and in [3,3,3-$(CO)_3$-3,1,2-*closo*-$MC_2B_9H_{11}$] metallacarboranes to longer M–CO distances *trans* to boron (see Table 2 of ref.[3]). The effects are also visible in metallacarboranes with a heterogeneous exopolyhedral ligand set. Here the preferred molecular conformation will be that in which the exopolyhedral ligand with the stronger or strongest *trans* influence will tend to lie opposite the cage carbon atom(s), exopolyhedral ligands of weak *trans* influence tending to lie opposite the cage boron atoms. We have previously named this phenomenon exopolyhedral ligand orientation (ELO).[4] Amongst many examples of ELO are the preferred *cisoid* conformations in indenyl and naphthalene metallacarboranes[5] and the motivation to redetermine the structure of [3,3-(κ^2-NO_2)-3-PPh_3-3,1,2-*closo*-$RhC_2B_9H_{11}$].[4]

The origin of a preferred ELO is electronic, and hence the interpretation of a molecular structure in terms of ELO assumes no significant competing steric effects. For this reason ELO analysis is best done by using carborane ligands with only H substituents, for example $[L_xMC_2B_9H_{11}]$ species. In this paper we explore, through ELO considerations, the relative *trans* influences of CO and PPh_3, initially by analysis of $[(CO)_2(Ph_3P)MC_2B_9H_{11}]$ and $[(CO)(Ph_3P)_2MC_2B_9H_{11}]$ and related structures in the literature, and then by the synthesis and structural characterisation of $[(CO)_3(Ph_3P)MoC_2B_9]$ and $[(CO)_2(Ph_3P)_2MoC_2B_9]$ species, the former both with and without methyl substituents on the cage C atoms. Unexpected equal Mo–CO distances in *trans*-[3,3-$(CO)_2$-3,3-$(PPh_3)_2$-3,1,2-*closo*-$MoC_2B_9H_{11}$] prompted us to study this species by DFT calculation, as a consequence of which we also prepared and studied the analogous PEt_3 complex, which was isolated in two isomeric forms.

Results and Discussion

CO and PPh_3 are two of the most common exopolyhedral ligands encountered in metallacarborane chemistry, and it is of interest to use ELO considerations to probe their relative *trans* influences (alternatively known as structural *trans* effects). Coe and Glenwright classify both CO and PPh_3 as "moderate *trans* influence ligands"[6] but go on to point out that analysis of the structures of $[M(CO)_5PPh_3]$ for relatively electron-rich metals (M = Cr,[7] Mo,[8] W,[9] and V[10]) suggests that, in terms of *trans*

[a] *Institute of Chemical Sciences, Heriot-Watt University, Edinburgh, EH14 4AS, UK*
E-mail: a.j.welch@hw.ac.uk
http://heteroborane.eps.hw.ac.uk

Supporting information and ORCID(s) from the author(s) for this article are available on the WWW under https://doi.org/10.1002/ejic.201700492.

influence, CO > PPh_3 since in all cases the M–CO distance *trans* to PPh_3 is shorter than those *cis* to PPh_3 (interestingly, for the relatively electron-poor metal Tc^+ there is no significant difference between the M–CO distances,[11] perhaps indicating the importance of π back-bonding on *trans* influence). On the other hand, See and Kozina conclude, from analysis of square-planar d^8 and low-spin octahedral d^6 complexes, that the relative *trans* influence is CO < PPh_3.[12]

The relative *trans* influences of CO and PPh_3 in metallacarboranes can be assessed by considering exopolyhedral ligand orientations (ELOs) of structurally characterised literature compounds. When the search is restricted to only {3,1,2-*closo*-$MC_2B_9H_{11}$} fragments to minimise the possible influence of intramolecular steric crowding on conformation, there is only one $[(CO)(PPh_3)_2MC_2B_9H_{11}]$ species, [3-CO-3,3-$(PPh_3)_2$-3,1,2-*closo*-$RuC_2B_9H_{11}$] (*BIHQUE*),[13] and one $[(CO)_2(PPh_3)MC_2B_9H_{11}]$ species, [3,3-$(CO)_2$-3-PPh_3-3,1,2-*closo*-$FeC_2B_9H_{11}$] (*KISBIX*),[14] in the Cambridge Structural Database (CSD).[15] Key ELO data for these, together with those of the closely related species [3-μ-$(PPh_2CH_2PPh_2)$-{3,3-$(CO)_2$-3,1,2-*closo*-$RuC_2B_9H_{11}$}$_2$] (*HIZQUC*),[16] are presented in Tables 1 and 2.

Table 1. ELO data for [3-(CO)-3,3-$(PPh_3)_2$-3,1,2-*closo*-$RuC_2B_9H_{11}$] (°, Å).

CSD code	M	θ_{CO}	θ_P, M–P	θ_P, M–P
BIHQUE	Ru	**131.52(16)**	–118.33(13), 2.3873(7)	*15.50(15)*, 2.4021(7)

Table 2. ELO data for $[(CO)_2(P)MC_2B_9H_{11}]$ compounds (°, Å).

CSD code	M	θ_{CO}, M–CO	θ_{CO}, M–CO	θ_P
KISBIX	Fe	**–133.5(6)**, **1.762(13)**	113.1(6), 1.754(13)	*–12.8(6)*
HIZQUC	Ru	**–130.2(4)**, **1.881(7)**	114.3(4), 1.886(8)	*–11.5(4)*
		127.4(3), **1.886(7)**	–113.6(4), 1.889(6)	*8.5(3)*

Initially, the published cage C atom positions in each database structure were checked by the vertex-to-centroid distance (VCD) method,[4] and they were found to be correct in all three cases. Then, for each ligand, the parameter θ, which defines the ligand orientation, was calculated as described in Figure 1. In essence, ligands with high $|\theta|$ lie *trans* to the cage C atoms whilst ligands with low $|\theta|$ lie *trans* to cage B. In all cases one ligand (bold) lies at a $|\theta|$ value of about 125–135°, one lies at about 110–120° and the remaining ligand (italics) lies at about 5–15°. For *BIHQUE* the unique CO ligand lies at highest $|\theta|$; this confirms that, of the three ligands present, it has the greatest *trans* influence. The two PPh_3 ligands have quite different θ values; that at intermediate $|\theta|$ (less *trans* to B) has a significantly shorter Ru–P bond than that at low $|\theta|$ (more *trans* to B), as expected. In *KISBIX* one of the two CO ligands is at highest $|\theta|$, the other is intermediate, and the unique PPh_3 ligand resides at lowest $|\theta|$, and the same pattern is seen in both crystallographically independent cages in the related species *HIZQUC*. Unfortunately the crystallographic study of neither *KISBIX* nor *HIZQUC* is sufficiently precise for statistically significant differences in the M–CO distances to be observed. Nevertheless, these data strongly indicate that in mixed CO/PPh_3 compounds containing the {3,1,2-*closo*-$MC_2B_9H_{11}$} fragment the *trans* influence of CO is greater than that of PPh_3.

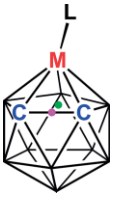

Figure 1. The ELO of ligand L is described by the torsion angle θ, where θ = L–M–*A*–*B*, *A* is the centroid of the metal-bound C_2B_3 face (green dot) and *B* is the centroid of the C–C connectivity (purple dot).

In comparison to the number of known $[L_3MC_2B_9H_{11}]$ species (L = same or different ligands) there are relatively few $[L_4MC_2B_9H_{11}]$ compounds,[17] and atomic coordinates for only four such species could be found in the CSD. Note that an $\{ML_2L'_2\}$ or $\{ML_2L'L''\}$ fragment introduces the possibility of "*cis*" or "*trans*" configurations of the L ligands.

ELO data for *cis*-[3,3-$(CO)_2$-3,3-$(Cl)_2$-3,1,2-*closo*-$ReC_2B_9H_{11}]^-$ (*FINWIJ*),[18] *cis*-[3,3-$(CO)_2$-3,3-$(SPh)_2$-3,1,2-*closo*-$MoC_2B_9H_{11}]^{2-}$ (*TOJREP*),[19] *trans*-[3,3-$(PPh_3)_2$-3-H-3-Cl-3,1,2-*closo*-$OsC_2B_9H_{11}$] (*TEXYUQ*),[20] and *trans*-[3,3-$(PPh_3)_2$-3-H-3-Cl-3,1,2-*closo*-$RuC_2B_9H_{11}$] (*QEXWAS*)[21] are presented in Table 3. The data for *FINWIJ* and *TOJREP* clearly demonstrate that CO has a stronger *trans* influence than the ligands Cl and SPh, respectively, since the *cis*-CO ligands adopt positions defined by high $|\theta|$ values. In *TEXYOQ* and its analogue *QEXWAS* the $|\theta|$ values clearly indicate that H has the strongest, and Cl the weakest, *trans* influence of the three types of ligand present (H, Cl, PPh_3), as fully expected.[6]

Having established that in $[L_3MC_2B_9H_{11}]$ species the *trans* influence of CO is greater than that of PPh_3 it was of interest to determine the relative *trans* influences of these ligands in the relatively unexplored class of $[L_4MC_2B_9H_{11}]$ compounds. We therefore targeted complexes [3,3,3-$(CO)_3$-3-PPh_3-3,1,2-*closo*-$MoC_2B_9H_{11}$] and [3,3-$(CO)_2$-3,3-$(PPh_3)_2$-3,1,2-*closo*-$MoC_2B_9H_{11}$] (the latter as either or both the *cis*- and *trans*-isomers) for synthesis and structural study. Although these specific compounds were previously unknown, the related cage-C-methylated analogues [1,2-Me_2-3,3,3-$(CO)_3$-3-PPh_3-3,1,2-*closo*-$MoC_2B_9H_9$] (**I**) and [1,2-Me_2-3,3-$(CO)_2$-3,3-$(PPh_3)_2$-3,1,2-*closo*-$MoC_2B_9H_9$] (**II**) were reported by Stone et al. in 1993.[22] Interestingly, both **I**

Table 3. ELO data for $[L_2L'_2MC_2B_9H_{11}]$ and $[L_2L'L''MC_2B_9H_{11}]$ species.

CSD code	M	θ values (°)			
FINWIJ	Re^-	θ_{CO} 133.4(4)	θ_{CO} –137.1(4)	θ_{Cl} 43.7(3)	θ_{Cl} –48.1(3)
TOJREP	Mo^{2-}	θ_{CO} 133.5(6)	θ_{CO} –141.0(7)	θ_{SPh} 32.3(4)	θ_{SPh} –49.6(5)
TEXYUQ	Os	θ_H 165.9(17)	θ_{Cl} –13.41(18)	θ_P 88.3(2)	θ_P –115.5(18)
QEXWAS	Ru	θ_H 166.9(11)	θ_{Cl} –13.62(11)	θ_P 91.93(10)	θ_P –122.26(0)

and **II** are afforded by the protonation of [PNP][1,2-Me_2-3,3-$(CO)_2$-3-(η-C_3H_5)-3,1,2-*closo*-$MoC_2B_9H_9$] {PNP = $[N(PPh_3)_2]^+$} in the presence of excess PPh_3. Whilst the formation of **II** simply represents replacement of the 4-e-donor $[C_3H_5]^-$ ligand by two PPh_3 ligands, the co-formation of **I** can only be explained by "CO-stealing" by an electron-deficient [1,2-Me_2-3,3-$(CO)_2$-3-PPh_3-3,1,2-*hypercloso*-$MoC_2B_9H_9$] species. CO-stealing must also occur in the decomposition of [1,2-Me_2-3-CO-3-PPh_3-3-(η-PhC_2Ph)-3,1,2-*closo*-$MoC_2B_9H_9$] to give **I** amongst a mixture of products, although interestingly the non-cage-C-methylated analogue, [3-CO-3-PPh_3-3-(η-PhC_2Ph)-3,1,2-*closo*-$MoC_2B_9H_{11}$], is reported as stable towards decomposition under the same conditions.[23]

Treatment of an equimolar mixture of [PNP][3,3-$(CO)_2$-3-(η-C_3H_5)-3,1,2-*closo*-$MoC_2B_9H_{11}$] (**1**, prepared analogously to the $[NEt_4]^+$ salt[22]) and PPh_3 in CH_2Cl_2 (DCM) with one equivalent of HBF_4•OEt_2 afforded moderate yields of the carbonyl–phosphine molybdacarboranes [3,3,3-$(CO)_3$-3-PPh_3-3,1,2-*closo*-$MoC_2B_9H_{11}$] (**2**, 27 %) and *trans*-[3,3-$(CO)_2$-3,3-$(PPh_3)_2$-3,1,2-*closo*-$MoC_2B_9H_{11}$] (**4**, 26 %) following work-up involving column chromatography on silica. Compound **4** is formed in much improved yield (65 %) if three equivalents of PPh_3 are used. The cage-C-methylated analogue of **2**, [1,2-Me_2-3,3,3-$(CO)_3$-3-PPh_3-3,1,2-*closo*-$MoC_2B_9H_9$] (**3**), was also prepared, again in modest yield (29 %), by protonation of [PNP][1,2-Me_2-3,3-$(CO)_2$-3-(η-C_3H_5)-3,1,2-*closo*-$MoC_2B_9H_9$] in the presence of one equivalent of PPh_3. Clearly the isolation of the tricarbonyl species **2** and **3** from dicarbonyl precursors represents further evidence of carbonyl-stealing, the driving force for which is presumably the formation of 12-vertex, 13-skeletal electron pair *closo* species in accord with polyhedral skeletal electron pair theory.[24]

Compounds **2**, **3** and **4** were all isolated as moderately air-sensitive yellow/orange solids and were initially characterised by elemental analysis (except for **2** which proved to be too unstable for reliable results) and multinuclear NMR spectroscopy (NMR spectra of all new compounds reported in this paper are available as Supporting Information). All three compounds have time-averaged C_s molecular symmetry in solution at room temperature. In the case of **2** this is evident from the $^{11}B\{^1H\}$ NMR spectrum, showing a 2:2:2:2:1 pattern from high to low frequency (one resonance of integral 2 must be a 1+1 co-incidence), for **3** it is clear from the observation of only one resonance for the CH_3 protons, and for **4** it is apparent from both the 1:1:2:2:2:1 pattern in the $^{11}B\{^1H\}$ NMR spectrum and the presence of equivalent PPh_3 ligands in the $^{31}P\{^1H\}$ NMR spectrum.

Compounds **2**, **3** and **4** were also studied crystallographically. A perspective view of a single molecule of **2** is shown in Figure 2. Table 4 hosts relevant ELO data, and Figure 8 provides a pictorial view of the orientation of the exopolyhedral ligands. One carbonyl ligand, C33O33, has the greatest $|\theta|$ and P1 the smallest $|\theta|$, as might have been anticipated from the established relative *trans* influences of CO and PPh_3 in [$L_3MC_2B_9H_{11}$] species. Moreover, the Mo–C33 bond length is significantly the

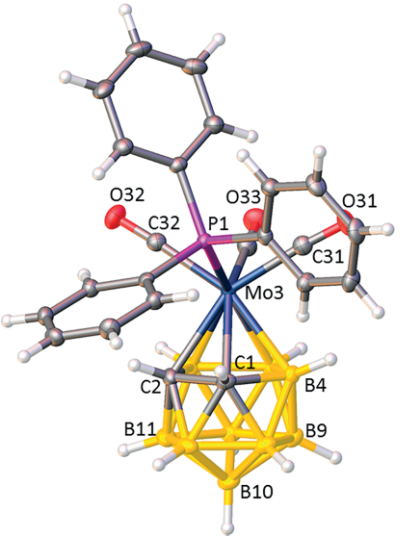

Figure 2. Molecular structure of **2** with thermal ellipsoids drawn at the 50 % probability level except for H atoms. Selected interatomic distances (Å): Mo–C1 2.3684(16), Mo–C2 2.3508(17), Mo–B7 2.3709(19), Mo–B8 2.3962(19), Mo–B4 2.4013(19), Mo–C31 2.0108(18), Mo–C32 2.0049(18), Mo–C33 1.9877(19), Mo–P1 2.5601(4), C31–O31 1.139(2), C32–O32 1.144(2), C33–O33 1.144(2), C1–C2 1.601(2).

Table 4. ELO and bond length data for compounds **2**–**6** (°, Å).

	2	**3**	**4**	**5**	**6**
θ_{C31O31}	117.25(12)	–80.7(3)	179.26(10)	139.65(4)	143.87(7)
Mo–C31	2.0108(18)	2.023(5)	1.9728(17)	1.9605(8)	1.9805(13)
C31–O31	1.139(2)	1.132(6)	1.152(2)	1.1587(10)	1.1697(15)
θ_{C32O32}	–69.49(13)	99.1(3)	–0.04(12)	–138.12(4)	–39.33(8)
Mo–C32	2.0049(18)	2.003(4)	1.9725(16)	1.9643(8)	1.9977(13)
C32–O32	1.144(2)	1.134(5)	1.156(2)	1.1611(10)	1.1694(16)
θ_{C33O33}	–155.21(11)	9.5(3)			
Mo–C33	1.9877(19)	2.000(6)			
C33–O33	1.144(2)	1.145(6)			
θ_{P1}	25.03(11)	–170.85(18)	88.64(9)	52.26(4)	52.34(6)
Mo–P1	2.5601(4)	2.5309(14)	2.5301(5)	2.5675(2)	2.5417(4)
θ_{P2}			–91.70(9)	–49.67(4)	–124.79(6)
Mo–P2			2.5267(5)	2.5743(2)	2.5190(4)

shortest of the three Mo–CO distances, as expected for the carbonyl ligand "most *trans*" to cage C. In compound **3** (Figure 3) the ELO is completely different, the $\{(CO)_3PPh_3\}$ unit having been effectively rotated approximately 180° about the metal–carborane axis such that the P1 is now *trans* to cage C. Since it now lies *trans* to cage carbon, which has a weaker *trans* influence than cage boron, the Mo–P distance in **3** is significantly shorter than that in **2**, 2.5309(14) vs. 2.5601(4) Å. Presumably, steric crowding between the PPh_3 ligand and the upward pointing methyl groups on the cage C atoms is responsible for the observed ELO in **3**, emphasising that it is necessary to use only unsubstituted (other than H) carborane ligands (or those substituted only on atoms not directly connected to the metal atom) when interpreting metallacarborane structures in terms of a preferred ELO.

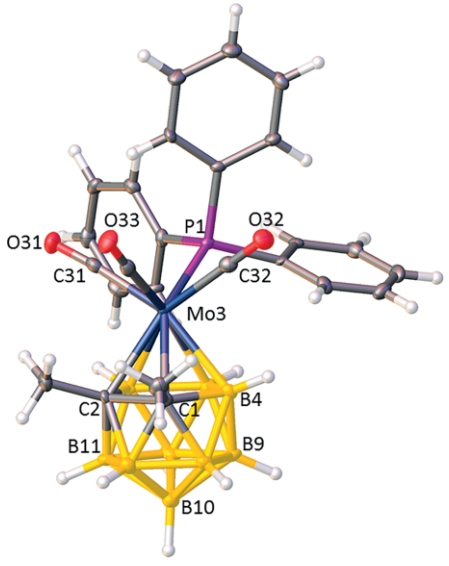

Figure 3. Molecular structure of **3** with thermal ellipsoids as in Figure 2. Selected interatomic distances (Å): Mo–C1 2.386(5), Mo–C2 2.375(5), Mo–B7 2.369(5), Mo–B8 2.390(6), Mo–B4 2.374(6), Mo–C31 2.023(5), Mo–C32 2.003(4), Mo–C33 2.000(6), Mo–P1 2.5309(14), C31–O31 1.132(6), C32–O32 1.134(5), C33–O33 1.145(6), C1–C2 1.668(7), C1–C11 1.516(7), C2–C21 1.523(7).

The dicarbonylbis(triphenylphosphine) species **4** is only afforded as the *trans*-isomer – presumably the *cis*-isomer would be too sterically crowded. As shown in Figures 4 and 8 the $\{(CO)_2P_2MoC_2B_9H_{11}\}$ fragment of the molecule has almost exact C_s symmetry in the solid state about a plane passing through the CO ligands and Mo3. Thus the two PPh_3 ligands have θ values which are effectively equal but opposite in sign, and effectively equivalent Mo–P bond lengths. The two CO ligands lie on the molecular mirror plane, one *trans* to the cage C–C connectivity and the other *trans* to B8. With only two as opposed to three carbonyl ligands, it is not surprising that there is greater individual Mo–CO π back-bonding in **4**, as evidenced by the significantly shorter and longer Mo–CO and C–O distances in **4**, respectively, than those in **2** and **3**. What is surprising, however, is the apparent equivalence of the carbonyl ligands in **4**. In spite of the fact that C31O31 lies *trans* to cage C and C32O32 lies *trans* to cage B, the Mo–CO distances (and the C–O distances) are exactly the same. To understand this unusual result, compound **4** has been studied by DFT calculations.[25]

Optimisation of the full molecule, starting from the crystallographic model, resulted in no significant change in the structure and afforded only slightly different Mo–CO distances, Mo–C31 1.969 Å, Mo–C32 1.980 Å. However, following replacement of PPh_3 by the smaller, less electron-withdrawing analogue PH_3, re-optimisation resulted in a much greater difference in Mo–CO lengths, Mo–C31 1.975 Å, Mo–C32 1.997 Å. This perhaps suggests that the unexpected equivalence of the Mo–CO lengths in the crystallographic study of **4** might at least in part be a consequence of intramolecular steric crowding. Figure 5 is a space-filling representation of the structure of **4** looking towards (left) C32O32 and (right) C31O31, and shows that each carbonyl ligand appears to be tightly surrounded by four adjacent Ph groups.

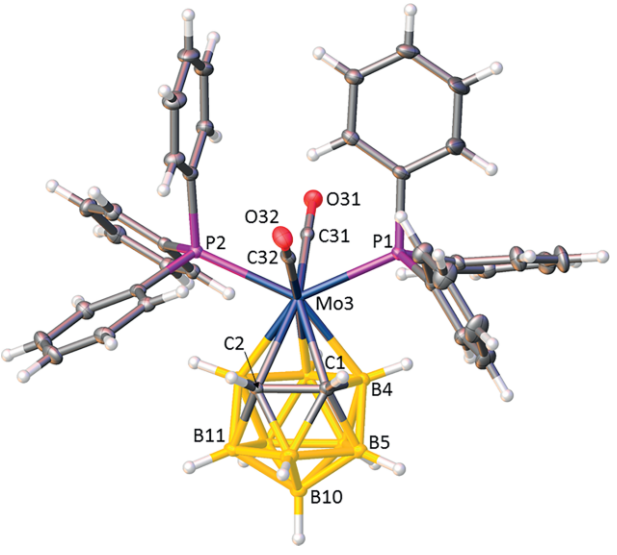

Figure 4. Molecular structure of **4** with thermal ellipsoids as in Figure 2. Selected interatomic distances (Å): Mo–C1 2.3701(17), Mo–C2 2.3743(16), Mo–B7 2.4065(18), Mo–B8 2.4690(18), Mo–B4 2.3932(19), Mo–C31 1.9728(17), Mo–C32 1.9725(16), Mo–P1 2.5301(5), Mo–P2 2.5267(5), C31–O31 1.152(2), C32–O32 1.156(2), C1–C2 1.588(2).

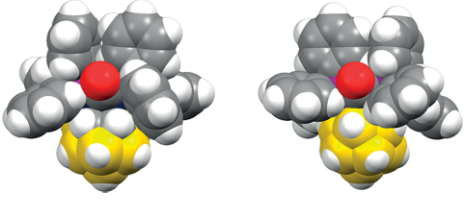

Figure 5. Space-filling representations of compound **4** looking (left) towards C32O32 and (right) towards C31O31.

This prompted us to target less-crowded analogues of **4**. Treatment of **1** with one equivalent of $HBF_4{\cdot}OEt_2$ at –78 °C followed by addition of three equivalents of PEt_3 afforded, following work-up involving column chromatography, both *cis*-[3,3-$(CO)_2$-3,3-$(PEt_3)_2$-3,1,2-*closo*-$MoC_2B_9H_{11}$] (**5**, 23 %) and *trans*-[3,3-$(CO)_2$-3,3-$(PEt_3)_2$-3,1,2-*closo*-$MoC_2B_9H_{11}$] (**6**, 6 %) as yellow/orange and bright yellow, slightly air-sensitive solids, respectively. We assume that, in contrast to the analogous reaction with PPh_3, the *cis*-isomer is accessible because of reduced steric crowding. In further contrast to the PPh_3 reaction, there was no evidence of the formation of a tricarbonyl monophosphine

derivative. Although the *trans*-isomer **6** is afforded as only a minor product, substantial amounts of **6** are easily prepared by the clean, quantitative conversion of *cis*-**5** to *trans*-**6** in refluxing THF.

Compounds **5** and **6** were initially characterised by elemental analysis (satisfactory in both cases) and multinuclear NMR spectroscopy. The ^{1}H NMR spectra of the two isomers differ mainly with respect to the resonances assigned to the ethyl protons, these appearing as three multiplets (6 H, -CH_2-; 6 H, -CH_2-; 18 H, -CH_3) for **5** and two apparent quintets (12 H, -CH_2-; 18 H, -CH_3) for **6**. The ^{11}B spectra of the isomers are fairly similar, both having a 1:1:2:2:2:1 integral pattern of resonances between about –2 and +20 ppm, although with individual resonances at measurably different chemical shifts. The greatest difference, not surprisingly, is seen in the $^{31}P\{^{1}H\}$ spectra, with singlet resonances at about 22 ppm for the *cis*-isomer and about 40 ppm for the *trans*-isomer.

Compounds **5** and **6** were also studied crystallographically (Figures 6 and 7). A perspective view of a single molecule of **5** is given in Figure 7, and the orientation of the metal–ligand set with respect to the carborane face is shown in Figure 8. The *cis*-isomer **5** has effective C_s symmetry with the carbonyl and phosphine ligands related pairwise across the effective mirror plane. Consequently, in terms of ELO the θ values for the CO ligands are essentially equal but opposite in sign, as are the θ values for the PEt_3 ligands. Moreover, the Mo–CO bond lengths are barely statistically different, and this is equally true of the Mo–P bond lengths [the small variations in distance reflect the high precision (low e.s.d. values) of the determination rather than chemically meaningful differences].

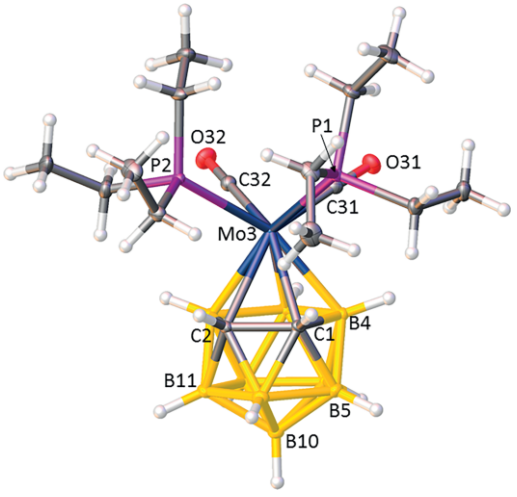

Figure 6. Molecular structure of **5** with thermal ellipsoids as in Figure 2. Selected interatomic distances (Å): Mo–C1 2.4148(7), Mo–C2 2.4162(8), Mo–B7 2.3900(9), Mo–B8 2.3864(9), Mo–B4 2.3792(9), Mo–C31 1.9605(8), Mo–C32 1.9643(8), Mo–P1 2.5675(2), Mo–P2 2.5743(2), C31–O31 1.1587(10), C32–O32 1.1611(10), C1–C2 1.5971(11).

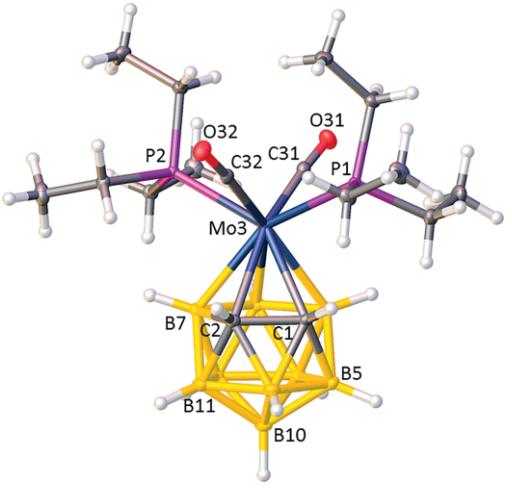

Figure 7. Molecular structure of **6** with thermal ellipsoids as in Figure 2. Selected interatomic distances (Å): Mo–C1 2.3930(13), Mo–C2 2.4309(13), Mo–B7 2.4305(16), Mo–B8 2.4467(15), Mo–B4 2.4176(16), Mo–C31 1.9805(13), Mo–C32 1.9977(13), Mo–P1 2.5417(4), Mo–P2 2.5190(4), C31–O31 1.1697(15), C32–O32 1.1694(16), C1–C2 1.6101(19).

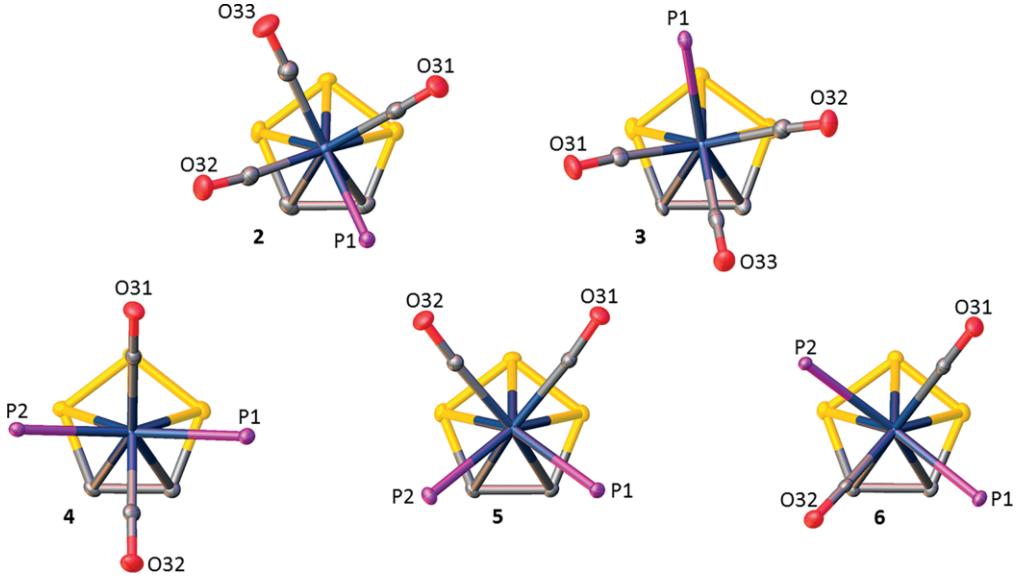

Figure 8. The orientations of the {$Mo(CO)_3P$} and {$Mo(CO)_2P_2$} fragments of compounds **2**–**6** projected onto the C_2B_3 carborane ligand faces.

The *trans*-isomer **6** is shown in Figure 7, and in this structure the two carbonyl ligands and the two phosphine ligands are distinct. C31O31 lies at high $|\theta|$, being sited nearly opposite C2, whereas C32O32 has a relatively low $|\theta|$, lying *trans* to a B–B connectivity. Consequently the Mo–CO bond lengths are quite different, Mo–C31 being the shorter by about 0.02 Å. Recall that a difference in Mo–CO bond lengths of this magnitude (again Mo–C31 being the shorter) was predicted by the DFT calculation on *trans*-[3,3-$(CO)_2$-3,3-$(PH_3)_2$-3,1,2-*closo*-$MoC_2B_9H_{11}$]. A similar difference (for the same reasons) exists between the two Mo–P bond lengths; P2 lies at high $|\theta|$ and is about 0.02 Å closer to Mo than P1, which lies at low $|\theta|$.

Conclusions

Analysis of literature structures suggests that in mixed CO/PPh_3 metallacarboranes the *trans* influence of CO is greater than that of PPh_3, and this is generally confirmed by consideration of the exopolyhedral ligand orientations (ELOs) in new carbonyl–phosphine molybdacarboranes. However, intramolecular steric crowding can compromise these orientations (noted in comparison of the structures of **2** and **3**) or can lead to unexpected bond lengths within the metal–ligand fragment (comparison of the structures of **4** and **6**).

Experimental Section

Materials and General Procedures: All experiments were performed, unless otherwise stated, under an atmosphere of nitrogen using standard Schlenk techniques, with subsequent manipulations and purifications carried out in air. Tetrahydrofuran (THF) was distilled from sodium/benzophenone, petroleum ether (40–60 °C, petrol) from sodium, with DCM and MeCN were distilled from CaH_2. All solvents were freeze-pump-thawed three times prior to use. $CDCl_3$ and CD_2Cl_2 were dried with 4 Å molecular sieves. Column chromatography was conducted on 60 Å silica supplied by Fisher and used as received. 1,2-*closo*-$C_2B_{10}H_{12}$ was purchased from Katchem Ltd. and $Mo(CO)_6$ from Fluorochem, and both were used without further purification. All other reagents were purchased from Sigma Aldrich Ltd. and also used without further purification. [1,2-Me_2-1,2-*closo*-$C_2B_{10}H_{10}$],[26] [$HNMe_3$][7,8-R_2-7,8-*nido*-$C_2B_9H_{10}$] (R = H or Me),[27] [$Mo(CO)_2(\eta$-$C_3H_5)(MeCN)_2Br$][28] and [PNP][1,2-Me_2-3,3-$(CO)_2$-3-(η-C_3H_5)-3,1,2-*closo*-$MoC_2B_9H_9$][22] were prepared by literature methods. NMR spectra were recorded with a Bruker DPX-400 spectrometer; chemical shifts are reported relative to residual protonated solvent peaks (^1H, ^{13}C), or to external standards (^{11}B: BF_3•OEt_2, ^{31}P: H_3PO_4). All spectra were recorded at 298 K and are provided as Figures S1–S29 in the Supporting Information. Elemental analyses (EA) were carried out with an Exeter CE-440 elemental analyser.

[PNP][3,3-$(CO)_2$-3-(η-C_3H_5)-3,1,2-*closo*-$MoC_2B_9H_{11}$] (1): The synthesis of this salt is closely related to that of the analogous $[NEt_4]^+$ salt reported by Stone et al.[22] Thus, to a solution of [$HNMe_3$][7,8-*nido*-$C_2B_9H_{12}$] (0.75 g, 3.86 mmol) in THF (18 mL) at –78 °C was added a solution of *n*BuLi in hexanes (2.5 M, 3.10 mL, 7.72 mmol), and the resulting mixture was warmed to ambient temperature and stirred for 1 h. The mixture was then frozen in liquid N_2, and solid [$Mo(CO)_2(\eta$-$C_3H_5)(MeCN)_2Br$] (1.38 g, 3.86 mmol) was added before warming to ambient temperature and stirring for a further 30 min. The mixture was re-frozen, and solid [PNP][Cl] (2.22 g, 3.86 mmol) was added before warming once again to ambient temperature and stirring for a further 30 min. All volatiles were then removed under high vacuum to yield a dark yellow/brown solid, which were purified by cold column chromatography (MeCN/dry ice jacket), to furnish the product [PNP][3,3-$(CO)_2$-3-(η-C_3H_5)-3,1,2-*closo*-$MoC_2B_9H_{11}$] (**1**) as a bright-yellow solid, which slowly decomposes in air. Yield: 1.86 g, 56 %.[29] ^1H NMR (400 MHz, CD_2Cl_2): δ_H = 7.70–7.63 (m, 6 H, Ph), 7.55–7.44 (m, 24 H, Ph), 3.32 (tt, J_{HH} = 10.7, J_{HH} = 7.1 Hz, 1 H, CH_2CHCH_2), 2.92 (d, J_{HH} = 7.1 Hz, 2 H, CH_2CHCH_2), 1.83 (s, 2 H, CH), 1.10 (d, J_{HH} = 10.7 Hz, 2 H, CH_2CHCH_2) ppm. $^1H\{^{11}B\}$ NMR (400 MHz, CD_2Cl_2): δ_H = 7.70–7.63 (m, 6 H, Ph), 7.55–7.44 (m, 24 H, Ph), 3.32 [tt (unresolved), 1 H, CH_2CHCH_2], 2.92 (d, J_{HH} = 7.1 Hz, 2 H, CH_2CHCH_2), 2.27 (s, 1 H, BH), 2.09 (s, 1 H, BH), 1.88 (v. br. s, 1 H, BH), 1.83 (s, 2 H, CH), 1.64 (s, 2 H, BH), 1.34 (s, 4 H, BH), 1.10 (d, J_{HH} = 10.7 Hz, 2 H, CH_2CHCH_2) ppm. $^{11}B\{^1H\}$ NMR (128 MHz, CD_2Cl_2): δ_B = –4.2 (s, 1 B), –7.3 (s, 2 B), –12.2 (s, 1 B), –13.9 (s, 2 B), –19.3 (s, 3 B) ppm. ^{11}B NMR (128 MHz, CD_2Cl_2): δ_B = –4.2 (1B, d, $^1J_{BH}$ = 131 Hz), –7.3 (d, $^1J_{BH}$ = 136 Hz, 2 B), –12.2, (d, 1 B , unresolved due to overlap with peak at –13.9 ppm), –13.9 (d, $^1J_{BH}$ = 141 Hz, 2 B), –19.3 (d, $^1J_{BH}$ = 150 Hz, 3 B) ppm.

[3,3,3-$(CO)_3$-3-PPh_3-3,1,2-*closo*-$MoC_2B_9H_{11}$] (2): To a solution of **1** (0.50 g, 0.58 mmol)[29] and PPh_3 (152 mg, 0.58 mmol) in DCM (20 mL) at 0 °C was added neat HBF_4•OEt_2 (0.08 mL, 0.58 mmol), producing a dark red-brown solution. The mixture was then warmed to ambient temperature and stirred for 1 h before removing all volatiles under high vacuum. The resulting brown solids were eluted with DCM/petroleum ether (30:70) on a silica column, two well-separated yellow/orange bands moving down the column. The higher R_f band was collected and identified as [3,3,3-$(CO)_3$-3-PPh_3-3,1,2-*closo*-$MoC_2B_9H_{11}$] (**2**), isolated as a moderately air-sensitive yellow/orange solid. Yield: 92 mg, 27 %. ^1H NMR (400 MHz, CD_2Cl_2): δ_H = 7.62–7.56 (m, 3 H, Ph), 7.54–7.48 (m, 6 H, Ph), 7.33–7.24 (m, 6 H, Ph), 2.53 (s, 2 H, CH) ppm. $^1H\{^{11}B\}$ NMR (400 MHz, CD_2Cl_2): δ_H = 7.62–7.56 (m, 3 H, Ph), 7.54–7.48 (m, 6 H, Ph), 7.33–7.24 (m, 6 H, Ph), 3.09 (s, 1 H, BH), 2.53 (s, 2 H, CH), 2.18 (s, 1 H, BH), 2.13 (s, 2 H, BH), 1.77 (s, 3 H, BH), 1.67 (s, 2 H, BH) ppm. $^{11}B\{^1H\}$ NMR (128 MHz, CD_2Cl_2): δ_B = –0.2 (s, 2 B), –3.2 (s, 2 B), –11.3 (s, 2 B), –14.9 (s, 2 B), –17.9 (s, 1 B) ppm. ^{11}B NMR (128 MHz, CD_2Cl_2): δ_B = –0.2 (2 B, d, $^1J_{BH}$ = 126 Hz), –3.2 (2 B, d, $^1J_{BH}$ = 141 Hz), –11.3 (2 B, d, $^1J_{BH}$ = 136 Hz), –14.9 (d, $^1J_{BH}$ = 150 Hz, 2 B), –17.9 (d, unresolved due to overlap with peak at –14.9, 1 B) ppm. $^{31}P\{^1H\}$ NMR (162 MHz, CD_2Cl_2): δ_P = 47.4 (s) ppm. Single crystals were grown from DCM at –20 °C, and the crystals contain one molecule of DCM of solvation per molecule of **2**. The second, lower R_f, band was also collected and identified as [3,3-$(CO)_3$-3,3-$(PPh_3)_2$-3,1,2-*closo*-$MoC_2B_9H_{11}$] (**4**) (yield 125 mg, 26 %), subsequently prepared in significantly higher yield by targeted independent synthesis, as described below.

[1,2-Me_2-3,3,3-$(CO)_3$-3-PPh_3-3,1,2-*closo*-$MoC_2B_9H_9$] (3): To a solution of [PNP][1,2-Me_2-3,3-$(CO)_2$-3-(C_3H_5)-3,1,2-*closo*-$MoC_2B_9H_9$] (0.47 g, 0.53 mmol) and PPh_3 (0.14 g, 0.53 mmol) in DCM (25 mL) at 0 °C was added neat HBF_4•OEt_2 (0.08 g, 0.53 mmol), and the mixture was warmed to ambient temperature before stirring for 1 h. All volatiles were then removed, and the resulting dark solids were purified by column chromatography, eluting with DCM/petroleum ether (35:65), to furnish the product, [1,2-Me_2-3,3,3-$(CO)_3$-3-PPh_3-3,1,2-*closo*-$MoC_2B_9H_9$] (**3**), as an orange/yellow, slightly air-sensitive solid. Yield: 89 mg, 29 %. ^1H NMR (400 MHz, CD_2Cl_2): δ_H = 7.61–7.40 (m, 15 H, Ph), 2.08 (s, 6 H, Me) ppm. $^1H\{^{11}B\}$ NMR (400 MHz, CD_2Cl_2): δ_H = 7.61–7.40 (m, 15 H, Ph), 3.01 (br. s, 1 H, BH), 2.17 (br. s, 2 H, BH), 2.11 (br. s, 2 H, BH), 2.08 (s, 6 H, Me), 1.98 (br. s, 2 H, BH), 1.81 (br. s, 1 H, BH), 1.76 (br. s, 1 H, BH) ppm. $^{11}B\{^1H\}$ NMR (128 MHz, CD_2Cl_2): δ_B = 0.0 (s, 2 B), –3.1 to –8.8 (7B, overlapping resonances, maxima at –4.5, –5.7, –7.1); ^{11}B NMR (128 MHz, CD_2Cl_2): δ_B = 0.0

(2B, d, $^1J_{BH}$ = 131 Hz), –3.1 to –8.8 (7B, overlapping resonances, maxima at –3.9, –5.1, –6.3, –7.6); $^{31}P\{^1H\}$ NMR (162 MHz, CD_2Cl_2): δ_P = 51.3 (s) ppm. $C_{25}H_{30}B_9MoO_3$ (571.74): calcd. C 49.8, H 5.02; found C 49.7, H 5.12. Single crystals were grown from DCM/petroleum ether at –20 °C.

***trans*-[3,3-(CO)$_2$-3,3-(PPh$_3$)$_2$-3,1,2-*closo*-MoC$_2$B$_9$H$_{11}$] (4):** To a solution of **1** (0.50 g, 0.58 mmol)[29] and PPh_3 (455 mg, 1.73 mmol) in DCM (20 mL) at 0 °C was added neat $HBF_4{\cdot}OEt_2$ (0.08 mL, 0.58 mmol), producing a dark red-brown solution. The mixture was then warmed to ambient temperature and stirred for 1 h before removing all volatiles under high vacuum. The resulting brown solids were eluted with DCM/petroleum ether (30:70) on a silica column, a well-defined bright orange band moving down the column preceded by a small amount of a very faint yellow band. The faint yellow band was collected and identified as monophosphine complex (**2**), whilst the major orange band was collected and identified as *trans*-[3,3-(CO)$_2$-3,3-(PPh$_3$)$_2$-3,1,2-*closo*-MoC$_2$B$_9$H$_{11}$] (**4**), a moderately air-sensitive, yellow/orange solid. Yield: 309 mg, 65 %. ^1H NMR (400 MHz, CD_2Cl_2): δ_H = 7.72–7.60 (m, 8 H, Ph), 7.54–7.35 (m, 18 H, Ph), 7.27–7.15 (m, 4 H, Ph), 2.15 (s, 2 H, CH) ppm. $^1H\{^{11}B\}$ NMR (400 MHz, CD_2Cl_2): δ_H = 7.72–7.60 (m, 8 H, Ph), 7.54–7.35 (m, 18 H, Ph), 7.27–7.15 (m, 4 H, Ph), 2.72 (s, 1 H, BH), 2.41 (s, 1 H, BH), 2.15 (s, 2 H, CH), 1.78 (s, 2 H, BH), 1.23 (s, 3 H, BH), 1.07 (s, 2 H, BH) ppm. $^{11}B\{^1H\}$ NMR (128 MHz, CD_2Cl_2): δ_B = 0.2 (s, 1 B), –2.5 (s, 1 B), –7.1 (s, 2 B), –11.6 (s, 2 B), –15.8 (s, 2 B), –22.1 (s, 1 B) ppm. ^{11}B NMR (128 MHz, CD_2Cl_2): δ_B = 0.2 (d, $^1J_{BH}$ = 113 Hz, 1 B), –2.5 (d, $^1J_{BH}$ = 112 Hz, 1 B), –7.1 (d, $^1J_{BH}$ = 129 Hz, 2 B), –11.6 (br. s, 2 B), –15.8 (br. s, 2 B), –22.1 (br. s, 1 B) ppm. $^{31}P\{^1H\}$ NMR (162 MHz, CD_2Cl_2): δ_P = 62.6 (s) ppm. $C_{40}H_{41}B_9MoO_2P_2$ (808.94): calcd. C 59.4, H 5.11; found C 58.7, H 5.06. Single crystals were grown from $CDCl_3$ at 20 °C (the crystals contain two molecules of $CDCl_3$ per molecule of metallacarborane).

***cis*-[3,3-(CO)$_2$-3,3-(PEt$_3$)$_2$-3,1,2-*closo*-MoC$_2$B$_9$H$_{11}$] (5) and *trans*-[3,3-(CO)$_2$-3,3-(PEt$_3$)$_2$-3,1,2-*closo*-MoC$_2$B$_9$H$_{11}$] (6)**

To a solution of **1** (0.31 g, 0.36 mmol)[29] in CH_2Cl_2 (12 mL) at –78 °C was added neat $HBF_4{\cdot}OEt_2$ (0.05 mL, 0.36 mmol), and the mixture was stirred for 30 min to yield a dark red-brown solution. Neat PEt_3 (0.16 mL, 1.08 mmol) was then added, and the mixture was warmed to ambient temperature and stirred for 4 h. All volatiles were then removed under high vacuum to furnish an oily red solid, which was eluted onto a silica column with DCM/petroleum ether (50:50), yielding two well-separated yellow bands.

The major, slower-moving band was collected and all volatiles were removed to furnish a yellow/orange solid, which slowly darkened in air; it was identified as *cis*-[3,3-(CO)$_2$-3,3-(PEt$_3$)$_2$-3,1,2-*closo*-MoC$_2$B$_9$H$_{11}$] (**5**). Yield: 44 mg, 23 %. ^1H NMR (400 MHz, $CDCl_3$): δ_H = 2.87 (br. s, 2 H, CH), 2.10–2.00 (m, 6 H, -CH_2-), 1.99–1.88 (m, 6 H, -CH_2-), 1.24–1.15 (m, 18 H, -CH_3) ppm. $^1H\{^{11}B\}$ NMR (400 MHz, $CDCl_3$): δ_H = 3.12 (br. s, 1 H, BH), 2.87 (br. s, 2 H, CH), 2.10–2.00 (m, 6 H, -CH_2-), 1.99–1.88 (m, 6 H, -CH_2-), 1.82 (br. s, 2 H, BH), 1.48 (br. s, 2 H, BH), 1.24–1.15 (m, 18 H, -CH_3) [analysis of the relative integrals suggest that at least 3 further BH resonances lie beneath the phosphine CH_2 resonance at 2.10–2.00 (2 × BH), and CH_3 resonance at 1.24–1.15 ppm (1 × BH), respectively] ppm. $^{11}B\{^1H\}$ NMR (128 MHz, $CDCl_3$): δ_B = –0.2 (s, 1 B), –3.0 (s, 1 B), –4.6 (s, 2 B), –12.5 (s, 2 B), –15.9 (s, 2 B), –19.4 (s, 1 B) ppm. ^{11}B NMR (128 MHz, $CDCl_3$): δ_B = –0.2 (d, J_{BH} = 131 Hz, 1 B), –3.0 (d, 1 B, coupling not resolved due to overlap with peak at –4.6 ppm), –4.6 (d, J_{BH} = 145 Hz, 2 B), –12.5 (d, J_{BH} = 137 Hz, 2 B), –15.9 (d, J_{BH} = 149 Hz, 2 B), –19.4 (d, J_{BH} = 152 Hz, 1 B) ppm. $^{31}P\{^1H\}$ NMR (162 MHz, $CDCl_3$): δ_P = 22.1 (s) ppm. $C_{16}H_{41}B_9MoO_2P_2$ (520.68): calcd. C 36.9, H 7.94; found C 36.9, H 8.07. Single crystals were grown from $CDCl_3$/petroleum ether at 5 °C.

The minor, faster moving band was collected and furnished a bright yellow solid which also slowly darkened in air and was identified as *trans*-[3,3-(CO)$_2$-3,3-(PEt$_3$)$_2$-3,1,2-*closo*-MoC$_2$B$_9$H$_{11}$] (**6**). Yield: 12 mg, 6 %. ^1H NMR (400 MHz, $CDCl_3$): δ_H = 2.59 (br. s, 2 H, CH), 2.16 (12 H, apparent quintet, -CH_2-), 1.23 (18 H, apparent quintet, -CH_3) ppm. $^1H\{^{11}B\}$ NMR (400 MHz, $CDCl_3$): δ_H = 2.98 (br. s, 1 H, BH), 2.59 (br. s, 2 H, CH), 2.16 (12 H, apparent quintet, -CH_2-), 1.96 (br. s, 3 H, BH), 1.76 (br. s, 3 H, BH), 1.35 (br. s, 2 H, BH), 1.23 (18 H, apparent quintet, -CH_3) ppm. $^{11}B\{^1H\}$ NMR (128 MHz, $CDCl_3$): δ_B = –1.4 (s, 1 B), –4.6 (s, 1 B), –6.5 (s, 2 B), –12.5 (s, 2 B), –16.9 (s, 2 B), –20.2 (s, 1 B) ppm. ^{11}B NMR (128 MHz, $CDCl_3$): δ_B = –1.4 (d, J_{BH} = 122 Hz, 1 B), –4.6 (d, 1 B, coupling not resolved due to overlap with peak at –6.5 ppm), –6.5 (d, J_{BH} = 142 Hz, 2 B), –12.5 (d, J_{BH} = 131 Hz, 2 B), –16.9 (d, J_{BH} = 150 Hz, 2 B), –20.2 (d, J_{BH} = 160 Hz, 1 B) ppm. $^{31}P\{^1H\}$ NMR (162 MHz, $CDCl_3$): δ_P = 40.6 (s) ppm. $C_{16}H_{41}B_9MoO_2P_2$ (520.68): calcd. C 36.9, H 7.94; found C 36.8, H 8.12. Single crystals were grown from $CDCl_3$/petroleum ether at 5 °C.

Thermolysis of 5 to 6: An orange solution of **5** (20 mg, 0.04 mmol) in THF (20 mL) was heated to reflux for 18 h. After cooling to ambient temperature all volatiles were removed under high vacuum to furnish a yellow solid, analysis (by ^{11}B and ^1H NMR spectroscopy) of which indicated a clean and quantitative conversion of *cis*-isomer **5** to *trans*-isomer **6**.

Crystallographic Studies

Diffraction data from compounds **2** and **4** were collected at 120 K with a Rigaku Oxford Diffraction SuperNova diffractometer at the University of Edinburgh, whilst data from **3** were collected at 100 K with a Rigaku FR-E+ diffractometer by the UK National Crystallography Service at the University of Southampton. Data from **5** and **6** were collected at 100 K with a Bruker X8 APEXII diffractometer at Heriot-Watt University. In all cases Mo-K_α *X*-radiation was used with crystals mounted in inert oil on a cryoloop and cooled in a stream of cold N_2. Using OLEX2[30] structures were solved by direct methods using the SHELXS[31] or SHELXT[32] programme and refined by full-matrix least-squares (SHELXL).[31] There was no evidence for twinning and all the metallacarborane cages were fully ordered. Compound **2** crystallises with one molecule of DCM per metallacarborane, **4** with two molecules of $CHCl_3$ per metallacarborane, and **5** with one molecule of $CHCl_3$ per metallacarborane, the last partially disordered. Cage C atoms bearing only H substituents were distinguished from B atoms by the VCD[4] and BHD[33] methods. H atoms bound to cage B or cage C atoms were allowed to refine positionally whilst H atoms bound to other C atoms were constrained to idealised geometries; C_{phenyl}–H = 0.95 Å, $C_{primary}$–H = 0.98 Å, $C_{secondary}$–H = 0.99 Å, $C_{tertiary}$–H = 1.00 Å. All H displacement parameters, U_{iso}, were constrained to be 1.2 × U_{eq} (bound B or C) except Me H atoms [U_{iso}(H) = 1.5 × U_{eq} C(Me)]. Table S1 (Supporting Information) contains further experimental details.

CCDC 1543882 (for compound **2**·CH_2Cl_2), 1543883 (for compound **3**), 1543884 (for compound **4**·2$CHCl_3$), 1543885 (for compound **5**·$CHCl_3$) and 1543886 (for compound **6**) contain the supplementary crystallographic data for this paper. These data can be obtained free of charge from The Cambridge Crystallographic Data Centre.

Acknowledgments

We thank the Leverhulme Trust for supporting A. P. M. R. and J. J. J. (project RPG-2014–286). We are grateful to Prof. S. A. Macgregor for the DFT calculations on compound **4** and its PH_3

analogue, and for helpful discussions. We also thank the UK National Crystallography Service for data collection of compound **3**. A. R. is an Erasmus exchange student from the Phillips-Universität Marburg, Germany.

Keywords: Carboranes · Steric effects · Electronic effects · Carbonyl ligands · Phosphane ligands

[1] a) D. M. P. Mingos, *J. Chem. Soc., Dalton Trans.* **1977**, 602–610; b) D. M. P. Mingos, M. I. Forsyth, A. J. Welch, *J. Chem. Soc., Dalton Trans.* **1978**, 1363–1374.
[2] a) A. J. Welch, *J. Chem. Soc., Dalton Trans.* **1975**, 1473–1478; b) G. K. Barker, M. Green, F. G. A. Stone, A. J. Welch, *J. Chem. Soc., Dalton Trans.* **1980**, 1186–1199; c) G. K. Barker, M. P. Garcia, M. Green, G. N. Pain, F. G. A. Stone, S. K. R. Jones, A. J. Welch, *J. Chem. Soc., Chem. Commun.* **1981**, 652–653.
[3] S. L. Powley, G. M. Rosair, A. J. Welch, *Dalton Trans.* **2016**, *45*, 11742–11752.
[4] A. McAnaw, G. Scott, L. Elrick, G. M. Rosair, A. J. Welch, *Dalton Trans.* **2013**, *42*, 645–664.
[5] a) D. E. Smith, A. J. Welch, *Organometallics* **1986**, *5*, 760–766; b) G. Scott, A. McAnaw, D. McKay, A. S. F. Boyd, D. Ellis, G. M. Rosair, S. A. Macgregor, A. J. Welch, F. Laschi, F. Rossi, P. Zanello, *Dalton Trans.* **2010**, *39*, 5286–5300; c) G. Scott, G. M. Rosair, A. J. Welch, *J. Organomet. Chem.* **2012**, *721–722*, 78–84; d) A. McAnaw, M. E. Lopez, D. Ellis, G. M. Rosair, A. J. Welch, *Dalton Trans.* **2013**, *42*, 671–679.
[6] B. J. Coe, S. J. Glenwright, *Coord. Chem. Rev.* **2000**, *203*, 5–80.
[7] a) H. J. Plastas, J. M. Stewart, S. O. Grim, *Inorg. Chem.* **1973**, *12*, 265–272; b) B. Ndiaye, S. Bhat, A. Jouaiti, T. Berclaz, G. Bernardinelli, M. Geoffroy, *J. Phys. Chem. A* **2006**, *110*, 9736–9742.
[8] F. A. Cotton, D. J. Darensbourg, W. H. Ilsley, *Inorg. Chem.* **1981**, *20*, 578–583.
[9] M. J. Aroney, I. E. Buys, M. S. Davies, T. W. Hambley, *J. Chem. Soc., Dalton Trans.* **1994**, 2827–2834.
[10] D. Rodewald, F. Sussmilch, D. Rehder, *An. Quim.* **1996**, *92*, 269–274.
[11] A. E. Miroslavov, A. A. Lumpov, G. V. Sidorenko, E. M. Levitskaya, N. I. Gorshkov, D. N. Suglobov, R. Alberto, H. Braband, V. V. Gurzhiy, S. V. Krivovichev, I. G. Tananaev, *J. Organomet. Chem.* **2008**, *693*, 4–10.
[12] R. F. See, D. Kozina, *J. Coord. Chem.* **2013**, *66*, 490–500.
[13] D. D. Ellis, S. M. Couchman, J. C. Jeffery, J. M. Malget, F. G. A. Sone, *Inorg. Chem.* **1999**, *38*, 2981–2988.
[14] S. S. Lee, C. B. Knobler, M. F. Hawthorne, *Organometallics* **1991**, *10*, 670–677.
[15] C. R. Groom, F. H. Allen, *Angew. Chem. Int. Ed.* **2014**, *53*, 662–671; *Angew. Chem.* **2014**, *126*, 675. For this search we used ConQuest version 1.19.
[16] J. C. Jeffery, P. A. Jelliss, E. Psillakis, G. E. A. Rudd, F. G. A. Stone, *J. Organomet. Chem.* **1998**, *562*, 17–27.
[17] R. N. Grimes, *Carboranes*, 3rd ed., Academic Press, Burlington, MA, USA, **2016**.
[18] M. J. Fischer, P. A. Jelliss, L. M. Phifer, N. P. Rath, *Inorg. Chim. Acta* **2005**, *358*, 1531–1544.
[19] J.-H. Kim, E. Hong, J. Kim, Y. Do, *Inorg. Chem.* **1996**, *35*, 5112–5113.
[20] I. T. Chizhevsky, P. V. Petrovskii, P. V. Sorokin, V. I. Bregadze, F. M. Dolgushin, A. I. Yanovsky, Yu. T. Struchkov, *Organometallics* **1996**, *15*, 2619–2623.
[21] D. N. Cheredilin, F. M. Dolgushin, I. D. Grishin, E. V. Kolyakina, A. S. Nikiforov, S. P. Solodovnikov, M. M. Il'in, V. A. Davankov, I. T. Chizhevsky, D. F. Grishin, *Russ. Chem. Bull.* **2006**, *55*, 1163–1170.
[22] S. J. Dossett, S. Li, F. G. A. Stone, *J. Chem. Soc., Dalton Trans.* **1993**, 1585–1591.
[23] S. J. Dossett, S. Li, D. F. Mullica, E. L. Sappenfield, F. G. A. Stone, *J. Chem. Soc., Dalton Trans.* **1993**, 3551–3557.
[24] a) K. Wade, *J. Chem. Soc., D* **1971**, 792–793; b) D. M. P. Mingos, *Nat. Phys. Sci.* **1972**, *236*, 99–102.
[25] Full details of the DFT calculations will be published subsequently: S. A. Macgregor, to be published.
[26] H. D. Smith, T. A. Knowles, H. Schroeder, *Inorg. Chem.* **1965**, *4*, 107–111.
[27] M. F. Hawthorne, D. C. Young, P. M. Garrett, D. A. Owen, S. G. Schwerin, F. N. Tebbe, P. A. Wegner, *J. Am. Chem. Soc.* **1968**, *90*, 862–868.
[28] R. G. Hayter, *J. Organomet. Chem.* **1968**, *13*, P1–P3.
[29] The requisite purification of this compound by column chromatography to remove a dark red/brown material led, unavoidably, to some decomposition to yield a mixture of salt **1** and [PNP][7,8-*nido*-$C_2B_9H_{12}$] in a 2:1 ratio based on analysis by ^{11}B NMR spectroscopy. This yield is, therefore, calculated from an overall yield of solid of 2.58 g, factoring in the presence of [PNP][7,8-*nido*-$C_2B_9H_{12}$]. Purification of the compound on a small scale by recrystallisation from DCM/petroleum ether at –20 °C produced a small number of well-formed crystals suitable for the full spectroscopic characterisation but, due to low yields in the recrystallisation, the bulk material was employed without further purification in subsequent reactions (in which [PNP][7,8-*nido*-$C_2B_9H_{12}$] should be a spectator species).
[30] O. V. Dolomanov, L. J. Bourhis, R. J. Gildea, J. A. K. Howard, H. Puschmann, *J. Appl. Crystallogr.* **2009**, *42*, 339–341.
[31] G. M. Sheldrick, *Acta Crystallogr., Sect. A* **2008**, *64*, 112–122.
[32] G. M. Sheldrick, *Acta Crystallogr., Sect. A* **2015**, *71*, 3–8.
[33] A. McAnaw, M. E. Lopez, D. Ellis, G. M. Rosair, A. J. Welch, *Dalton Trans.* **2014**, *43*, 5095–5105.

Received: May 3, 2017